A retino-cortical model to study movement-generated waves in the visual system

Jérôme Emonet

UNIVERSITÉ CÔTE D'AZUR | ÉCOLE DOCTORALE SCIENCES ET TECHNOLOGIES DE L'INFORMATION ET DE LA COMMUNICATION

THÈSE DE DOCTORAT

Un modèle rétino-cortical pour étudier les ondes générées par le mouvement dans le système visuel

Jérôme EMONET

Equipe Biovision

Centre INRIA d'Université Côte d'Azur

Présentée en vue de l'obtention du grade de docteur en Informatique d'Université Côte d'Azur

Dirigée par : Bruno Cessac, *Directeur de Recherches INRIA, Université Côte d'Azur.*
Alain Destexhe, *Directeur de Recherches CNRS NeuroPsi, Université Paris-Saclay.*

Soutenue le : 28 novembre 2024

Devant le jury composé de :
Frédéric ALEXANDRE, *Directeur de Recherches INRIA Université de Bordeaux*
Viktor JIRSA, *Directeur de Recherches CNRS Université d'Aix-Marseille*
Michael BERRY, *Professeur agrégé Université de Princeton*
Joana CABRAL, *Professeur assistant Université de Minho*
Frédéric CHAVANE, *Directeur de Recherches CNRS Université d'Aix-Marseille*

PROJET FINANCÉ PAR L'ANR - PROJECT FUNDED BY THE ANR

UNIVERSITÉ CÔTE D'AZUR | ÉCOLE DOCTORALE SCIENCES ET TECHNOLOGIES DE L'INFORMATION ET DE LA COMMUNICATION

THÈSE DE DOCTORAT

A retino-cortical model to study movement-generated waves in the visual system

Jérôme EMONET

Biovision team

Centre INRIA d'Université Côte d'Azur

A thesis submitted in fulfillment of the requirements for the degree of Doctor in Computer Science from the Université Côte d'Azur

Directed by : Bruno Cessac, *INRIA Research Director, Université Côte d'Azur.*
Alain Destexhe, *NeuroPsi CNRS Research Director, Université Paris-Saclay.*

Defended on : 28 november 2024

In front of a jury composed of :
Frédéric ALEXANDRE, *INRIA Research Director Université de Bordeaux*
Viktor JIRSA, *CNRS Research Director Université d'Aix-Marseille*
Michael BERRY, *Associate Professor Princeton University*
Joana CABRAL *Assistant professor University of Minho*
Frédéric CHAVANE, *CNRS Research Director Université d'Aix-Marseille*

PROJET FINANCÉ PAR L'ANR - PROJECT FUNDED BY THE ANR

Un modèle rétino-cortical pour étudier les ondes générées par le mouvement dans le système visuel

Jury :

Rapporteurs :

Frédéric ALEXANDRE, Directeur de Recherches INRIA, Université de Bordeaux

Viktor JIRSA, Directeur de Recherches, Université d'Aix-Marseille

Examinateurs :

Michael BERRY, Professeur agrégé, Université de Princeton

Joana CABRAL, Professeur assistant, Université de Minho

Bruno Cessac, Directeur de Recherches INRIA, Université Côte d'Azur.

Frédéric CHAVANE, Directeur de Recherches, Université d'Aix-Marseille

Alain Destexhe, NeuroPsi Directeur de Recherches CNRS, Université Paris-Saclay.

Résumé

Le système visuel est capable de traiter rapidement et efficacement des mouvements complexes dans des scènes visuelles riches. Une partie de ce traitement a lieu dans la rétine et le cortex. En particulier, la connectivité latérale permet de générer des ondes induites par des objets en mouvements. Dans notre travail, nous nous intéressons particulièrement à l'implication de ces ondes dans deux mécanismes de la perception du mouvement : l'anticipation et l'omission saccadique. L'anticipation est le nom donné à l'ensemble des mécanismes du système visuel permettant d'avancer dans le temps la représentation du stimulus dans la rétine ou le cortex. Leur but est de compenser le retard d'environ 100 ms qui se produit lors du traitement visuel au niveau de la rétine. Avec un tel retard, nous ne pourrions pas attraper un objet en mouvement. L'omission saccadique est un mécanisme qui permet d'ignorer les mouvements oculaires très rapides appelés saccades oculaires. Ces saccades nous permettent d'explorer la scène visuelle bien que nous ne les percevions pas (omission saccadique). L'hypothèse actuelle est que l'omission saccadique ne se produit qu'en présence de mouvements oculaires. Cependant, une hypothèse alternative soutient le rôle indispensable des stimuli périsaccadiques. Des expériences sur les saccades sans mouvement oculaire ont montré qu'en présence de stimuli périsaccadiques (avec un taux de rafraîchissement suffisamment élevée, 1440 Hz), les individus perçoivent une barre en mouvement plus lente, plus nette, avec une amplitude réduite et sans traînée. Cela créé un mouvement que le système visuel pourrait facilement effacer grâce à la propagation d'ondes suppressives, déjà présentes dans les mouvements apparents, par le biais de la connectivité latérale dans le cortex. Dans ce mécanisme potentiel d'omission saccadique, la représentation la plus récente de l'objet en mouvement inhibe les plus anciennes grâce aux ondes suppressives.

L'objectif de cette thèse est d'étudier les mécanismes d'anticipation et d'omission saccadique sous le point de vue de la modélisation. Pour ce faire, nous utilisons un modèle rétino-cortical appelé « modèle Chimère ». Il contient d'abord un modèle rétinien composé de cellules bipolaires, amacrines et ganglionnaires interconnectées, avec un contrôle de gain sur les cellules bipolaires et ganglionnaires. La sortie rétinienne est envoyée à un modèle cortical, un réseau de colonnes corticales, chacune correspondant à des équations de champ moyen, capables de produire l'intensité du signal d'un pixel dans l'imagerie dépendante du voltage. La sortie du modèle peut donc être comparée à des expériences biologiques. Ce modèle rétino-cortical a été implémenté dans la plateforme Macular créée à l'INRIA. Cette thèse présente le modèle chimère, certaines de ses propriétés dynamiques et son implémentation, avant d'y étudier l'anticipation et l'omission saccadique. Après une calibration du modèle reproduisant des expériences réalisées dans le laboratoire de F. Chavane, nous montrons comment différents paramètres expérimentaux (vitesse de la barre, contraste) et physiologiques (intensité de la sortie rétinienne, connexions des cellules amacrines, contrôle de gain, intensité des connexions corticales, ...) impactent l'anticipation au niveau de la rétine et du cortex. Pour l'omission saccadique, nous reproduisons d'abord les ondes suppressives observées avec le mouvement apparent avant d'étudier la réponse rétino-corticale de stimuli correspondant au mouvement avec ou sans stimuli périsaccadiques affichés à une fréquence de rafraîchissement de 60Hz (vidéoprojecteurs classiques) ou de 1440Hz (vitesse de rafraîchissement à laquelle un effet de traînée est perçu). Nous étudions également l'impact des phases statiques et le rôle potentiel de la propagation d'ondes suppressives.

Mots-clés : Neurosciences computationnelles, Modèle rétino-cortical, Vision du mouvement, Anticipation visuelle, Saccade simulées, Ondes d'activité.

Abstract

The visual system is able to process complex movements quickly and efficiently in rich visual scenes thanks to a processing taking place in the retina, the LGN, and the visual cortex. Especially, lateral connectivity enables the generation of waves that only appear when a moving object is present. In our work, we are particularly interested in the involvement of these waves in two mechanisms of motion vision: anticipation and saccadic omission. Anticipation is the name given to the set of mechanisms in the visual system to bring forward in time the representation of the stimulus in the retina or cortex. Their aim is to compensate for the 100ms delay in visual processing in the retina. With such a delay, we would not be able to catch a moving object. Saccadic omission is a mechanism for ignoring very rapid eye movements known as ocular saccades. These saccades enable us to explore the visual scene although we do not perceive them (saccadic omission). The current hypothesis is that saccadic omission only occurs in the presence of eye movements. However, an alternative hypothesis supports the indispensable role of perisaccadic stimuli. Experiments on saccades without eye movement have shown that in the presence of perisaccadic stimuli (with a sufficiently high frame rate, 1440 Hz) individuals perceive a slower, sharper moving bar, with reduced amplitude and no smear. This creates a movement that the visual system could easily erase. This process could be caused by the propagation of suppressive waves, already exhibited in apparent movements, through lateral connectivity in the cortex. In this potential mechanism of saccadic omission the most recent representation of the moving object inhibits older ones thanks to suppressive waves.

The aim of this thesis is to study the mechanisms of anticipation and saccadic omission from a modelling perspective. To this end, we are using a retinal-cortical model known as the 'Chimera model'. It first contains a retinal model made up of bipolar, amacrine and ganglion cells interconnected, with gain control on the bipolar and ganglion cells. The retinal output is sent to a cortical model, a network of cortical columns, each corresponding to mean-field equations, capable of producing the signal intensity of a pixel in voltage-dependent imaging. The output of the model can therefore be compared with biological experiments. This retino-cortical model has been implemented in the Macular plateform created at INRIA. This thesis introduces the Chimera model, review some of its dynamical properties, and discuss its implementation, before studying anticipation and saccadic omission. After a calibration of the model reproducing experiments made in F. Chavane lab, we show how different experimental (bar speed, contrast) and physiological (retinal output intensity, amacrine cells connections, gain control, cortical connections intensity, ...) impact anticipation at the level of the retina and in the cortex. For saccadic omission, we first reproduce the suppressive waves observed with apparent movement before studying the retino-cortical response of stimuli corresponding to movement, with or without perisaccadic stimuli, displayed at a refresh rate of 60Hz (classical video projectors) or 1440Hz (refresh speed at which a smear effect is perceived). We also study the impact of static phases and the potential role of suppressive wave propagation.

Keywords : Computational neuroscience, Retino-cortical model, Motion vision, Visual anticipation, Simulated saccades, Activity waves.

Contents

Introduction en Français

La vision

La perception visuelle est un processus aussi complexe qu'essentiel pour beaucoup d'organismes et l'être humain n'y fait pas exception. Cette capacité à détecter les radiations lumineuses de l'environnement, ainsi qu'à y trouver un sens, a toujours été intimement liée à notre survie, et plus généralement à la nécessité de nous déplacer, d'interagir avec le monde extérieur. On doit cette aptitude au système visuel dont la porte d'entrée est l'œil. Les rayons lumineux traversent ce dernier pour venir activer des cellules photoréceptrices au fond de l'œil, dans la rétine. Ces rayons lumineux engendrent un signal électrique traité par les couches neuronales successives de la rétine, avant d'être envoyé au thalamus, par le biais du nerf optique, puis de rejoindre l'aire visuelle primaire (V1). Cette région du cerveau a pour rôle de différencier des propriétés particulières de l'image (orientation, fréquences spatiales, mouvement...). Le système visuel fait ensuite intervenir de nombreuses autres zones corticales responsables de traitements toujours plus complexes et intégrés. Tout ceci est rendu possible via le traitement préliminaire de l'information visuelle par la rétine, qui est bien plus qu'une simple caméra. C'est dans la rétine que naîssent une trentaine de canaux d'information constituant autant de représentations différentes et complémentaires du monde, chacune associée à une modalité de la vision. C'est également dans la rétine que commencent les traitements d'un certain nombre de propriétés comme la représentation de l'orientation, la couleur ou encore le mouvement des objets perçus. Le système visuel est aussi capable d'analyser des mouvements rapides et complexes dans des scènes visuelles extrêmement riches et complexes. Dans la rétine, comme dans le cortex, ce sont les propriétés particulières du réseau neuronal qui permettent d'analyser ces mouvements. Dans ce contexte, deux mécanismes nous intéressent tout particulièrement : l'anticipation et l'omission saccadique.

L'anticipation

La vision du mouvement présente un défaut majeur qui réside dans la lenteur du procédé de phototransduction (conversion de la lumière en variations de potentiel électrique) au sein des photorécepteurs. Cela induit un délai de 100 ms entre la capture de photons par les photorécepteurs et l'arrivée du signal électrique rétinien dans le cortex visuel primaire [1]. Un tel retard entre la réalité et notre perception rendrait la vision non effective. Face à un danger tel qu'un prédateur ou une voiture se déplaçant à 50 km/h, notre perception de ces derniers accuserait un retard de 1.4 m sur le mouvement réel. En d'autres termes, le danger aurait déjà parcouru 1.4 m avant que notre système visuel ne détecte le début du mouvement réel. Cet exemple permet de souligner la gravité qu'aurait un retard de cette ampleur. Moins dramatiquement, un tel retard devrait nous empêcher d'attraper un objet en mouvement. Mais alors, comment les espèces animales peuvent-elles alors se reposer sur la vision pour chasser ou fuir ? Le système visuel a mis en place des mécanismes d'anticipation pour compenser ce défaut. Ces derniers se mettent uniquement en place pour des objets en mouvement, mais restent inactifs pour des objets fixes. L'anticipation permet d'avancer dans le temps la représentation neurale des futures positions de l'objet en mouvement et ainsi de compenser le retard dû à la phototransduction. Cette compensation dépend bien sûr de la vitesse de l'objet et devient inopérante pour des objets trop rapides. Des mécanismes d'anticipation ont été mis en évidence dans la rétine et dans le cortex visuel primaire. Dans la rétine, deux types d'anticipation ont été mis au jour. Le premier, dit par "adaptation", correspond à un chute plus précoce du pic d'activité des cellules de sortie de la rétine afin de l'avancer [1]. Ce pic est ce à quoi répondent principalement les cellules corticales, et son avancement leur permet donc de répondre plus tôt. Le second type, dit par "prédiction", correspond quand à lui à un décalage plus précoce de l'intégralité de la réponse rétinienne. Dans les deux cas, des cellules rétiniennes spécifiques, les cellules amacrines, semblent également être à l'origine du processus [2]. Au sein du cortex visuel primaire, un autre procédé d'anticipation, dit "par latence", a été identifié [3]. Dans ce cas, le mouvement de l'objet entraîne la propagation d'une onde d'activité transmise par la connectivité latérale des colonnes corticales excitées par la barre, vers d'autres colonnes corticales plus distantes. Les colonnes corticales sont, en quelque sorte, les unités de traitement dans le cortex visuel. Elles sont constituées de quelques milliers de neurones avec une organisation spécifique. L'onde d'activité induite par un objet en mouvement permet aux colonnes corticales distantes de répondre de façon plus précoce. Récemment, S. Souihel et B. Cessac ont soulevé l'hypothèse que l'anticipation rétinale puisse présenter des caractéristiques similaires à l'anticipation corticale par latence. Un objet en

mouvement pourrait produire, par le biais du réseau des cellules amacrines, une onde d'activation précoce des cellules ganglionnaires.

L'omission saccadique

Les saccades oculaires sont des mouvements oculaires très rapides, se produisant environ 3 fois par seconde, avec une vitesse maximale de 500 °/s, et une vitesse moyenne de 200 °/s [4, 5]. Ce processus est essentiel pour explorer rapidement une scène visuelle et en saisir les informations essentielles. Il est également à l'origine de nos capacités de reconnaissance faciale et de lecture. Lors d'une saccade, la représentation de la scène visuelle se déplace à la même vitesse que la saccade. Cependant, nous ne percevons aucun flou de mouvement. Au contraire, la scène visuelle reste stable, claire et précise. C'est ce qu'on appelle "l'omission saccadique". Une explication actuelle de ce phénomène est basée sur un signal appelé "décharge corollaire" [6]. Cette copie de la commande oculaire motrice engendre une perte de sensibilité visuelle au mouvement appelée "suppression saccadique", pendant la saccade. Cependant, cette explication a ses limites. Lorsqu'un stimulus est montré à un sujet uniquement pendant une saccade, pas avant ni après, alors le stimulus est perçu mais avec une traînée. Cela signifie que la décharge corollaire ne suffit pas à expliquer l'omission saccadique. En revanche, l'ajout de stimuli périsaccadiques avant et/ou après la saccade permet de faire disparaître la traînée. Les stimuli périsaccadiques agissent donc comme des masques qui vont cacher le mouvement du stimulus [7]. C'est dans ce contexte qu'est né l'explication alternative d'une omission saccadique supportée par ces masques périsaccadiques.

Des expériences psychophysiques récentes [8] ont réussi à effacer la traînée dans une saccade simulée, sans aucun mouvement des yeux, chez le sujet humain. Dans ces expériences, les mouvements de saccades oculaires ont été reproduits en utilisant un stimulus se déplaçant à la vitesse de la saccade et affiché avec un appareil ayant une fréquence d'images de 1440 Hz. Traditionnellement, les stimuli dans les expériences psychophysiques sont affichés à une fréquence de 60 Hz. A 60 Hz, les sujets observent un mouvement apparent, avec une traînée autour de la trajectoire du stimulus. L'utilisation d'un taux de rafraîchissement de 1440 Hz permet de supprimer cet effet. Dans l'expérience, deux types de stimuli ont été utilisés : une simple barre blanche en mouvement (_M_) ou la même barre en mouvement précédée et suivie de phases statiques : masques avant et arrière (SMS). Seul le stimulus _M_ conduit à la traînée, alors que le SMS en est exempt et permet de percevoir un mouvement plus lent et plus court. Par conséquent, le masquage du mouvement (SMS) n'est pas suffisant pour éviter la perception du mouvement de la barre, mais pourrait le rendre plus facile à ignorer. Des processus supplémentaires, comme la suppression saccadique, seront nécessaires pour supprimer complètement le mouvement. Une hypothèse, proposée pour expliquer ce masquage temporel du mouvement est soutenue par des expériences dans le cortex visuel primaire du singe réalisées par Frédéric Chavane et son équipe (Institut des Neurosciences de la Timone) montrant des ondes suppressives se propageant dans la direction opposée d'un mouvement et provenant d'ondes d'activité [9]. Ces ondes suppressives se propagent aux zones précédemment activées par le mouvement et suppriment ainsi l'activité résiduelle. Cet effet suppressif de la dernière position du stimulus vers la précédente pourrait expliquer l'effacement de la traînée. À partir de ces expériences, on peut donc se demander si le masquage temporel des mouvements peut être expliqué par des ondes suppressives se propageant dans le cortex et dans la rétine.

Contexte de la thèse. Cette thèse étudie, sous l'angle de la modélisation, les mécanismes d'anticipation et d'omission saccadique en utilisant un modèle intégré rétine-cortex, appelé "Chimera model", présenté ci-dessous.

Le travail sur l'anticipation s'inscrit dans le cadre d'une précédente collaboration, l'ANR Trajectory (https://team.inria.fr/biovision/anr-trajectory/) entre Frédéric Chavane, Alain Destexhe, Olivier Marre, Bruno Cessac et Selma Souihel (ancienne doctorante) visant à mieux comprendre comment les mécanismes d' anticipation dans la rétine et le cortex se combinent. C'est dans le cadre de la thèse de Selma Souihel, dirigée par Bruno Cessac, que le "Chimera model" a été initié. Cependant, il n'a pas été finalisé, et la thèse de Selma Souihel a essentiellement porté sur la modélisation de l'anticipation dans la rétine. Notre premier objectif a été de finaliser le "Chimera model". D'une part, du point du modèle lui-même, en étudiant son comportement dynamique et recherchant des plages de paramètres donnant lieu à un comportement stable et biologiquement plausible. D'autre part, du point de vue de la simulation. Une grande partie de notre activité de thèse a en effet consisté à porter le modèle sur la plateforme de simulation Macular (https://team.inria.fr/biovision/Macular-software/), décrite dans le chapitre 2, de façon à obtenir des simulations rapides et réalistes (avec notament une taille de cortex raisonable), en deux dimensions. Cela nous a permis d'avoir des résultats nouveaux sur le rôle respectifs des mécanismes d'anticipation dans la rétine et le cortex. Au delà de l'anticipation, le "Chimera model" et la plateforme Macular permettent de simuler le complexe rétine cortex, avec des entrées visuelles réalistes (films), en faisant varier notament des paramètres physiologiques parfois impossible à contrôler expérimentalement. En particulier, nous avons réussit à mettre en oeuvre un modèle amélioré ayant la capacité de reproduire l'anticipation par prédiction.

Le travail sur l'omission saccadique s'inscrit, lui, dans le cadre de la collaboration ANR Shooting Star (https://team.inria.fr/biovision/anr-shootingstar/), entre Mark Wexler, Frédéric Chavane, Olivier Marre, Alain Destexhe

et Bruno Cessac visant à tester l'hypothèse d'omission saccadique par ondes suppressives. Notre objectif était de tenter reproduire les ondes d'activité corticale avec le "Chimera model" et d'y simuler des saccades. Ceci, afin de repoduire les résultats expérimentaux de M. Wexler et F. Chavane, et d'étudier l'existence et la nature d'ondes suppressives. A l'aide de la plateforme Macular nous avons pu ainsi mettre en évidence un effet de traînée plutôt observée avec un taux de rafraichissement à 1440 Hz qu'à 60 Hz, avec un modèle mathématique simple permettant de comprendre cet effet. Nous avons aussi constaté la perte dans l'identité du stimulus à 1440 Hz. Nous mettons également en évidence d'une suppression des phases statiques sur le mouvement et une différence de réponse corticale entre les stimuli M et SMS. Enfin, nous montrons comment des phases statiques de tailles différentes de la phase mouvante peuvent influencer sur la réponse à celle-ci.

Le chimera model

Le "Chimera model" vise à modéliser et simuler le complexe rétine-cortex, en "négligeant" le thalamus i.e. en le considérant comme un simple relais. Nous faisons cela dans un soucis de simplicité du modèle bien que le thalamus soit plus qu'un simple relais [10, 11]. Il s'agissait aussi de disposer d'une plateforme de simulation associée, permettant de jouer des entrées rétiniennes réalistes (films). Le terme "Chimera model" provient du fait que le modèle de rétine a été calibré à partir de données sur la souris alors que le modèle cortical a été calibré à partir de données sur le singe [12, 13, 9]. Nous discutons cet aspect plus en détail dans la thèse. La modélisation a l'avantage de pouvoir ici palier aux lacunes expérimentales qui ne permettent pas de mesurer la rétine et le cortex en même temps et de modifier "à la main" des paramètres physiologiques impossibles à contrôler expérimentalement. La modélisation octroie aussi la possibilité de pouvoir identifier les facteurs suffisant pour engendrer l'anticipation et l'omission saccadique.

Ce modèle rétino-cortical produit une activité correspondant à l'intensité des pixels en imagerie à colorant sensible au voltage (VSDI) en réponse à une stimulation rétinienne. Le modèle de rétine est basé sur de précédents travaux sur la rétine de souris [1, 14, 15, 16]. Il simule un graphe constitué de cellules bipolaires, amacrines et ganglionnaires. Le champ récepteur des cellules bipolaires est une fonction qui permet de reproduire la réponse des photorécepteurs et des cellules horizontales. Les cellules bipolaires disposent d'un système de contrôle de gain connu pour reproduire l'anticipation par adaptation. Les cellules amacrines sont, quant à elles, utilisées dans le but de mettre en place une connectivité latérale qui pourrait être à l'origine de l'anticipation par prédiction mais également de la propagation d'ondes au sein de la rétine. Le modèle cortical a été créé à partir d'expériences chez le macaque. Il utilise des réseaux connectés de modèles de champs moyens représentant chacun une colonne corticale. Pour chaque colonne corticale, on compte un modèle de champ moyen correspondant à sa population excitatrice et un à sa population inhibitrice. A cela s'ajoute une connectivité latérale entre les colonnes où les signaux se propagent à une vitesse de 300mm/s. On obtient en sortie l'intensité du pixel d'imagerie voltage dépendante (VSDI) contenant la colonne corticale. Ce modèle était utilisé dans le but de reproduire des résultats d'imagerie optique voltage dépendant.

Macular

Macular est un logiciel élaboré, sous la direction de Bruno Cessac, par des ingénieurs du Service d'Etudes et Développement (SED) de l'Inria, ainsi que par des doctorants dont je fait partie. Il s'agit d'une plateforme modulaire de simulation de rétine et de cortex visuel primaire. Elle permet de reproduire l'activité spontanée ou la réponse à des stimuli visuels en condition de vision normale, altérée (pharmacologie, pathologie...) ou prosthétique. Macular se structure en ensemble de couches pour reproduire l'architecture de la rétine. Chaque couche est composée d'un type d'objet pouvant être une cellule ou une population d'une colonne corticale. Le tout est ensuite interconnecté par le biais de synapses pouvant incorporer ou non un délai dynamique. Dans notre cas, le "Chimera model" reçoit une entrée spatio-temporelle sous la forme d'une vidéo. Une description complète est donnée dans le chapitre 2.

Plan de thèse

Le premier chapitre est destiné à introduire ensemble l'ensemble des connaissances nécessaires à la compréhension de cette thèse ainsi que de l'état de la littérature sur les différents sujets que nous aborderons.

Dans un second chapitre, nous introduisons le "Chimera model" et discutons ses élements et sa dynamique. En particulier, nous montrons que, sous certains régimes de paramètres, le modèle présente des instabilités pathologiques (oscillations) qu'il a fallu contrôler. Nous présentons ensuite le logiciel Macular et l'implémentation du "Chimera Model". Nous expliquons en particulier, comment nous l'avons adapté pour réaliser des simulations bi-dimensionnelles ainsi que les différentes modifications effectuées pour le rendre plus proche de la réalité. Nous détaillons aussi la calibration du modèle que nous avons effectué afin de reproduire les premiers résultats expérimentaux sur les ondes corticales induites par les objets en mouvement.

Le troisième chapitre est consacré au mécanisme d'anticipation. Après avoir introduit des mesures quantitatives, expérimentalement accessibles, de l'anticipation, nous étudions l'effet d'un certain nombre de paramètres associés au stimulus - tels que le contraste, la vitesse-; physiologiques - tels que la portée des connections corticales-; ou encore phénoménologiques - tels les paramètres contrôlant l'anticipation rétinienne, le contrôle de gain et/ou la

connectivité latérale amacrine. Un résultat important de ce travail est de montrer comment la réponse VSDI, mesurable expérimentalement, est modifiée de façon visible par les mécanismes d'anticipation rétiniens, mettant en évidence les rôles respectifs de l'anticipation par avancement du pic d'activité (rétine) et l'anticipation par latence (cortex). Nous montrons également comment le réseau amacrine influe sur la réponse rétinienne et corticale à un objet en mouvement.

Le quatrième chapitre est consacré à l'omission saccadique. Nous reproduisons tout d'abord des ondes suppressives similaires aux expériences de Frédéric Chavane. Nous utilisons ensuite des stimuli de Mark Wexler (mouvement simple ou mouvement entourant des phases statiques) affichés à un taux de rafraîchissement de 60 Hz ou 1440 Hz pour comprendre l'impact que peuvent avoir la phase statique et la vitesse de rafraichissement sur l'activité corticale, comment la phase statique déclenche potentiellement des ondes suppressives et quels en sont les paramètres importants. Ceci pour là aussi mieux discerner les rôles respectifs de la rétine et du cortex V1 dans ce mécanisme.

Dans la conclusion, nous montrons un modèle rétino-cortical fonctionnel capable de reproduire à la fois les expériences d'anticipation [3] et d'ondes suppressives [9] dans le cortex visuel primaire. Ce modèle rétino-cortical nous a permis de souligner l'importance de l'output rétinien fourni au cortex, de la vitesse de la barre ainsi que de l'équilibre des connexions excitatrices et inhibitrices. Il nous a également permis de montrer le transfert de l'anticipation par rétine dans le cortex malgré une réduction de l'anticipation corticale. Nous avons pu voir la capacité des deux types d'anticipation rétinienne se combiner favorablement pour l'anticipation corticale. Dans le contexte de l'omission saccadique, nous avons découvert une perte de continuité engendrée par un faible taux de rafraîchissement sur un stimulus se déplaçant à la vitesse d'une saccade. Nous montrons de plus un plus grand smear dans le cas d'un stimulus possédant des phases statiques. Nous observons le shape-dragging uniquement pour des phases statiques plus grande que celle en mouvement. Enfin, nous reproduisons l'onde suppressive dans un mouvement apparent mais nous ne mettons en évidence qu'une gaussienne inhibitrice dans le cas des stimuli de saccades simulées avec phases statiques.

Le texte comprend également des annexes décrivant dans un premier temps les différents sets de paramètres utilisés tout au long de la thèse. Une seconde annexe décrivant plus en détail les équations de mean-field du modèle et sa connectivité. Enfin, le dernier montre un résultat préliminaire que nous avons commencé à étudier sur les paramètres de mise en forme de la réponse rétino-corticale.

Introduction (english)

Vision

Visual perception is a complex process, essential for many organisms, including humans. The ability to detect and make sense of light coming from the environment has always been intimately linked to our survival, and more generally to the need to move around and interact with the outside world. We owe this ability to the visual system, whose gateway is the eye. Light rays pass through the eye to activate photoreceptor cells at the back of the eye, in the retina. These light rays generate an electrical signal that is processed by successive layers of neurons in the retina, before being sent to the thalamus via the optic nerve and on to the primary visual area (V1). The role of this region of the brain is to differentiate specific properties of the image (orientation, spatial frequency, movement, etc.). The visual system then involves many other cortical areas responsible for increasingly complex and integrated processing. All this is made possible by the preliminary processing of visual information by the retina, which is much more than just a camera. It is in the retina that around thirty "information channels" are created, each representing a different and complementary view of the world, each associated with a different mode of vision. It is also in the retina that the processing of a number of properties begins, such as the representation of orientation, colour and the movement of perceived objects. The visual system is also capable of analysing rapid and complex movements, in extremely rich and complex visual scenes. In the retina, as in the cortex, it is the specific properties of the neural networks that enable these movements to be analysed. In this context, two mechanisms are of particular interest to us in this thesis: anticipation and saccadic omission.

Anticipation

A major flaw in motion vision is the slowness of the phototransduction process (conversion of light into variations of electrical potential) within the photoreceptors. This results in a delay of 100 ms between the photons captured by the photoreceptors and the arrival of the retinal electrical signal in the primary visual cortex [1]. Such a delay between reality and our perception would render vision ineffective. Faced with a danger such as a predator, or a car moving at 50km/h, our perception of them would lag behind the real movement by 1.4 m. In other words, the danger would have already travelled 1.4 m before our visual system detected the start of the actual movement. This example highlights the seriousness of a delay of this magnitude. Less dramatically, such a delay should prevent us from catching a moving object. With such a delay, how can animal species rely on vision to hunt or flee? The visual system has developed anticipatory mechanisms to compensate for this defect. These are only put in place for moving objects, but remain inactive for stationary objects. Anticipation allows the neural representation of future positions of the moving object to be brought forward in time, thereby compensating for the delay caused by phototransduction. Of course, this compensation depends on the speed of the object and becomes inoperative for objects that are too fast. Anticipatory mechanisms have been demonstrated in the retina and in the primary visual cortex. Two types of anticipation have been identified in the retina. The first, known as "adaptation", corresponds to an earlier fall in the peak activity of the retinal output cells in order to bring it forward [1]. This peak is what the cortical cells mainly respond to, and bringing it forward therefore enables them to respond earlier. The second type, known as "predicting", corresponds to an earlier shift in the entire retinal response [2]. In both cases, specific retinal cells, the amacrine cells, seem to be at the origin of the process. Within the primary visual cortex, another process of anticipation, known as 'latency anticipation', has been identified [3]. In this case, the movement of the object leads to the propagation of a wave of activity transmitted by the lateral connectivity of the cortical columns excited by the bar to other more distant cortical columns. The cortical columns are, in a way, the processing units in the visual cortex. They are made up of a few thousand neurons with a specific organisation. The wave of activity induced by a moving object enables the more distant cortical columns to respond earlier. Recently, S. Souihel and B. Cessac have hypothesised that retinal anticipation may have characteristics similar to latency cortical anticipation. A moving object could produce an early ganglion cell activation wave via the amacrine cell network.

Saccadic omission

Ocular saccades are very rapid eye movements, occurring about 3 times per second, with a maximum speed of 500 °/s, and an average speed of 200 °/s [4, 5]. This process is essential for rapidly exploring a visual scene and grasping the essential information. It is also at the root of our facial recognition and reading abilities. During a saccade, the representation of the visual scene moves at the same speed as the saccade. However, there is no motion blur. Instead, the visual scene remains stable, clear and precise. This is known as 'saccadic omission'. A current explanation of this phenomenon is based on a signal called 'corollary discharge' [6]. This copy of the ocular motor command causes a loss of visual sensitivity to movement called 'saccadic suppression' during the saccade. However, this explanation has its limits. When a stimulus is shown to a subject only during a saccade, not before or after, then the stimulus is perceived but with a trail. This means that the corollary discharge is not sufficient to explain saccadic omission. On the other hand, adding perisaccadic stimuli before and/or after the saccade makes it possible to eliminate the drag. The perisaccadic stimuli therefore act like masks that hide the movement of the stimulus [7]. It is in this context that the alternative explanation of a saccadic omission supported by these perisaccadic masks was born.

Recent psychophysical experiments [8] have succeeded in erasing the smear in a simulated saccade without any eye movement in the human subject. In these experiments, eye saccade movements were reproduced using a stimulus moving at the speed of the saccade and displayed with a device having a frame rate of 1440 Hz whereas, traditionally, stimuli in psychophysical experiments are displayed at a rate of 60 Hz. At 60 Hz, subjects observe an apparent illusory movement, with a smear around the trajectory of the stimulus. Using a refresh rate of 1440 Hz eliminates this effect. In the experiment, two types of stimuli were used: a simple moving white bar (_M_) or the same moving bar preceded and followed by static phases: front and static masks (SMS). Only the _M_ stimulus led to a smear, whereas the SMS was free of smear and allowed a slower, shorter movement to be perceived. Therefore, motion masking (SMS) is not sufficient to avoid the perception of the bar, but could make it easier to ignore. Additional processes, such as saccadic suppression, will be required to completely suppress the movement. One hypothesis proposed to explain this temporal motion masking is supported by experiments in the primary visual cortex of monkeys performed by Frédéric Chavane lab (Institut des Neurosciences de la Timone) showing suppressive waves propagating in the opposite direction of a motion and originating from activity waves [9]. These suppressive waves propagate to areas previously activated by the movement and thus suppress their residual activity. This suppressive effect from the last stimulus position to the previous one could explain the erasure of smear. On the basis of these experiments, we can therefore ask whether the temporal masking of movements can be explained by suppressive waves propagating in the cortex and retina.

Thesis context This thesis studies, from a modelling perspective, the mechanisms of anticipation and saccadic omission using an integrated retina-cortex model, called the 'Chimera model', presented below.

The work on anticipation is part of a previous collaboration, the ANR Trajectory (https://team.inria.fr/biovision/anr-trajectory/) between Frédéric Chavane, Alain Destexhe, Olivier Marre, Bruno Cessac and Selma Souihel (former doctoral student) aimed at gaining a better understanding of how anticipation mechanisms in the retina and cortex work together. The Chimera model was first developed as part of Selma Souihel's thesis, supervised by Bruno Cessac. However, it was not finalised, and Selma Souihel's thesis focused mainly on modelling anticipation in the retina. Our first objective was to finalise the Chimera model. Firstly, from the point of view of the model itself, by studying its dynamic behaviour and looking for ranges of parameters giving rise to stable and biologically plausible behaviour. Secondly, from the point of view of simulation. A large part of our work during the thesis consisted of porting the model to the Macular simulation platform (https://team.inria.fr/biovision/Macular-software/), described below, in order to obtain fast and realistic simulations (including a reasonable cortex size) in two dimensions. This enabled us to obtain new results on the respective roles of anticipation mechanisms in the retina and cortex. In addition to anticipation, the Chimera model and the Macular platform can be used to simulate the retina-cortex complex, using realistic visual inputs (films) and varying physiological parameters that are sometimes impossible to control experimentally.

The work on saccadic omission is part of the ANR Shooting star collaboration (https://team.inria.fr/biovision/anr-shootingstar/) between Mark Wexler, Frédéric Chavane, Olivier Marre, Alain Destexhe and Bruno Cessac aimed at testing the hypothesis of saccadic omission by suppressive waves. Our aim was to generate cortical activity waves using the Chimera model and to simulate saccades. The aim was to reproduce the experimental results of M. Wexler and F. Chavane, and to study the existence and nature of suppressive waves. Using the Macular platform, we were able to highlight a drag effect that was more noticeable with a refresh rate of 1440 Hz than at 60 Hz, using a simple mathematical model to understand this effect. We also observed a loss of stimulus identity at 1440 Hz. We also demonstrate the suppression of static phases in movement and a difference in cortical response between the M and SMS stimuli. Finally, we show how static phases of different sizes can influence the response to the moving phase.

Chimera model

The 'Chimera model' aims to model and simulate the retina-cortex complex, 'neglecting' the thalamus i.e. considering it as a simple relay. We did this for the sake of simplicity of the model, even though the thalamus is more than just

a simple relay [10, 11]. The aim was also to have an associated simulation platform, enabling realistic retinal inputs (films) to be played. The term 'Chimera model' comes from the fact that the retinal model was calibrated using mouse data whereas the cortical model was calibrated using monkey data [12, 13, 9]. We discuss this aspect in more detail in the thesis. Modelling has the advantage of being able to compensate for experimental shortcomings, which make it impossible to measure the retina and cortex at the same time and to modify 'by hand' physiological parameters that are impossible to control experimentally. Modelling also makes it possible to identify the factors that are sufficient to generate saccadic anticipation and omission.

This retino-cortical model produces activity corresponding to the intensity of pixels in voltage-sensitive dye imaging (VSDI) in response to retinal stimulation. The retinal model is based on previous work on the mouse retina [1, 14, 15, 16]. It simulates a graph made up of bipolar, amacrine and ganglion cells. The bipolar cell receptive field is a function that reproduces the response of photoreceptors and horizontal cells. Bipolar cells have a gain control system known for reproducing adapting anticipation. Amacrine cells are used to set up lateral connectivity, which could be at the origin of predicting anticipation as well as wave propagation within the retina. The cortical model was created on the basis of experiments with macaques [12, 13, 9]. It uses connected networks of mean-field models, each representing a cortical column. For each cortical column, there is one mean field model corresponding to its excitatory population and one to its inhibitory population. In addition, there is lateral connectivity between the columns where the signals propagate at a speed of 300 mm/s. The output is the intensity of the voltage-dependent imaging pixel (VSDI) containing the cortical column. This model was used to reproduce voltage-dependent imaging results.

Macular

Macular is a software package developed, under the direction of Bruno Cessac, by engineers from Inria's Research and Development Department (SED), as well as by doctoral students including myself. This is a modular platform for simulating the retina and primary visual cortex. It can be used to reproduce spontaneous responses or responses to visual stimuli under conditions of normal vision, altered vision (pharmacology, pathology, etc.) or prosthetic vision. Macular is structured in layers to reproduce the architecture of the retina. Each layer is composed of a type of object, which may be a cell or a population of a cortical column. The whole is then interconnected by synapses that may or may not incorporate a dynamic delay. In our case, the 'Chimera model' receives a spatio-temporal input in the form of a video. A full description is given in chapter 2.

Thesis outline

The first chapter is intended to provide a general introduction to the knowledge required to understand this thesis and the state of the literature on the various subjects we will be addressing.

In the second chapter, we introduce the Chimera model and discuss its elements and dynamics. In particular, we show that, under certain parameters regimes, the model exhibits pathological instabilities (oscillations) that had to be controlled. We then present the Macular software and the implementation of the Chimera Model. In particular, we explain how we adapted it to carry out two-dimensional simulations, and the various modifications made to bring it closer to reality. We also detail the calibration of the model that we carried out in order to reproduce the initial experimental results on cortical waves induced by moving objects.

The third chapter is devoted to the anticipation mechanism. After introducing experimentally accessible quantitative measures of anticipation, we study the effect of a number of parameters associated with the stimulus - such as contrast and speed -, physiological parameters - such as the range of cortical connections - and phenomenological parameters - such as those controlling retinal anticipation, gain control and/or lateral amacrine connectivity. An important result of this work is to show how the experimentally measurable VSDI response is visibly modified by retinal anticipation mechanisms, highlighting the respective roles of anticipation by advancing peak activity (retina) and anticipation by latency (cortex). We also show how the amacrine network influences the retinal and cortical response to a moving object. In particular, we have succeeded in implementing an improved model with the ability to reproduce predicting anticipation.

The fourth chapter is devoted to saccadic omission. We first reproduce suppressive waves similar to Frédéric Chavane's experiments. We then use Mark Wexler stimuli (simple motion or motion surrounding static phases) displayed at a refresh rate of 60 Hz or 1440 Hz to understand the impact that static phase and refresh rate can have on cortical activity, how static phase potentially triggers suppressive waves and what the important parameters are. The aim is also to gain a better understanding of the respective roles of the retina and V1 cortex in this mechanism.

In the conclusion, we show a functional retino-cortical model capable of reproducing both anticipatory [3] and suppressive wave [9] experiences in the primary visual cortex. This retino-cortical model enabled us to highlight the importance of the retinal output supplied to the cortex, the speed of the bar and the balance of excitatory and inhibitory connections. It also enabled us to show the transfer of retinal anticipation to the cortex despite a reduction in cortical anticipation. We were able to see the capacity of the two types of retinal anticipation to combine favourably for cortical

anticipation. In the context of saccadic omission, we found a loss of continuity caused by a low refresh rate on a stimulus moving at the speed of a saccade. We also show a greater smear in the case of a stimulus with static phases. We observe shape-dragging only for static phases that are larger than the moving phase. Finally, we reproduce the suppressive wave in apparent motion but show that an inhibitory Gaussian is present in the case of simulated saccade stimuli with static phases.

The text also includes appendices describing the different sets of parameters used throughout the thesis. A second appendix describes in more detail the model's mean-field equations and its connectivity. Finally, the last one shows a preliminary result that we have started to study on the shaping parameters of the retino-cortical response.

Chapter 1

State of the art

1.1 Visual system

1.1.1 The retina

Introduction to retina

The retina is the organ where visual signals are received and where the first processing of visual information takes place. It is a thin neurosensory membrane composed of several layers (Fig. 1.1B, C) and located at the back of the eye [17]. This position allows it to receive the light from outside, concentrated in the crystalline lens. Light passes through the entire depth of the retina up to the outer nuclear layer (ONL), made up of photoreceptors (Fig. 1.1A).

The cells of the retina have two special properties. The majority of retinal cells do not have well-defined axons and only make local connections with their neighbours via dendrites or small axonal processes. In addition, they don't spike either, and respond with continuous and gradual changes in their potential.

Photoreceptors

These light-sensitive retinal cells are able to carry out the phototransduction process which transforms the light signal into an electrical signal [18]. Darkness causes them to hyperpolarise the photoreceptors and increase the release of glutamate. Then, they transfer this signal to synapses with bipolar and horizontal cells in the outer plexiform layer (OPL) [17]. There are two main types of photoreceptor [18]. The first are the rods, which are more sensitive to light but do not discriminate colour, only grey levels. They are saturated during the day and are therefore only used for scotopic vision. The second are the cones which require greater light intensity and can therefore produce photopic vision. They are crucial for seeing details, contrasts and colours [19]. The cones are a family including three subtypes, each of which detects a different colour: red, green or blue.

Bipolar cells

Bipolar cells are located in the inner nuclear layer (INL) and contact ganglion and amacrine cells in the inner plexiform layer (IPL) [17]. There are around ten bipolar subtypes in the mouse retina [20]. Little is known about their response because their intermediate position makes them difficult to record. Bipolar cells constitute the first level of integration within the retina. They bring together the activity of a localized region of photoreceptors, building up the central 'receptive field'. In addition to this central receptive field, there is also a peripheral receptive field which produces an effect opposite to that of the central zone (inhibition or excitation) [21]. It remains unclear whether this is due to a direct connection with the horizontal cells (feedforward) or an indirect action via the photoreceptors (feedback) [22]. There are two main types of bipolar cells, which are depolarised or hyperpolarised by glutamate and depend on the receptor expressed on their synapses. In the presence of light, the so-called 'ON' cells have an active central receptor field that is depolarised and a hyperpolarised periphery that is inhibited (Fig. 1.2A, B). In the case of 'OFF' bipolar cells, the opposite occurs, with the periphery activated by light and the center inactivated (Fig. 1.2C, D). Bipolar cells are sensitive to the difference in activity between their photoreceptors and those in their vicinity. The aim of this mechanism is to improve contrast vision and visual acuity. [23, 21]

Horizontal cells

Horizontal cells are inhibitory GABAergic neurons responsible for feedback on photoreceptors and feedforward modulation of bipolar cells [21]. The horizontal cells are hyperpolarised by light, making them active. Their main role is to shape the center-surround receptive fields of the bipolar cells. There are only 2 subtypes of horizontal cells in mammals [24].

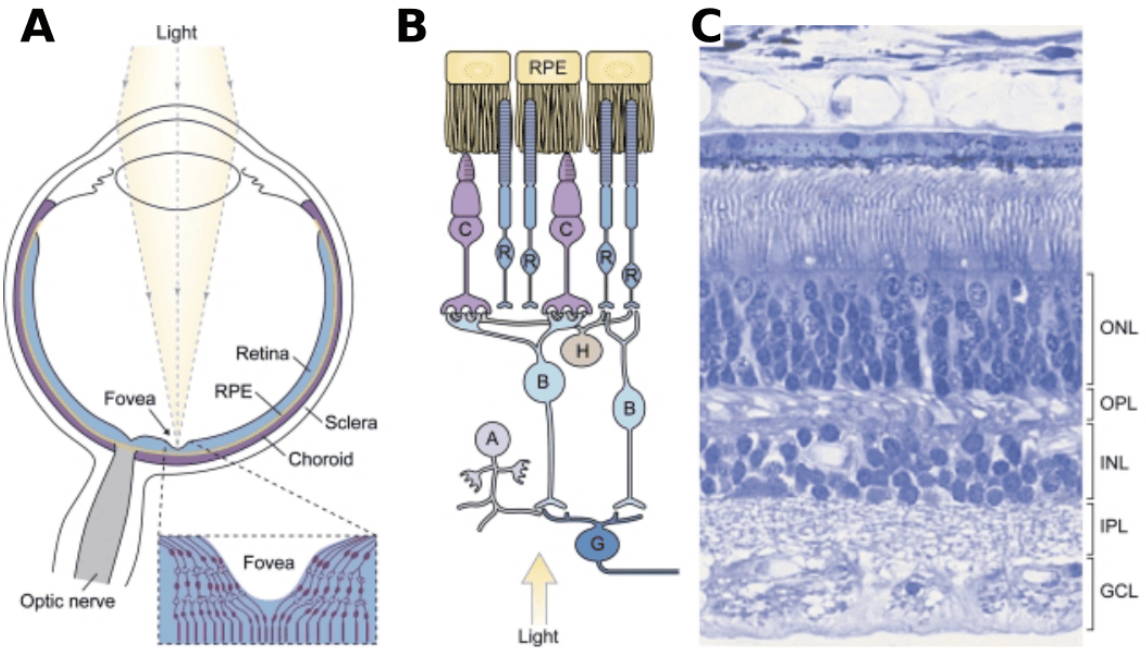

Figure 1.1: **Illustration of the organisation of the retina. A)** Diagram of an eye: light enters through the iris, passes through the crystalline lens and ends up on the retina. At the center of the retina is the fovea, in which is located the small depression where the photoreceptors are naked, the fovea. The optic nerve is where the ganglion axons are grouped together. **B)** Diagram of the organisation of the different cells in the depth of the retina. Each cell is associated with a letter: ganglion cells (G), amacrine cells (A), bipolar cells (B), horizontal cells (H), cone cells (C) and rod cells (R). **C** Microscopic image of the retina. The outer nuclear layer (ONL) with photoreceptor nuclei, the outer plexiform layer (OPL) with photoreceptor/bipolar cell synapses, the inner nuclear layer (INL) with bipolar and amacrine cell nuclei, the inner plexiform layer with synapses between bipolar, amacrine and ganglion cells and the ganglion cell layer (GCL) with their nuclei. Adapted from [17].

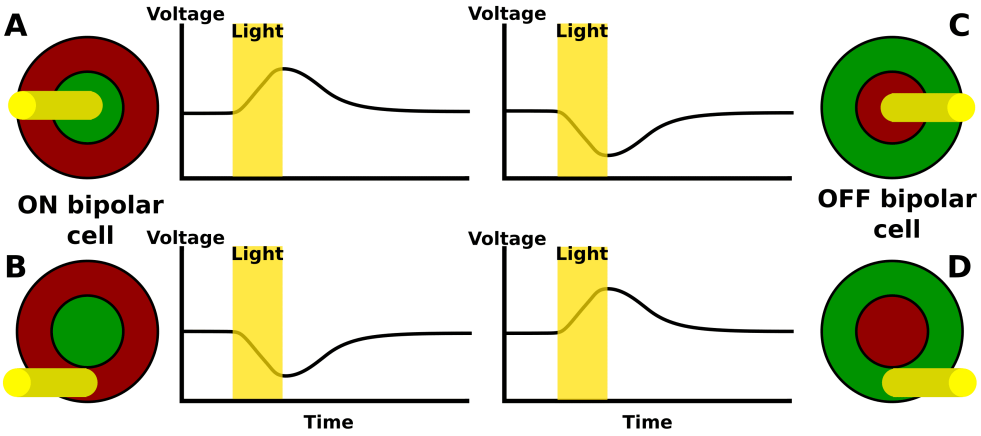

Figure 1.2: **Fonctionnement des cellules bipolaires ON et OFF. A-D)** Diagram of the bipolar cell receptive field, separated into a central and peripheral region (left). The green region corresponds to that activated by light and the red to that inhibited by it. A beam of light is sent to one of the two regions (yellow cylinder). The voltage in response to this beam of light is shown over time (right). The yellow rectangle shows the interval when the light beam is present. We show this for 4 conditions. Firstly, we have an ON bipolar cell illuminated at its center **(A)** or periphery **(B)**. Then we have a bipolar cell illuminated in its center **(C)** or its periphery **(D)**.

Amacrine cells

Amacrine cells are activated by bipolar cells. They generate feedback inhibition on bipolar cells to refine the center/surround receptive field and regulate the gain of the feedforward signal. They also feedforward inhibit ganglion cells to complexify the spatio-temporal components of the receptive field. In some cases, they can also inhibit lateral connectivity with other amacrine cells [21]. Almost all are axonless and their signals are carried by dendrites [25]. A distinction is made between wide-field amacrine cells responsible for transient activity via long-distance connections and localised to a single layer of the retina, and narrow-field amacrine cells for connectivity between layers over a long period of time [26]. The amacrine cells are the retinal cell family with the most different representatives (45 subtypes in mice) [20]. They participate in the creation of the different parallel channels encoded in ganglion cells. Some amacrines are dedicated to specific visual processes, while others are more versatile.

We can take as an example the amacrine starburst cells which release GABA onto ganglion cells or other starburst cells depending on the direction of movement [27]. This property is due to two factors. Firstly, the ability of starburst dendrites to respond more to movements from the soma towards the dendrites. Secondly, an asymmetry in the expression of cholinergic (excitation) and GABAergic (inhibition) receptors.

Ganglion cells

Ganglion cells are the least represented cells in the retina. There are 1 million ganglion cells for over 100 million photoreceptors [21] in humans. They correspond to the second and last level of integration of the retina. They can be ON, OFF [28] or both [29]. The axons of ganglion cells are grouped together in the optic nerve, a the bench of RGCs axons connecting the retina to the thalamus LGN. Because of this long distance i.e. larger than a centimeter, distance beyond which action potentials are necessary to transmit neuronal voltages, ganglion cells are the only spiking cells in the retina. Each ganglion cell encodes a local property of the visual field (direction of movement, orientation of an object, expansion of an object, local movement, contrast, colour, etc) [30, 31]. There are at least a dozen of subtypes of ganglion cells in the mouse, with very different morphologies, as well as their receptive fields. All the cells of a given subtype pave the retina in a regular fashion, with no overlap between their receptive fields. This mosaic of ganglion cells makes it possible to create around thirty different versions of the visual world [32, 33]. Each subtype has a uniform morphology, the same physiological properties and a similar gene expression [31].

Retina organisation

At the center of the retina is the fovea, an area of maximum cell density composed exclusively of cones [34, 35]. These cones are unique in that they are connected to just one bipolar cell, which also contacts just one ganglion cell. This gives this area very high visual acuity. In contrast, in the peripheral part of the retina, each ganglion cell brings together the activities of many bipolar cells, which in turn bring together the activities of a whole region of photoreceptors. Moreover, the further away you are from the fovea, the more the cone density is reduced, leaving only rods.

Within the retina there are two major neuronal pathways: parvocellular and magnocellular [36, 37]. The first is the parvocellular (P) pathway, which is made up of "midget" cells representing the majority of cells in the fovea. They are responsible for managing shapes and colours. They have a small dendritic tree which gives them high spatial resolution but they have a low temporal resolution. They receive inputs from a single cone type (red or green). The center and surround may be associated with a different cone. They are mainly responsible for the red/green colour axis. The blue/yellow axis is carried by another very small pathway. The magnocellular pathway, on the other hand, is responsible for motion detection [38]. This is made possible by these "parasol" cells, which have very high temporal resolution and very wide receptive fields. They receive inputs from all types of cones without colour specificity and are therefore insensitive to the chromaticity of the stimulus. As a result, they will perceive two stimuli of different colours but the same luminance as identical.

1.1.2 Lateral geniculate nucleus of the thalamus

The thalamus is a nuclear complex located in the diencephalon and composed of the hypothalamus, epythalamus, ventral thalamus and dorsal thalamus. It acts primarily as a relay center, redirecting all sensory inputs and motor outputs [39]. The thalamus is lateralised, with each of its halves responsible for the contralateral part of the visual field. The lateral geniculate nucleus (LGN) is located in the ventral part of the thalamus. It is in this region that the majority of fibres from the retina synapse are located. The LGN is made up of 6 layers. Layers 2, 3 and 5 receive axons from the temporal retina of the ipsilateral eye. Axons from the nasal retina of the contralateral eye synapse go into the other layers [40]. Only 7% of thalamic inputs come from the retina, the remainder coming equally from inhibitory connections from the reticular nucleus of the thalamus (TRN), the primary visual cortex and the parabrachial nucleus (PBN) (see Fig. 1.3) [41].

The cells of the LGN are mainly thalamo-cortical cells divided between a very large magnocellular class in layers 1 and 2 and a very small parvocellular class in layers 3 to 6 (Sec. 1.1.1 for more information on parvo and magnocellular pathways) [40]. Thalamo-cortical cells make almost no connections in the LGN. The LGN also contains inhibitory

interneurons which inhibit the thalamo-cortical cells. When a signal is sent to the cortex, a copy is also sent to the reticular cells of the TRN, which will retrocontrol the thalamo-cortical cells by inhibiting them. The axons of the thalamo-cortical cells reach the primary visual cortex and establish connections in layer 4 [42]. In response, layers 5 and 6 of the cortex send feedback to the thalamo-cortical and reticular neurons. The cortex thus has considerable control over the thalamus.

The LGN has long been considered to be a simple relay because it does not generate complex receptive fields. In fact, it reproduces the receptive fields of ganglion cells in the thalamus (ON/OFF) in thalamo-cortical neurons [43] and interneurons [44]. The LGN also has retinotopy like the retina [45] (see section 1.1.3 for the definition of retinotopy). However, the thalamus is not just a relay, as it controls the flow of information to the cortex. To do this, it uses networks and cells with complex properties.

Thalamo-cortical cells have the capacity to adopt a burst or tonic discharge behaviour depending on the resting potential imposed by their synaptic inputs [46]. The tonic mode seems to be the one that dominates during wakefulness. For the same input, the response of a thalamo-cortical cell changes according to the mode it is in. The tonic mode is associated with a linear response that preserves the properties of the input [41]. The burst mode, on the other hand, has the particularity of generating a non-linear response as a function of the intensity of the input. It also has a much stronger signal-to-noise ratio. For this reason, burst is seen as a transient increase in detectability that could signal the presence of an unexpected visual cue to the cortex.

Regarding the organisation of the network in which the LGN is found, the retinal neurons are activating the thalamo-cortical neurons and the interneurons [41]. The parabrachial neurons generate direct or indirect excitation (disinhibition) of the thalamo-cortical neurons. In the case of cortical fibres, they excite both thalamo-cortical neurons and inhibitory neurons. The exact effect depends on the exact configuration of these connections, which remains unknown.

Cortical or parabrachial pathways also have the capacity to initiate the transition from burst to tonic mode by activating metabotropic receptors. The same can be observed for the reverse transition with inhibition of TRN or interneurons.

For all these reasons, the hypothesis of an organisation of LGN afferent fibres with a driver (retinal input) responsible for transmitting the signal from the retina and modulators (parabrachial, cortical and reticular axons) has emerged.

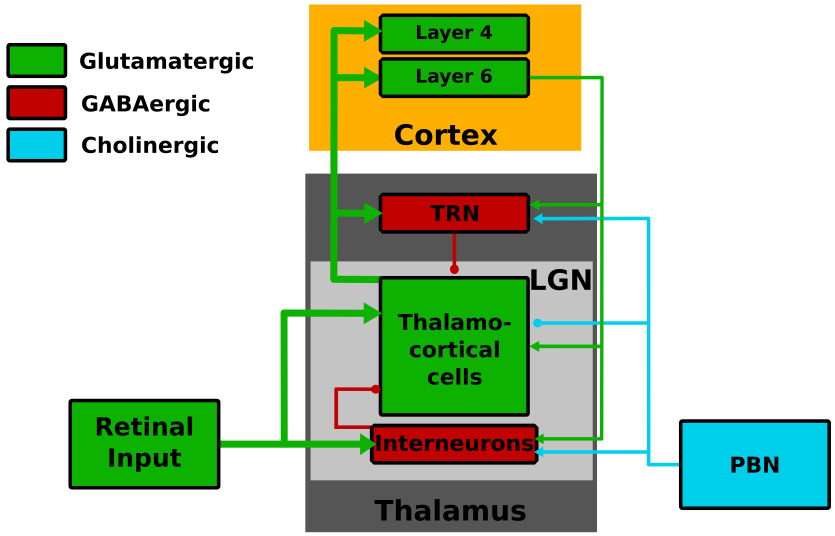

Figure 1.3: **Diagram of the LGN network.** On the right are the inputs from the lateral geniculate nucleus (LGN) originating from the retina. The LGN (light grey) is divided between thalamo-cortical cells and inhibitory interneurons. The LGN is part of the thalamus (dark grey), which includes the thalamic reticular nucleus (TRN). Layers 4 and 6 of the cortex (orange) participate in this network. There is also the parabrachial nucleus (PBN) (blue). The retina sends excitatory fibres to the two subpopulations of the LGN. The thalamo-cortical cells send excitatory fibres to the TRN and the cortex. The cortex in turn excites the TRN as well as the cortico-thalamic cells and interneurons. The interneurons inhibit and the TRN inhibits the thalamo-cortical cells. The PBN sends excitations to the interneurons and TRNs while inhibiting the thalamo-cortical cells. The neurotransmitter type of the neurons is indicated by the colour of the rectangles and arrows: glutamatergic (green), GABAergic (red) and cholinergic (blue).

1.1.3 The visual cortex

General organisation

The visual cortex is the set of brain regions specialised in the processing of visual information (Fig. 1.4). It entirely covers the occipital lobe at the back of the skull, where most of the visual cortex is concentrated. It also includes other regions in the temporal and parietal lobes. The thalamic-cortical neurons of the LGN project to the primary visual area (V1) located in the occipital lobe [40]. This very first area carries out initial processing before sending the signal to the secondary visual area (V2). At this stage, there is a branch which leads to two pathways with distinct roles [47, 48]. The first is the dorsal pathway, which deals with the processing of movement and the coding of localisation ("how" pathway). It passes through the dorsomedial area, the medial temporal area and the parietal cortex. The second is the ventral pathway, responsible for shape and object recognition and long-term memory ("what" pathway). It passes through visual area V4 and then the temporal lobe. Beyond this are the associative areas of the parietal and frontal lobes [49]. They receive sensory information from several sensory systems, process it together and interpret it. It is possible to describe three levels of organisation within the visual system.

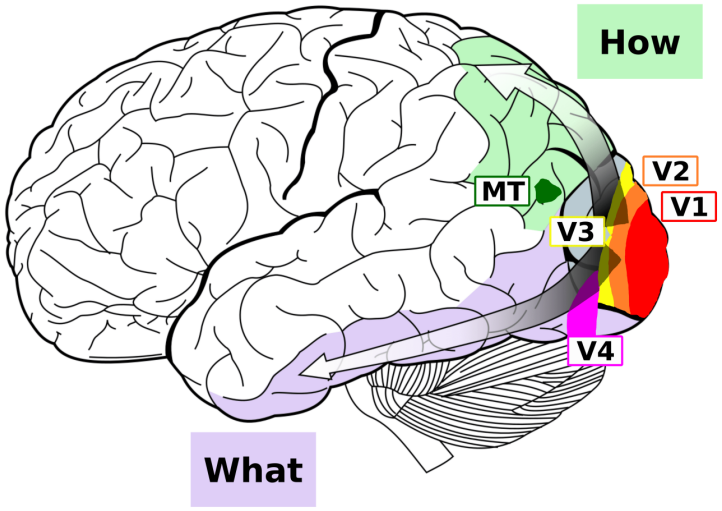

Figure 1.4: **Illustration of the visual cortex.** The signal arrives first in V1 (red) before travelling through V2 (orange), V3 (yellow) and then splitting off. The ventral pathway responsible for 'what' (purple) starts from V4 (pink) and extends deep into the temporal cortex. The dorsal pathway responsible for 'where' (light green) starts from middle temporal area (dark green) and goes into the parietal lobe. Adapted from wikipedia.

The deep cortical hierarchy represents the final level of organisation of the visual cortex. This hierarchy has been established on the basis of all the connections in the visual cortex and their direction [50]. The flow of information circulates within this network. Some connections are made in the direction of this hierarchy (feedforward), others go backwards (feedback) or establish connections of the same hierarchical level (lateral connectivity). The further one progresses in the hierarchy of visual processing areas, the more complex and specialised the receptive fields of the cells become [51]. Thus, in the temporal area, neurons are activated by the presence of specific two-dimensional shapes in their spatial receptive field [52]. A distinction is made between areas of early vision, which isolate all the most basic aspects of an image (movement, colour, orientation, etc.), and areas of high-level vision, which possess conceptual or thematic modalities. They are the place where connections and features converge [53]. At this stage, the definition of receptive field is no longer sufficient because it is no longer reduced solely to the spatial dimension. The receptive field extends to all the dimensions of the stimulus features. We should speak of a preferential or selective response [54].

The cortical column is the smallest level of organisation. It is a functional unit of the cortex, initially defined by several characteristics [55]. They are made up of neurons specific to the same modality, so they all respond in the same way to a given stimulus. All the neurons in a column may, for example, respond to the same angle of orientation of the object [56] or to a single tactile modality [57]. Cortical columns show very strong connectivity within the column and little with its neighbourhood. In addition, their size is highly conserved in mammals, with only the number of columns varying between species [58]. This definition has evolved with the discovery of many different types of cortical columns in visual areas. They now correspond above all to a vertical grouping of cells that share the same selectivity to a feature. Cortical columns are mainly present in the visual cortex and only a few areas have shown the presence of functional cortical columns (V3, mediotemporal area) [59].

The cortical map is the intermediate level of organisation of the visual cortex that is also found in other sensory or motor cortices [60]. These cortical maps are an organisation of the feature space to which the selective neurons belong, within the cortical area. Neurons with very similar selectivity to stimulus features are grouped together in sub-regions of the cortical area. There is thus a continuum of neuron selectivity within the cortex.
Two examples of this concept can be described in figure 1.5. Our first example is the retinotopic maps present in the LGN or V1 [61] (Fig. 1.5A-C). Neurons excited by close visual field positions are also anatomically adjacent. This space-dependent cortical map of the visual field is more specifically called a topographical map. Retinotopic maps are present in all areas of the occipital lobe (V1, V2, V3, V4, ML). The retinotopic maps of the LGN and V1 are described as first order because they are simple and continuous. From V2 onwards, the retinotopic maps become more complex and the retinotopy becomes partial because certain regions, whose receptive field has a similar spatial position, are no longer adjacent [62]. The second example is the orientation map in V1 (Fig. 1.5D). Neurons selective to a specific orientation are surrounded by neurons selective to a very close orientation angle [63]. There are about fifteen cortical maps in humans [64].

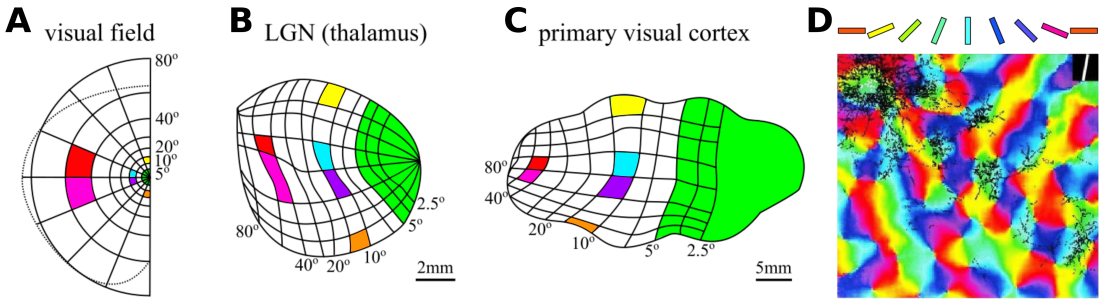

Figure 1.5: **Example of cortical maps. A)** Visual field representation. **B, C)** Cortical map of visual field representation in **(B)** LGN and **(C)** V1. The distance of the visual field **(A)** as well as the cortical maps **(B,C)** are expressed in degrees of visual angle. The fovea is shown in green while 6 areas have been colourised to highlight them in the visual field and each cortical map. **D)** Cortical map of orientation selectivity in V1. Each colour is associated with a particular bar orientation (top). A, B, C are adapted from [61] and D from [63].

V1 Area

The primary visual area (V1) is the entry point to the visual cortex. V1 neurons are organised with retinotopy close to the retina. The V1 areas of each hemisphere receive information from the contralateral visual field, except for the fovea which projects entirely onto the two hemispheres [65]. Within the V1 cortex, the projection of the fovea is over-represented in relation to its size in the retina [66]. There are a few cells with the same center/surround receptive field [67] but the majority have more elaborate receptive fields.

Area V1 is composed of cortical columns organised according to two features [56]. First, there are cortical columns that are specific to precise stimulus orientations. These columns are then grouped into parallel bands where each column is specific to one eye (ocular dominance column). Simple, complex and hypercomplex cells are the three types of cell that make up the cortical orientation columns (see below).

A number of features are supported by V1 [68] :

- Linear and oriented patterns (bars, gratings or edges) as well as spatial frequency (gratings). To achieve this, two types of cells are used : simple cells and complex cells [69, 70]. Simple cells have receptive fields that can vary with dissociated ON and OFF parts. This makes them sensitive to the position of the bar or the phase of the grating. Complex cells have extremely varied receptive fields, which are difficult to analyse and generally have overlapping or mixed ON and OFF parts. They respond whatever the phase or position of the stimulus.
- Detection of the ends of bars or gratings. This feature requires hypercomplex cells [71]. Their response is maximum for small bars or edges. If the size of the bar increases, the response will decrease as the bar starts to excite OFF portions of the receptive fields.
- Absolute depth of an object by calculating the difference in angle between the object and the two eyes [72]. This processing requires neurons receptive inputs from both eyes.
- Slow temporal frequency of linear and oriented patterns. Certain simple and complex cells are sensitive to the direction of a movement as well as its speed if it is not too fast [73]. These cells remain mainly present in eccentric positions.

- Colour of a bar supported by double-opponent cells. They have a central and peripheral receptive field that responds to two different colours. A distinction is made between cells sensitive to red and green and those sensitive to blue and yellow [74]. Their receptive field is slightly selective to orientation.

The theory still accepted today explains the mode of formation of the cortical maps of V1 on the basis of the particular distribution of the feedforward fibres of the LGN on layer 4 of V1 [43]. For the moment, only the V1 retinotopy and the occular dominance columns have found an anatomical substrate to explain them. The other cortical maps remain unexplained. This theory is being increasingly challenged today with the accumulation of anatomical evidence on the importance of the existence of a microcircuit that could be involved in the creation of cortical maps. Some of this evidence points to the importance of local modulatory feedback within the cortical column, between different layers [75]. A number of anatomical results also point to the important responsibility of lateral excitatory and inhibitory connectivity within the same cortical layer [76]. Studies have emphasised the importance of inhibition within V1. Inhibitory cells have a slightly wider and weaker orientation selectivity, which allows them to accentuate the orientation selectivity of excitatory cells in V1. They are also recruited by both the LGN and areas higher in the hierarchy in order to modulate V1. Finally, inhibition modulates brain states to amplify communication between neurons and reduce noise [77].

V2 Area

Area V2 has a second-order retinotopy [62]. This means that retinotopy is present but with some discontinuity In the case of V2, this discontinuity is located at the level of its horizontal axis. The visual field is cut off and separated along the entire length of the horizontal axis. It receives its inputs from area V1 and sends feedback to V1 which reinforces the suppression caused by the peripheral parts of V1's receptive fields [67].

In addition to processes shared with V1 (orientation, colour, absolute depth), V2 analyses a number of specific features [68, 73] :

- Contours defined by superimposing different textures.
- Determining whether each edge belongs to a given surface. Perception tends to attribute edges to one surface, which is an object, while the second surface is background. These cells are also selective according to the direction in which the surface with the edges is located. [78].
- Relative depth between two image planes.

The increasing complexity of the features processed by the visual areas from V2 onwards makes it difficult to study their receptive fields. Despite this, one study found four types of receptive fields [79]. A first part of the receptive fields were V1-like. A second part had very elongated complex receptive fields. Some of the receptive fields had complex shapes with multiple preferential orientations. These receptive fields are made up of separate excitatory and inhibitory portions that take on elaborate shapes. Finally, a small proportion of the receptor fields had a center-surround structure, as in LGN.

"What" ventral pathway

The ventral pathway groups together a set of regions specialising in the identification of objects [68, 73]. In hierarchical order it is made of :

- V4 area with selectivity for orientation, colour, depth, simple shapes, contours caused by a motion differential, curves and colour hue.
- The posterior inferior temporal area (PIT) is selective to the combination of several features (simple shape, colour, size, orientation) present on the fovea. It is retinotopic.
- Anterior inferior temporal area (AIT) is selective for moderately complex 2D shapes [52], colour, depth, texture and 3D shapes. AIT codes for sub-parts of objects.

"How" ventral pathway

The dorsal pathway is made up of regions specialised in spatial vision [68, 73] which eventually project into the premotor areas of the frontal lobe. In hierarchical order it is constituated from :

- The middle temporal area (MT) processes the speed and direction of movement, depth, movement gradients and any element generated by movement. It has cortical columns for this purpose. Its neurons have a very wide receptive field and mainly receive input from the magnocellular pathway, which encodes movement more effectively [38].

- Medial superior temporal (MST) is selective to movement, expansion, rotation, orientation and speed of movement, as well as to movements generated by head or eye movement. They have even wider receptive fields than MT.
- Caudal intraparietal area (CIP) is selective to inclined or curved flat surfaces, 3D orientation of elongated stimuli and position in depth.
- Lateral intraparietal area (LIP) contains a salience map which is used to determine where in the visual field to direct attention and perform occular saccades.

1.2 Saccades

1.2.1 Saccadic vision

In our daily lives, we we are all the time scanning our environment, whether consciously or unconsciously. Carrying out any task requires us to move our gaze many times from one point to another. This is because we need to use our central vision, which is the most accurate. This involves moving our eye to place each point of interest on our fovea. These eye movements are called "saccades" and we make them on average 3 times a second [5]. Let's take the example of an 'ordinary' task. I want you to take the time to read this sentence and focus on each moment when you stop on a word like this one, but also on each time you move from one word to another. While you were reading the previous sentence, you made 37 saccades to move your gaze over each word, one by one. During the movement of a saccade, our eyes move at an average speed of 200 degrees/s and can reach peak speeds of up to 500 degrees/s [4]. Each saccade is separated by moments of pause when we keep our eyes still to take in information from the environment. These fixations can last 300 ms or more depending on whether our attention is directed on something or not [5]. Did you notice the movements between each fixations? Did your visual field move at high speed from one letter to the next? Or did it remain stable throughout to allow you to complete your task without any problems?

At the speed at which the saccades are moving, you should be able to see the movement with a motion blur in most cases. However, when you make a saccade, your perception of the entire visual field shifts without leaving any trace of the movement that may have occurred in between. Our visual system is aware that these movements are merely parasitic movements arising from our own movements and that they must be ignored so as not to contaminate the perception of the visual environment. Without it, you would perceive a scene moving at high speed 3 times per second. This break in attention that occurs during the movement of a saccade is called "saccadic omission" [7]. It is accompanied by a second phenomenon called saccadic suppression.

The term saccadic suppression refers to a biological phenomenon that causes a reduction in visual system activity during a saccade. Note that this suppression must nevertheless be accompanied by a saccadic omission to avoid seeing a completely black frame between the two saccade fixations. This suppression is due to a decrease in the perception of saccade movements [80]. This saccadic suppression has been demonstrated in the magnocellular pathway [81]. Burr et al. presented an isoluminance or luminance grating in motion during a saccade or fixation. The luminance stimulus presents a grating and a background of different luminance (black/yellow) whereas in equiluminance the grating and background are of different colours but identical luminance. The perception of the luminance stimulus during a saccade is different to that during fixation, so the phenomenon of saccadic suppression is present. At the same time, during fixations, movement is perceived better in luminance than in isoluminance. This means that motion is perceived by cells that do not detect colours. This is the particularity of the magnocellular pathway. In humans, suppression is found in the LGN, V1 but also V2, V3 and MT [82]. Deletion remains more pronounced in LGN and V1. The site of suppression could therefore be on the LGN or in V1 but accompanied by indirect feedback on the LGN. In the LGN, magnocellular and parvocellular cells show a sharp drop in discharge frequency starting 50 ms before the saccade and continuing throughout its duration [83]. This is followed by a considerable amplification of the discharge frequency after the saccade. In the retina, the projection of a video reproducing a saccade leads to inhibition after the start of the saccade, generated by amacrine cells [84]. The retina may play a role in saccadic suppression, but it cannot be the sole cause. Phosphenes (light sensations without stimuli) caused by electrical stimulation in the visual cortex are suppressed. So, this is evidence of suppression without activation of the retina [85]. Finally, the exact site of this suppression remains very uncertain. The mechanism thought to be at the origin of the omission is motion masking and the one at the origine of suppression is corollary discharge.

1.2.2 Corollary discharge

The corollary discharge corresponds to a copy of the occulomotor command which is sent to the eye muscles to generate a saccade [6]. This command therefore contains all the information necessary for the saccade. This explanation makes it possible to justify why we observe a suppression which is initiated even before the movement has begun.

The corollary discharge is thought to be created in the intermediate superior colliculus. Neurons in this region send the motor command that triggers the saccade. These neurons form a map of the amplitudes and directions of the saccades.

The corollary discharge passes via the dorsomedial thalamic nucleus (MD) and then the frontal eye field (FEF). All these neurons are activated before a saccade [86]. Inhibition of MD causes a shift in the perception of the visual field just after a saccade. This effect is explained by the role of the corrolary discharge in creating the continuity perceived between two saccades despite the disappearance of the latter [87, 88]. The corrolary discharge creates a remapping of the neurons' receptive fields in many regions of the visual cortex (V2, V3, V4, FEF, SC) [6]. This corresponds to reassigning to each receptive field the response that corresponds to the new position in the visual field that they will occupy after the saccade [89, 90]. This makes it possible to switch between the visual field before and after the saccade. There is a second negative version of corrolary discharge which originates from a connection of a neuron in the superficial superior colliculus with an inhibitory interneuron [91]. This suppression travels through the inferior pulvinar (IP) and middle temporal cortex (MT). It also begins before the saccade and inhibition of the neuron in the superior colliculus relieves the suppression in MT. Saccadic suppression could therefore be caused by corrolary discharge.

1.2.3 Temporal motion masking

Campbell and Wurtz devised an experiment which revealed the importance of fixations before and after on the perception of a saccade (saccadic omission) [7]. They performed saccades preceded and/or followed by fixation in the dark or in bright light. A motion blur was perceived in the case of fixations in the dark, but the increase in fixation time in the light condition masked it. This was the first instance of backward temporal masking. This temporal masking is associated with an illusion in which the flash of an object is less well perceived if it is followed or preceded by the flash of an object [92]. The forward mask which precedes the object masks the weaker activity generated by the object. The feedback mask, on the other hand, inhibits the object's activity.

Another series of experiments on saccades showed that our visual system is able to detect speeds of up to 800 degrees/s when a low spatial frequency stimulus is used [80]. Building on this, it was subsequently shown that motion displayed during a saccade performed without pre- or post-saccadic stimuli can be seen in the context of low spatial frequency grating [93]. This demonstrates that motion is not completely suppressed during saccades. Conversely, the addition of increasingly long pre- and postsaccadic stimuli leads to the progressive disappearance of the perception of this movement [94].

More recently, Duyck et al. developed a new procedure for creating simulated saccades. These simulated saccades correspond to the display of a grating moving at the average speed of a saccade (176 degrees/s) and displayed at a frame rate of 1440 Hz. This very high frame rate is used to ensure that the movement of the saccade, because of its speed, will be perceived as continuous by the cortex. In comparison, our eye would be capable of a frame rate of up to 250 Hz in the case of natural images [95]. In the case of a traditional frame rate of 60 Hz, such rapid movement is no longer continuous but apparent. This study showed a reduction in the amplitude of the perceived saccade for longer peri-saccadic mask durations. Other unpublished studies also seem to show a reduction in speed. The perception of movement would therefore be reduced but not totally erased.

Mark Wexler has also shown the presence of a smear observable at 60 Hz but which is erased at 1440 Hz to allow the stimulus movement to be perceived (unpublished). Using the same saccade procedure simulated at high frame rate, Wexler and Cavanagh demonstrated a new illusion which they called shape-dragging [96]. This illusion appears when a simulated saccade is performed where the peri-saccadic masks have a different shape to the object that is moving in the saccade. In this context, the object that the observer perceives as moving in the saccade is the object that makes up the perisaccadic masks. It is the same shape and size. Based on these two observations by Mark Wexler (disappearance of the smear at 1440 Hz and shape-dragging) the ANR shooting star was created with the aim of exploring the biological substrates underlying these two effects. This study is being carried out at the level of the retina and the cortex, as well as by modelling both. It is this modelling that is the subject of part of this thesis.

In conclusion, it is possible that the blur observed in the saccade-only condition is caused by suppression by corrolary discharge alone without saccadic omission. Conversely, the results of Duyck and Wexler show a clear perception of the moving bar in the presence of a static phase but no saccadic omission. It is possible that saccadic omission is the result of these two effects combined. It has been suggested that the suppressive effect of the corrolary discharge reduces the response in the LGN during the saccade. At the same time, this suppression is followed by a strong amplification of the response in the LGN [83]. It could contribute to increasing the strength of the backward mask response and facilitate temporal masking [97].

1.3 Motion processing

1.3.1 Retinal motion anticipation

The retina is not just a reactive encoder, it is able to respond in a proactive way, especially with regards to stimuli. In visual processing, it is able to extrapolate and estimate how the visual stimulus is the most likely to behave in a near future, given the information of the past. This is, of course, based on the assumption that the stimulus is predictable to

some extent. In particular, several studies have suggested that the predictability of stimuli can be learned from spatial and temporal regularities, arising e.g. in a deterministic trajectory.

Prediction is a rather wide concept. If by this term, one refers to motion extrapolation, studies have reported that it already starts at the level of the retina. Berry et al. [1] have first shown that local gain control mechanisms, occurring at the level of retinal bipolar and ganglion cells, can explain a form of local anticipation for a moving bar, by advancing the peak in the retinal ganglion cells response. This explains the change in the shape of response observed in experimental data - bringing the ganglion cells to their activity peak earlier than when they respond to a flashed bar - without modifying the time at which their activity starts increasing, i.e. when the bar enters in their receptive field. Another study by Johnston et al. [98] has emphasized the role of lateral inhibition in the elicitation of anticipatory mechanisms at the retinal level. They have proposed that motion anticipation can be mediated via feed-forward inhibition from amacrine cells inputs that specifically suppress the response to the moving object in the latter half of the receptive field. This mechanism as well truncates the response and yields an early response peak. According to the authors, this "adaptation anticipation" occurs at the level of synapses. It requires each excitatory synapse to be more distal than an inhibitory synapse on the pathway. The latter will inhibit its EPSP and generate a shift forward (anticipation) of the peak. Thus, there must be an excess of inhibitory synapses compared to excitatory ones. In this case, motion anticipation arises from the general properties of the retina connectome and from the feedforward inhibition that ganglion cells receive from amacrine cells. Souihel and Cessac [14] explored, in a modelling study, another potential anticipatory effect of amacrine cells. In addition to the feed-worward effects discussed in [98] feedback inhibition due to amacrine cells could induce a wave of activity further anticipating the bipolar cell response and thereby enhancing the effect of gain control. Finally, Menz et al. [2] observed that motion anticipation can, in addition to a peak advancement by truncation of the response, arise by advancing the *onset* of the response, with a strong anticipatory effect. They hypothetize that this effect may come from amacrine cells: hyper-polarizing these cells would provide a dis-inhibitory input to ganglion cells prior to the object crossing the receptive field center.

1.3.2 Cortical motion anticipation

The cortex is not left out either, with its ability to extrapolate and estimate trajectories. It has also been shown that anticipation is further carried out at the level of the primary visual cortex [99, 100, 101, 3]. Jancke et al. [99] first demonstrated the existence of anticipatory mechanisms in the cat primary visual cortex. They recorded cells in the central visual field of area 17 of anesthetized cats, responding to small squares of light, either flashed or moving in different directions, and with different speeds. When presented with the moving stimulus, these cells show a reduction of neural latencies, as compared to the flashed stimulus. Subramaniyan et al. [101] have reported the existence of similar anticipatory effects in the macaque primary visual cortex, showing that a moving bar is processed faster than a flashed bar. They give two possible explanations to this phenomenon : either a shift in the cells receptive fields, induced by motion, or a faster propagation of motion signals. Consistent with the study by Jancke et al., they reported a speed dependence of the response latency as well as a luminance dependence. However, Subramaniyan et al. note that the motion representation delays are not reduced to zero, irrespective of the experimental setting of the flash lag effect. As a consequence, moving objects representation in V1 should be mislocalized. This observation is in favor of a collaborative work conducted, on the one hand, by the retina and V1 to help reducing the latencies, and, on the other hand, by other specialized brain regions which carry out predictive computations. Learning and training seem also to play important roles in calibrating the response of the nervous system to a giving moving object. Finally, Benvenuti et al. [100, 3] have studied the trajectory-based activity in V1. They have compared voltage sensitive dye imaging responses for different cortical locations along a bar trajectory. By centering all positions on the same relative time events (bar centered in the middle of the receptive field), they have highlighted a gradient in the response (see also Fig. 3.1). The further the bar starts from the current position of a cortical column the earlier its activity rises. They gave convincing arguments that this increase is carried by the lateral connectivity in the cortex.

1.3.3 Cortical suppressive wave

Chemla et al. [9] identified the generation of a suppressive wave in the primary visual cortex of macaque monkeys using apparent movement stimuli. Apparent motion is an illusion associated with certain types of stimuli. This fake motion is characterised by an impression of movement perceived by the cortex, even though the visual stimulus is only a flash of distinct objects ordered from a precise spatio-temporal sequence. For the illusion to occur, the objects must be flashed at regular intervals in time and distance. These intervals constraint the perceived speed of the apparent movement.

Two white dots of 0.25 degree of visual angle were successively flashed against a black background. The left dot is flashed first, lasts 100 ms, then the right dot is flashed within a delay of 50 ms. This flash has also a duration of 100 ms. The distance between the dots was set to 1 or 2 degrees. The authors observed an apparent speed ranging from 5 to 66.6 degree/s by varying the flash duration of the stimuli. They exhibited a specific non-linearity present in the response to apparent movement. For this, they calculated the difference between the cortical (V1) activity generated by the complete stimulus and the sum of cortical activity generated by the isolated white dots making up the apparent

motion. On this basis, they observed a mechanism of suppressive waves propagation that we are going to describe and reproduce with our model. In addition to this, they also used a cortical model based on Di Volo's paper [13] described in section 2.2.1. Their simulated cortical area has a periodic geometry and consists of only one dimension. The retinal inptus received by the cortical columns corresponds to a stereotyped drive mimicking the retina. Their model allows the use of static or dynamic adaptation. One difference between this model and Di Volo's paper is the presence of external drive and retinal input feed to the inhibitory population. In our case, our geometry is just a plane where each edge is zero. This allows us to use real visual stimuli and a spatial orientation of up/down and left/right. Connectivity was biased towards inhibitory excitation. Chemla et al. also set up a gain on inhibitors for certain experiments. This gain has the same role of reinforcing inhibition as our biased connectivity but the methodology for achieving this is not the same. In their case, the gain is an amplification factor that increases the slope of the inhibitory transfer function (B.1). Finally, the cortex of our model receives realistic retinal input from a model of the retina processing the visual stimulus presented to it. This retina allows us to study the activity of the cortex as a function of a whole spectrum of different biologically inspired retinal responses. In our simulations, for the sake of simplicity, we have kept the retina static, although we can modify the time scale parameters. In addition, we only have a static adaptation, which is a little less precise. The Chema et al. model made it possible to reproduce the suppression wave and to study the effect of a few parameters on it. Our aim is to reproduce the same type of wave.

1.4 Models

1.4.1 Retinal model

This model is made of 3 bidimensional layers whose structure is shown in Fig. 2.3: A layer of bipolar cells (BCs), a layer of amacrine cells (ACs) and a layer of retinal ganglion cells (RGCs). The layers are rectangle grids, with the same dimension $L_x \times L_y\ mm^2$ and the same number of cells, N. BCs are labelled with an index $i = 1 \dots N$, ACs are labelled with an index $j = 1 \dots N$, RGCs with an index $k = 1 \dots N$. Cells are located on the nodes of their grid layer and are spaced by a distance δ mm in both directions x, y. Spatial coordinates are noted $\vec{x} = (x, y)$ and the coordinates of, e.g., BC i are (x_i, y_i).

The 3 layers ought to be parametrised by a vertical coordinate, z. However, this parametrisation is implicit in the retinal layers label BCs, ACs, RGCs and we are not going to use a vertical distance between layers. Since all layers have the same grid spacing, δ, and the same number of neurons, there is a vertical alignment of nodes: the BC with index $i = 10$ is vertically aligned with the AC of index $j = 10$ and the RGC with index $k = 10$. This given, we define the Euclidean distance between a cells i, in layer 1, and a cell j, in layer 2 as $d(i,j) = \sqrt{(x_i - x_j)^2 + \left(y_i - y_j^2\right)}$. That is, we do not consider the vertical distance, for simplicity. The distance $d(i,j)$ is used for connectivity patterns.

There is indeed an interlayer connectivity. The connectivity from BCs to ACs is characterized by a connectivity matrix Γ_A^B, with entries $\Gamma_{A_j}^{B_i} = 1$ if there is a connection from BC i to AC j, and $\Gamma_{A_j}^{B_i} = 0$ otherwise. In the paper, the connectivity structure of Γ_A^B is called "nearest-neighbours+1": the BC with coordinate i connects to the AC with coordinate i and with the four nearest neighbours of this AC. The synaptic weight from BC i to AC j is then $W_{A_j}^{B_i} = w_A^B \Gamma_{A_j}^{B_i}$ where the parameter $w_A^B \geq 0$ controls the excitatory synapses amplitude. This form of synaptic weigths allows us to tune the synaptic intensity from BCs to ACs with the unique parameter w_A^B. The connectivity from ACs to BCs is also characterized by a synaptic weight matrix W_B^A with entries $W_{B_i}^{A_j} = w_B^A \Gamma_{B_i}^{A_j}$, $w_B^A \leq 0$ (inhibition from AC j to BC i) where Γ_B^A is "one to one" (AC j only connects to BC with index $i = j$). The synapse from BC i to RGC k corresponds to "Gaussian pooling" [1] where $W_{G_k}^{B_i} = w_G^B \frac{e^{-\frac{d(i,k)^2}{2\sigma^2}}}{2\pi\sigma^2}$ with $w_G^B \geq 0$. Likewise, the connectivity from AC j to RGC k is characterized by a synaptic weight $W_{G_k}^{A_j} = w_G^A \frac{e^{-\frac{d(j,k)^2}{2\sigma^2}}}{2\pi\sigma^2}$ with $w_G^A \leq 0$. Synaptic weights are expressed in Hz. The different types of connectivity are summarized in the appendix B.2.

Cell types have characteristic times, expressed in seconds, corresponding to the integration time of their response to external influence and including synaptic delay. Here, we consider that all BCs have the same characteristic time, τ_B. Likewise, all ACs have a characteristic time, τ_A, and RGCs a characteristic time, τ_G.

The dynamics of cells is based on their voltage. We note V_{B_i} the voltage of BC i and so on. Voltage rectification takes place below a certain threshold (eq. (1.3)). In addition, BCs and RGCs have gain control, a desensitization when activated by a steady illumination. (eq. (1.5), (1.8)), characterized by an activation variable A_{B_i} for BCs, A_{G_k} for RGCs [102]. The dynamics of voltages and activations is given by eq. (1.2) below.

BCs receive a visual input featuring the pre-processing of a visual stimulus via photo-receptors and horizontal cells. In this study, a visual stimulus is a grey scale video, that is a function $\mathcal{S}(\vec{x}, t) \in [\,0, 1\,]$ where 0 corresponds to black

and 1 to white. The pre-processing of this visual stimulus via photo-receptors and horizontal cells is modelled by a spatio-temporal convolution:

$$\left[\mathcal{K}_{B_i} \overset{\vec{x},t}{*} \mathcal{S}\right](t) \equiv V_{i_{drive}}(t), \tag{1.1}$$

where $\mathcal{K}_{B_i}(\vec{x},t)$ is a spatio-temporal kernel, centered at the coordinate of the BC i, and called "OPL kernel" (where "OPL" stands for "Outer Plexiform Layer" `https://www.ncbi.nlm.nih.gov/books/NBK11518/`). Spatially, this is a Gaussian with a center of radius σ_c and sstemporally, a gamma function with a characteristic time τ_c (see appendix A.1 for the value of these parameters). Therefore, the OPL input of BCs is monophasic in space and time. As shown in [16] the presence of lateral inhibition (here, by ACs) allows nevertheless to generate biphasic profiles in space and in time for the BCs response. Note that the spatial RF is circular: we do not consider orientation selective cells in this paper. In the definition of $\mathcal{K}_{B_i}$ there is a multiplicative factor, $\mathcal{C}$, which allows us to control the amplitude of $V_{i_{drive}}(t)$. This is used, in section 3.2.1, to modify the amplitude of the retinal input to the cortex.

The joint evolution of BCs, ACs, RGCs, driven by the stimulus $\mathcal{S}$ is given by the following set of equations. We use the standard notations of dynamical systems theory, where the time variable is omitted except for the non autonomous term (here, the drive term). We refer to the papers [14, 15, 16] for detail about this model.

$$\left\{\begin{array}{rcl}
\frac{dV_{B_i}}{dt} & = & -\frac{V_{B_i}}{\tau_B} + \sum_{j=1}^{N_A} W_{B_i}^{A_j}\, V_{A_j} + V_{i_{drive}}(t), \\
\frac{dA_{B_i}}{dt} & = & -\frac{A_{B_i}}{\tau_{a_B}} + h_B\, \mathcal{N}_B(V_{B_i}), \\
\frac{dV_{A_j}}{dt} & = & -\frac{V_{A_j}}{\tau_A} + \sum_{i=1}^{N_B} W_{A_j}^{B_i} R_B\left(V_{B_i}, A_{B_i}\right), \\
\frac{dV_{G_k}}{dt} & = & -\frac{V_{G_k}}{\tau_G} + \sum_{j=1}^{N_A} W_{G_k}^{A_j}\, V_{A_j} \;+\; \sum_{i=1}^{N_B} W_{G_k}^{B_i}\, R_B\left(V_{B_i}, A_{B_i}\right), \\
\frac{dA_{G_k}}{dt} & = & -\frac{A_{G_k}}{\tau_{a_G}} + h_G\, \mathcal{N}_G(V_{G_k}),
\end{array}\right. \tag{1.2}$$

where, in addition to voltages, we have introduced the activity variables, A_{B_i} for BCs, A_{G_k} for RGCs, ruling the gain control mechanisms on these cell type. There is no gain control on ACs. BCs are, in addition, rectified. The function:

$$\mathcal{N}_B(V_{B_i}) = \left\{\begin{array}{ll} 0, & \text{if} \quad V_{B_i} \leq \theta_B; \\ V_{B_i} - \theta_B, & \text{else,} \end{array}\right. \tag{1.3}$$

models this BCs voltage rectification, where θ_B is the rectification threshold. The BCs output to ACs and RGCs is then characterized by a non linear response to its voltage variation, given by :

$$R_B\left(V_{B_i}, A_{B_i}\right) = \mathcal{N}_B\left(V_{B_i}\right)\, \mathcal{G}_B\left(A_{B_i}\right), \tag{1.4}$$

where the function:

$$\mathcal{G}_B(A) = \left\{\begin{array}{ll} 0, & \text{if} \;\; A \leq 0; \\ \frac{1}{1+A^6}, & \text{otherwise.} \end{array}\right. \tag{1.5}$$

implements the gain control of BCs as a function the activity variable A_{B_i} [1].

As ganglion cells are spiking cells, their response function is:

$$R_G\left(V_{G_k}, A_{G_k}\right) = \mathcal{N}_G(V_{G_k})\, \mathcal{G}_G(A_{G_k}). \tag{1.6}$$

This function corresponds to a probability of firing within a small time interval. Thus, it is expressed in Hz. Consequently, α_G is expressed in Hz mV^{-1} and N_G^{max} in Hz. A non-linearity is fixed so as to impose an upper limit over the firing rate. Here, it is modeled by a piece-wise linear function :

$$\mathcal{N}_G\left(V\right) = \left\{\begin{array}{ll} 0, & \text{if} \quad V \leq 0; \\ \alpha_G(V - \theta_G), & \text{if} \quad \theta_G \leq V \leq N_G^{max}/\alpha_G + \theta_G; \\ N_G^{max}, & \text{else.} \end{array}\right. \tag{1.7}$$

We have, for the RGCs gain control:

$$\mathcal{G}_G(A) = \left\{\begin{array}{ll} 0, & \text{if} \quad A \leq 0; \\ \frac{1}{1+A}, & \text{else.} \end{array}\right. \tag{1.8}$$

which actually differs from the non-linearity in the BCs gain control, following [102]. The gain control rate, h_B for BCs, h_G for RGCs, expressed in Hz mV^{-1}, tunes the intensity of the gain control. In particular, if $h_B = 0$, $A_{B_i} \to 0$ exponentially fast so that the gain $\mathcal{G}_B(A) = 1$. The same remark holds for RGCs.

Parameters values of the model can be found in the appendix A.1.

1.4.2 Cortical model

This is a two dimensional model composed of two populations of cortical columns: excitatory (E) and inhibitory (I), located in a cortical area of dimension $\alpha L_x \times \alpha L_y$, where α is a magnification factor from retina to cortex. Cortical columns represent the spatial average of cortical neurons at a space scale roughly corresponding to one pixel of voltage sensitive dye imaging (VSDI signal) [103]. This model has actually been employed in [9] to reproduce the VSDI response to a simple visual stimuli (apparent motion) in the awake monkey primary visual cortex (V1). Cortical spatial coordinates are noted $(x, y) \equiv \vec{x}$. We thus use the same notations as for the retina, to alleviate notations, although there is a magnification factor between these two systems of coordinates.

The activity of cortical columns is represented by their average firing rate: ν_E for excitatory columns, ν_I for inhibitory columns. The equations for cortical neurons dynamics are based on a mean-field model of Adapting Exponential (AdEx) neurons [10, 12, 13]. The types of neurons modelled were chosen on the basis of their electrophysiology: regular-spiking (RS) excitatory neurons and fast-spiking (FS) inhibitory neurons [104]. This model was derived under the hypothesis that the network dynamics is Markovian at a timescale of a few ms and stationary for a duration T. One describes then the collective dynamics through a master equation formalism developed by El Boustani and Destexhe [105]. This system can reproduce asynchronous irregular regime, a typical feature of the awake states, as well as Up and Down states, characteristic of sleep or anesthesia states [13, 106].

The spatially extended dynamical system reads:

$$\begin{cases} T\,\frac{\partial \nu_E(\vec{x},t)}{dt} = -\nu_E(\vec{x},t) \,+\, F_E\left[\,\nu^{aff}(\vec{x},t) \,+\, \nu^{drive} \,+\, A_E^E\,\nu_E^{input}(\vec{x},t)\,,\, A_E^I\,\nu_I^{input}(\vec{x},t)\,\right] \\ T\,\frac{\partial \nu_I(\vec{x},t)}{dt} = -\nu_I(\vec{x},t) \,+\, F_I\left[\,\nu^{aff}(\vec{x},t) \,+\, \nu^{drive} \,+\, A_I^E\,\nu_E^{input}(\vec{x},t)\,,\, A_I^I\,\nu_I^{input}(\vec{x},t)\,\right], \end{cases} \tag{1.9}$$

where $\nu_E(\vec{x},t)$ (resp. $\nu_I(\vec{x},t)$) is the population rate of the excitatory (resp. inhibitory) cortical column located at $\vec{x}$, at time t. T is the characteristic integration time.

In eq. (1.9) the functions F_E (resp. F_I) are the transfer functions of excitatory (resp. inhibitory) neurons. They describe the firing rate of population E (resp. I) as a function of the excitatory and inhibitory rates ν_E and ν_I. Their form is made explicit in the appendix, section B.1. The term $\nu^{aff}(\vec{x},t)$ in eq. (1.9) corresponds to the retino-thalamic input (sensory drive). As the thalamus is not considered here (we assimilate it to a simple relay) this input comes directly from the RGCs. There is a direct correspondence, a retinotopy, between a point in the retina (RGC), and a point in V1 (cortical column). Here, this mapping is linear. There is just a magnification factor α from the retina to V1. Each RGC inputs a cortical column and $\nu^{aff}(\vec{x},t)$ is the firing rate emitted by the RGC that inputs the cortical column located at $\vec{x}$. Note that, in the absence of gain control or amacrine connectivity, the retinal model is reduced to a convolution cascade [14, 15, 16]. In this case, the input $\nu^{aff}(\vec{x},t)$ is therefore similar to the one used in [3]. In the transfer functions F_E, F_I, we include a spatially uniform external drive ν^{drive}. This drive represents the background constant input coming from the rest of the brain.

$\nu_E^{input}(\vec{x},t)$ (resp. $\nu_I^{input}(\vec{x},t)$) are excitatory (resp. inhibitory) inputs coming from the column itself or from other cortical columns. They are multiplied by an amplification connectivity factor A_{post}^{pre}, where pre and $post \in E, I$ stands respectively for "pre synaptic" and "post synaptic". In our case $A_E^E = A_I^I = A_E^I = 1$ and $A_I^E = 1.5$. This connectivity corresponds to the observed physiology of the real cortex. We have:

$$\begin{cases} \nu_E^{input}(\vec{x},t) \,=\, \int_{\mathbb{R}} \mathcal{N}_E(\vec{x}-\vec{x}')\,\nu_E(\vec{x}', t-||\vec{x}'-\vec{x}||/v_c)\,d\vec{x}' \\ \nu_I^{input}(\vec{x},t) \,=\, \int_{\mathbb{R}} \mathcal{N}_I(\vec{x}-\vec{x}')\,\nu_I(\vec{x}', t-||\vec{x}'-\vec{x}||/v_c)\,d\vec{x}' \end{cases} \tag{1.10}$$

where $\mathcal{N}_E, \mathcal{N}_I$ are 2D circular Gaussian connectivity kernels with mean-square deviation σ_E, σ_I:

$$\mathcal{N}_X(\vec{x}) \,=\, \frac{e^{-\frac{1}{2}\frac{\|\vec{x}\|^2}{\sigma_X^2}}}{2\pi\sigma_X^2}, \tag{1.11}$$

with $X = E, I$. This form follows e.g. [12], although our connectivity kernel is two dimensional in contrast to their paper. Thus, σ_E, σ_I control the two dimensional cortical extent of the excitatory and inhibitory connections. Note, that, due to the normalisation of the Gaussian the shorter the cortical extent the larger the amplitude of the synaptic weight $\mathcal{N}_X(\vec{x})$ (see section 3.2.3 for a consequence of this). The parameter v_c is the speed of axonal conduction (assumed to be a constant). Equations (1.10) therefore express that the excitatory input $\nu_E^{input}(\vec{x},t)$ is the sum of the incoming excitatory activity from the connected columns arising with a delay $||\vec{x}'-\vec{x}||/v_c$ depending on the distance between the columns and the axonal conduction speed.

The cortical model is designed to reproduce the pixels intensity of voltage sensitive dye imaging, corresponding to a variation of fluorescent luminosity with respect of the fluorescent baseline. Its expression depends on the average membrane potential of the excitatory and inhibitory populations in the column located at $\vec{x}$, at time t. Its expression is given by equation (B.11) in the appendix, section B.1.

Remark. Note that this type of cortical model can exhibit pathological (i.e. model induced) oscillations due to bifurcations when some parameters become too large (such as ν^{drive} or the conduction speed). This phenomenon is well known and has been reported in the literature [107]. We observe as well such oscillations when parameters such as the retinal output amplitude becomes too large. This is commented in the afferent section.

1.5 Conclusion

However, one can ask at which stage of the visual system do these predictions start taking place. At the level of the early stages of the visual system ? Or in late-stage processors ? At the current state of the art there are convincing benches of evidence that anticipation takes place along the pathway from retina to cortex. This has been observed with a large diversity of recording conditions (in vitro, in vivo, anesthetized, awake), for different animal models (rodent, cat, monkey . . .). This suggests that there might exist a synergy between the retina, the thalamus-LGN and the cortex to optimize anticipation. This leads to a natural question: How does the dynamical response of the retina to a moving object affect the dynamics changes in the cortex ?

We will also investigate how the cortex can respond to stimuli mimicking saccades and how this activity can be influenced by the frame rate of the stimulus used in the experiments. We will also try to determine whether it is possible that the mechanisms of smear reduction and shape-dragging can be generated in the cortex. Finally, we will go further by exploring the suppressive interaction that could be generated between responses to peri-saccadic stimuli and movement. The aim of all this will be to gain a better understanding of the extent to which V1 cortex is responsible for the phenomena generated during saccades?

Along these lines, the purpose of this thesis is to answer these two questions, using a computational model, grounded on experimental studies performed at the Institut des Neurosciences de la Timone, in F. Chavane Lab, as well as preexisting models themselves grounded on experiments. Rather than developing a biologically plausible model for one species, the aim of this article is to reconcile two sets of work that have been conducted to model different species, and to study the potential effect of known retinal anticipatory mechanisms on cortical anticipation. The model consists first of a retinal model developed in [14] to confront several potential mechanisms of retinal anticipation (gain control, amacrine cells) and further studied in [15, 16]. This retina model is used as an input to a cortical mean-field model of V1, previously developed by A. Destexhe and his collaborators [12, 9], and calibrated on experimental VSDI signal data on the monkey cortex V1, performed in F. Chavane Lab. Note that, as further discussed in the text, we will not consider the effects of the thalamus (LGN) in this work. More precisely, it will be transparent, considered as a simple relay.

Chapter 2

The Chimera model in Macular

2.1 Macular

2.1.1 Introduction to Macular

I introduce here the software Macular, which I used intensively in my thesis, and to the development of which I contributed significantly. Macular is a visual system simulation platform coded in C++/Python at INRIA by the SED (experimentation and development service at Inria). It allows reproduce experimental retinal or cortical response to chosen visual stimuli movies in normal or altered vision. Macular is constructed as a layer-by-layer replica of the visual system. The first layer of this simulated system can receive a visual input corresponding to a stimulus video. It is also possible to provide nothing in order to observe spontaneous activity. Furthermore, Macular offers the opportunity to use inputs corresponding to models of retinal prostheses. Once the experimental results have been successfully reproduced, Macular grants the ability to change easily all the model parameters to explore and predict new results. The main aim of Macular is to provide neuroscientists with a tool capable of reproducing experimental results and also predicting new results. Some of these results may not be experimentally verifiable.

Macular consists of 4 main objects :

- *Cell object* can be biological cell but also networks of cells such as cortical columns. Each cell is associated to a state. This is a vector with a number of state variable defined by the model. Cell state evolves in time by following specific functions. These functions take into account inputs of the system and a set of parameters. Inputs can be external or synaptic. Parameters are constants, chosen by the user between each simulations. Cells can also have multiple outputs. For example, the amacrine cells in our model have a state V defining their voltage: $V = -\frac{V-V_L}{\tau_A} + V_{syn}$. This is a differential equation for the voltage dynamics. Two parameters are used in this formula: the characteristic time of the amacrines (τ_A) and their leak potential (V_L). The last variable V_{syn} corresponds to the synaptic inputs received by the amacrine cell.
- *Synapse object* are the connections existing between cells of same or differents types. They have a cellular input, an synaptic amplification factor parameter and a function defining what is their output. Note that this amplification factor is the same for all synaptic connections of the same type. It should be distinguished from the connectivity weight, the value of which depends on the type of connectivity (Gaussian, uniform, etc.). Among these parameters, synapses have a conduction speed that allows them to set a delay corresponding to propagation or integration. For example, in our model, the synapse connecting the amacrines to the bipolars is defined by its output: $w_b^a \times V_{pre}$. This is made up of the synaptic amplification factor parameter w_b^a and the voltage of the pre-synaptic cell V_{pre}.
- *Cell layers* are the second level of organisation in Macular. A layer represents a two dimensional grid with a defined size and density. Each layer groups together a single type of Macular cell with the same set of parameter values. The cells in a layer can be interconnected.
- *Graph object* is composed of cell layers connected between them with synapses (Fig. 2.1). Each layers can send or receive multiple synapses. The size and the number of cells in a layer or synaptic connection length is defined during the graph generation. During this step are also set the synaptic weights of each synaptic connection depending on the connectivty type. Macular graphs can be saved in files.

Macular has a number of pre-defined connectivity types:

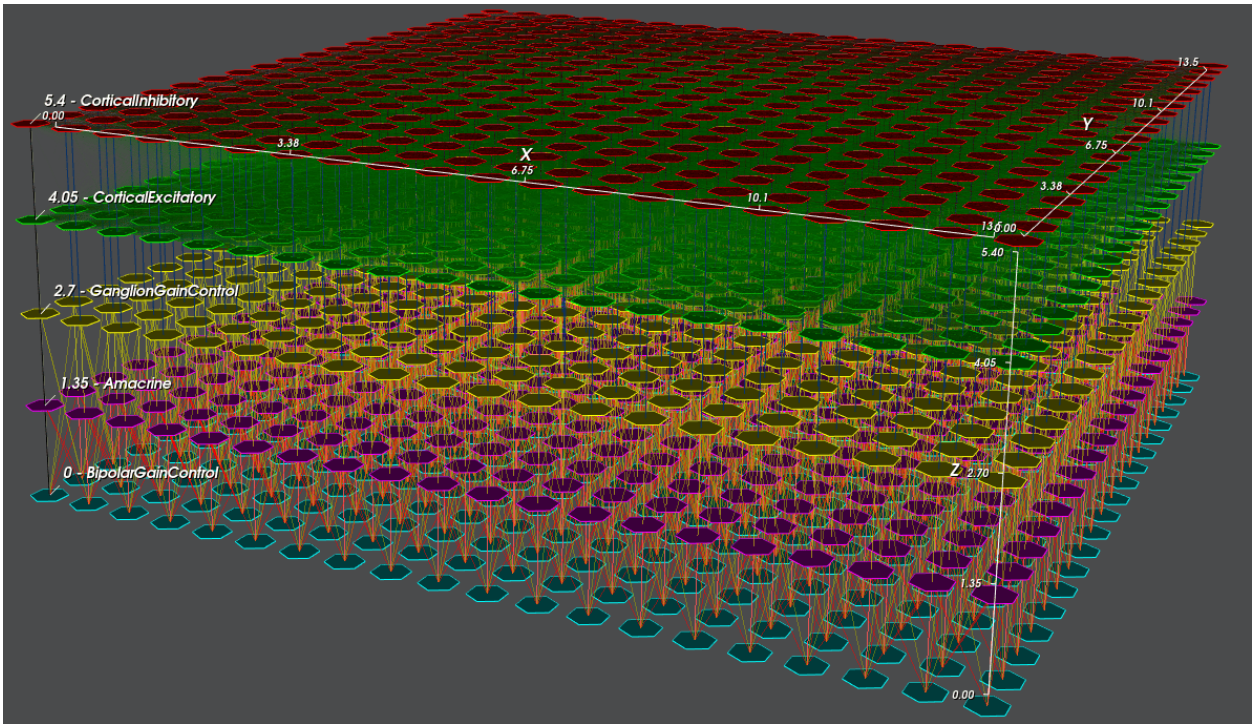

Figure 2.1: **The Chimera model in Macular.** This graph is made up of 5 layers whose bottom-up axis reproduces the retino-cortical pathway. Each layer is made up of 20x20 Macular cells. In this example, we have one layer for each cell type bipolar, amacrine and ganglion cells, then the primary visual cortex with its excitatory and inhibitory populations. Synapses connecting the cells can be seen between each layer. They appear as lines between layers, with colours depending on their type.

- *One to one* connectivity connects Macular cells with the same spatial position in another layer.
- *Nearest neighbor* connects all Macular cells with their 4 nearest adjacent cells.
- *Nearest neighbor + 1* connects Macular cells to their 4 nearest neighbours as well as to the cell in the same position as it in the post-synaptic layer.
- *Fully connected* creates a graph where all the Macular cells within one layer, or between two layers, are connected with a uniform weight.
- *Radius connected* connects all the Macular cells in a given radius with a uniform weight.
- *Gaussian* connectivity also connects all Macular cells in a radius $d_{[pre,post]} <= 3\,\sigma$. However, each Gaussian connection has a varying Gaussian synaptic weight W_{post}^{pre} which depends on this same distance via a Gaussian profile :

$$W_{post}^{pre} = \frac{e^{-\frac{d^2[pre,post]}{2\,\sigma^2}}}{2\pi\,\sigma^2}. \tag{2.1}$$

  Note that the normalisation holds for a two dimensional Gaussian distribution. This equation does not actually integrates the boundary conditions, for simplicity, but they are taken into account in Macular.

Macular's first major advantage is its modularity. The user can implements their own cells and synapses and then use them in their own graph. Macular allows users to generate the graph of their choice by connecting the cells in the way they want. Macular also provides a number of generic cells and synapses.

The second major advantage of this platform is its simplicity. Macular has two easy-to-use graphical interfaces. One GUI, Macular Graph Simulator is used for simulation, parameters setting, graph creation and to visualise different aspects of the simulation in real time (stimulus, layer activity, specific selected cell response, 3D graph). This GUI is made up of views that users can organise as they wish. Figure 2.2 shows an example of how this GUI is organised. The GUI structure and all Macular parameters and states can be saved in reimportable session files. The other GUI,

called the Macular Template Engine, is used for creating cells and synapses from scratch (input, parameters, vector field, functions). The user doesn't need to master a programming language to use Macular. They just need to have the equations, parameters and corresponding units for the model and enter them in specific cells. The physical units must be consistent. Several differential equation solvers are also available. Note that a programmer with Python and C++ skills can perform all these operations without using the graphical interface.

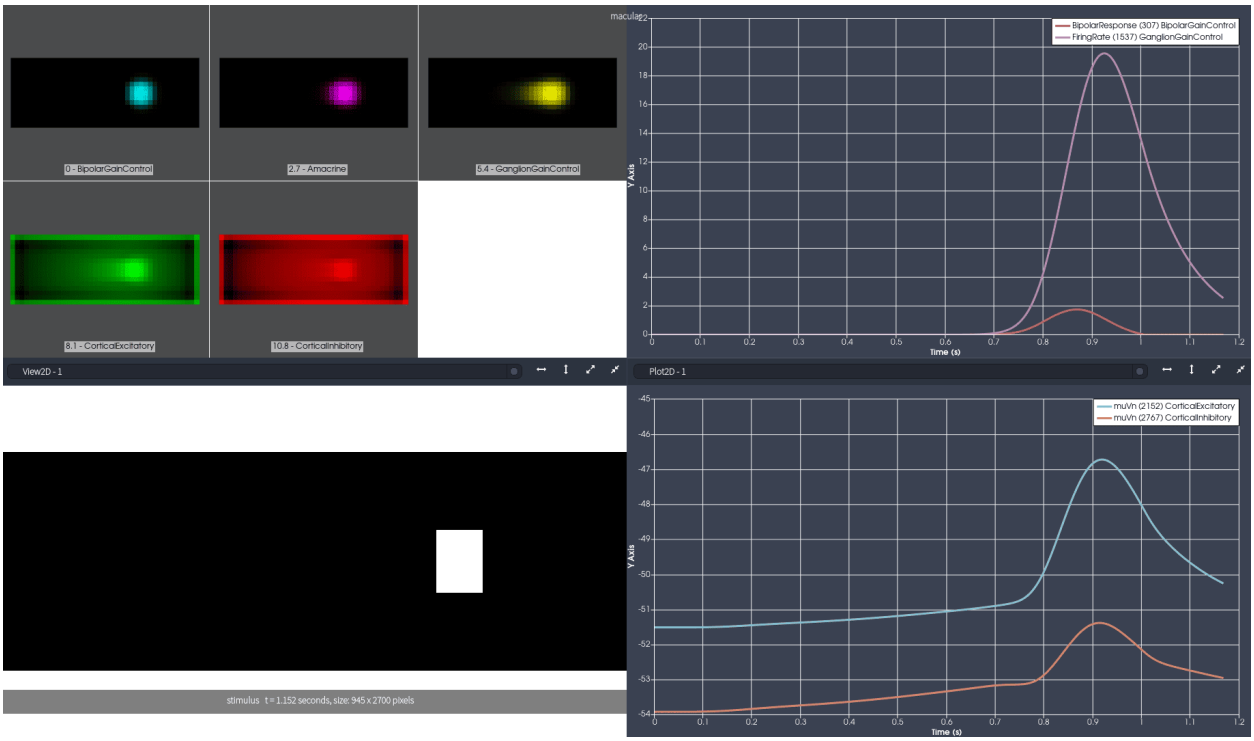

Figure 2.2: **Macular simulator graphic interface.** On the top left are heatmaps of the five layers of our model : bipolar cells (cyan), amacrine cells (magenta), ganglion cells (yellow), excitatory cortical population (green) and inhibitory cortical population (red). On the right are shown the temporal evolution of outputs chosen by the user. At the top is the response of a bipolar (red) and the firing rate of a ganglion (pink). At the bottom is the mean voltage of the excitatory (blue) and inhibitory (orange) populations. Stimulus, heatmaps and graphs are refreshed in real time when simulation progresses.

2.1.2 Spatio-temporal representations in Macular

A visual scene is a spatio-temporal event. It is therefore important to carefully handle space and time.
Within Macular, 4 spatial representations co-exist, each of them has to match :

- *Movie, in pixels.* The input of Macular is a movie where each pixel is defined by a light intensity level corresponding to a grey level from 1 to 255. Colour management is not implemented. All RGB video is processed in greyscale.
- *Visual field in degree of visual angle.* This is the actual representation of the visual environment and of the bipolar receptive fields that integrate the visual field. Degrees of visual angle are a more precise unit of measurement than metres. They do not depend on the distance at which objects are perceived. The "pixels per degree" parameter is used to manage the conversion between the movies spatial units and the visual field units. The variable δ_x is associated with the distance of a pixel in degrees of visual angle.
- *Retinal space in millimeters or micrometers.* Millimeters are the default unit used by Macular. Micrometers are automatically converted to millimeters. The appropriate conversion factor must be used to convert between the degrees of visual angle of the visual field and th metric system. This factor varies according to the animal species under consideration.
- *Cortical space in millimeters or micrometers.* This conversion factor is different from that for the retina. So there will also be a conversion factor between retinal and cortical spatial representation.

The choice of millimeters as the default unit was motivated by the use of conduction velocities and connectivity radii most often expressed with mm rather than in degrees of visual angle in the literature of the retina. Despite this choice within Macular, for the remainder of this thesis we have decided to express the results of our experiments in degrees of visual angle in the same way as the paper from which we drew inspiration [3].
The degree per mm ratio is implicit, unlike the pixel per degree ratio, which is explicitly defined as a Macular parameter. It is the user's responsibility to use the appropriate conversion factors to ensure consistency between the size of the simulated area and the radii of connectivity between the visual field and the retinal/cortical spaces. In the Chimera model, we set a degree per mm parameter of 3.33 in the retina and 0.33 in the cortex. This means that to simulate an area of 18.45×3.15 degrees we set the area of the retinal layers at 5.535×0.945 mm and the cortical layers at 55.35×9.45 mm. The area in degrees is defined as a function of the number of pixels and the "pixel per degree" parameter. We set this to 300, which requires a stimulus of 5535×945 pixels. If we also want to establish Gaussian connections of 5 degrees radius in the cortex, then we need to set the radius of their connectivity to 15 mm.
Another parameter implicitly defined in Macular is the distance between cells δ_x. This is defined as a function of the size of the simulated area and the number of cells on the x and y axes. We have a cortical area of 18.45×3.15 degrees made up of 83×15 cells. The value of δ_x is identical in the horizontal and vertical directions, and is calculated from : $\delta_x = \frac{L_x}{n_{cells_X} - 1}$. The result is $\delta_x = 0.225$ degrees.

Macular's temporal dimensions can be divided into 3 groups :

- *Movie in frame index.* A video is a succession of images. The time of a video is therefore defined by the index of the current frame.
- *Real time in millisecond or second.* This represents the elapsed time of the stimulus as well as cellular and synaptic processes. The duration of a frame δ_t is used to convert a video frame index into real time. All the characteristic times of biological processes are expressed in this temporal representation.
- *Integration in second.* They correspond to the time steps of the integrator of differential equations dt (eg : Runge-Kutta).

2.1.3 Spatio-temporal conditions in Macular

To ensure that the different spatial and temporal representations co-exist correctly, certain conditions should be validated to prevent errors in the simulations.
Two conditions on temporal representations :

- $\delta_t \ll \tau_{cell}$, the time between each frame must be much less than those used to integrate the different cells. In this way, the speed of the bar is slow enough to give the cells time to activate before the bar leaves their receptive field.
- $dt \ll \delta_t$, the time step for integrating the differential equations must be much smaller than the duration of the frames. This produces smooth response curves, not stair-stepped.
- $\delta_x \ll \sigma_c ell$, the radius of the cell receptive field must exceed the size of a pixel in degrees of visual angle. The receptive field needs to contain enough pixels to integrate the video image correctly. This also gives the cells more time to integrate.
- $\sigma_c ell \ll L_{X,Y}$, the radius of the cell receptive field must be sufficiently smaller than the sizes of the visual field. The size of the visual field must be adapted to that of the receptive field.

The last condition to meet involves both time and space. It comes into play when we use stimuli from a moving object: $v_{stim} \leq \frac{2\sigma_{cell} + l_X}{\tau_{cell}}$. The speed of the object must not exceed the response speed of the cells. The cells must have enough time to integrate the movement of the object. The peak of the time component of the receptive field must occur while the object is still in the receptive field. If the characteristic time of the receptive field τ_{cell} decreases, the integration of the object will be increased and will be able to support higher object speeds.

It may be possible to play with these different conditions to test particular cases of the retino-cortical model. This is what we do in the chapter 4.2. In this chapter, we play in particular with the last condition on the speed object and the first condition between the δ_t and the τ_{cell}.

2.1.4 Spatial accuracy and frame rate of stimuli

An important part of my thesis is based on the use of various speed and frame rate stimuli. In this context, I had the opportunity to learn how to create and simulate stimuli in Macular.

The first difficulty to take into account is the precision of the spatial dimensions of the stimulus. When you want to impose a spatial dimension on an element of the stimulus (length, width, speed), you are always forced to round up or

down the number of pixels. This round-off can lead to a more or less significant shift in the spatial dimension actually applied to the stimulus element. There is an essential parameter for limiting the amplitude of this shift: pixel per degree. This parameter acts as the spatial resolution of the stimulus. If we increase its value sufficiently, the pixels will have a sufficiently low value in degrees so that one pixel more or less will cause negligible variation. On the contrary, decreasing it would cause a drop in the precision of the spatial dimensions.

A spatial precision that is too low creates another problem when you want to simulate at high frame rates. It is possible to obtain a bar speed of less than 1 pixel/frame. This means that the bar will not move with each frame and that the effective frame rate will therefore be reduced. This is particularly true for simulating slow speeds which require the bar to move a very small distance each frame. As a consequence, the spatial resolution (pixel per degree) must be very high.

For a bar speed of 6 degrees/s travelling at 1440 Hz, the stimulus travels 0.004 degrees in one frame. I decided to set my pixel per degree at 300 for a spatial resolution of 0.0033 degrees/pixel (1 µm of retina). As a result, the value of a pixel in degrees is negligible. If necessary, this pixel per degree value can be adapted to work with smaller spatial dimensions. It should be noted, however, that increasing the size of the stimulus also generates a time cost during the Macular simulation. A decision therefore needs to be made between performance and accuracy.

For stimulus speed studies, I recommend creating different stimuli for each speed condition. Macular offers to modify the value of frame per second (δ_t) to change the speed of the stimulus with a single video. This method was not appropriate in my case though. This seems practical and avoids having to create new videos with different pixel/frame motion speeds. However, changing the speed of the bar in this way also changes the frame rate of the stimulus. As this thesis demonstrates, the frame rate is not a parameter to underestimate as the results obtained will be a mixture of effects caused by frame rate and bar speed.

2.1.5 Getting started with Macular

Macular targets users in the community of modellers and biologists. For this reason, it was necessary for Macular to be tested by users with these skills. As a biologist by training, I was able to play this role, while developing my thesis model. Using Macular for the first time was relatively straightforward. The presence of clear GUIs guided me. I was able to quickly create my first graphs and Macular sessions and run simulations.

The difficulties I encountered with my model gradually pushed me to understand Macular more and more. I didn't initially have any skills in C++ and all my knowledge came from learning before my internship in the Biovision team and from interacting with members of the team and members of the SED INRIA, particularly during an early two-week coding sprint. A coding sprint is a period of time during which the development team meets to focus on a piece of code with the aim of producing a list of tasks to be carried out on the code. All this led to a better understanding of Macular. Organised into around twenty modules, Macular is the biggest piece of code I've ever worked with.

The initial help from the Macular developers gave me an initial overview of the most important files in the package. From there, I was able to gradually move from module to module to understand them. Running tests also enabled me to confirm the roles of the various functions present. The availability of the developers to ask questions also reinforced my learning. Today, I can navigate Macular very easily and modify its code.

2.1.6 Macular improvements

My regular use of Macular, my understanding of it and the improvement of my C++ skills have enabled me to contribute to the development of the platform throughout my thesis. Firstly, I was able to implement a number of functionalties and fixes myself. Secondly, I was also able to help identify and reproduce numerous bugs that I was able to pass on to the development teams when I couldn't solve them on my own. Finally, I also thought about and identified the needs for new features to be implemented.
Most of the fixes and new features were implemented as part of 3 coding sprints (16-24 May 2022, 6-30 November 2023, 2-5 April 2024). In this context, I was responsible for listing and organising all the bugs and new features to be worked on. My most important role was to check that each add-on worked properly and that my results were not regressed in Macular. I also had to check that the add-on met my expectations. As a biologist user, my role also extended to active participation in thinking about the various tasks to be carried out and the best way of implementing them. Finally, I was also sometimes able to assist the development team on the programming side.

Unit management Especially, I have highlighted a major problem in the management of units in Macular. This resulted in a lack of clarity that caused a lot of confusion. Discussions with my thesis supervisor led us to the conclusion that there was a need for explicitly defined units in Macular. We needed to reduce the risk of inconsistent units within or between cells, while leaving the choice to users. Based on this observation, the SED developed a new version of Macular in which each parameter is defined with a physical quantity chosen from a list. Once the quantity has been chosen, the unit must also be selected from a second list. For example, you can choose "Voltage" as the physical

quantity and "V" or "mV" as the unit. Macular automatically converts the chosen unit to its default unit. This prevents any inconsistency in the units. I was able to contribute to this project by testing and checking the units in my model.

This problem of managing units was also found in Macular's spatio-temporal representations. As we explained in the section 2.1.2, Macular co-exists with 4 spatial representations. In reality, there is a 5th dimensionless spatial representation internal to Macular that I called "Macular units". This is the internal dimensionless representation used by Macular in its calculations. Initially, to create a graph, it was required to enter the size of the graph used in Macular's internal representation. This size defined the value of internal δ_x and δ_y used in Macular's calculations. Consequently, it was important to enter all the connectivity radii or the conduction velocity in this 5th spatial representation. It was therefore necessary to perform calculations to navigate between this representation and the biological representations in meters. To remedy this, it could be possible to simply enter the size of the area to be simulated directly in mm or degrees of visual angle when creating the graph, instead of Macular units. The simulated area size was defined by the pixel per degree parameter and the stimulus size in pixels. However, the realisation of this solution required the introduction of a new functionality as we needed to be able to simulate graphs with layers of different sizes.

Patches I also had to solve additional problems, mostly associated with the connectivity. In order to work, Gaussian connectivity takes a connectivity radius as input and uses it to calculate its sigma, which is 3 times smaller. In the case of intra-layer connections, the input that was received was treated as a sigma instead of the radius. This consistency problem led to the use of connectivity radii 3 times larger than expected. We therefore reintroduced the calculation of the sigma from the radius.

In biology, the cells in a cortical column send a majority of their output to the other cells in the cortical column. This can be summed up by the presence of a strong auto-connectivity. This auto-connectivity is normally present in the cortical model, but not in our initial Chimera model. This poses a problem because it should be their strongest source of input. We have therefore modified the implementation of our Gaussian models to take account of the connections between the cortical columns themselves.

Among the other types of connectivity, nearest neighbour should correspond to a connection between a cell and its closest environment. In modelling terms, this corresponds to the 4 directly adjacent cells. However, we discovered that our nearest neighbour had been configured to connect all the cells within a given radius. We renamed this nearest neighbour 'radius neighbour' before creating a radius neighbour function connecting only the 4 nearest neighbours.

Other problems lay in the management of synaptic inputs. Firstly, there was a duplication of excitatory cortical inputs, normally counted only once. This resulted in far too much excitation of the system. In addition, inhibitory inputs were also used as excitatory inputs. As a result, the excitation of the system was still too high.

The last of these corrections was made for the Gaussian weight. We noticed that by changing the connectivity distance and the spacing between cells so as to keep the same ratio, we obtained a different Gaussian profile instead of a constant one. We first tried to implement dynamic normalisation. This solution was complex to implement and in the meantime we have found another. Our weights were not dimensionless as they should have been but had a unit in mm^{-2}. To make it dimensionless we multiplied it by the spacing between the δ_x and δ_y cells.

New features Over the course of the coding sprints, Macular has been enhanced with new features that I have contributed to implement. Graph generation has been improved by making it possible to create several inter-layer synapses of the same type with different parameters, create several intra-layer synapses and use several layers of cells of the same type with different parameters. Parameter management has also been enhanced with the ability not to reset parameters when re-initialising the simulation, and the ability to save and then import the state of the system so as not to have to run a transient. A new specific fibre conduction velocity parameter has been added to the synaptic parameters. This was previously global for all synapses. Finally, there have been a number of improvements to make Macular easier to use for users, including the possibility of deleting cell types and synapses, the introduction of a batch to simulate Macular in a terminal and a considerable increase in the speed of simulations, which were far too slow. This required a refactoring of the cells and synapses as well as parallelization.

Exploring The Virtual Brain (TVB) During the first coding sprint at the start of my thesis (16 to 24 May 2022), we also studied the possibility of connecting Macular with a cortical simulation software called The Virtual Brain (https://www.thevirtualbrain.org/tvb/zwei/brainsimulator-software). It was in this context that I studied in detail the TVB code, which I was introduced to during a stay in Alain Destexhe's team. The Virtual Brain is a Python program created by the Human Brain Project under the supervision of Viktor Jirsa. The software simulates an entire brain, with each region corresponding to a mean field model based on several works [105, 12, 13]. Users can define the number of regions to be modelled and their names. The connectivity between the regions will be defined using a connectivity file containing tractography data. These are experiments that determine whether two brain regions are connected and how strongly.

Taking into account all these features of TVB it was an interesting opportunity to connect it with Macular and that's why we spent two weeks with the SED to study this possibility. Linking the retina part of Macular to TVB requires sending an output file containing the activity of retinal ganglion cells from Macular to TVB. But all TVB stimuli are generated by discretising a spatial and temporal function, and there is no way of importing a data file and using it to create a stimulus. However, this first problem could be solved because TVB offers the opportunity to create its own stimuli. A second complication is associated with the spatiality of the stimulus, which is not fully managed by TVB. The TVB graph consists only of a set of regions defined at a single point, which are not subdivided into sub-regions. There is therefore no spatial component within the cortical regions in TVB. This is not compatible with the stimulus from our retina, which have a two spatial representation with a resulution that can vary. Connecting Macular to TVB would require the outputs of each of our ganglion cells to be connected to a sub-region of V1 cortex. This is feature which is currently not available in TVB although this feature is currently being developed by its developers.

For these reasons, the Macular - TVB assembly has been set aside for the time being.

Macular documentation The development of my knowledge of Macular has also enabled me to play an active part in writing exhaustive documentation on the implementation, structure and operation of Macular. In particular, I was able to describe how to create, parameterise and simulate the retino-cortical model developed for this thesis. `https://Macular.gitlabpages.inria.fr/Macular/user_doc/Macular/main.html`.

2.2 The Chimera model

2.2.1 Initial Macular implementation

The retinal-cortical model we use in this thesis was developed in previous work. It is a fusion of the two models of retina and cortex presented in the introduction (respectively section 1.4.1 and 1.4.2). These two models were assembled by Frédéric Chavane, Alain Destexhe, Mattéo Di Volo, Selma Souihel and Bruno Cessac. In addition to the mathematical formulation, this work gave rise to a C++ code (Selma Souihel's thesis in collaboration with Mattéo Di Volo) [108]. This code was implemented in the Macular platform.

Here, It is important to emphasize several of the biggest differences between our implementation and that of Zerlaut et al. and Di Volo et al. [12, 9, 13] as they impacted and constrained the implementation in Macular. The Zerlaut et al. model is composed of a one-dimensional area of cortical columns separated between an excitatory and inhibitory population. Di Volo et al. model was initially one-dimensional but has been adapted to a two-dimensional area. These cortical columns are inter-connected by a lateral Gaussian connection with a dynamic delay depending on the distance and conduction velocity of the fibres. In addition the cortical area has a periodic ring-shaped geometry. At the edges, the connectivity connects the cortical columns present at the two opposite edges. In these one dimensional ring models the calculation of the Gaussian weights is based on a formula using a one-dimensional normalisation with no boundary. In contrast, we have two dimensional scenes with a bottom, a top, a left, a right, thus no periodic boundary conditions are acceptable. Instead, we used zero boundary conditions.

Another difference lays in the retino thalamic input. Each cortical column receives a stereotyped retino-thalamic input that mimics the input from the retina. In the previous models, this input is received only by the excitatory population, not by the inhibitory population. The excitatory population is also the only one to receive a background input (ν_{ext}) which reproduces the activity constantly coming from the other regions of the cortex. This activity ensures that cortical columns are never totally inactive, even in the absence of a stimulus. The inhibitory population only receives excitatory inputs from the excitatory population of the cortex. Each cortical column has an adaptation variable which reproduces its capacity to inactivate in the event of excessive activity. In the case of Zerlaut et al., this variable is static. In Di Volo et al. case, the adaptation becomes dynamic and enables us to obtain results that are more stable and closer to AdEx neural network models [13].

The major difference in our retino-cortical model lies in the use of a retinal model to create and send retinal inputs to the cortex. Our retinal input is therefore driven by a real visual stimulus. Because of the retinal spatialisation, we are therefore forced to adopt a geometry with a top, a bottom, a right, a left. As a consequence, we can't manage edges from a periodic geometry (rings) as is the case in all traditional models. Instead, we have to opt for zero edge management, which means that the cells located on the edges will receive less input than the others. The existence of these edges will have a direct influence on the cortical cells or columns close to them. We believe that these properties take us further away from biological reality than simple zero edges.

In our case, we can act on the cortex by modifying the parameters of the retina to create responses with different intensities and activity profiles that reproduce specific features of biology. Selma Souihel initially added this retinal input only to the excitatory population of the model, as did the input from the rest of the cortex (ν_{ext}). Our model subsequently evolved to incorporate the presence of retinal and external drive on the inhibitory population as well [109]. It was also added a bias in favour of inhibitor excitation. Finally, we have switched to a two-dimensional Gaussian

formula to simulate two-dimensional areas. As regards the adaptation of the cortical columns, we have retained the static adaptation of Zerlaut in an initial concern to limit the excessive calculation time that would be generated by an additional differential equation.

This model is a "chimera" model in the following sense. While the design and parameters of the cortical model are based on previous works on the monkey visual cortex, the retinal model is essentially based on previous works dealing with mice retinas. In addition, as mentioned above, there is no thalamus, or, more precisely, it is transparent, considered as a simple relay. In this sense, our model resembles more a "Frankenstein" creature than a real, actual organism. However, we believe that it captures the main mechanisms in the retino-cortical entanglement. Also, the advantage of such a model, with its joint simulation platform, is that one can easily modify the parameters of such or such components and see how it modifies the observed response. This is actually the main philosophy of this work where we vary physiological parameters, such as the conduction speed, or the effect of amacrine cells, that cannot be easily varied experimentally. This also means that the chimera model could be made closer to monkeys by adjusting the retina model to experimental results on monkeys retinas (that we didn't have). Note that a feature of the simulator Macular is precisely to afford such changes in the retina design.

The first graph (illustrated in Figure 2.3) that we retrieved at the beginning of this thesis formed the skeleton from which we added and modified certain elements to improve it:

- *Bipolar layer* receives an external input corresponding to the result of the convolution between the spatio-temporal stimulus (video) and the photoreceptor receptive field. This receptive field may or may not include the effect of horizontal cells with a center/surround. In this graph the bipolar is OFF without surround. The bipolar cells send their output one-to-one to the amacrine cells and with a 540 µm Gaussian to the ganglion cells with a weight of 0.15.
- *Amacrine layer* is excited by the bipolars before inhibiting them with nearest neighbour + 1 connectivity. This corresponds only to the feedback inhibition in Figure 2.3.
- *Ganglion cell layer* pool together the activity of bipolar cells. Each cell then contacts a single excitatory column with a weigth of 20 Hz. The activity of this cell is first multiplied by the density of ganglion cells in the retina ($400mm^{-2}$) to obtain the ganglion response per mm^{-2}. This is then divided by the cortical density ($4000mm^{-2}$) to evenly distribute the retinal response across the cortical column.
- *Excitatory cortical layer* is activated by ganglion cells. It sends synapses to the inhibitory cortical layer and to itself, with radii of connectivity of 2.7 mm and 3.6 mm respectively.
- *Inhibitory cortical layer* receives ganglion cells and then sends them one-to-one to the excitatory populations. They also contact each other within a radius of 1.8 mm.

In addition to this graph, we also had a stimulus from Selma. A 180-frame video of a 60x60 pixels square. In the context of the default set of Macular parameters, the pixel ratio in degrees of visual angle is 5. This gives a field of view of 12×12 degrees. The stimulus is a vertically centered black bar moving from left to right on a white background. The bar measures 5×15 pixels or 1×3 degrees and moves at 20 degrees/s for a $\delta_t = 0.005$ s. The switch between degrees and millimeters require to multiply by two conversion factors that are respectively $f = 0.3$ mm/deg in the retina and $f = 3$ mm/deg in the cortex [110, 111]. All the layers in this graph have grids of 20×20 cells within a square area of 3.6 mm for the retina and 36 mm for the cortex. The spacing between cells is therefore 190 µm and 1.9 mm respectively.

Our first simulations were therefore carried out with this graph and Selma's stimulus, in addition to the parameter values that were present by default in Macular. Details of this initial set of parameters can be found in appendix A.2.

2.2.2 Model calibration

Initial parameter set.

The first, necessary, step was to calibrate the cortical model in order to be sure that it correctly reproduces the results of biological experiments, especially the one made by Benvenuti and his colleagues on the monkey primary visual cortex with VSDI signaling [3] (Fig. 2.4). This experiment have shown the existence of anticipatory cortical waves when a white moving bar at 6°/s is presented to monkeys 4.5. The time evolution of VSDI intensity has been centered at the time which the centre of the bar is at the middle of the receptive field. This allows to show that cortical columns far from the initial bar position are activated earlier than the one close to it. This is due to an anticipation wave supported by the lateral connectivity in the cortex. More details on this mechanism are given in the next chapters.

These results had already been partly reproduced by [108] who had designed the retino-cortical model. Despite this, the first simulations carried out with the implementation described in the previous session (2.2.1) were not successful.

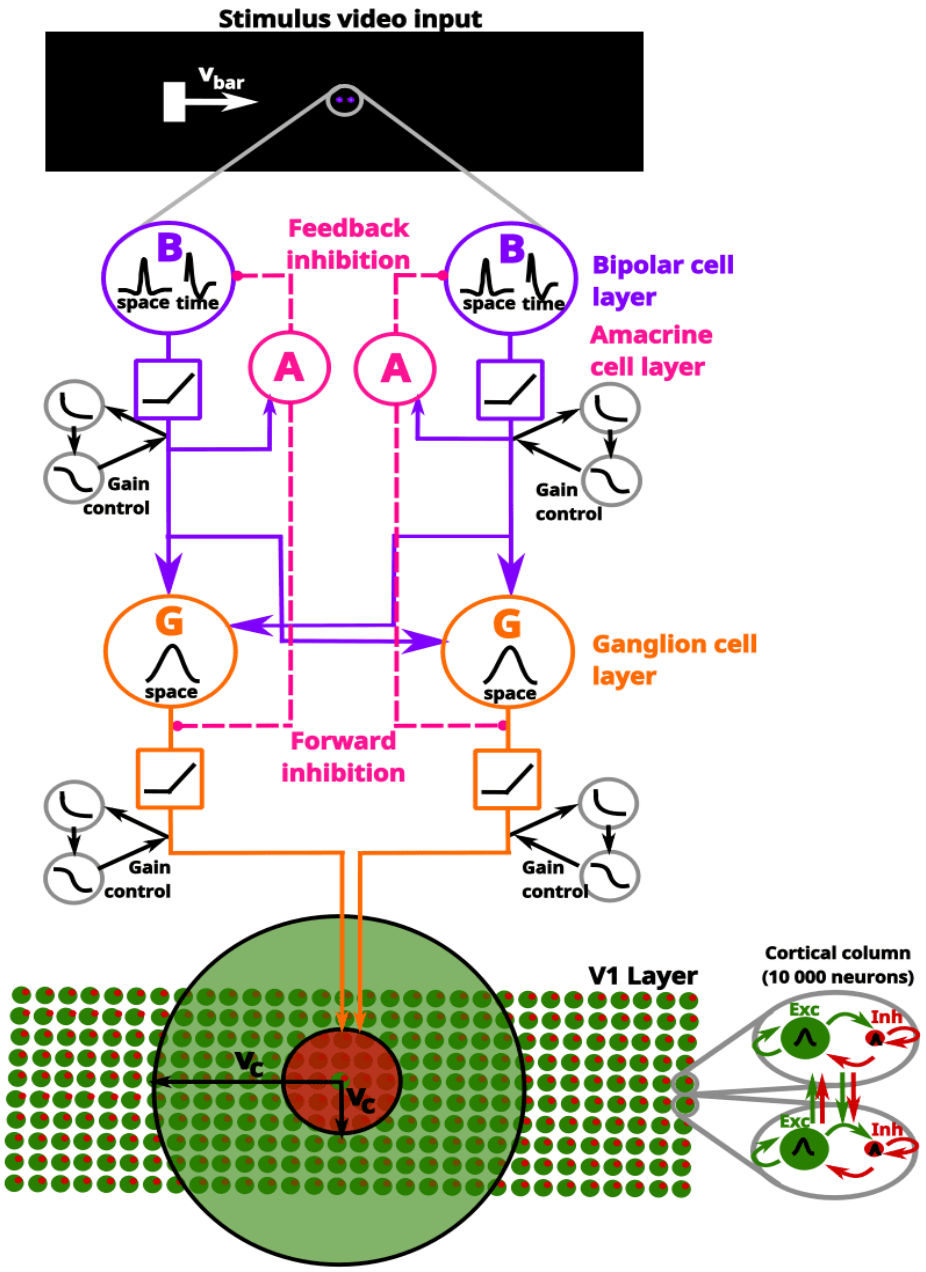

Figure 2.3: **Synthetic view of the retino-cortical model.** A stimulus is perceived by the retina, triggering a response. **From top to bottom**: The stimulus is first convolved with a spatio-temporal receptive field (black traces labelled "space" and "time" in the purple circles), that mimics in the Outer Plexiform Layer (OPL) the concerted activity of photoreceptors and Horizontal cells and is fed to Bipolar cells (purple circles). This response is rectified by a low voltage threshold (purple squares). Bipolar cells responses are then pooled to retinal Ganglion cells (orange). The firing rate response of a Ganglion cell is a sigmoidal function of the voltage (orange square). Gain control can be applied at the Bipolar and Ganglion cells level (grey circles) triggering anticipation by a shift in the time to peak. The Bipolar cells activity is modulated by lateral inhibition through Amacrine cells (pink). The Ganglion cells response (firing rate) is sent to cortical columns in the primary visual cortex depicted, at the bottom right, as two interconnected mean field units (circles) corresponding respectively to excitatory (green) and inhibitory (red) population. Cortical columns are connected together by an excitatory (big green circle) and inhibitory (big red circle) lateral connectivity. Note that we assume the same conduction velocity v_C for both connectivities.

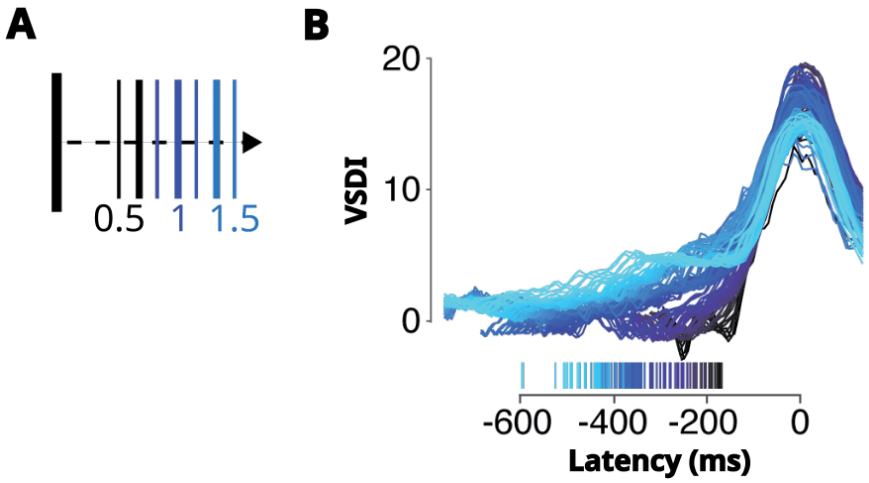

Figure 2.4: **Experimental results from Benvenuti et al. used as a calibration model A) The different bar positions** in the visual field are represented by a color gradient. The darker the colour, the closer the cortical column is to the origin of the bar. **B) Experimental response of cortical columns** located on the trajectory of a moving bar. Each curve was centered on the moment when the center of the bar was at the center of the cortical columns' receptive field.

For example, Figure 2.5 shows the very strange response obtained by our first graph and parameter set. The cortical response seems to be in a state of saturation. This saturation is caused by the presence of the external drive and the model's inability to support this input.

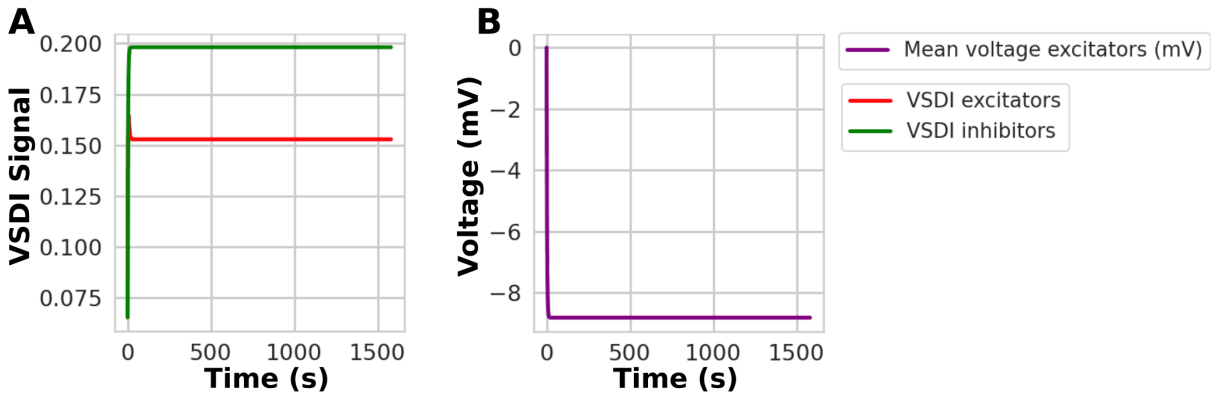

Figure 2.5: **Cortical response of the initial implementation of the retino-cortical model** with a darkfield stimulus. **A)** VSDI signal from excitators (green) and inhibitors (red). **B)** Excitatory mean voltage (purple).

Connectivity and parameters consistency

To improve the retino-cortical model, I had to expand the model's outputs to better understand the different of the equations. All of this combined with dimensional analyses of these same equations.

It was also at this stage that I added more comments and corrected the existing ones and their units. During these calibrations, I set the ganglion and cortical firing rates at 30 Hz and 40 Hz respectively modifying the value of the activity amplification factor received by the bipolar cells ($\mathcal{C}$) 1.4.1. I chose values fairly far from the saturation value (200 Hz) but not too low to give me some freedom for future experiments.

Exploring Macular enabled us to improve connectivity in our model. The cortical connections in Selma Souihel's retino-cortical model used one-to-one connectivity between excitatory and inhibitory populations. Only the intra-population connections used Gaussians. In Di Volo's case, the connections between populations of different types were made by a Gaussian. We therefore decided to use this same structure for the cortical connections in our model. To do this, we added a Gaussian connectivity from the excitatory population to the inhibitory one and vice versa.

Our aim was to incorporate additional elements of biology, under the guidance of Frédéric Chavane and Alain Destexhe. We incorporated retinal and external drive (ν_{ext}) into the excitatory inputs received by the inhibitory population. We also introduced a connectivity biased towards excitation of the inhibitory population. This translates into the implementation of an amplification factor $A_I^E = 1.5$ on the synaptic inputs coming from the excitatory population and sent to the inhibitory population (1.9).

We also discovered the presence of a variable substitution in the calculation of σ_V and τ_V. The parameters τ_E and τ_I were replaced by Q_E and Q_I respectively. In our case, this meant using much higher values for τ_E and τ_I.

It was through this further development of the retino-cortical model that we were also able to highlight a number of inconsistencies within our set of parameters. To resolve these inconsistencies, we configured a new set of parameters corresponding to the one described by Zerlaut et al. [12].

At retinal level, we decided to use ON bipolar cells and therefore to invert the stimulus contrast: a moving white bar on a black background. We also increased the size of the cortical area, the speed of the bar and the conduction speed of the fibres to get closer to that used by Benvenuti et al. Unlike Zerlaut's parameter set, we set the retino-thalamic input ν_{Aff} to 0. In fact, our input comes directly from the retinal model. We also used a much lower integration time because we observed artefacts arising from under-integration (sawtooth curve). For details of all the modified parameters in this section, please refer to the appendix A.3.1.

It was the implementation of all these changes that led to the result illustrated in Figure 2.6 A. We can see that the response of the cortical columns close to the bar are active much earlier the further they are from the origin of the bar. This means they have a greater latency. So we're seeing anticipation. However, there is also a significant drop in the VSDI signal just before its peak. This pre-peak drop is not present in the biological results of Benvenuti et al. visible in figure 2.4 B. It is therefore an artefact whose origin we need to elucidate and then remove it.

Following on from the inconsistencies noted for the various parameters, we realised the existence of the 5th spatial representation internal to Macular as detailed in the section 2.1.6. As a result, spatial parameters were overestimated by a factor of 1.7 in our simulations. The effective length of the connections was 8.7 mm instead of 15 mm for the excitators and 1.74 mm instead of 3 mm for the inhibitors. The effective fibre conduction velocity was actually 174 mm/s instead of 300 mm/s. These corrections generated a huge amount of instability in the form of oscillations and an increase in the pre-peak drop (Fig. 2.6 B). As mentioned in section 1.4.2, the cortical model is known to exhibit pathological activity in the form of regular oscillations associated with bifurcations. In specific regions of the parameters space where the small changes in parameters can shift the state of the system from a rest state to oscillations [13].

In order to remove these two simulation artefacts, carried out a new set of changes to the parameters of our model. The distance and conduction speed parameters of this set were selected to be as close as possible to those of Selma Souihel's article [14]. Details of these modified parameters can be found in the appendix A.3.2. We also removed all the cortical columns located 1 degrees or less from the edges to limit edge effects.

We also set out to drastically reduce the external drive (ν_{ext}) to avoid oscillations in the steady state. This resulted in zero mean excitatory and inhibitory discharge frequencies in the steady state.

Figure 2.7 shows the result of this simulation in this case. We note the presence of a lot of oscillations despite the set of parameters in more close to biology than the previous one. We had one major issue, the shape of the response is formed by a succession of 2 positive peaks and 1 negative drop. In this setting, the VSDI or mean voltage The pre-peak drop is even higher, without knowing why. We speculate that this shape is associated with an inhibitory/excitatory imbalance. The first rising phase would be initiated by excitatory lateral connectivity, the pre-peak drop by the arrival of too much inhibition and the second large peak by the onset of the retinal input. Lateral inhibition would therefore be stronger than lateral excitation, enough to completely counterbalance it. On the other hand, the retinal feedforward input is much stronger than the lateral connectivity, which enables it to compensate for the inhibition. The good point was that oscillations are less present for lower external drive.

Stabilisation of the cortical model

After numerous unsuccessful attempts to get rid of the oscillations and the inhibitory drop. We started to think about implementing two new properties of the retino-cortical model already studied and used by Mattéo DiVolo [13]. The first property is the use of dynamic adaptation. Adaptation is a variable reproducing neurons desensitization following a high activity. The second property is the use of a second-order retino-cortical model including the dynamics of the variances and co-variances of the sub-threshold statistical quantities (μ_V, σ_V and τ_V).

Unfortunately, the slowness of our simulations meant that we did not immediately implement these two solutions, which would have required us to implement several more differential equations. The simulation time would have been drastically increased. In preparation for work on dynamic adaptation, we modified the parameter set to use the one found in The Virtual Brain (section 2.1.6). The transfer function fitting parameters have been changed (10 parameters

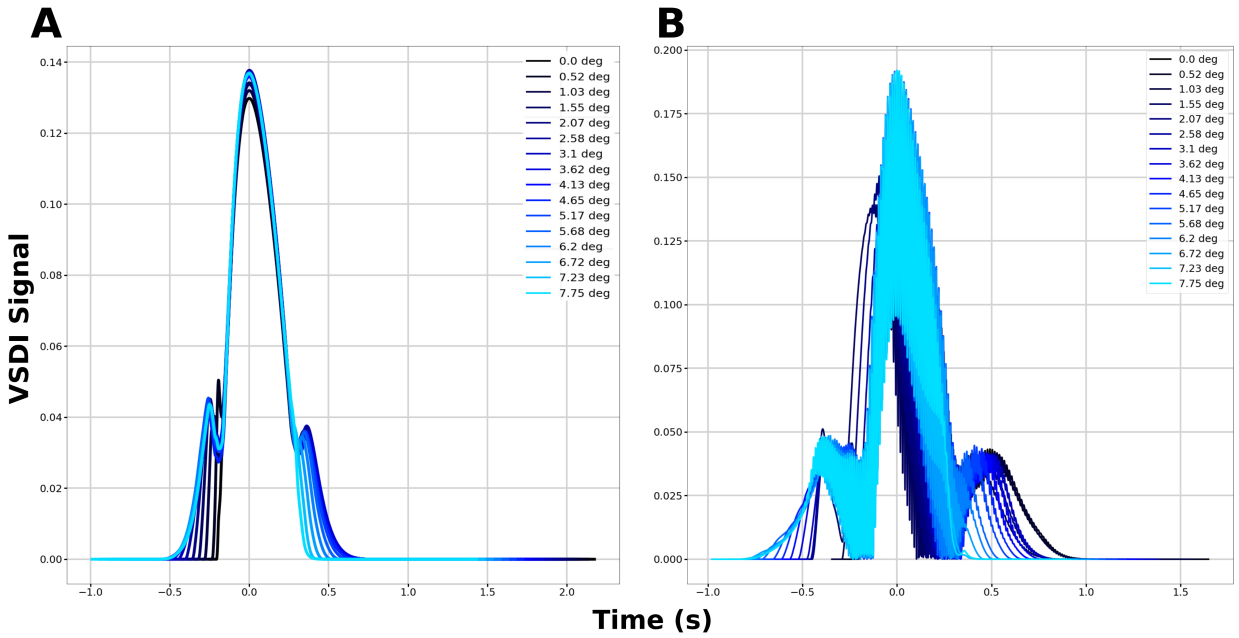

Figure 2.6: **Cortical response of the first corrections of the implementation of the retino-cortical model** with a 0.5×1.5 degrees bar moving at 6deg/s on a 31×31 cell grid of 6×6 degrees. **A)** VSDI signal with correction of inputs (retinal excitation on inhibitors, biased connectivity) and Gaussian (self-connection, equal intra and inter-layer Gaussian). **B)** VSDI signal with correction for inputs, Gaussian and spatial parameters (length of connectivity, conduction velocity). The legend on the two graphs corresponds to the position in degrees of the cortical column relative to the origin of the bar. The lighter the blue colour, the further the cortical column is from the origin of the bar.

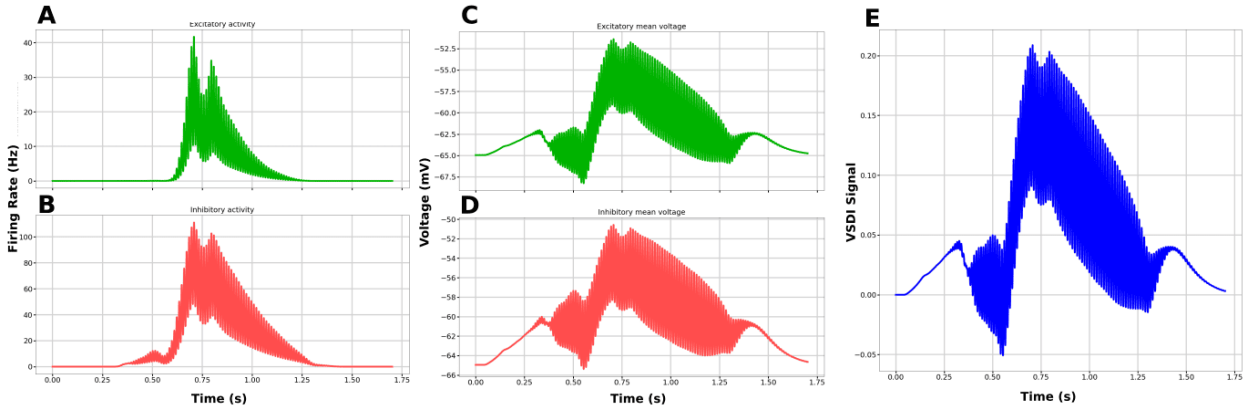

Figure 2.7: **Cortical response of the distance-optimised retino-cortical model** with a 0.67×2 degrees bar moving at 6deg/s on a 37×37 cell grid of 8.1×8.1 degrees. **A,B)** Excitatory (green) and inhibitory (red) activity. **C,D)** Excitatory (green) and inhibitory (red) mean voltage. **E)** VSDI signal.

instead of 11). This parameter set has some differences from that of Di Volo et al. [13]. All these differences are listed in appendix A.3.3. The most notable parameter is the decrease in the excitatory quantal conductance Q_E. This means that the excitation is attenuated. When we tested this new set, we noticed that these parameters were much more stable and made the oscillations disappear (Fig. 2.8 A). However, the pre-peak drop problem was still present.

In this set, we also switched to longitudinal graphs instead of square graphs. Because of the reduction in the height of the simulated area, we were forced to reduce the height of the bar, which we set equal to the new height of the simulated area. This graph format allows us to produce much longer motion trajectories while minimising the computation time required. This transition was also motivated by the desire to study the origin of the inhibitory drop. We began to think that it might be edge effects. To verify this, we wanted to increase the length of the simulated areas.

To do this, we also had to reduce the width of the area because our simulations were too time-consuming. A simulation showed that a simulation with 20×4 cells had almost the same cortical response as with 20×20 cells. The results with longer longitudinal graphs did not ultimately change anything, and edge effects do not seem to be an issue.

Balance of excitation and inhibition

The reason for the pre-peak drop was eventually found in the bipolar cells. In our retino-cortical model, retinal cells have an activation threshold. In our parameter set, this threshold was non-zero in bipolars. A parameter value inherited from Berry's model equation [1]. With this threshold to 0 mV, the drop disappears (Fig. 2.8 B). We think that this threshold excessively slows down the system's response because bipolars have to pass the threshold before to send excitation to ganglion cells. As a consequence, there is a desynchronisation in the activation of bipolar cells in response to the bar. Once this threshold was removed, all the bipolar cells in contact with the bar were activated without delay. As a result, the response of the cortical columns is also more synchronised and their response is more stable. This finally restores the balance between excitation and inhibition that had apparently been broken by the desynchronisation of responses.

According to Mattéo Di Volo's advice, inhibitors should always be 5 times more active than exictators. This was no longer true our case, the excitators were too high. So to calm the excitators we increased their inhibitory quantal conductance Q_i. This increases the inhibitors' control over the system. We also took the opportunity to reduce the value of τ_B, which we felt was too high, and set it at 50 ms. The changes made to the parameters are listed in the appendix A.3.4. The result obtained with these parameters can be seen in figure 2.8 C. We chose not to display the curves closest to the edges of the cortex, which were more strongly affected by edge effects. We can see that there is a nice anticipation with the cells far from the origin of the bar (light blue) activating before the others. There are no more oscillations or drops, just small peaks after each latency.

However, our curve is still quite different from the biological reality (Fig. 2.4 A). Indeed, our curve is too symmetrical and the latency slopes increase too abruptly. The increase in latency should be more gradual and the part of the curve after the peak should have cortical columns with more condensed response curves than the part before the peak.

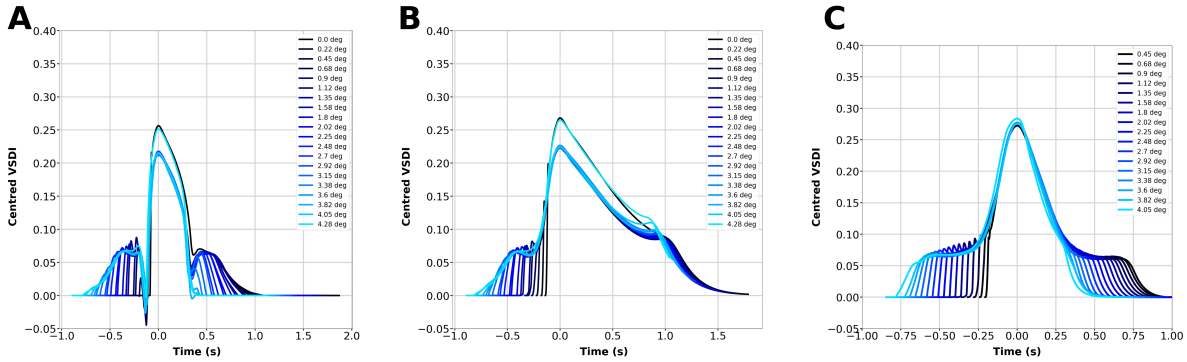

Figure 2.8: **Cortical response of the retino-cortical model with new P parameters and bipolar threshold** with a 0.67×0.9 degrees bar moving at 6deg/s on a 20×4 cell grid of 4.28×0.9 degrees. **A)** VSDI signal with the new P parameter set for the transfer function. **B)** Same as A but without bipolar threshold. **C)** Same as B with a set balancing inh/exc.

Steady-state cortical activity

The previous results were still not close enough to what we were looking for. To be viable, Di Volo's Di volo advised us on the importance of always having a cortical model in a non null steady-state activity. This is the condition that has to be met to obtain a network dynamic that is asynchronous and irregular as in an awake brain. We therefore decided to develop a set of parameters revolving around a non-negligible external drive. We set it at 2 Hz, as in Di Volo's article [13]. However, the introduction of this external drive has led to the disappearance of latency. We hypothesised that the addition of external drive increased the overall level of activity and could therefore drown out latency. To remedy this, we decreased the inhibitory quantal conductance of the excitatory population. The aim is to remove some of the inhibition received by the excitators in order to increase excitation in the network.

Inspired from biology we have also increased the size of the connections from the OPL to the bipolars by following the literature [112, 113]. The characteristic time of ganglion cells was also increased to correspond to the same value recommended by Olivier Marre. We extended it to other cells due to a lack of values in the literature.

We have also redefined the size of the graph to use the same size as Benvenuti et al. It was also at this stage that we applied our new methodology for creating stimuli as explained in the section 2.1.4. This allows us to improve the accuracy of all the model's spatial parameters and to set a frame rate equal to 60 Hz. The appendix A.3.5 catalogues all these changes in the retino-cortical model.

This new set of parameters finally produces curves very close to what we were looking for (Fig. 2.9 A). The anticipation is present, and the slopes of the latencies have no intermediate peaks or drops. They also increase much more gradually, as seen in the experiment by Bienvenuti et al. These curves are also asymmetric, as desired. The response curves after the peak are much more condensed. We believe that using a higher characteristic time of retinal cells has had a crucial effect on this loss of asymmetry by creating a terminal part of the curve that decreases more slowly.

Simulation of large cortical area

A remaining problem with this new set lies in its instability for simulations on large networks (41×15 cells), which would reduce possible edge effects and would be preferable for experiments on simulated saccades. After a series of tests, the connectivity probability parameter, known for its ability to reduce oscillations, was selected to stabilise the network. We can see that using this parameter at $pconnec = 0.0375$ ((Fig. 2.9 B) strongly alters the graph obtained previously (Fig. 2.9 A).

The last modification to be implemented was produced following the second coding sprint (November 2023) where we considerably increased the speed of Macular. This enabled us to simulate quite larger graphs: 83×15 cells (18.45×3.15 degrees) (Fig. 2.9 C). The results are close to those of the two previous models, with a clearly visible and clean anticipation. Increasing the horizontal size of the simulated area has become essential for studying the anticipation of very slow speeds or high amplitudes. Indeed, larger speeds or amplitudes increase the capacity of latency to grow over very long distances. If we want to see their dynamics correctly, the distance of the cortical area must be greater than that of the latency.

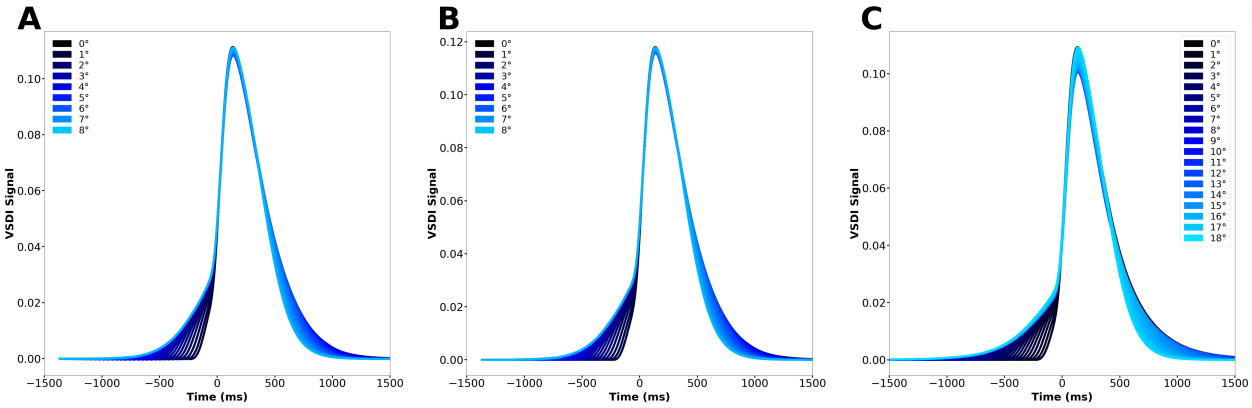

Figure 2.9: **Cortical response of the retino-cortical model with external drive non null** with a 0.67×0.9 degrees bar moving at 6deg/s on a various grid size. **A)** VSDI signal with parameter set including non-zero external drive and 41x5 graph. **B)** Same as A with a new parameter set based on a connection probability (pconnec) of 0.0375. **C)** Same as B with 83x15 cells and a new parameter set based on asymmetric retinal/cortical layers.

2.3 Conclusion

In conclusion, all of these trials and errors were gradually aggregated to give a final set of parameters detailed in the appendix A.1 and illustrated by the diagram of the retino-cortical model in figure 2.3. Throughout these simulations I developed a large number of stimuli of different proportions to adapt to each simulation.

The last result obtained highlights the success of our calibration of the retino-cortical model to reproduce the anticipation by cortical latency observed by Benvenuti [3]. We used the same speed of 6 deg/s and obtained an anticipation speed very close to theirs. Our retino-cortical model is now ready to study anticipation in more detail and continue with simulated saccade.

Chapter 3

Anticipation waves

3.1 Introduction

In this paper, benvenuti et al. [3] demonstrate the presence of an anticipatory wave that propagates ahead of feedforward bar activity in macaque primary visual cortex. This anticipation is carried by the lateral connectivity of V1. The retino-cortical model was calibrated so as to reproduce these results. Note however that, although our color gradient is similar to the one used by these authors, it corresponds to different positions. Indeed, in our simulations, the cortical area used is bigger than in their experiments (18 degrees versus 7 degrees). A larger simulated cortical area was indeed needed to be able to correctly observe the effect of certain parameters such as bar speed or cortical latency.

3.1.1 Indicators for anticipation

From now, both simulated retinal and cortical areas are 2D spaces of 81×15 retinal cells. As two consecutive retinal or cortical columns are spaced by $0.225°$ of visual angle these areas correspond to $18.225° \times 3.375°$. Using the conversion factor of about 0.3 mm per degree in the retina, approximated from `https://www.ncbi.nlm.nih.gov/books/NBK11556/` and 3 mm per degree in the cortex for humans this gives a retinal area of $\sim 5.46 \times 1\ mm^2$ and a cortical area of $54.6 \times 10\ mm^2$ with a spacing of $67.5\ \mu m$ between retinal cells and $675\ \mu m$ between cortical columns. We discard the first and the last horizontal degree in all figures to reduce boundaries effects, giving thus an effective cortical space of $16.45°$ long.

In this paper, we mainly consider the motion of a bar, moving horizontally, from left to right, along the x axis with a constant speed v_B. The bar starts to move at time $t = 0$ where the center of the RF of the cortical column located at $x = 0$ coincides with the middle of the bar. The bar has dimensions 0.67×0.9 degrees of visual angle, i.e. its height is small compared to the vertical extent of the retina and the cortex. As a consequence, we will consider, in the definition of anticipation indicators, that the bar response is characterized by two dimensional graphs, with one spatial dimension, x, and the time, t.

Cortical anticipation

In this section, we define several indicators related to the cortical activity when responding to the moving bar. These indicators are here introduced in a case where the sensory drive of the cortical model consists of the retinal response to a white bar with neither gain control nor amacrine cells. This especially means that the retina is passive. We refer this as control conditions (CTL). All parameters are given in the table A.1 of the appendix. The illustrative figure 3.1 corresponds to a bar moving at $6°/s$ (equivalent to 18 mm/s in the cortex). This is also the value of the default bar speed.

The indicators for cortical anticipation are based on the typical VSDI signal curves, shown in Fig. 3.1A, and reproducing the experimental observations made by [3]. We first define quantities attached to individual columns, i.e. depending on the spatial coordinate x.

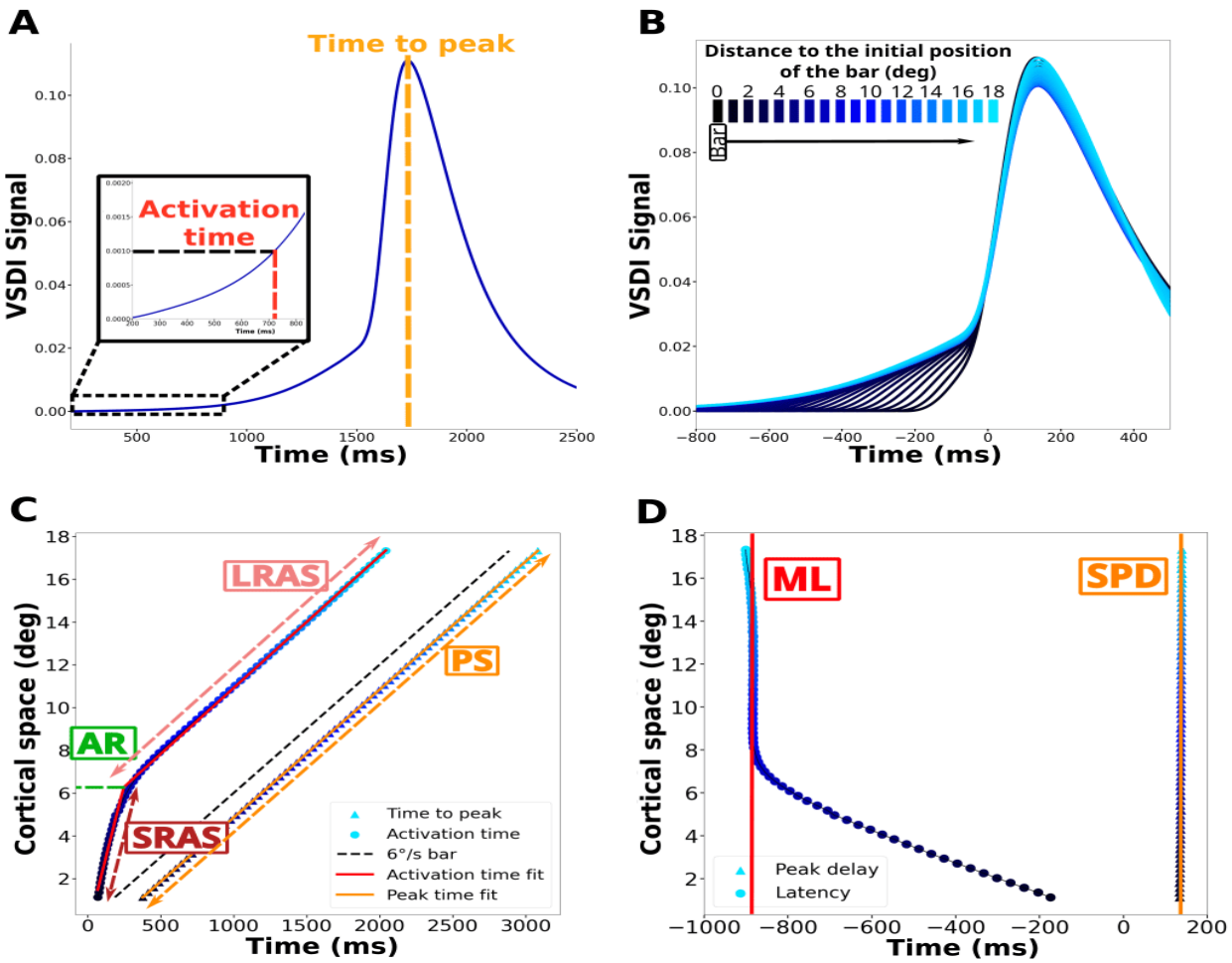

Figure 3.1: **The paradigm of cortical anticipation by latency. A) Typical time course of the VSDI signal response** for a fixed cortical column located at x. The time to peak corresponds to the yellow dotted line. The insert shows a zoom of the proximal part of the curve where the activation time is computed (the black dotted line corresponds to the threshold θ, see text.). **B) Global representation of the spatio-temporal VSDI responses using a collapse of the VSDI signals**. The curves corresponding to cortical columns located at different spatial locations are shifted so that their maximum coincides. Then, these curves are colored so that the different cortical columns positions in the V1 field are represented by a color gradient (displayed on the top of the figure), from black ($x = 0$ degree, point where the bar starts) to light blue ($x = 18.45$ degree). The legend at the top left represents the color gradient (from black to light blue) associated with the position of the cortical column. **C) inverted time space representation** where the cortical space (x coordinate, in degrees of visual angle) is represented as a function of time (in ms). The dotted black line corresponds to the displacement of the center of the moving bar. This is a straight line, $x = v_B\, t$ (the center of the bar is located at $x = 0$ when $t = 0$). The *time to peak*, $t_P(x)$, is represented by triangles, colored according to the color gradient. The curve (orange line) is a straight line too, with equation $x = v_B\,(t - t_P(0))$, where $t_P(0)$ is the time to peak for the column located at $x = 0$. The *peak speed* (PS) is the slope of this curve (thus, in CTL conditions, this is the bar speed, v_B). The activation time, $t_{ON}(x)$ is represented by circles colored according to the color gradient. The curve represents a crossover between two regimes, well fitted by straight lines (red curves), and separated by an inflection point. The spatial position of this inflection point is the *anticipation range (AR)*. The slope of the first linear part (dark red dashed arrow) corresponds to the *short-range activation speed (SRAS)*. The slope of the second linear part (light red dashed arrow) is the *long range activation speed (LRAS)*. In CTL conditions, this slope is equal to v_B. **D) Maximal latency (ML) and Standard Peak Delay (SPD)**. The cortical space is represented as a function of the latency (in ms). The latency increases until saturation (red vertical line), at a time called *maximal latency (ML)*. The peak delay (triangle) is constant and equal to the standard peak delay (SPD), (yellow vertical line).

Local indicators.

- $t_{center}(x)$ is the time when the middle of the bar reaches the center of the receptive field of the column located at x. We have $t_{center}(0) = 0$.
- **The activation time (AT)**, $t_{ON}(x)$, is the time when the VSDI signal response becomes larger than a threshold $\theta = 0.001$.
- **The latency** is $t_L(x) = t_{ON}(x) - t_{center}(x)$. Since $t_{ON}(x) \leq t_{center}(x)$, the latency can be negative or equal to 0. The latency increases therefore when its value become more negative.
- **The time to peak (TTP)** is the time $t_P(x)$ when the VSDI signal has its maximum (see Fig. 3.1B).
- **The peak delay** is $t_{PD}(x) = t_P(x) - t_{center}(x)$. This quantity can, a priori, have any sign, although in CTL conditions it is always positive. This value can be negative though due to e.g. to the retina influence.

The latency, $t_L(x)$, depends on the distance of the column to the point where the bar started. To illustrate this dependence we use a color code, similarly to the paper [3]. The different cortical columns positions in the V1 field are represented by a color gradient (see Fig. 3.1B), from black ($x = 0$ degree, point where the bar starts) to light blue ($x = 18.45$ degree). Although, for a spatio-temporal representation x, t, there is a redundancy between the x coordinate and the color, this representation is actually quite didactic and insightful. Especially, as shown in Fig. 3.1B, if one shifts all these curves so that their peak coincides, one observes a change in the shape of the response prior to the peak: the latency increases with the distance to the bar origin, so that the columns start to respond earlier and earlier. Following [3] we interpret this as a *cortical anticipation by latency*. We now introduce global indicators to quantify this form of anticipation.

Global spatial indicators. Although the latency corresponds to a time as a function of space, it is useful to invert the axes and, instead, to represent space as a function of time: the curve $t_L(x)$ becomes $x(t_L)$ by a simple symmetry with respect to the first diagonal. The cortical space, ploted in function of the activation time and the time to peak have characteristic shapes illustrated in Fig. 3.1C. This allows us to define four spatial indicator, following Benvenuti et al. [3]:

- **The anticipation range (AR)** is the maximal spatial limit of anticipation, the maximal distance at which cortical columns constructively interact to anticipate motion, as argued in [3]. It corresponds to the ordinate of the inflexion point in Fig. 3.1C. Beyond this spatial position, anticipation saturates because lateral connectivity, which causes anticipation, has a finite radius. Consequently, beyond the anticipation range, the slope of the activation time becomes constant (Fig. 3.1C), the activation time is no longer affected by the lateral cortical propagation, but only by the bar speed.
- **The short-range activation speed (SRAS)** is the slope of the activation time before the inflection point (Fig. 3.1 C). This speed, actually sums up two different contributions: the bar speed and the anticipation speed carried by lateral connectivity (Fig. 3.1C).
- **The Long range activation speed (LRAS)** is the slope of the activation time after the inflection point. This cortical region is characterized by an absence of lateral cortical connectivity influence. In our model, its slope is only constrained by the bar speed. We mention this quantity because it is expected to vary due to feedback effects [3] and would become relevant with a model including a thalamus-LGN (see discussion).
- **The Peak speed (PS)** is the slope of the time to peak curve. It is parallel to the moving bar curve. It is constant in our case, because the bar speed is constant.

Global temporal indicators. One can also plot x as a function of the latency (see figure 3.1D). We obtain two temporal indicators, illustrated in Fig. 3.1D:

- **The maximal latency (ML)**. One observes that the latency of cortical columns close from the starting point of the bar (black circles) increases until saturation as the columns are located further and further from the starting point of the bar. The saturation value is the maximal latency.
- **The standard peak delay (SPD)**. In contrast to ML, the peak delay is actually independent of x, in all the cases studied in the paper. We discuss this homogeneity in the discussion section. We call this value the SPD.

Interpretation. The figure 3.1 essentially shows that the moving bar triggers a wave of cortical activity, transmitted by the columns sensing the bar to the distant columns via the lateral connectivity, at a speed which accumulates the bar speed and the axonal velocity (Fig. 3.1B and C). This reproduces the observations of Benvenuti et al. [3] and was interpreted by the authors as an indication that cortical anticipation mainly holds by latency. The accumulation of the signals sent by the columns sensing the bar, via the lateral connectivity, advances the time when the distant

columns - not yet sensing the bar - start nevertheless to respond to it. This is the explanation of the change in the early VSDI response profile (before the peak), in Fig. 3.1B, as a function of the color gradient. One observes therefore that the latency becomes more and more negative with the distance of the cortical column to the position where the bar starts, Fig. 3.1D, meaning that the cortical columns are informed earlier and earlier that something is arriving. This observation holds until a saturation value, the maximal latency, where the gain of anticipation provided by the lateral cortical connectivity reaches a maximum. This suggests that cortical connectivity and axonal velocity impacts anticipation (sections 3.2.3, 3.2.4). As developed below, we also observe an anticipation by peak shift, where the peak in the VSDI signal is advanced with respect to the peak in the RGCs response.

Retinal anticipation

Anticipation has also been observed in the retina, according to different modalities. The first characterization was provided Berry et al. [1]. It is characterized by a shift in the peak of the ganglion cell response to a moving object, occurring before the peak response to the same object when flashed [1, 102]. This can be explained by gain control which has the effect of advancing the peak response of the cell's activity. In our model, this effect can arise at the level of BCs or RGCs. A detailed study was published in [14]. It shows that, with gain control, anticipation time grows with the size and the contrast of the bar while it decreases with its velocity. In our retina model, amacrine cells can also induce anticipation by advancement of the peak, independently of gain control, although these two effects can constructively combine. We qualify this peak shift mechanism as *peak anticipation* or *adapting anticipation* (using the terminology of [98]) since BCs and RGCs adapt according to their level of activity. Therefore, we quantify retinal anticipation by a RGC peak shift and we define the same peak-based quantities as for the cortical case (time to peak and SPD).

3.1.2 Model calibration result

The figure 3.1 illustrates the result of our model in CTL conditions, with a bar speed of $6°/s$. Our model reproduces the shape of the latency curve shown in [3], Fig. 4: cortical columns far from the bar origin are activated much earlier than the ones close to the bar origin. This curve is divided in two regimes, reproduced by our model, commented in section 3.1.1 and illustrated in Fig. 3.1. In the first regime (short-range activation) the slope have a value of $24.8°/s$ in experimental data and of $21.3°/s$ in simulated data. The inflection point differs though: $2°$ in experiments and $6.3°$ in simulations. Also, the activation in our model can occur up to 880 ms before the center of the bar arrives at the center of the receptive field (i.e. a maximal latency of -880 ms) while in [3] it is said that "latency scatter for the medium and long trajectories that fully covered a wide range of values from 0 to -400 and -800 ms". We finally note a difference in the time of the peak, very close to zero in experiments (Fig. 4D of [3]) but located at 139 ms in the simulation. To understand these discrepancies, it is important to note that our simulations are made in control conditions i.e. without any retinal anticipation mechanism, whereas such mechanisms are presumably present in experimental conditions. Indeed, as commented later, adding retinal anticipation reduces these differences (section 3.3). Taken together, these results provide a good basis for further explorations on the role of retinal and cortical effects on anticipation with discrepancies expected to be reduced in the presence of a realistic retinal input.

3.2 Cortical anticipation depends on stimulus features and on physiological parameters

We now study study, in CTL conditions, the dependence of anticipation on several parameters, such as the bar speed or contrast, and physiological parameters, such as the conduction speed following the modalities described in section 3.2. The default value of the parameters, including the bar speed, are those reported in the Appendix A.1.

3.2.1 Increasing the retinal output amplitude enhances anticipation

We varied the retinal output amplitude (ROA), sent by retinal ganglion cells, in a range from 1 to 50 Hz (figure 3.3). For this, we increased the amplitude $\mathcal{C}$ of the OPL kernel (eq. (1.1)). This has the effect of increasing the firing rate of the RGCs in a linear way (Fig. 3.2). Note that we are still in CTL conditions here, the retina is passive. Increasing the retinal input increases almost linearly the VSDI signal (Fig. 3.3 E) with a slight saturation presumably due to the sigmoid activation functions F_E, F_I in the mean field model of cortical columns (eq. (1.9)). Here, we chose to stay in the almost linear range. Indeed, we observed that increasing too much the amplitude of the input leads to pathological oscillations which, as mentioned above, are artefacts of the cortical model.

The collapse of VSDI signals, shown in Fig. 3.3 A (1 Hz) and Fig. 3.3 B (35 Hz), has globally the same shape as the paradigmatic figure 3.1A, although we observe a clear difference in the latencies between A and B. This is a first indication that increasing the ROA enhances anticipation by latency. Fig. 3.3 C shows the temporal profile of the VSDI signal for the cortical column located at the center of the lattice ($x = 9°, y = 1.35°$). One observes an increase in the slope before the peak, resulting in an increase of the maximal latency (ML) which becomes more negative as shown in Fig. 3.3 F (red trace). There is a saturation for large retinal inputs amplitude though. Along the same lines, we plot, in 3.3 D, the spatial VSDI signal for the time when the central cortical column reaches its maximum. Note that

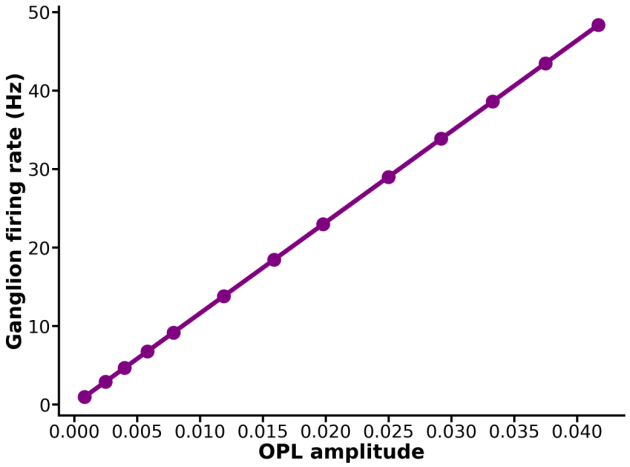

Figure 3.2: **The amplitude of the retinal output changes linearly with the amplitude of the OPL.**

the x coordinates has been shifted so that the central cortical column is actually located at $x = 0$ in this figure. We observe a spread of the left part of the peak and a more abrupt slope on the right part, as the ROA increases. Those combined effects results in a increase of the anticipation range (AR) as shown in Fig. 3.3 F (green trace), with again a saturation effect. Finally, the spatial and temporal effects combine to increase the short range anticipation speed (SRAS). Therefore, anticipation by latency becomes more prominent (ML and AR) and spreads faster (SRAS) as the ROA increases.

Interestingly, we also observe a slight anticipation by peak shift. This appears in Fig. 3.3 C where we remark a shift of the time to peak as the ROA increases. For a more quantitative study we have plotted in Fig. 3.3 H the SPD as a function of the ROA. It is constant for RGCs, but essentially decreases for the cortex. This figure also shows the difference between the cortical and retinal SPD, which is negative, meaning that the VSDI peak arises earlier than the RGC frequency peak. Thus, in addition to show anticipation by latency, the VSDI signal is also a bit in advance on the RGC peak. This effect is primary due to the cortical lateral connectivity. It decreases when the cortical extent decreases as further commented in section 3.2.3. It is enhanced when the retinal input increases, up to some maximum at about 35 Hz, where the difference is maximal, i.e. where the VSDI peak anticipates the most the RGC frequency peak. However, beyond 35 Hz, we start to observe (small) oscillations in the VSDI signal so that the increase of the curve after 35 Hz might be an artefact of the model. It is interesting to note that even at small retinal amplitudes (1Hz), the cortex remains 8.8 ms ahead of the retina. In Fig. 3.3 I we have plotted the time profile of the frequency response near the peak for the central RGC, and, in Fig. 3.3 J, the time profile of the VSDI, near the peak for the central cortical column. The red traces correspond to a 1 Hz ROA and the green traces to 35 Hz. The green traces have actually been rescaled to match the amplitude of the red ones. This is to show that, in addition to a simple rescaling (which makes the RGC response overlap in Fig. 3.3 I), there are, in the cortex, non linear effects which modify the shape of the response and thereby impact the anticipation.

To summarize, an increase in the ROA non-linearly enhances the anticipation which extends further, earlier and faster, with a saturation when the amplitude of the retinal input becomes too large. Rising the ROA increases the overall activity level transmitted laterally by cortical columns. Thus, more distant cortical columns are above the threshold earlier as shown by the increase in ML and AR. The results also demonstrate the presence of a mechanism in the cortex enabling anticipation by peak shift, an effect which increases with the amplitude of retinal input. This effect is quite weaker though than the anticipation by latency (maximum 15 ms for the peak delay and minimum 200 ms for the latency).

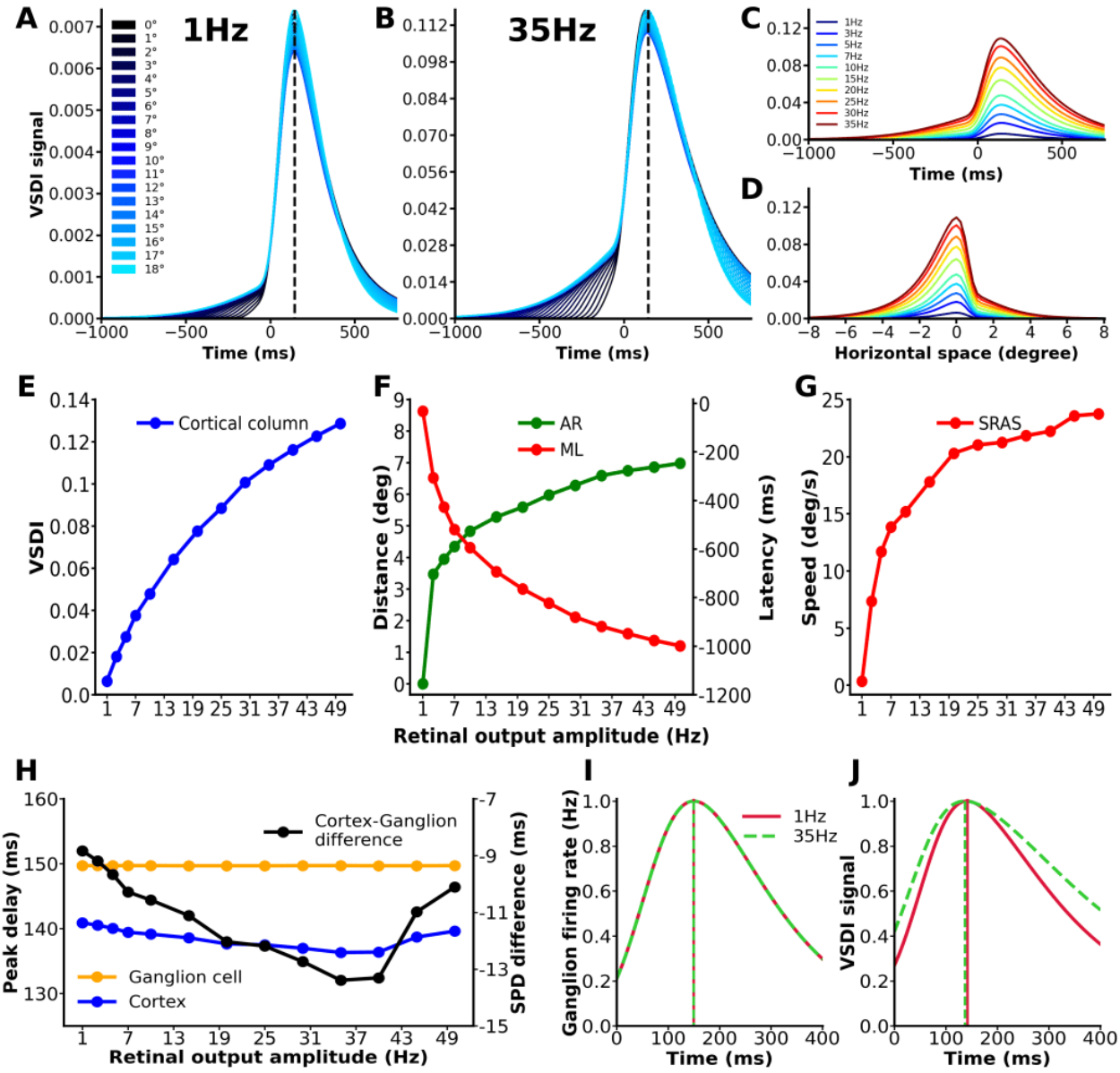

Figure 3.3: **The effect of the retinal output amplitude (ROA) on the cortical response. VSDI signal response to ROA at A,** 1 **Hz and B)** 35 **Hz.** The color bar on the left of Fig. A represents the color gradient introduced in section 3.1.1. **C) Temporal VSDI signal** in response to increasing retinal amplitude for the cortical column located at the center of the lattice ($x = 9°, y = 1.35°$). **D) Spatial VSDI signal** in response to increasing retinal amplitude, for the time where the central cortical column reaches its maximum. The x coordinates has been shifted so that the central cortical column is actually located at $x = 0$. **E) VSDI signal amplitude** of the central cortical column versus the ROA. **F) Temporal and spatial indicators**: maximal latency (red, scale on the right) and anticipation range (green, scale on the left) versus the ROA. **G) Speed indicator**: short-range activation speed (red) versus the ROA. **H) Retino-cortical SPD variation** versus the ROA for the central cell. The ganglion firing rate SPD is plotted in orange and the VSDI signal in blue (scale on the left). In black, is represented the difference between the cortical and RGC SPD (scale on the right). A negative value means a cortical peak arising earlier than the RGC peak. **I) Shape of the central RGC response profile to the moving bar**, for 1 Hz (red) and 35 Hz (dashed green). Note that the red trace is normally quite smaller than the green trace, but we have rescaled it to show that the difference between 1 Hz and 35 Hz, at the retinal input level, is only a rescaling. This contrasts with **J) VSDI signal**, where the same rescaling let also appear distortions due to the non linearities in the cortical model. The dotted vertical lines in I, J correspond to the peaks in the RGCs firing rate or VSDI signal at 1 Hz (red) and 35 Hz (green).

Stimulus contrast. We assessed the impact of the stimulus contrast in the movies by increasing it from 0.1 to 1 by increments of 0.1. As we checked (Fig. 3.4) the effect is completely equivalent to increasing the amplitude $\mathcal{C}$ of the OPL kernel and thus, the amplitude of the retinal input.

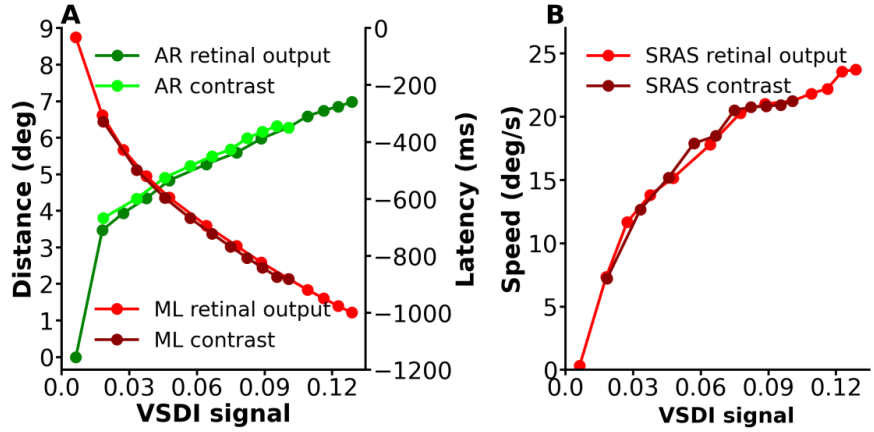

Figure 3.4: **Stimulus contrast and retinal output amplitude comparison. A) Temporal and spatial indicators in function of VSDI amplitude**: Maximal latency with retinal output (red) or stimulus contrast (dark red) variant. Anticipation range with retinal output (green) or stimulus contrast (light green) variant. **B) Speed indicator**: short-range activation speed with retinal output (red) or stimulus contrast (dark red) variant.

3.2.2 Cortical anticipation non monotonously depend on the bar speed

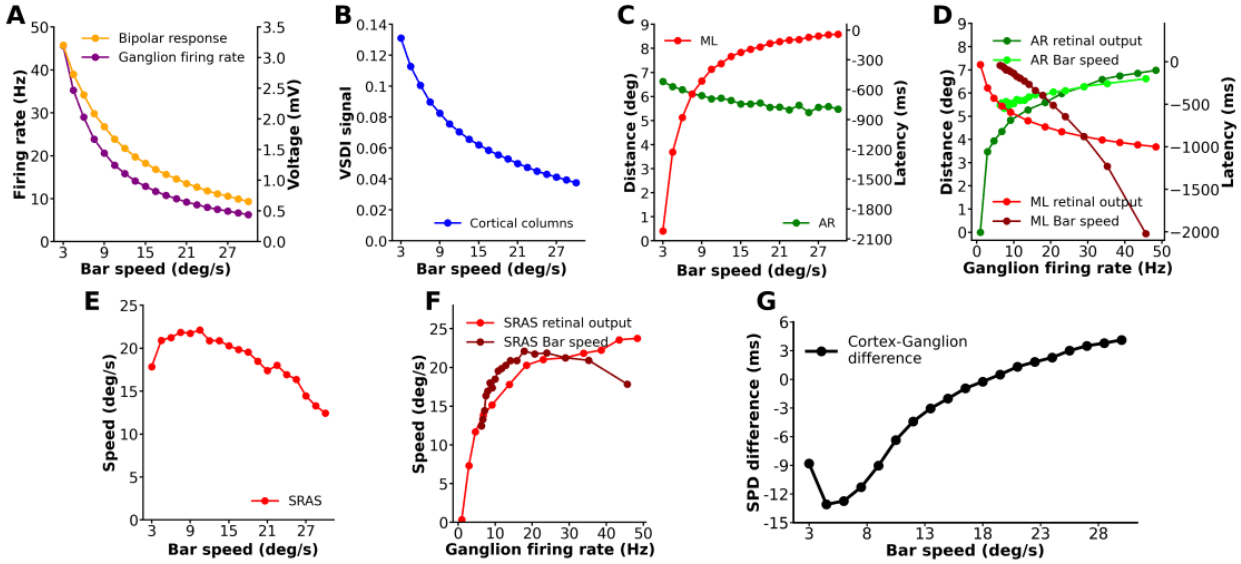

Figure 3.5: **The effect of the bar speed on the cortical response. A) decay** of the BC voltage peak and RGC firing rate (ROA) as the bar speed increases. **B) VSDI signal amplitude** of the central cortical column. **C) Temporal and spatial indicators**: maximal latency (red) and anticipation range (green) in function of the bar speed. **D) ML and AR as a function of the RGC firing rate**, in the case where the firing rate is constrained by the retinal input (red for ML, dark green for AR) and in the case where the firing rate is constrained by the bar speed (brown for ML, light green for AR). **E) Speed indicator** : short-range activation speed (red) versus the bar speed. **F) SRAS as a function of the ganglion firing rate**, in the case where the firing rate is constrained by the retinal input (red) and in the case where the firing rate is constrained by the bar speed (brown). **G) SPD difference** between cortical VSDI and ganglion firing rate.

We have done simulations with speeds ranging from $3\ ^\circ/s$ (equivalent to 18 mm/s of the cortex) to $30\ ^\circ/s$ (resp. 90 mm/s in the cortex), still in conditions where the retina is passive, with the default parameters of Appendix A.1. Our results are summarized in Fig. 3.5. The first remark is that, increasing the bar speed decreases the amplitude of the

retinal input. This is because the OPL kernel $\mathcal{K}_{B_i}$ in eq. (1.1) has less time to integrate the stimulus. We actually see the decrease in the BCs activity and RGCs activity as the bar speed increases (Fig. 3.5 A). This induces a decrease in the VSDI signal activity (Fig. 3.5 B). Thus, from the conclusions of the previous section, one expects a reduction of the anticipation by latency. Increasing the bar speed indeed diminishes the ML and the AR (Fig. 3.5C).

Is this effect on ML and AR only due to the ROA reduction or are there more subtle, non linear, effects hidden ? To address this question we plotted ML, AR as a function of the ROA itself controlled by the bar speed and compared to the case of Fig. 3.3 F where the ROA was under direct control. (Fig. 3.5 D). For the range of bar speeds that we explored the ROA varies in the interval $[10, 45]$ Hz, a bit less that the range of retinal inputs explored in the previous section. In the common interval of variation, we observe that the AR, when it is controlled by a direct variation of the ROA (dark green curve) behaves almost linearly, similarly to the case when the retinal input is tuned by the bar speed (dark green curve), although with a smaller slope in this case. In contrast, the ML decreases non linearly, and goes to saturation when the ROA is directly tuned (red trace) whereas it decreases sharply and slightly non linearly in the case where the ROA is tuned by the bar speed (brown trace). This evidences that the decay in ML and AR versus the bar speed is not only due to the decay in the ROA but includes additional, non linear effects.

Similarly, we studied the effect of the bar speed on the SRAS, Fig. 3.5 E. This quantity shows an increase up to $9°/s$ (2.7 mm/s in the retina, 27 mm/s in the cortex), then a decrease, suggesting the existence of a range of preferred speeds where anticipation by latency is optimal. Note that this effect cannot be explained only by the decrease of the ROA, as shown by Fig. 3.5 F. The red trace (direct control of ROA) is rather different from the curve where ROA is controlled by the bar speed (brown trace).

One actually expects three distinct effects as the bar speed increases. First, a decrease of the VSDI signal, since the OPL convolution kernel has less time to integrate the stimulus, directly impacting the anticipation. Second, a cortical column integrates the retinal signal as well but if the speed of the bar is very small (say, even static) its response occurs within a characteristic time quite shorter than the time it takes to the bar to reach the next column. In other words, when the bar arrives to the next column, the activity coming from the previous one has dropped to zero. This does not allow the columns to build up a non linear propagating front travelling faster than the bar. As the bar speed increases this front takes place and anticipation gradually increases. However, the lateral cortical connectivity has less time to build up long range excitation. Thus, as a third effect, the activity generated by this bar eventually catches up the one carried by the lateral connectivity. In consequence, the speed of anticipation is gradually overwhelmed by the speed of the bar. This last effect explains the maximum observed in the SRAS. Beyond this point anticipation by latency is more and more driven by the decay of the VSDI signal, as the bar speed approaches the conduction speed (although we are far from this limit in our bar speed range).

Finally, we investigated the role of the bar speed on the anticipation by peak shift (Figs. 3.5 G). The SPD shows up a minimum at about $4.1°/s$, where the advance of the cortical SPD with respect to the RGC SPD is maximal. After this minimum there is a non linear, sigmoidal like, increase of the SPD, which switches from negative to positive at about $16°/s$. Thus, for larger speed, the cortical peak is delayed with respect to the RGC peak. This effect of the SPD can be explained as follows. An increase in the speed causes a reduction in the RGC response (Fig. 3.5 A) and cortical SPDs before stabilising above $9\ °/s$. The RGC SPD actually stabilizes at a time which is nearly the characteristic integration time of the RF, about 100 ms, as expected from a direct integration of (1.1). This explains the observed saturation.

To sum up increasing the bar speed first decreases the amplitude of the retinal input. In parallel, one observes a monotonous decrease of ML and a (moderate) decay of AR. However, this detrimental effect on anticipation is not only due to the decay of the output; additional, non linear effect take place. This is prominent when observing the SRAS which shows a "preferred" speeds range (at about $9°/s$) where it is maximal. This preferred speed is also the place where the SPDs of RGCs and cortex saturate. We also observe a slight anticipation by peak shift (overwhelmed by anticipation by latency) with a "preferred" speed at about $4.1°/s$.

3.2.3 The role of excitatory and inhibitory connections length on cortical anticipation

We have next explored the influence of the excitatory and inhibitory connectivity lengths on cortical anticipation, an effect which cannot be studied experimentally (Fig. 3.6). We need to recall first a salient feature of the model. The cortical connectivity is modeled by a *normalized* Gaussian kernel (section 1.4.2, eq. (1.11)) where the cortical extent (excitatory or inhibitory) is the mean square deviation of the Gaussian. As a consequence, the shorter the cortical extensions, the more the Gaussian connectivity profile is concentrated around the cortical column's receptive field, with a higher weight. Inversely, increasing the cortical extensions spreads the Gaussian and reduces its weights. Therefore, acting on the Gaussian mean square deviation dramatically influences the value of the mean cortical column voltage for the excitatory and inhibitory populations as well as their polarisation in the steady state, with, thereby a significant impact on the VSDI signal, AR, and ML. This is illustrated in Fig. 3.6.

We maintained the ratio between the two respective lengths to a constant ratio of 0.2 so as to keep the balance between excitation and inhibition extents. The excitatory extent was then varied from 1° to 7° and the inhibitory extent from 0.2° to 1.4°. The first prominent effect, observed in Fig. 3.6 A, is the behaviour of the VSDI signal. In contrast to the previous cases, it is non monotonous. It decays up to a minimum at about 2° before increasing. To better understand this behaviour we have plotted, in Fig. 3.6 E, the peak of the excitatory mean voltage (called $\mu_{V,E}$ in the appendix B.1) as a function of the excitatory cortical extent (dark green) while the light green curve represents the excitatory mean voltage at rest. The difference between the two, "mean voltage difference", is shown in Fig. 3.6 F (dark green). Likewise, Fig. 3.6 G shows the peak of the inhibitory mean voltage (brown) and inhibitory mean voltage at rest (red), while the red trace in Fig. 3.6 G shows the difference between these two quantities. The total VSDI signal as a function of the cortical extent is a linear combination of these two traces, (eq. (B.11), appendix B.1).

When the cortical extent increases from 1° up to 2° we observe that the excitatory and inhibitory mean voltages increase while the mean voltage differences decreases, explaining the observed decay of the VSDI signal. This decrease is due to the fact that the mean voltage at rest increases faster than the peak mean voltage, for both population. As anticipated above, this behaviour can be explained by the Gaussian connectivity profiles. Increasing the cortical length decreases the intensity of the coupling between two cortical columns. Short extensions give a concentrated Gaussian with strong weights but short range influence. When the inhibitory cortical extent is 0.2° (resp. 1° for the excitatory cortical extent), the inhibitory Gaussian is so concentrated that its weight far exceeds that of the excitatory. This inhibitory dominance gives rise to a strong steady-state hyperpolarisation and an overall sensitisation of the cortical column which reacts more strongly to the stimulus. This hyperpolarisation is reduced by the elongation of the inhibitory extensions above 0.2°. This mean votage difference decreases leading to a reduction in the VSDI. From 2°, we observe a decay in the steady state voltage for excitatory and inhibitory population, corresponding to a new phase of hyperpolarisation at rest. When the cortical extent increases, the excitatory and inhibitory weights decrease thereby diminishing the mean voltage at rest. In contrast, the mean voltage peak increases for excitators and have a moderate variation for inhibitors. As a consequence, the mean voltage differences increase, leading to an increase of the VSDI.

We observe a positive effect on anticipation by latency since AR and ML increase when the cortical extent increases (Fig. 3.6 B) as well as SRAS (Fig. 3.6 C) with a saturation for an excitatory and inhibitory length respectively at 7° and 1.4°. Here, it is interesting to note that the measured AR is always larger than the length of the corresponding excitatory connectivity (black dotted line, Fig. 3.6B). The cortical columns are therefore influenced beyond the excitatory extent, and, therefore also earlier, promoting anticipation. This is particularly true up to 4° where this effect is maximal. Beyond 7°, the AR and ML start to saturate. We believe that this arises because the Gaussian extent increases at the expense of proximity activity until the weights on the periphery of the Gaussian become insufficient to activate the cortical columns, corresponding to this limit of 7°.

We observe that the SPD is also affected by the increase in cortical extent, Fig. 3.6 D. For cortical extent smaller than 2° the cortical peak is delayed with respect to the RGC peak. In particular, as the connections length tends to 0, the SPD difference (black trace) in Fig. 3.6 tends to 0. This justifies our comment in section 3.2.1 where we claimed that the difference between RGC and VSDI SPD is primary due to the cortical lateral connectivity. Beyond 2° the cortical SPD decreases (while the RGC SPD obviously stays constant), Fig. 3.6 D, so that the VSDI signal peak is more and more in advance to the RGC peak with a saturation at about 5°. The time scale of this peak delay (maximum -14 ms) is quite lower than the ML though.

Therefore, anticipation is enhanced by increasing the length of excitatory and inhibitory fibres at a constant ratio for values inferior to 7°. This improvement also involved an earlier shift in the VSDI peak. These effects are highly dependent on changes in the Gaussian profile. The effect is the strongest with an excitatory length of 4° and an inhibitory length of 0.8°. This is close to the physiological connectivity that we use in the rest of the paper.

3.2.4 The role of conduction velocity

We finally investigate the influence of fibre conduction velocity between cortical columns on anticipation in control conditions (Figure 3.7), in the range $100 - 333\ ^\circ/s$. The effects are rather easy to resume and are shown in Fig. 3.7. There is no effect on the VSDI signal. The ML slightly decreases while the AR slightly increases. More interesting is the behaviour of SRAS which is increasing almost linearly. In the paper [3] Benvenuti et al. proposed a phenomenological, physiologically plausible model of lateral cortical integration in response to a moving bar (Fig. 3 of their paper). In their model, SRAS increases linearly with a 1:1 ratio to the fibre conduction speed (Fig. 3D of their paper). In our model, which integrates more biological features, we also observe a (quasi)-linear behaviour but the slope, ~ 0.035 is far from 1. In our opinion, this is because they only used lateral excitation while inhibitory lateral connectivity also plays an important role. Inhibition acts as in impediment to the activation of cortical columns, explaining the small slope. The increase in fibre conduction speed is also accompanied by a very slight decrease of 0.6 ms in the shift between the cortex and the ganglion cells SPD (3.7 E).

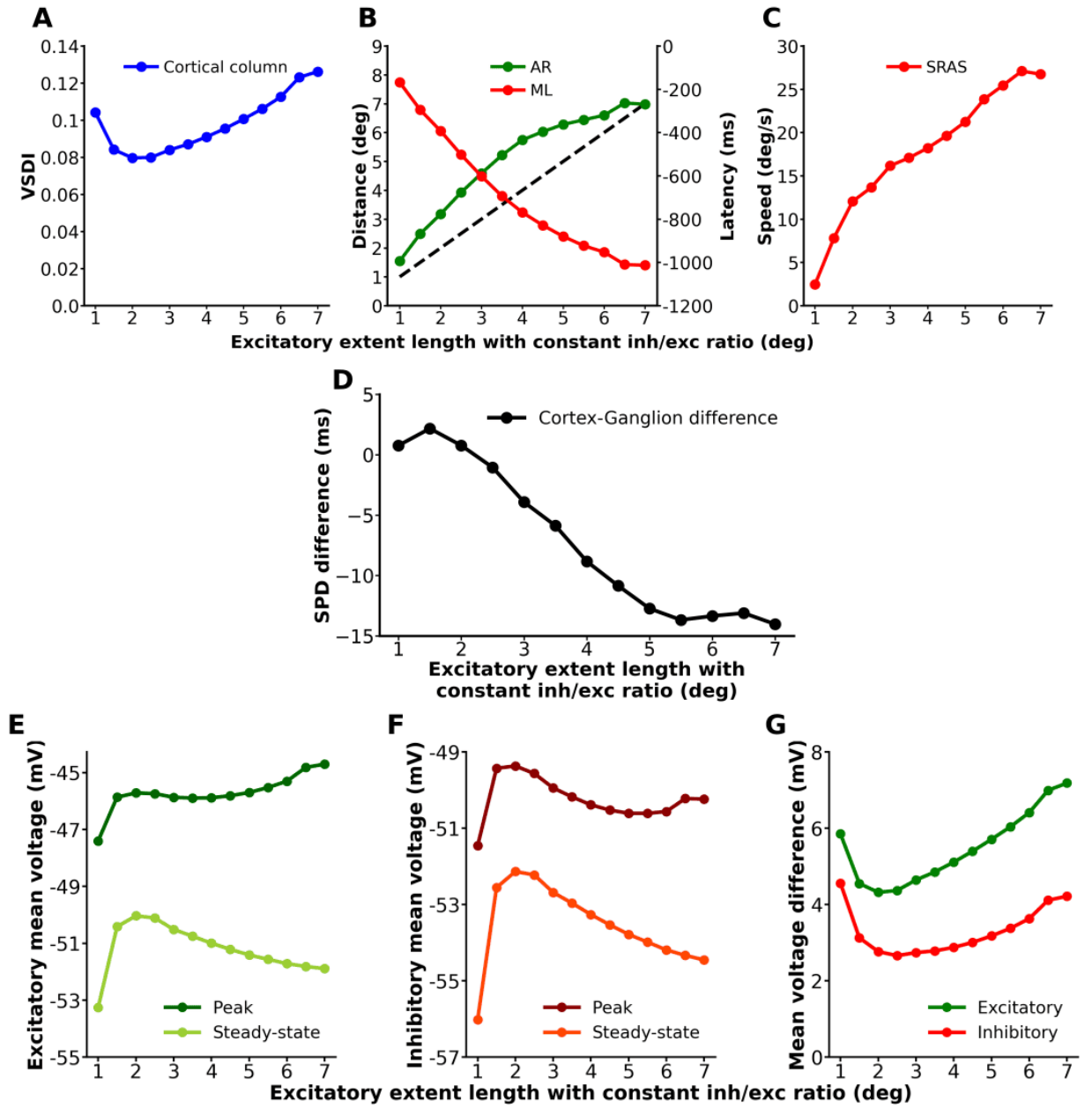

Figure 3.6: **The effect of excitatory and inhibitory connectivity length on the cortical response.** In the whole figure, the variable on abscissa is the excitatory cortical extent, but recall that there is a constant ratio with the inhibitory extent. **A) VSDI signal amplitude** of the central cortical column versus the cortical extent length. **B) Temporal and spatial indicators:** anticipation range (green) and maximal latency (red) in function of excitatory. The black dotted line represents the equality between distance and length of excitatory connectivity. **C) Speed indicator :** short-range activation speed (red) in function of excitatory extent. **D) Difference** between RGC SPD and VSDI signal SPD. **E) Excitatory mean voltage** at the peak (dark green) and at the steady-state (light green). **F) Inhibitory mean voltage** at the peak (dark red) and at the steady-state (light red). **G) Mean voltage peak amplitude** for excitators (green) or inhibitors (red). This is the difference between the average peak voltage and the steady state voltage.

To sum up, the only remarkable effect induced by an increase in the conduction velocity is a linear increase in the SRAS, similar to what has been conjectured by Benvenuti et al. in [3], but with a quite smaller slope, due to lateral inhibition.

We have shown that our cortical model can reproduce the cortical anticipation observed experimentally, although with some quantitative discrepancies, and explored effects that cannot be studied in an experimental setting. The anticipation

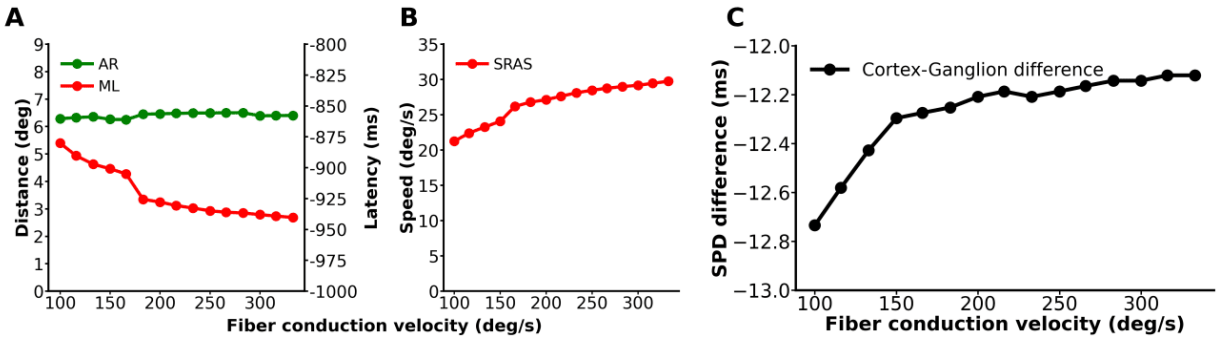

Figure 3.7: **The effect of fibre conduction velocity on the cortical response A) Temporal and spatial indicators:** anticipation range (green) and maximal latency (red) in function of excitatory and inhibitory extent. **B) Speed indicator:** short-range activation speed (red) in function of fibre conduction velocity. **C) Difference** between RGC SPD and VSDI signal SPD.

in our model clearly results from the propagation of activity in an excitatory/inhibitory balanced horizontal network. We have also shown that, in addition to latency, cortical anticipation has a peak shift component. The ability of this system to anticipate is closely linked to a few parameters. Increasing the amplitude (Fig. 3.3) or the length of connectivity at a constant inh/exc ratio (Fig. 3.6) improves the ability to anticipate by shift and latency. On the contrary, increasing the speed of the bar (Fig.3.5) first increases anticipation then decreases it, beyond a "preferred speed". Finally, increasing the conduction velocity of cortical fibres (Fig.3.7) allows anticipation to propagate more rapidly in the cortex, as expected. This propagation remains limited by inhibition though.

3.3 Cortical anticipation is influenced by the retina

We now investigate how the cortical response behaves if the retinal drive is itself generating peak anticipation during the integration of the motion. Our retina model first implements gain control following [1, 102]. This has the effect of advancing the peak response of ganglion cells' activity. The effect increases with the size and the contrast of the bar while it decreases with its velocity [108, 114]. Anticipation in the retina can also be studied from the point of view of the population, taking into account the interactions between the different cells. We have therefore implemented amacrine cell connectivity and designed a retinal circuit capable, under certain conditions, of improving retinal anticipation. Theoretical and numerical results concerning the role of lateral connectivity in retinal anticipation of motion trajectories can be found in [108, 114]. Note that, in general, these mechanisms generating peak anticipation also modify the time profile of the RGCs response to the moving bar (see Fig. 3.8 E, 3.10 E). The resulting effect on the cortical response is thus not only a shift in the VSDI signal peak, but a change in its global shape as well (see e.g. Fig. 3.8 F, 3.10 F or Fig. 3.12). This entails potential changes in the VSDI signal amplitude and in the latency. In general, the global effect is quite entangled.

Gain control and amacrine cells connectivity cause, on one hand, a decrease in the ROA, and on the other hand, a shift of the response peak earlier while changing its shape. Now, as we saw above, decreasing the amplitude of the retinal input impacts the cortical response. Thus, to isolate the effect of e.g. gain control on anticipation we need to compare the situation with gain control to the situation with no gain control, while the ROA are identical. The set of control simulations where no effect (gain control or amacrine cells network) is present, but where the amplitude of the retinal input is rescaled to match the case where the effect is present is called "equivalent retinal output amplitude" (EROA).

3.3.1 Gain control in the retina enhances cortical anticipation

In the model, gain control can be present in BCs or RGCs. We ran simulations with increasing values of the strength of these two gain controls and compare these results to EROA conditions.

Variation of BCs gain control. We first simulated the response to the moving bar with a bipolar gain control (parameters h_B in eq. (1.2)) varying between 0 and 9.2 mV/s. As shown in [108, 115] gain control triggers the appearance of adapting anticipation in the cortex. We investigate here what is the induced effect on cortical anticipation, by latency and by peak shift.

The increase in h_B is first associated to a moderate decrease in the amplitude of the VSDI signal (Fig 3.8A). This was expected since the strength of gain control in BCs reduces the amplitude of the retinal response. We observe however a slight deviation of the VSDI signal compared to the EROA condition: the amplitude of the VSDI signal remains larger. This is because, when h_B increases, gain control changes the shape of the BC response (not shown) and thereby the

RGC profile integrated by the cortex (Fig. 3.8 E, F). Anticipation by latency (AR and ML) is slightly favoured for small values of h_B (≤ 4.3 mV/s) before being attenuated. There is no difference with EROA for AR. In the case of the ML, the decreasing regime is less marked than for EROA condition. For a gain control of 9.2 mV/s, ML increases by 7.6% more than EROA (Fig. 3.8 B). This indicates an additional positive effect of gain control on ML, which partially compensates for the anticipation decay due to retinal amplitude output reduction. The SRAS increases much more than in the EROA condition (Fig. 3.8 C). In comparison, it is 26.7% faster than the speed observed in EROA for BCs gain control at 9.2 mV/s. This effect is strong enough to compensate and even reverse the slight decrease due to the reduction in the amplitude of the retinal input.

Concerning the anticipation by peak shift, the presence of BCs gain control results in a -77 ms (-51.5%) increase in RGC SPD between $h_B = 0$ and $h_B = 9.2$ mV/s (Fig. 3.8 E). This is accompanied by an earlier shift in the cortex peak of -72.5 ms (-53%) (Fig. 3.8 F), corresponding to a strong anticipation by peak shift. Note the difference in the response profiles for $h_B = 0$ (red traces) and $h_B = 9.2$ mV/s (green dashed traces) in the RGC response and in the VSDI response. Fig. 3.8 D illustrates the evolution of the RGC SPD (orange trace), the cortical SPD (blue trace), and the difference of these two quantities (black trace). This difference shows a maximum at $h_B = 4.9$ mV/s.

To sum up, this study demonstrates the direct influence of retinal peak anticipation on the cortex when increasing the BCs gain control. BCs gain control induces a earlier shift of the RGC peak, a reduced amplitude in the retinal input, and a change in the RGC response profile, with a corollary anticipation in the VSDI signal, by adaptation and by latency. However, the impact on anticipation depends on the level of BCs gain control. For small h_B (≤ 4.9) the main effect is an increase in the peak shift with no significant effect on the cortical anticipation by latency. For larger h_B anticipatory waves propagate faster (SRAS) than in EROA condition but with a reduced latency (ML) and a reduced range at which cortical columns begin to anticipate (AR). Large h_B lead to a reduction in the peak shift of the cortex, detrimental effects on ML and AR, while SRAS saturates. This suggests therefore that there is an optimal value for BCs gain control.

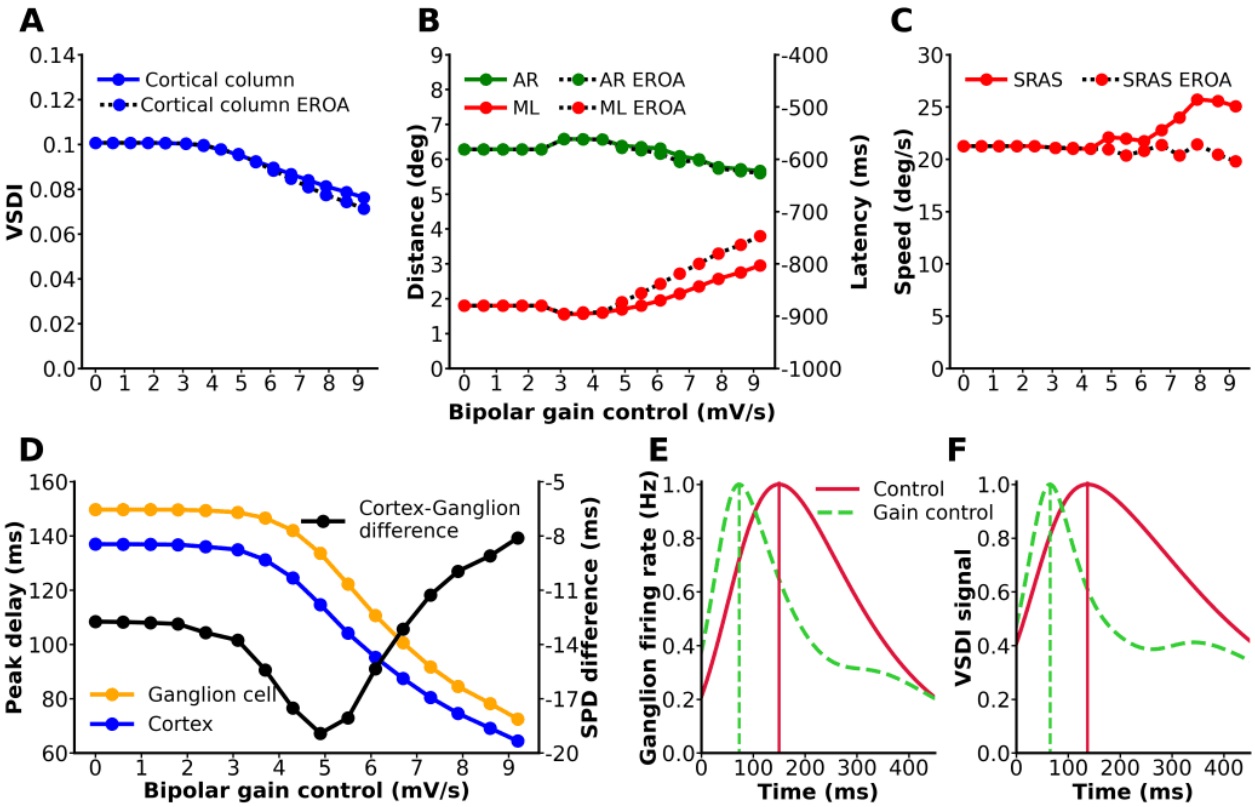

Figure 3.8: **The effect of bipolar gain control strength, h_B, on the cortical response. A) VSDI signal amplitude** of the central cortical column versus h_B. **B) Temporal and spatial indicators:** anticipation range (green) and maximal latency (red) versus h_B. **C) Speed indicator :** short-range activation speed (red) in function of bipolar gain control weight. In A, B, C, we also drawn the Equivalent Retinal Output Amplitude (EROA) curve. This is the dotted black curve with the same coloured symbols. **D) SPD** for RGCs (orange), VSDI signal (blue) for the central cell (scales on the left) and difference between RGC SPD and VSDI signal SPD (black, scales on the right). **E) Shape of the central RGC response profile to the moving bar**, without gain control (red) and with BC gain control (dashed green). Note that the two traces have been rescaled to have the same maximum. This is to emphasize the change in the shape of the response induced by BCs gain control. **F) VSDI signal**, same conditions. In E,F, the dotted lines correspond to the peaks in the RGC firing rate or VSDI signal without BCs gain control (red) and with it (green).

Variation of RGCs gain control. Here, we varied the RGCs gain control, h_G, from 0.18 mV^{-1}Hz to 0.54 mV^{-1}Hz (Fig. 3.9). Note that the range of values is very different from BCs gain control because the non linearity in the gain function is quite different (see eq. (1.5) versus (1.8)). The result shows strong similarities with BCs gain control though. The first similarity is that the stronger the gain control, the lower the VSDI signal (Fig. 3.9A) with a similar range of values, although the decay of the VSDI signal curve is identical to the EROA condition and has a different profile than for BCs gain control. As a second similarity, the RGCs gain control reduces AR and ML (Fig. 3.9B). However, this reduction is steeper and monotonous. Compared to EROA condition, AR remains unchanged while ML increases slightly (6.1% at 0.54 mV/s). The SRAS curve shows, in contrast, a big difference with the bipolar case. SRAS increases up to $h_G = 0.29$ mV/s before decreasing slightly (Fig. 3.9C). The EROA curve shows a smaller increase and a larger decrease. RGCs gain control has therefore a positive effect on SRAS (21.9% at 0.54 Hz). This effect is opposed to the negative effect of retinal amplitude reduction. Below 0.29 mV/s, the positive effect predominates before being overwhelmed by the reduction in retinal amplitude.

We observe an increase in the peak shifts in the retina and in the cortex by the addition of RGCs gain control. The RGCs arises 50.5 ms earlier for $h_G = 0.54$ mV/Hz compared to control conditions, $h_G = 0$ (Fig. 3.9 E) while the cortical SPD occurs up to 52 ms earlier (-38.1%) in the cortex (Fig. 3.9 F). As shown by Fig. 3.9D, when h_G increases, the RGC SPD (orange trace) decreases as well as the cortical SPD (blue trace), while the difference between the two decreases for small values of h_G (< 0.1 Hz/mV) and then stays constant (black trace). Fig. 3.9E, F also reveals a major difference with BCs gain control (compare to Fig. 3.8 E, F): the response profile of RGCs and cortical columns is quite

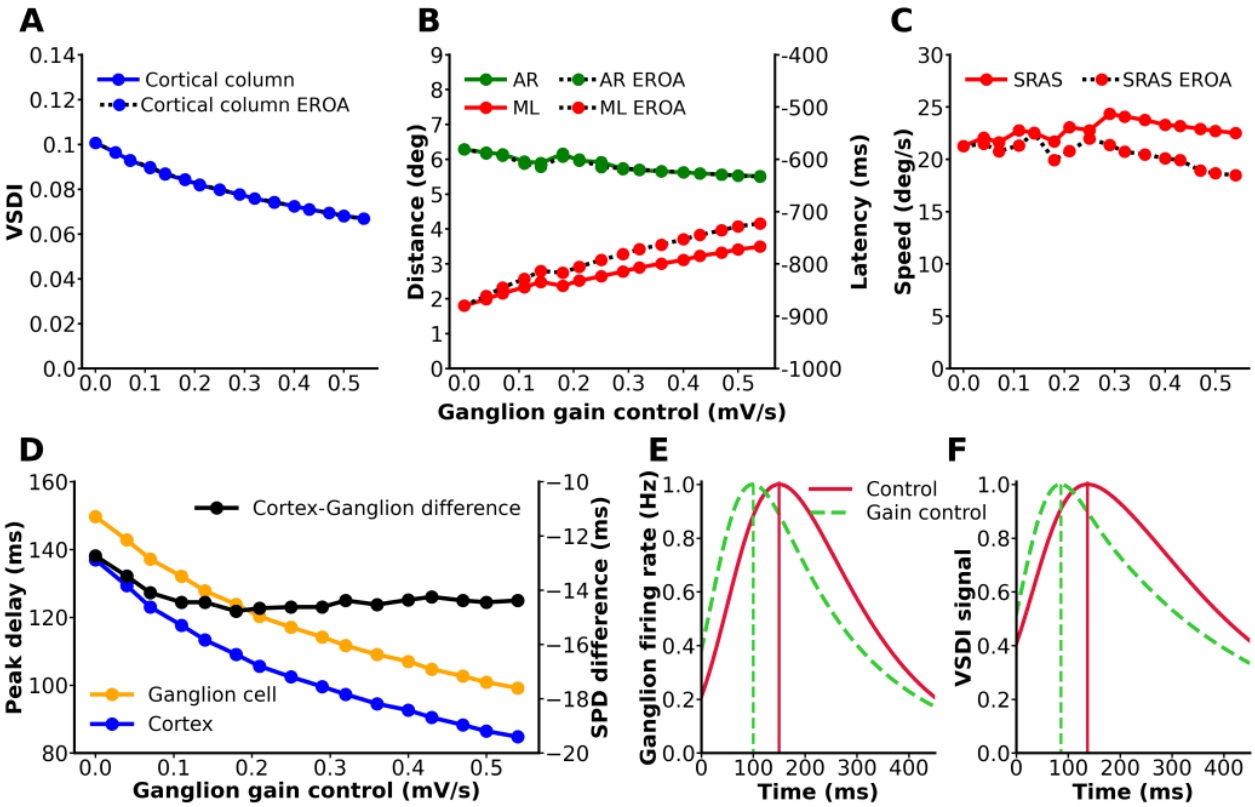

Figure 3.9: **The effect of RGCs gain control strength, h_G, on the cortical response.** The representation is the same as in Fig. 3.8

less modified than in the case of BC gain control. Essentially, RGC gain control only entails a peak shift. In contrast BCs gain control induces a cascade of convolutions up to the RGC, modifying the RGC response profile and the VSDI signal.

To conclude, the RGCs gain has a negative effect on cortical anticipation by latency while transferring the adaption anticipation coming from the retina and enhancing the intrinsic cortical shift. SRAS shows also some improvement in the presence of RGC gain control. A similar compensatory effect is observed in ML (compared to EROA), but not sufficient to compensate the decrease in ML. Finally, we mentioned in section 2.2.2 that the time of the peak in CTL conditions is located at 139 ms, while the peak observed in experiments (Fig. 4D of [8]) is very close to 0. We proposed that the discrepancy ought to be due to the absence of retinal anticipation mechanisms in CTL conditions. Here we see that combining the maximal peak shift due to BCs gain control (-72 ms) and the peak shift due to RGCs gain control (-52 ms) we arrive at a cumulative peak shift of -134 ms, so that, compared to CTL, the time to peak with gain control is close to 0, as observed in experiments.

3.3.2 The anticipatory role of amacrine cells

Here, we study the effect of lateral ACs inhibition. ACs, like horizontal cells, provide a lateral connectivity somewhat entangling the "vertical" information channels from photoreceptors to retinal ganglion cells via bipolar cells. Although some ACs can have excitatory connections (e.g. cholinergic) we mainly focus here on inhibitory effects of ACs. Amacrine cells constitute networks which modulate and can potentially propagate the response of BCs to a moving signal to other BCs and RGCs. This depends though crucially on the scaling between synaptic weights (w_B^A, w_A^B, w_G^A, w_G^B in the model) and characteristic integration times (τ_A, τ_B, τ_G in the model). A detailed study in [16] shows that tuning these parameters dramatically change the shape of the response to simple flashes (e.g. from monophasic response to biphasic), while [108, 115] emphasize the effect of stimulus induced wave propagation leading to an advancement of the peak time in RGCs. The network response to the moving bar also depends on the connectivity structure. By construction, our model has a feedback connectivity where BCs act on ACs which modulate BCs back. But, one can also study a feed-forward case where BCs input ACs without reciprocal connection, simply by setting $w_B^A = 0$. S. Ebert [116] shown in her thesis that the response is rather different. Especially, with feedback connections ACs can

induce effects similar to BCs gain control while modifying the spatio-temporal BC response (e.g. leading to biphasic or polyphasic responses even if the OPL input is monophasic [16]). The aforementioned studies were focusing on anticipation at the retinal level. Here, we analyse the impact on cortical anticipation, along the same lines as the previous sections, feed-forward versus feedback inhibition.

Feed-Forward amacrine inhibition. We study first the direct influence of feed-forward inhibition pathway with connectivity from BCs to ACs and from ACs to RGCs, respectively characterized by the parameters w_A^B and w_G^A in eq. (1.2). We varied $w_G^A \leq 0$, controlling the intensity of ACs synapses to RGCs, and $w_A^B \geq 0$, controlling the intensity of BCs synapses to ACs, from 0 to 1 Hz, restricting to the case $w_G^A = -w_A^B$. The other parameters are tuned to the control value (appendix A.1). The results are shown in Fig. 3.10. As expected, the inhibitory effect of ACs induces a decrease in the VSDI signal amplitude (Fig. 3.10 A). Note that the VSDI signal curve in this condition is essentially indistinguishable from the EROA curve, confirming that the effect of ACs on VSDI, in feedforward conditions, is only a drop in the amplitude of the retinal input. Fig. 3.10 B shows a detrimental effect of forward inhibition on the AR, as well as on the ML, although less important than in EROA. In contrast, the comparison of the SRAS obtained with feedforward inhibition and its corresponding EROA reveals a compensatory effect of the retinal amplitude. While EROA decreases fast, SRAS remains relatively constant suggesting a mechanism which counterbalances the decrease in speed due to the decrease in amplitude.

The most prominent effect occurs on the SPD of RGCs (orange trace) and VSDI signal (blue trace) which decrease sharply (Fig. 3.10 D), though with a difference becoming smaller and smaller in absolute value (black trace). These behaviors are accompanied by a strongly advancement of -104 ms (-69.4%) for the RGC spd (Fig. 3.10 E) and of -88 ms (-64.2%) for the VSDI signal peak (Fig. 3.10 F), when $\left| w_G^A \right| = w_A^B = 1$ Hz. Note that we observe also a small rebound of the VSDI signal (Fig. 3.10 F), arising when $\left| w_G^A \right|$ becomes large. When the bar arrives in their receptive field, BCs activity increases, increasing the ACs activity and their inhibitory effect on the RGC. When $\left| w_G^A \right|$ is large enough it takes over the excitation from BCs and the RGC firing rate drops to 0. Because the ACs have here a shorter time scale than BCs (corresponding e.g. to the peak of the green dashed curve in Fig. 3.10 E), their effect lasts shorter and the rebound corresponds to the residual activity coming from BCs.

Thus, the presence of feedforward inhibitory connectivity implements adapting anticipation within the cortex, with an increasing effect as the intensity the synaptic weights increases, while severely penalising cortical latency anticipation (AR, ML) and intrinsic cortical shift. Surprisingly, though, the speed of the anticipatory wave remains stable thanks to compensation for the decay of the amplitude of the retinal input. All these effects are not simply due to a decrease in the ROA but entail additional effects presumably due, as for gain control, to the difference in the BCs response profile.

Amacrine feedback inhibition. The feedback loops BCs $\rightarrow$ ACs $\rightarrow$ BCs induce a complex interaction between the moving object, the local cells response and the influence of these cells on distant cells, propagated via the lateral amacrine inhibition. The picture is that of a moving bar propagating in a non homogeneous landscape of activities modulated by the amacrine network. This entails specific effects, not present with a feedforward connectivity, such as the existence of resonant frequencies [15], a change in the shape of BCs response [16] or the existence of a preferred speed range at which adapting anticipation is maximal [116]. In addition, the feedback loop propagates inhibition producing a decay of the response before and after the peak. This actually differs from gain control, which only acts on the post-peak portion of the curve. It has been shown that these feedback effects can be characterized by (1) the characteristic integration times of BCs (τ_B) and ACs (τ_A); (2) the average intensity of the connection from BCs to ACs, $w_A^B \geq 0$, and ACs to BCs, $w_B^A \leq 0$. Actually, the relevant parameter is $\mu = -w_B^A w_A^B \tau^2$, where $\frac{1}{\tau} = \left| \frac{1}{\tau_B} - \frac{1}{\tau_A} \right|$. In particular, this shows that the synaptic weight effects of the feedback loop is characterized by the product $w_B^A w_A^B$. Here, we keep τ_A, τ_B constant and vary w_A^B with $w_B^A = -w_A^B$ from 0 to 12 Hz. The values of the other parameters are given in the Appendix A.1. The goal here is to show an example of the potential effects of this type of connectivity while a more exhaustive study would require to vary other parameters as well, a task well beyond the scope of this paper.

The result of our simulations are shown in Fig. 3.11. The amacrine feedback loop primarily drops the amplitude of the VSDI signal with no significant difference from the EROA (Fig. 3.11A). It also influences the ML as well as AR (Fig. 3.11B) with a slight optimum. A comparison with the corresponding EROA curve reveals a negative effect of the feedback loop in addition to that caused by the reduction in the amplitude of the retinal input, particularly for AR (-9.1 % at 12 Hz) but also for ML (-3.7 % at 12 Hz). On the opposite, the SRAS is a little bit higher. This increase contrasts with the reduction observed in the EROA condition. At 12 Hz, the difference with EROA is 39.3 %. This indicates a compensation of the retinal input decay by the amacrine feedback loop. This compensation counterbalances up to 6 Hz before being overtaken. The simulations also reveal an earlier SPD shift of 50 ms (-36.6 %) for RGCs (Fig. 3.11E) transmitted to the VSDI signal. We actually observe in Fig.3.11E and F, as in the previous section, a change in the shape of the RGCs response and VSDI (green traces), compared to control (red traces). The SPD for RGCs and VSDI signal, as well as their difference, versus w_B^A is shown in Fig. 3.11D. The RGC (orange trace) and cortical (blue trace)

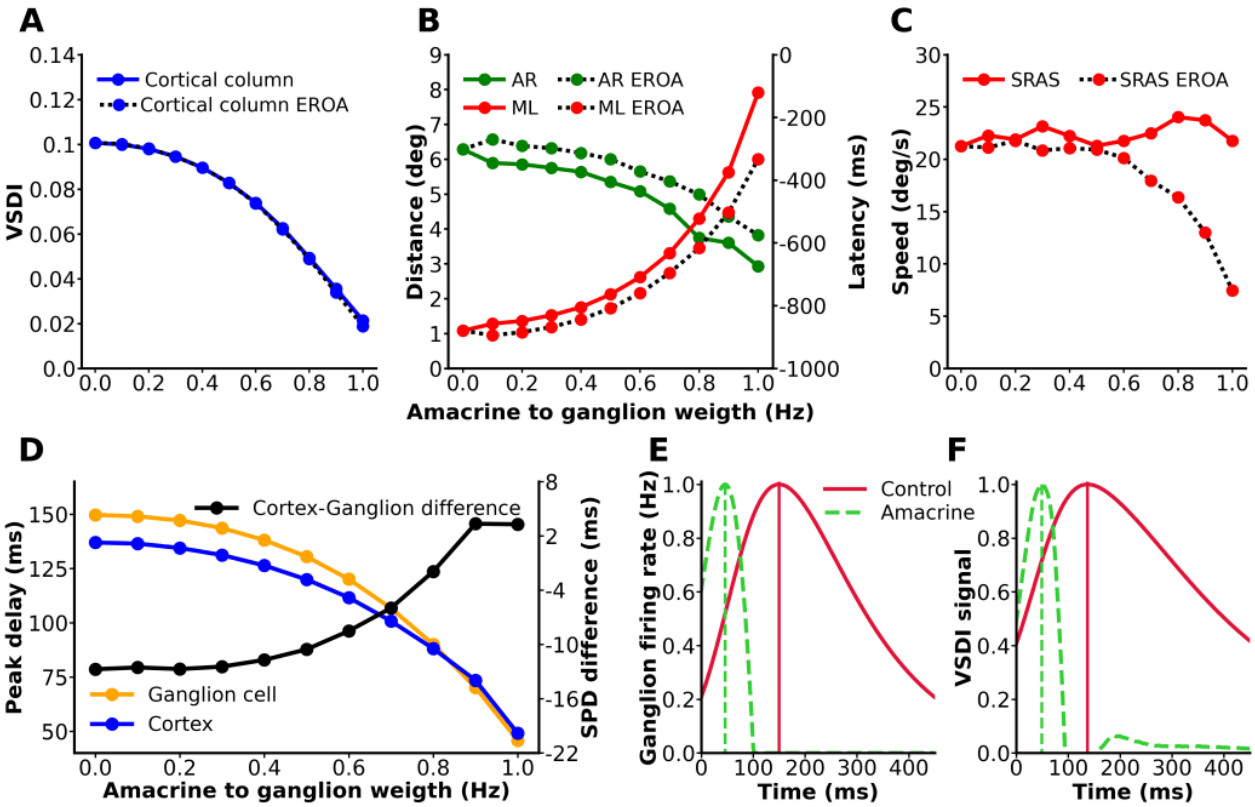

Figure 3.10: **The effect of forward inhibition, controlled by $w_G^A = -w_A^B$, on the cortical response. A) VSDI signal amplitude** of the central cortical column. **B) Temporal and spatial indicators:** anticipation range (green) and maximal latency (red). **C) Speed indicator :** short-range activation speed (red). **D)** SPD for RGCs (orange), cortical columns (blue) and difference between the cortical and RGC SPD (black). **E) Shape of the central RGC response profile to the moving bar**, without feedforward AC connection ($w_G^A = -w_A^B = 0$) (red) and when these parameters take the maximum value ($\left| w_G^A \right| = w_A^B = 1$ Hz, dashed green). Note that the two traces have been normalized to have the same maximum at 1 Hz. **F) VSDI signal**, same conditions. The dotted lines in E, F correspond to the peaks in the RGC firing rate or VSDI signal without feedforward AC connection (red) and with it (green).

SPDs increase but their difference diminishes (black trace). This shows an increase in retinal SPD at the expense of cortical SPD. The difference is minimal at $w_A^B = 12$ Hz but the SPD is maximal at this same connectivity value. A behavior similar to the feedforward effect but with a smoother slope.

These results demonstrate the capacity of amacrine retro-control to provoke adapting anticipation influencing the cortex. However, this is accompanied by a negative effect on cortical anticipation by latency mainly manifested by a drop in the AR, ML and of the cortical peak shift.

3.3.3 The anticipatory impact of the retina

We now synthesize our observations about the cortical correlates of the retinal anticipatory mechanisms. Although our investigations are absolutely non exhaustive - a more detailed study would require to vary a larger set of parameters in the model - it reveals several effects which are generic, i.e. present on a wide range of parameters value, although the *quantitative* observations may depend on these parameters. These generic effects are an advancement of the RGC output peak, a decrease in the ROA, and a global change in the shape of the firing rate response. This has an impact on the VSDI response, illustrated in the figures above and summarized in Fig. 3.12.

In Fig. 3.12 A, we compare the respective effect of BC and RGC gain control on the VSDI signal at the central cell. It is however rather difficult to compare quantitatively the effects of these two gain control mechanisms, as a systematic study would require to modify jointly h_B and h_G in a two dimensional map, a task beyond the scope of this paper. Here, we only compare the model response in a case where BCs and RGCs gain control are tuned so that the retinal output amplitude is the same (ROA $= 17.1$ Hz), that is $h_B = 8.554$ mV/s (magenta trace) and $h_G = 0.359$ mV/s (yellow trace). The first observation is a peak shift stronger for BC gain control than for RGC gain control. There is

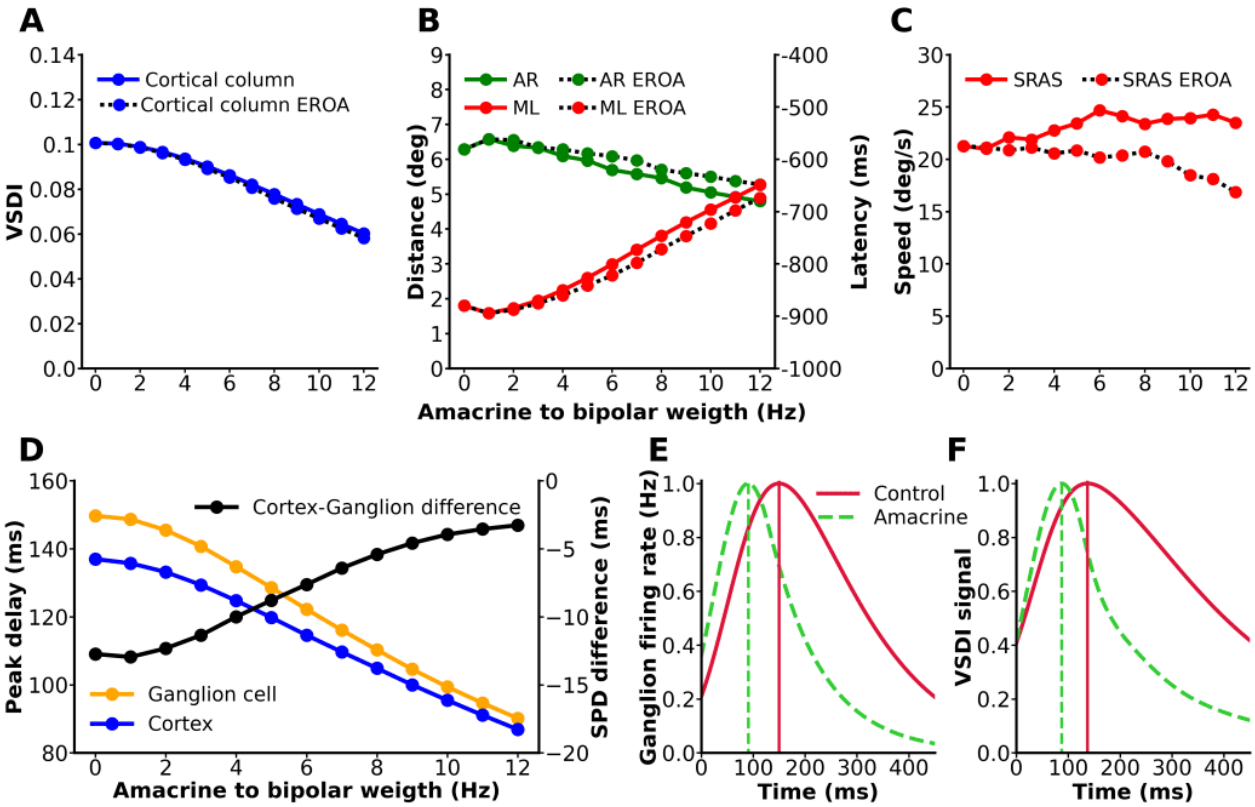

Figure 3.11: **The effect of ACs-BCs feedback loop on the cortical response. A) Amplitude quantity:** VSDI signal amplitude of the central cortical column versus the feedback loop weight. **B) Temporal and spatial indicators:** anticipation range (green) and maximal latency (red). **C) Speed indicator :** short-range activation speed (red) in function of amacrine to bipolar weight. **D)** SPD for RGCs (orange), cortical columns (blue) and difference between the cortical and RGC SPD (black). **E) Shape of the central RGC response profile to the moving bar**, without feedback AC connection ($w_B^A = -w_A^B = 0$) (red) and when these parameters take the maximum value ($\left| w_B^A \right| = w_A^B = 1$ Hz, dashed green). Note that the two traces have been rescaled to have the same maximum. **F) VSDI signal**, same conditions. The dotted lines in E,F correspond to the peaks in the RGC firing rate or VSDI signal without feedforward AC connection (red) and with it (green).

a SPD difference of 25 ms (36.7%). There is also a strong difference in the VSDI signal profile, after the pic. It is unfortunately not possible to compare this with the experimental results in [3] as the VSDI profiles they show (e.g. Fig. 4 D) is cut before the place where such a possible rebound may occur. Performing new experiments on a larger time scale would be a way to confirm the role of BC gain control on the VSDI signal profile. Finally, one sees a small variation in the early part of the curves, where latency is computed. The smallness of this variation is due to the scaling of the figure though, where we wanted to show the whole VSDI profile. Now, remember that cortical latency indicators are computed at the very beginning of the activity rising, when this activity exceeds a threshold of 0.001 (section 3.1.1). Thus, there is a small but significant effect on latency indicators. There is a difference of -1.2% for AR , -2% for ML and -7% for SRAS, in favour of BC gain control. This suggests that, overall, BC gain control is more effective. However, cortical anticipation by latency is slightly affected compared to adapting anticipation which is much higher. To sum up BCs control appears more effective at generating peak anticipation while limiting the impact on cortical latency anticipation and increasing the speed of anticipation.

In the same vein, Fig. 3.12 B compares the role of feedforward versus feedback amacrine cells connectivity, adjusting the control parameters $w_G^A = 0.7$ Hz (feedforward) and $w_B^A = 11$ Hz (feedback) so that the ROA are equal to 13.1 Hz. We observe here a small pic shift and a small change in latency while the main visible effect is a change in the shape of the VSDI profile after the peak. For these value of parameters, the AR actually decreases by -6.9% when comparing the feedback case to the feedforward case, the ML decreases of -6% and SRAS by -7.3 %. Finally, SPD arrives 9 ms later in the feedforward case than in the feedback case (10.6 %). Although the difference is rather tiny, a general conclusion would require a more systematic study. In particular, a comparison of Fig. 3.10 and Fig. 3.11 suggests a

better efficiency of amacrine connectivity in the form of a feedback loop. Adaptating anticipation is more pronounced while limiting the impact on cortical latency anticipation despite the smaller intrinsic cortical delay. On the basis of preliminary results obtained in [116] we actually believe that the main difference between the two effects would hold when varying the bar speed. We expect the presence of a preferred bar speed - where anticipation is maximum - in the feedback case and not in the feedforward case (where anticipation would grow monotonously until saturation).

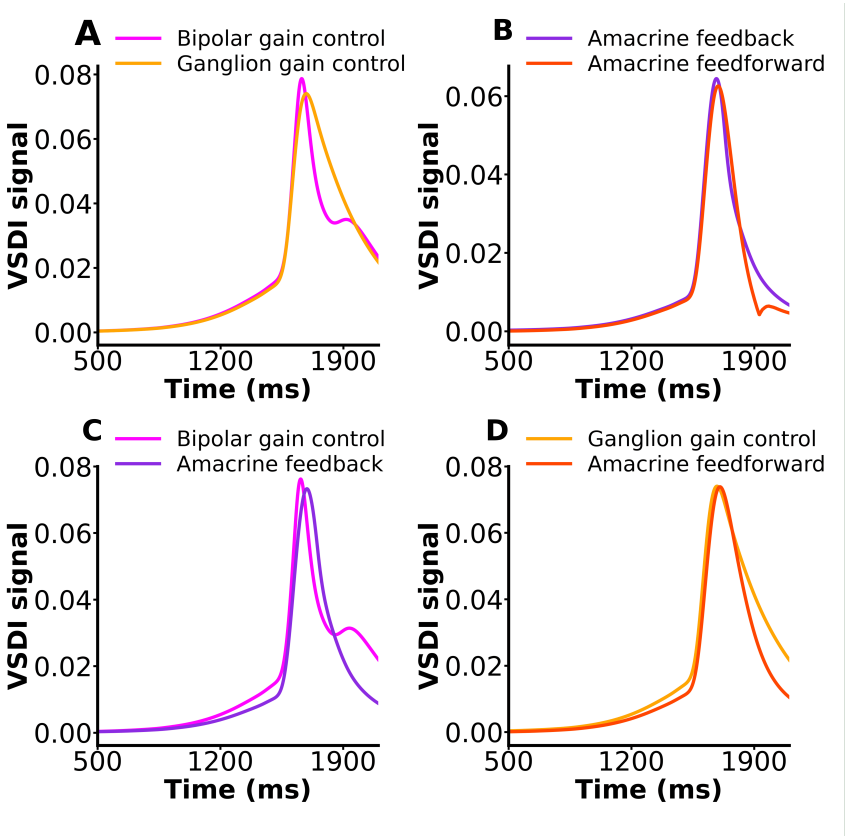

Figure 3.12: **Gain control and amacrine connectivity comparison. A) Temporal profile** of the VSDI response with a BC gain control $h_B = 8.554$ mV/s (magenta) and a RGC gain control $h_C = 0.359$mV/s (yellow). **B) Temporal profile** of the VSDI response with amacrine feedback connectivity weight $w_B^A = 11$ Hz (purple) and feedforward weight at $w_G^A = 0.7$Hz (orange). **C) Temporal profile** of the VSDI response with bipolar gain control $h_B = 8.554$ mV/s (majenta) and amacrine feedback connectivity weight $\left| w_B^A \right| = 11$ Hz (purple). **D) Temporal profile** of the VSDI response with ganglion gain control $h_G = 0.359$ mV/s (yellow) and amacrine feedforward connectivity weight $\left| w_G^A \right| = 0.7$ Hz (orange).

Fig. 3.12 C compares the BCs gain control to the ACs feedback still tuning the respective parameters so that the ROA are equal: BCs gain control $h_B = 9.2$ mV/s and the feedback loop $\left| w_B^A \right| = 9$ Hz (same ROA of 16.1 Hz). Considering the difference between AR in the BC gain control case and in the feedback connectivity case, we obtain a decrease of -8.4 %. This is -10.3% for ML, and -4.9% for SRAS, while SPD arises 36 ms later 55.2% and the intrinsic cortical SPD 3.4 ms (43%) after. In this example BCs gain control provides more anticipation with a visible effect on latency. Fig. 3.12 D compares as well the RGCs gain control to the ACs feedforward connectivity with $h_G = 0.36$ mV/s, $w_A^B = 0.6$Hz (ROA equal to 17 Hz). We observe a decrease of -10.1 % for AR, -11.3% for ML and -8.4 % for SRAS. The RGC SPD arises 17ms (18.1 %) later and the cortical SPD 6ms (41.4 %) later. For this set of parameters RGC gain control performs better than feedforward amacrine connectivity.

To sum up, this study provides an effective way of studying the potential impact of retinal anticipation mechanisms on cortical anticipation with a main drawback: parameters tuning. Although, the retinal model has been designed to have a minimal set of parameters (compared to a real retina) there are still quite a lot and a systematic study of the effects requires actually an (ongoing) systematic mathematical analysis (Cessac-Ebert, in preparation). Note that numerical simulations do not allow to effectively sample the parameter space of the retina model, while a mathematical analysis shows that some parameters (such as $\tau_A, \tau_B, w_B^A, w_A^B$) are actually dependent. Another alternative for parameter tuning

would be experimental tests. Experiments on the retina somewhat allow one to tune these parameters so as to match empirical responses. But, as said in the introduction, they mainly hold for mice (or salamanders). A more efficient way and a bigger challenge would be to tune these parameters from the observation of the V1 VSDI signal, on the basis of this model and of the afferent simulation platform. We actually made in this thesis a conjecture about the shape of the VSDI signal (presence of a rebound after the main peak) when, e.g., BCs gain control or ACs feedback connectivity is present. Their influence results in a mesurable effect on the VSDI signal profile. It would be interesting to test these conjectures in new experiments.

In this spirit, we would like to come to the remark made in section 2.2.2. In CTL condition (without retinal anticipation) the anticipation by latency is a bit too high (-880 ms for ML) compared to $\sim -400, -600$ ms in Fig. 4D of [3] (where this range of variations comes from feedback effects). We have actually shown that adding a realistic retinal output has the effect of reducing the anticipation by latency in our model, in a range compatible with experimental observations (see e.g. Fig. 3.10 B). The same holds for the anticipation range which was $6.3°$ in CTL conditions compared to $2°$ in experiments. Again, the retina has the effect of reducing this discrepancy. To get better insights on the parameters values experiments could for example focus more on the VSDI shape (e.g. after the peak) and also investigate the effects of the bar speed on peak anticipation and latency anticipation.

3.3.4 Reproduction of predicting anticipation in the retina

Creation of the anticipation model by prediction

"Predicting anticipation" is another form of retinal anticipation identified in the salamander by Menz et al. [2]. Some retinal ganglion cells in the salamander are capable of producing predicting anticipation in addition to adapting anticipation. This form of anticipation translates the entire peak without loss of amplitude. This effect is mainly supported by biphasic amacrine cells. These cells are characterised by an initial hyperpolarisation phase followed by a depolarisation phase. These two phases correspond respectively to disinhibition and inhibition of ganglion cells. According to Menz et al., this is the application of substractive gain control of biphasic amacrine activity on the response of retinal ganglion cells that enables this "predicting anticipation" to be generated (Fig. 3.13). Here, we aim to reproduce this new type of anticipation by recreating biphasic amacrine cells. With this idea in mind, we have developed a a few hypotheses on which we base our model.

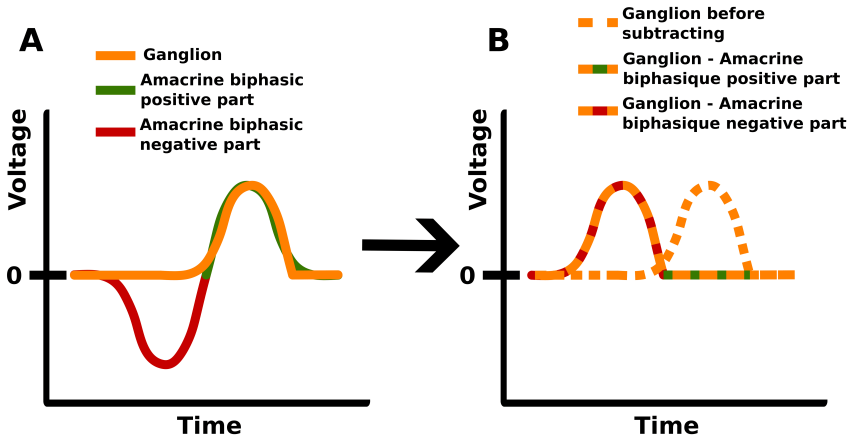

Figure 3.13: **Diagram of the subtraction of the biphasic amacrine voltage from the ganglionic voltage. A)** Hypothetical voltage curve of a ganglion cell (orange) and a biphasic amacrine cell with its positive (green) and negative (red) parts. The amplitude of these two parts are equal, so the profile is balanced. **B)** Result of subtraction between ganglion voltage and biphasic amacrine voltage. First we can see the result of the subtraction between the negative part of the biphasic amacrine voltage and the ganglion voltage (orange-red). The same applies to the subtraction of the positive part (orange-green). Finally, we have the ganglion voltage curve before subtraction (orange dotted line) for comparison; this is the response without lateral connectivity (feedforward).

We conjecture first that the disinhibition phase enables the early response peak to be set up (orange-red curve in Fig. 3.13B), while the inhibition would have the role of completely erasing the initial peak which would have occurred in the absence of the amacrines (orange-green curve in Fig. 3.13B). The inhibition phase also serves to stop the growth of the earlier peak when it reaches the amplitude of the displaced peak. We believe that to achieve this effect, it is important that the inhibition and disinhibition peaks are perfectly balanced (Fig. 3.13A). This allows the early part of the response to be amplified with the same amplitude as the terminal part of the response is reduced. If the inhibition is

strong enough to completely suppress the retinal ganglion cell peak, this means that its disinhibition is strong enough to create an earlier peak of the same amplitude.

On one hand, we assume that the depolarisation phase of biphasic amacrines comes from direct excitation by bipolar cells. An approximate measurement of the characteristic time of this depolarisation phase was made in Menz et al: 0.3 s. This depolarisation must correspond to the feedforward response of the retina. To achieve this, the connectivity between the bipolar and amacrine cells must be established at the same spatial position. On the other hand, we hypothesise that the presence of a first phase of hyperpolarisation of biphasic amacrines could be explained by the presence of a second type of amacrine responsible for inhibiting them. This inhibition must occur earlier than the feedforward response and must therefore be mediated by long-distance lateral connectivity. We suggest that these second amacrine cells type are also excited by bipolar cells. Finally, biphasic amacrine cells should be able to apply their disinhibition-inhibition to cells of the retinal feedforward pathway such as bipolar or ganglion cells.

On the basis of all these hypotheses we have developed a model as an extension for the retino-cortical model introduced in chapter 2.2 with the same parameter values. We then made a few modifications to the amacrine connectivity of the retina part of the model (Fig. 3.14. The amacrine cells still receive input from the bipolars although no longer one-to-one but within a given radius with uniform weights. There is also no longer any inhibition of ganglion cells. Instead, they inhibit in one-to-one a new type of amacrine cell that we have named "biphasic amacrine".

These biphasic amacrine cells also receive bipolar input and establish a one-to-one connection with the retinal ganglion cells. Note that the choice of a uniform lateral connectivity of the bipolars to the amacrines could also have been replaced by a connectivity of this type from the amacrines to the biphasic amacrines. The important thing is that, in the end, the inhibition from the amacrines to the biphasic amacrines is shifted. Unfortunately, We did not have enough biological information to determine which of these two situations is the more likely. We were able to identify the parameters that were essential for reproducing this predicting anticipation. The length of the radius between bipolar and amacrine increases the distance at which the amacrines start to activate. The biphasic amacrine characteristic time must be high enough to slow the rise and fall of their response. This results in a longer residual activity. Without this activity, we would obtain triphasic profiles. The third phase of a triphasic profile is a hyperpolarisation resulting from the activation of the amacrines by the bipolars, downstream in the trajectory of the bar.

We have also decreased the characteristic time of the amacrines was decreased to increase their slope and decay and thus accentuate the time lag between the inhibition of the amacrines on the biphasic amacrines and their feedforward response.

The different factors amplifying the connections between amacrines are also crucial. The two amplification factors on the bipolar-amacrine and biphasic amacrine-amacrine synapses control the amplitude of the voltage hyperpolarisation phase of the biphasic amacrine cell. On the other hand, we have the amplification factor of the biphasic bipolar-amacrine synapse which controls the amplitude of the depolarisation phase of the voltage of the biphasic amacrine cell. These three amplification factors had to be carefully selected to shape a balanced biphasic profile as in Fig 3.13A.

Finally, the amplification of the biphasic amacrine cells towards the ganglion cells serves to create a subtraction of the biphasic profile strong enough to suppress the feedforward response and create an earlier one. It is also necessary to establish a connectivity between the biphasic amacrines and the retinal ganglion cells.

The connectivity on the bipolars does not allow the amplification factors to be manipulated in such a way as to create the biphasic profile and then subtract it sufficiently. Indeed each change always has repercussions on the biphasic amacrines. Input and output has therefore to be decoupled.

We thus established a new set of parameters synaptic weight was set to 0.68 mm. The characteristic time of biphasic amacrines is $tau_{A_{Bi}} = 0.3$ s and that of amacrines is $tau_A = 0.005$ s. Connection amplification were set at 3.5 Hz between bipolars and amacrines, -4 Hz between amacrines and biphasic amacrines, 8 Hz between bipolars and biphasic amacrines and -0.4 Hz between biphasic amacrines and ganglion cells.

Finally, the weight between the retina and the cortex was reduced to 0.1 Hz. This reduction in retinal-cortical weight resulted in very weak VSDI signals in our control condition. Because of this, the latency was no longer visible because it was below the activation threshold we had set. For this reason, we decided to divide activation threshold by 10 define in Sec 3.2

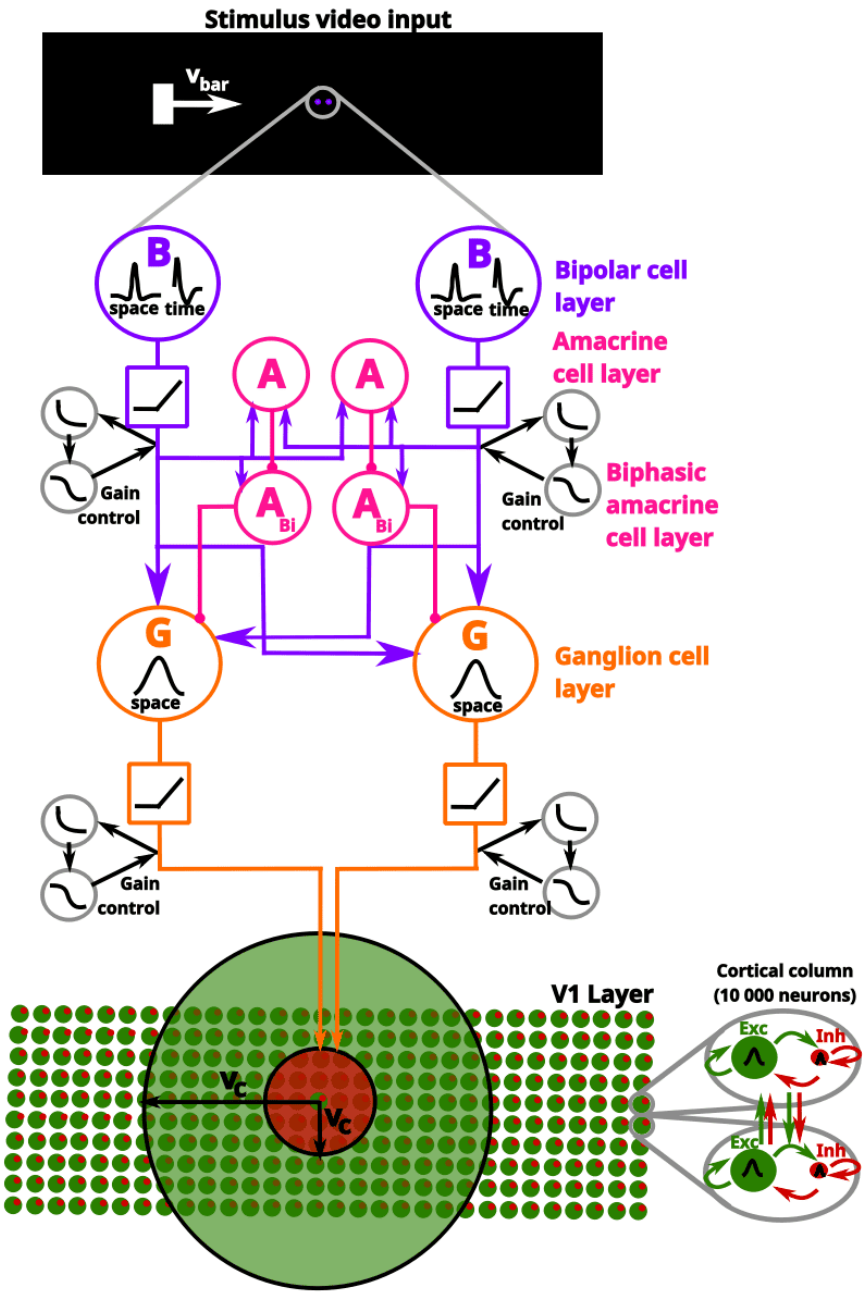

Figure 3.14: **Synthetic view of the retino-cortical model with biphasic amacrine.** This model is a modified version of the retino-cortical model used throughout this thesis and described in figure 2.3. The amacrine connectivity has been modified. Bipolar cells (purple circles) connect all amacrine cells (pink circle "A") or biphasic amacrine cells (pink circles "A_{Bi}") within a given radius. The amacrine cells then inhibit the biphasic amacrine cell in the same position. The biphasic amacrine cells in turn inhibit the ganglion cell at their position.

It is important to note that to facilitate the explorations leading to our results, we have reduced the size of the cortical size ($3.15 \times 9°$) compared to the rest of this thesis. This parameter set was applied in Macular to reproduce anticipation by prediction. We compared it to a control condition where the bipolar/amacrine and bipolar/amacrine bi-phasic amplification are 0.

Effect of the anticipation model by prediction on cortical anticipation

Figure 3.15A shows no variation in bipolar response. This contrast with the frequency of ganglion discharge where the peak of the predicting condition is earlier than the control (3.15B). In addition, this ganglion firing rate predicting peak is also earlier than the bipolar one see in A. In addition to this, the descending part of the curve falls sharply in the presence of predicting.

The voltage of ganglion cells (3.15C), in the absence of predicting, shows only one depolarising peak, whereas with prediction a second hyperpolarising peak appears, smaller and later than the depolarising peak. Amacrine cells are activated very early in the predicting condition, their voltage become a long plateau. In predicting condition, bi-phasic amacrine cells consist in one hyperpolarised peak followed by a depolarisated peak (3.15E). At cortical level, in the predicting case, the peak of the VSDI signal obtained (3.15G) happens 60 ms earlier and is higher compare to control (3.15F). The latency is also accentuated in the prediction condition. We can see a second rounded peak in the VSDI of the prediction condition. If we compare latency indicators, anticipation by prediction causes twice as much AR (3.15H), a slower speed (3.15I), and a latency 1.5 times earlier (3.15J). The ganglion peak arrives 95 ms earlier (3.15K) and the cortical peak 60 ms earlier (3.15L).

In the following, we use the term feedforward to refer to the response obtained in the control condition in the absence of any lateral connectivity. Our results show that the ganglion peak is shifted relative to the feedforward peak obtained in control condition without altering its amplitude. We believe that combining these two characteristics demonstrates the successful reproduction of predicting anticipation within the retina. It also demonstrates that a subtractive connection of the amacrine biphasic voltage to ganglion is enough to generate predicting anticipation. The hyperpolarised peak of amacrine biphasic voltage causes a strong disinhibition at the origin of the depolarize peak observed in the ganglion response in predicting condition. A little bit later, the depolarised peak in the voltage of the biphasic amacrines leads to the inhibition of the ganglion response, which falls sharply. This drop occurs at the precise moment when the amplitude of the predicted ganglion response has reached that of the control condition. We can see that this inhibition actually causes a very strong hyperpolarisation of the ganglion voltage. This hyperpolarisation masks the peak firing rate depolarisation caused by the feedforward (control) pathway. The shift in the ganglion firing rate peak in the predicting condition is explained by the earlier activation of ganglion cells excited by biphasic amacrines. In turn, biphasic amacrines activate earlier thanks to their long-distance lateral connectivity with bipolars.

The shape of the biphasic amacrine response is explained by the subtraction of the bipolar response by the amacrine voltage. The switch between the hyperpolarised and depolarised peaks depends on the amplification values of the biphasic bipolar-amacrine and biphasic amacrine-amacrine synapses. The slower dynamics of the biphasic amacrine cells enable them to counterbalance the long, constant inhibition they receive from the amacrines. If this were not the case, a third hyperpolarised peak could appear.

The shape of the amacrine curve can be explained by the use of a characteristic time that is sufficiently low in relation to the frame rate for the amacrines to perceive the image as static. The explanation of this phenomenon (shaping parameter r) is described in detail in the appendix C.

It should be noted that in our case, the activity of the biphasic amacrines is unbalanced. The hyperpolarised phase of the biphasic amacrine response is just over 2 times smaller than the depolarised phase. Balancing these two peaks required the use of a characteristic time that was too long compared with Menz et al (1 s). The use of an unbalanced voltage profile for biphasic amacrines resulted in the abrupt decrease in ganglion voltage or firing rate observed after the depolarised peak. But also the strong hyperpolarisation of the ganglion voltage. We do not know whether or not these two characteristics are observed in biology.

The VSDI signal in the presence of predicting anticipation in the retina is 84 ms earlier. In the predicting condition, the peak of the cortical response is 25 ms later than the ganglion response compared with the control condition. Prediction improved the overall delay in the peak while reducing the proportion that can be attributed to the cortical anticipation. Anticipation by retinal predicting also led to a reduction in SRAS and a sharp increase in AR and ML. We expected ML to increase due to the translation of the retinal response peak. However, the increase in ML is much greater than the increase in peak delay. This means that there is an additional effect of the predicting on the ML that is not due to the peak shift. Note that the AR and ML values are currently underestimated. Indeed, the current size of the cortical area is not long enough to observe the moment when latency is no longer increasing. This could also have minimised SRAS.

In the presence of the prediction, the VSDI peak is doubled due to potentially two phenomena. The first is a strong residual activation trail on either side of the bar trajectory. This contrasts with a total absence of activity on the bar trajectory. The biphasic amacrine cells on the edges of the trajectory are activated by the bipolars seeing the bar but not inhibited by the amacrines.

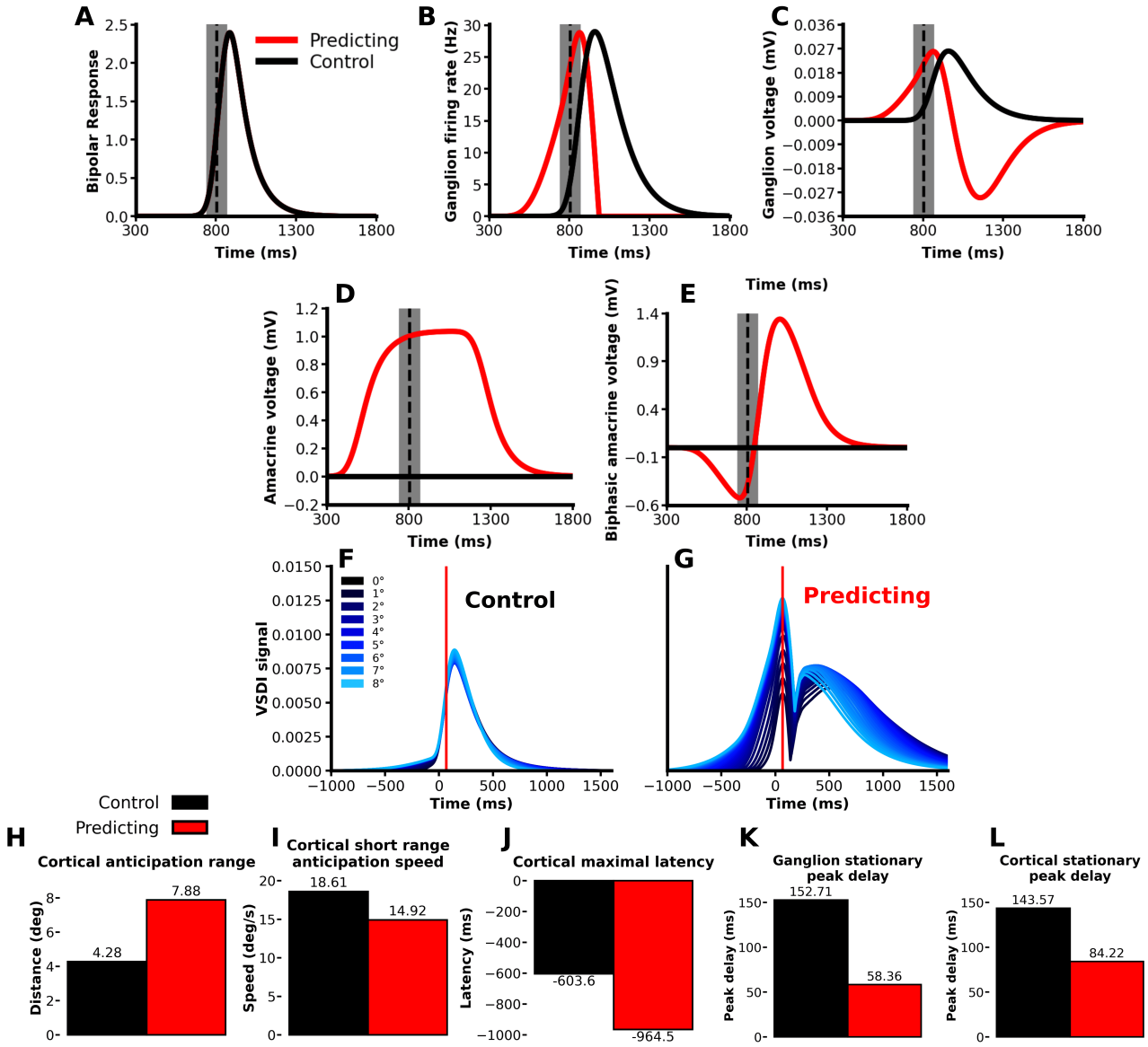

Figure 3.15: **Predicting anticipation in chimera model. A-E) Time profile** of bipolar cell response ((**A**), ganglion discharge frequency **(B)**, ganglion voltage **(C)**, amacrine voltage **(D)**, biphasic amacrine voltage **(E)** with control condition (black) or with predicting (red). The grey rectangles in the figures represent the time during which the bar is in the receptive field of the cortical column. The black dotted line is the time when the center of the bar passes through the center of the receptive field. **(F, G) Spatio-temporal representation** of the VSDIs centerd on the arrival of the bar at the center of the receptive field for the control condition **(F)** and the predicting condition (G). The red line corresponds to the peak time of the VSDI with predicting. The blue gradient corresponds to the distance between the cortical column and the origin of the bar trajectory. **H-L) Barplots** of the variation in RA **(H)**, SRAS **(I)**, ML **(J)**, ganglion SPD **(K)** and cortical SPD **(L)** for the control condition (black) and that with predicting (red).

3.3.5 Predicting and adapting anticipation interactions

Bipolar gain control and predicting anticipation

We are taking advantage of the reproduction of predicting anticipation in the retina to evaluate the extent to which this anticipation interacts with adapting anticipation. We start with the addition of gain control on bipolars in addition to predicting. We compare four conditions: control, predicting, gain control and predicting with gain control.

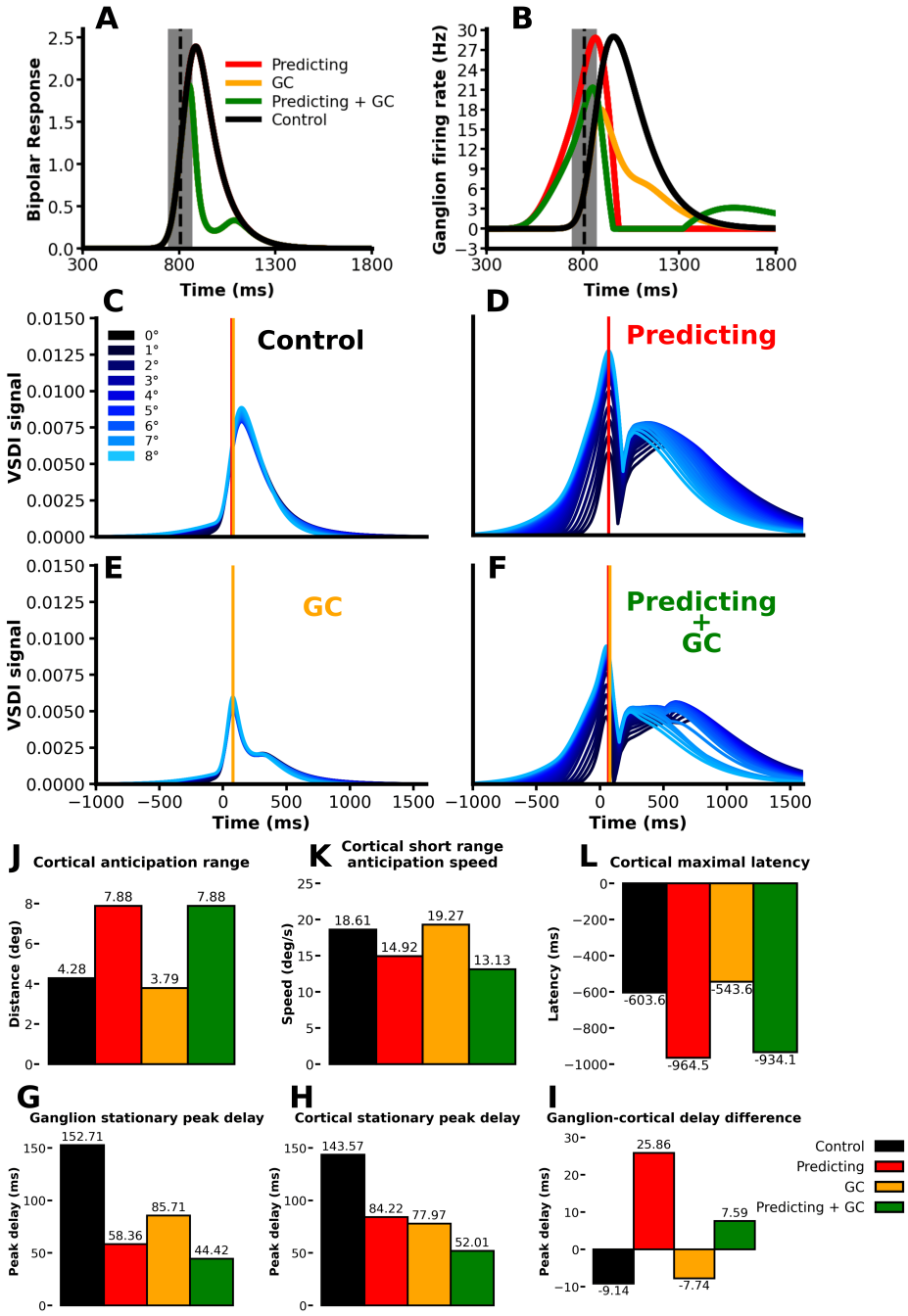

Figure 3.16: **Effect of bipolar gain control on predicting anticipation. A, B) Temporal profile** of bipolar cell response ((**A**) and ganglion discharge frequency **(B)** with the control condition (black), bipolar gain control (yellow), predicting (red) or both (green). The grey rectangles in the figures represent the time during which the bar is in the receptive field of the cortical column. The black dotted line is the time when the center of the bar passes through the center of the receptive field. **C-F) Spatio-temporal representation** of the centerd VSDIs as in Figure 3.15 for the control condition **(C)**, the predicting **(D)**, the bipolar gain control **(E)** or both (F). The red line corresponds to the peak time of the VSDI with predicting and the yellow line to that with gain control. **G-L) Barplots** of variation in RA **(G)**, SRAS **(H)**, ML **(I)**, ganglion SPD **(J)**, cortical SPD **(K)** and the difference between the two SPDs **(L)** for the control condition (black), predicting (red), bipolar gain control (yellow), both (green).

Bipolar cell responses in the presence of bipolar gain control and with or without predicting differ from those in the control or predicting condition (Fig. 3.16A). Their peak is also slightly earlier. In addition, there is a small peak at the

end of the curve. In the ganglion, the firing rate peak with predicting and bipolar gain control is the earliest, slightly earlier than that with predicting only (Fig. 3.16B). The peak with bipolar gain control is slightly later than that with predicting. We also observed a small peak in activity beyond 1300 ms. At the cortical level, the two conditions with predicting (Fig. 3.16D and F) have a stronger amplitude compare to condition control (Fig. 3.16D). In the case of the gain control condition, the amplitude is the smallest (Fig. 3.16E). The conditions with predicting both show a doubled VSDI peak.

The AR is longer in both cases where predicting is present and gain control is associated with the smaller AR value (Fig. 3.16J). On the other hand, SRAS is maximal in the gain control condition, not far from the control condition (Fig. 3.16K). The SRAS with predicting anticipation is weaker than without. ML is maximal with only predicting, followed closely by the predicting + gain control condition (Fig. 3.16L) and far from the condition without predicting. The two conditions without predicting have a much lower ML with a minimum in the gain control only case. The ganglion firing rate peak delay shift is 2 to 3 times lower in the presence of gain control or predicting (Fig. 3.16G). The gain control remains the weakest of the three. The peak of the VSDI signal is also well advanced by the gain control and the predicting (Fig. 3.16H) but more with gain control. This is reflected by a difference in SPD between the cortex and the ganglion cells which is negative only in the control and gain control conditions (Fig. 3.16I). The predicting condition shows the greatest delay in the ganglion peak.

In bipolar response, the second small peak for conditions with bipolar gain control is caused by a sufficiently rapid decrease in the bipolar response. Indeed, this decrease in bipolar response is accompanied by a reduction in gain control before the bar has left their receptive field. As a consequence, the bipolar is no longer under the influence of adaptation and can be activated again by the bar. In ganglion response, the second peak is explained by a triphasic voltage profile of biphasic amacrines. This is revealed by the more rapid post-peak decay ganglion voltage in the presence of gain control.

In this figure, AR and ML are again underestimated because of the distance of the simulated cortical area. Despite this, AR is greater with predicting and compensate in whole or in part for the loss of AR caused by gain control when the two retinal anticipations are combined. The same dynamic can be observed for ML.

Overall, the bipolar gain control and the predicting greatly improve the peak shift. However, it should be noted that the shift observed in the presence of predicting and bipolar gain control does not correspond to the linear sum of the two shifts caused by predicting or bipolar gain control alone. In ganglion cells, the difference between the control SPD and that with predicting and gain control is 1.5 times smaller than expected with the linear sum. For cortical SPD, it's 1.4 times less. This demonstrates a competition between both shift effects caused by bipolar gain control and predicting anticipation. Finally, we note that bipolar gain control increases the shift of the peak associated with latency anticipation. This effect can also be observed when bipolar gain control is combined with predicting. In this case, the cortical peak lags behind the ganglion peak, but much less than in the case of predicting alone. We can see a non-linear effect from the interaction between predicting and bipolar gain control. In fact, the difference between the two ganglion and cortical peaks is 2.05 times smaller than the linear sum of these two conditions alone. Bipolar gain control seems to counterbalance the negative effect of predicting anticipation on the delay of the cortical peak.

Ganglion gain control and predicting anticipation

We continue by adding ganglion gain control with predicting anticipation. The bipolar response is identical whatever the condition (Fig. 3.17A). In the presence of gain control and predicting, the ganglion peak becomes earlier than with predicting or gain control alone (Fig. 3.17B). The time to peak in the predicting condition is much earlier than in the gain control condition, which is itself earlier than in the control condition. The cortical response with ganglion gain control and predicting (Fig. 3.17F) causes a slightly higher peak than with gain control alone (Fig. 3.17E) but lower than the control condition (Fig. 3.17C) or predicting alone (Fig. 3.17D). We note that the presence of predicting anticipation accentuates latency (Fig. 3.17J) and ML (Fig. 3.17L). On the other hand, it reduces SRAS (Fig. 3.17K). The time taken to reach the ganglion peak is reduced a little by the ganglion gain control, a lot by the predicting and even more by both (Fig. 3.17G). The same is true for the peak of the VSDI signal, but with a weaker effect of predicting anticipation alone (Fig. 3.17H). These two changes in SPD generate a difference that is positive with predicting. The cortical peak therefore arrives later than the ganglion peak. Overall, the gain control improved this difference beyond that observed for the control condition.

We conjecture that ganglion gain control exhibits an effect similar to that of bipolar gain control when added to predictive anticipation. AR and ML are underestimate. The increase in AR and ML with predicting anticipation offsets the normally expected drop by adding extra gain control.

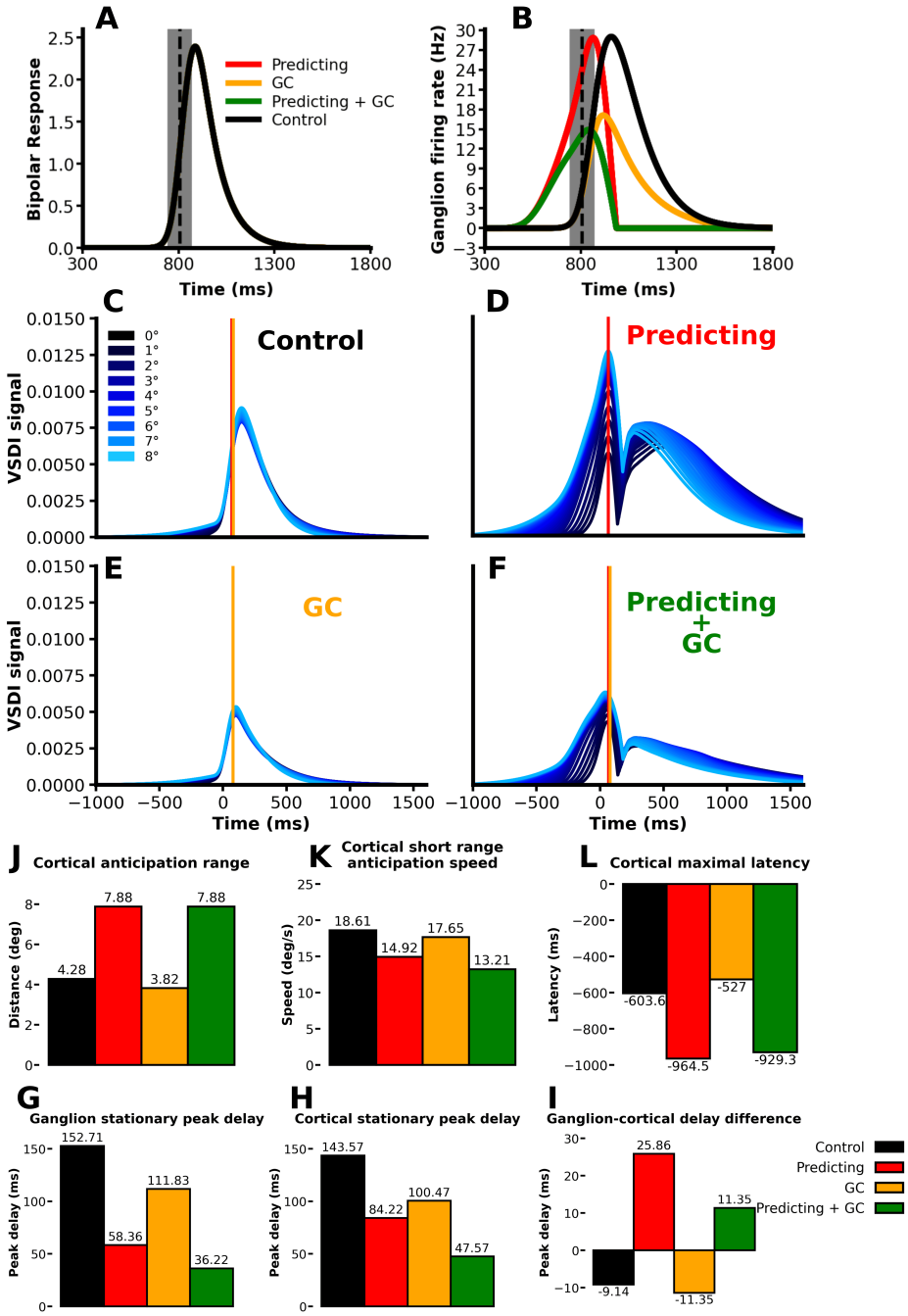

Figure 3.17: **Effect of ganglion gain control on predicting anticipation. A, B) Temporal profile** of bipolar cell response **(A)** and ganglion discharge frequency **(B)** with the control condition (black), ganglion gain control (yellow), predicting (red) or both (green). The grey rectangles in the figures represent the time during which the bar is in the receptive field of the cortical column. The black dotted line is the time when the center of the bar passes through the center of the receptive field. **C-F) Spatio-temporal representation** of the centerd VSDIs as in Figure 3.15 for the control condition **(C)**, predicting **(D)**, ganglion gain control **(E)** or both (F). The red line corresponds to the time of the VSDI peak with predicting and the yellow line to that with gain control. **G-L) Barplots** of variation in RA **(G)**, SRAS **(H)**, ML **(I)**, ganglion SPD **(J)**, the cortical SPD **(K)** and the difference between the two SPDs **(L)** for the control condition (black), predicting (red), ganglion gain control (yellow), both (green).

The change in spike time in the ganglion with predicting and gain control is 1.16 times smaller than with the addition of the lags caused by predicting and gain control alone. In the cortex, the linear sum of the predicting and gain control

condition is only 1.08 times stronger than the condition with both combined. The lower non-linearity in ganglion compare to bipolar could be explained by the choice of a weaker bipolar gain control. Finally, once again, gain control causes an improvement in the delay of cortical spikes over ganglion spikes, while predicting increases it. The difference between the delays does not behave linearly. The difference obtained between predicting and ganglion gain control is 1.65 less than we would have expected by summing the effects of both alone compared with the control. This means that the effect of the ganglion gain control on the cortical compensate for the the one in predicting.

Conclusion on adapting and predicting anticipation interaction

We first demonstrated our ability to reproduce a new form of retinal anticipation by predicting, never before reproduced, using our new model. In this context, we put forward a number of hypotheses on how this anticipation is formed and which parameters are important (characteristic time of the two types of amacrine cells, lateral connectivity, amplification factor). Our observations are consistent with the importance of subtraction between biphasic amacrine voltage to ganglion voltage for predicting anticipation as conjectured by Menz et al. The earlier hyperpolarisation phase is generated by lateral inhibition via another type of amacrine with a rapid characteristic time. The depolarisation phase results from feedforward input from bipolar cells. The hyperpolarisation phase generates disinhibition in the ganglion cells, which can go as far as forming a peak of the same amplitude as that of the feedforward obtained without lateral amacrine connectivity. The depolarisation phase creates an inhibition which suppresses the old feedforward peak, which will be replaced by the newly formed, earlier peak. This predicting anticipation improves some of the latency anticipation indicators (AR, ML, ganglion SPD, cortical SPD) but reduces others (SRAS, SPD difference). Despite this, we are aware that our model still has limitations that we would like to improve in the future.

Secondly, we tried to assess the extent to which predicting anticipation was influenced by adapting anticipation. In particular, we wondered whether these two types of anticipation could be compatible. We were able to see that in our results predicting anticipation seems to have a positive effect on AR, ML and both ganglion and cortical SPDs. On the other hand, it reduces SRAS and the difference between ganglion and cortical SPDs. In the case of adaptive anticipation with gain control, we observe more or less the opposite, with ML and AR decreasing while the difference in SPDs increases. On the other hand, both SPDs also increase in the gain control conditions. In our simulations, the two types of anticipation seem to partly compensate for each other's defect. Both improve on each other while bringing forward the ganglion and cortical peaks ever earlier. Our results therefore point to a combination of the two which would be favourable for anticipation in both the retina and the cortex. This seems to reinforce a hypothesis we developed during our work on the co-existence of so many anticipation mechanisms within the visual system. We suggest that all these anticipation mechanisms can fit together and interact in such a way as to limit each other's defect and ultimately obtain an ever greater shift in peak responses. It is also possible that each anticipation can be recruited according to the level of anticipation required for the speed of the object being processed. Anticipation cannot grow indefinitely because the lateral connections in biology are not. The accumulation of several parallel anticipation channels could overcome this limitation and increase anticipation efficiency without having to set up ever longer connections. An alternative hypothesis would be several anticipation processes in order to make different function for which it would be adapted.

For the future, we need to be able to confirm all this by using a graph of a more suitable size, but also parameters that are more and more optimised, as mentioned above. We also need to ensure that these results do not stem from the two potentially strange phenomena we have identified. Finally, we would like to be able to evaluate in a little more depth the effect of adapting anticipation on predicting anticipation. To do this, we want to test different levels of gain control. We could also evaluate the effect of adaptive anticipation with feedback or feedforward amacrine connectivity. The aim is to evaluate each time how the capacity for interaction between the two types of anticipation evolves.

Chapter 4

Suppressive waves in simulated saccades

In this final chapter, we study another type of phenomenon induced in the cortex by a moving object and enabled by the cortical lateral connectivity. The aim here is to study the different properties observed in the V1 response to simulated saccades. As a preliminary step, used also as a validation of the model, we first attempt to reproduce suppressive waves as our working hypothesis is that they are closely linked to the cortical response to simulated saccades. Another crucial experimental parameter we want to investigate is the frame rate of the video projector. Currently, many experiments use video projectors with a 60 Hz refresh rate without consideration of the impact of the frame rate. We therefore also want to better understand this impact on the visual system. After these two tests, we look at the properties of the simulated saccades. It is with this objective in mind that we are going to carry out a series of experiments. For each simulation we use the model and parameters (Macular graph) described in the chapter 2.2 and detailed in the appendix A.1. In each case the stimuli are designed to better address the questions we are rising.

4.1 Suppressive waves in apparent motion

Suppressive waves were demonstrated by Chemla et al. in area V1 of macaques [9]. To do this, they used apparent movements that generated illusions of movement. They noted the appearance of a suppressive wave in the apparent movement which moves from the most recent flashed point to the oldest. This suppression would be carried by the inhibitory gain control. We have adapted the stimulus used in Chemla et al. experiments to our setting. Two stimuli were created corresponding to two different Macular graphs and two different sets of parameters. The first stimulus measured 4.275×4.275 degrees (135×135 pixels, corresponding to 20×20 cells in our model) with a pixel/degree ratio of 31.6. The parameter set is the one described in section 2.2.2 and appendix A.3.4. The second stimulus has a size of 18.45×3.15 degrees (5535×945 pixels, 15×83 cells) with a pixel/degree ratio of 300. Its parameter set is the default one defined in the appendix A.1 and used in the anticipation chapter 3. For both stimuli, the white dots of the stimulus are disks with a diameter of 1 degrees (300 pixels) separated by 1 degree from the left and right of the center of the visual scene. Our white dots are therefore larger than Chemla et al, so as to obtain a sufficiently visible response in our setting. Our results are synthetized in Fig. 4.1 and 4.2.

Fig. 4.1 A shows the stimuli (top row) and the simulated VSDI signal response (see legend). The second row of this figure shows the response to the left dot. It has roughly a Gaussian shape which spreads over time before fading away. The next row shows the response to the right dot. It has the same shape and evolution as for the right dot, delayed in time. The last row of figure 4.1 A shows the VSDI signal response to the successive flash of the left and right dots. The Gaussian like activity generated by the first dot spreads out until it eventually reaches the position of the right dot, *before* this second dot is flashed. When this flash occurs (at 150 ms) the response to the left and right dot interfere (between 150 and 400 ms).

In order to better visualise the interactions of these two responses we use, in Fig. 4.1 B, the representation proposed by Chemla et al. This heatmap represents the VSDI signal response where time is on abscissa and the horizontal coordinate (degrees of cortex) is on the vertical axis. In this representation, the left dot is at the bottom, while the right dot is at the top. One sees the Gaussian spread, which increases with time and reaches the position where the top spot is located. Note that, obviously, the bottom response (left spot) arrives earlier than the top response (right dot). There is a delay of 11 ms between the appearance of the stimulus on the right and the increase in its activity.

This obvious ordering is in strong contrast to what is observed in Fig. 4.1 C where we used the method proposed by Chemla et al. to investigate the nature of the interaction between the two Gaussian spots corresponding to non linear

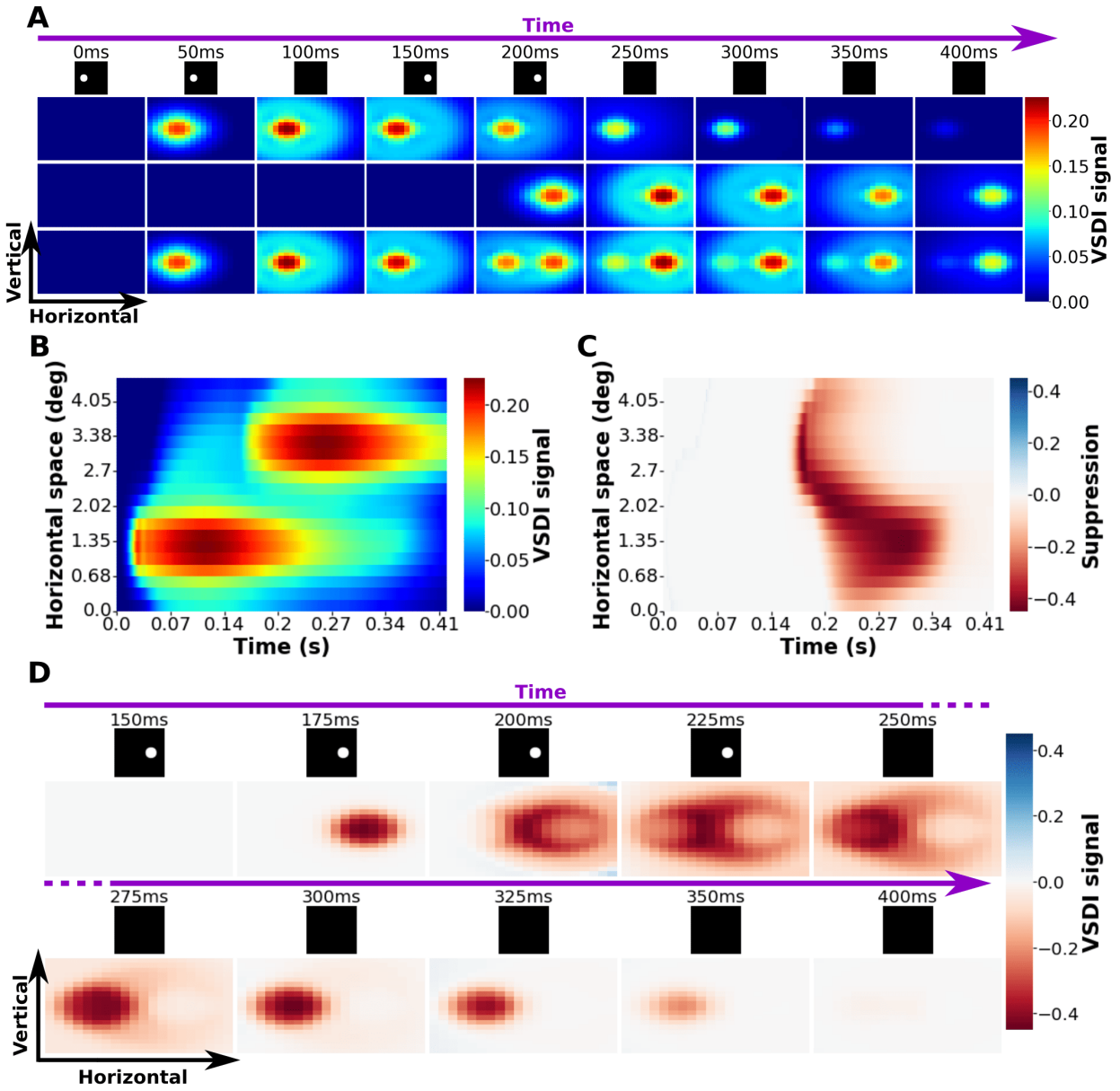

Figure 4.1: **The retino-cortical model reproduces the suppressive wave in apparent motion. A)** Time sequence of the VSDI signal map for different stimuli. Time is represented by the top purple arrow. The black squares below this arrow present the stimuli at different times. There are 3 stimuli: (1) a static white dot, on the left side of the black square, flashed during the time interval $[0, 100]$ ms; (2) a static white dot, on the right side of the black square, flashed during the time interval $[150, 200]$ ms; (3) the apparent motion corresponding to (1) followed by (2). The first line represents the activity (VSDI signal) generated by stimulus (1). The second line is the activity in response to stimulus (2). The last line is the activity of the apparent motion (stimulus (3)). **B)** Time-horizontal representation of VSDI signal to two-stroke apparent motion (stimulus (3)). We have adopted here the representation of [9], where time is on abscissa and the horizontal space on ordinate. **C)** Time-horizontal representation of the non linearity in response to the two-stroke apparent motion stimulus. The non-linearity is obtained by subtracting the sum of the flash activities of the isolated left and right dots from the activity of the apparent motion. Thus, this is the response to (1)+(2) minus the response to (3). **D)** Suppressive wave using the same representation as in A. Each time of the time sequence is accompanied by the stimulus frame of the corresponding time. This simulation was carried out with the parameter set of Sec. 2.2.2 and appendix A.3.4, a graph of 20×20 cells and square stimuli.

effects. This method consists of substracting from the apparent motion response (4.1 A top) the sum of the left stimulus response (4.1 A middle) and the right stimulus response (4.1 A bottom). The result is then normalised dividing it by the sum of the responses to the right and left stimuli. This non-linearity represents the part of the apparent motion response that cannot be explained by the mere response to the flash of the stimuli that makes it up. It is a prominent characteristic of the apparent motion. Using this methodology in Fig. 4.1 C we observe a suppressive wave (the red color corresponds to a negative effect) propagating *backwards*. The wave originates at the same time and in the same place as the spot of activity generated by the stimulus on the right thus, the last flashed dot, and moves toward the region corresponding to the first flashed dot. This region of negative activity fades abruptly to become an area of weak suppression, as a "shadow", which is clearly distinguishable from its surrounding positions where the suppression is visible. The suppression moves and becomes concentrated where the left stimulus was flashed. Therefore, the suppression starts in the most recent spot of activity and then spreads to the oldest. The level of suppression is relatively high. To make the suppressive wave more explicit we have also presented this suppression in the same representation as figure 4.1 A. Figure 4.1 D thus shows the propagation of a suppressive wave backwards, from right to left.

Chemla et al. conjectured that the size of the activity spots is linked to the extent of the lateral cortical connections. In this conjecture, the suppression wave would have the same spatial extension and the same speed as the response to a local stimulus (81.7 degrees/s). The cortical model used by the authors enabled them to reproduce a suppressive wave. An important parameter of this model is the cortical extent of the excitatory/inhibitory connections. They tuned it so as to obtain a VSDI response similar to the experimental one. The inferred size is close to the one reported in the literature. They also highlight that the suppression requires an inhibitory gain stronger than the excitatory gain and a model based on conductances. To remind you, this gain is an amplification coefficient for the slope of the transfer function. This means that for lower excitations, the inhibitors will increase their discharge frequency more strongly. They showed that with a current-dependent model, the interaction between the two spots of dot activity did not lead to suppression but, on the contrary, to reinforcement. They found that suppression increases with a reduction in external drive as well as with an increase in the synaptic timescale ratio (τ_E/τ_I) ratio or adaptation. They also conjectured the need for an asynchronous, irregular and spontaneous regime which only occurs for a *non-zero external drive*. According to them, as long as this regime is present, whatever the modified parameters, the suppression wave is almost always observed. They concluded that this suppression could be a kind of a dynamic normalisation of lateral connectivity, created by the excitatory/inhibitory balance and induced by the non-linearity of excitatory and inhibitory conductances. Its role would be to ensure that there is only one representation of the stimulus at a time in the cortex.

We also carried out a quantitative analysis of our results to compare them with those of Chemla et al. We reveal a maximum extension of the activity spot of around 4 degrees. This is a slightly smaller connection size than the the cortical extent of the excitatory connections (5 degrees). This size is also twice as small as the spatial extension measured by Chemla et al. (2 degrees). We believe that if the suppressive wave and the activity Gaussian are both due to lateral connectivity, we should be able to verify this by varying the length of the connections as well as the speed of fibre conduction. We actually conjecture that the size of the activity spots depends on the excitatory/inhibitory balance. We could evaluate this by varying the parameters affecting inhibition (excitatory/inhibitory connection amplification factor, inhibitory characteristic time, quantal conductance of inhibitors). Note that the duration of our activity spots is twice as long as Chemla et al. (400 ms compared with 200 ms). This discrepancy could be fixed by modifying the values of the characteristic times of the retina. This additional degree of freedom in our model, not present in the previous cortical models (including the one used by Chemla et al), allows us to better tune the simulation results to experiments, in a similar way as we did already in chapter 3. We have previously observed what looks very much like a suppression wave in Figures B and C. However, it is important to confirm this impression by quantitative measurement. However, it is important to confirm this impression with a quantitative measurement. To do this, we need to determine how the maximum suppression peak behaves over time. If this maximum peak remains at the same position, then what we have observed is simply a spot that spreads out gradually. On the other hand, if the maximum peak moves in space, this means that it is a propagating wave. This maximum peak moves from 2.7 degrees (left stimulus) to 1.6 degrees (right stimulus) at a speed of 11.4 degrees/s. The speed of propagation of the wave is half that of the spread of the Gaussian activity (25.8 degrees/s). This confirms the presence of a propagating suppressive wave. The wave suppresses up to -45% of the sum of the responses from the right and left stimuli, which is close to the -50% observed by Chemla et al. Unlike Chemla et al. biological results, our two speeds (gaussian activity and suppression) are different and much lower. It would be interesting to check whether this difference in velocity is explained by the difference in retinal characteristic times. Finally, the delay that we observed in the cortical response in relation to the stimulus flash is also present in the results of Chemla et al. but is twice as long (11 ms compared with 23 ms). In our model, this delay is reproduced by the characteristic time cascade, from the retinal layers, to cortical layers. In biology, this cascade corresponds to the time taken by the visual signal to "pass through" the visual system.

If we compare our results with those of the Chemla et al. cortical model, our suppression wave seems actually quite different from theirs. The article by Chemla et al. does not present any analysis of the behaviour of the maximum

peak of suppression. It is therefore not possible to conclude with certainty that their model reproduces the suppressive wave. Furthermore, the time-horizontal representations of the suppression seem to evoke the spreading of a Gaussian spot rather than a wave. A spot mainly located halfway between the two flashed points. On the contrary, in our result, we clearly have the displacement of a suppressive wave between the most recent and the oldest point. A behaviour closer to the biological results observed. This means that our model would have a parameterisation more favourable to suppressive waves. However, we do not know which parameters are responsible for this difference.

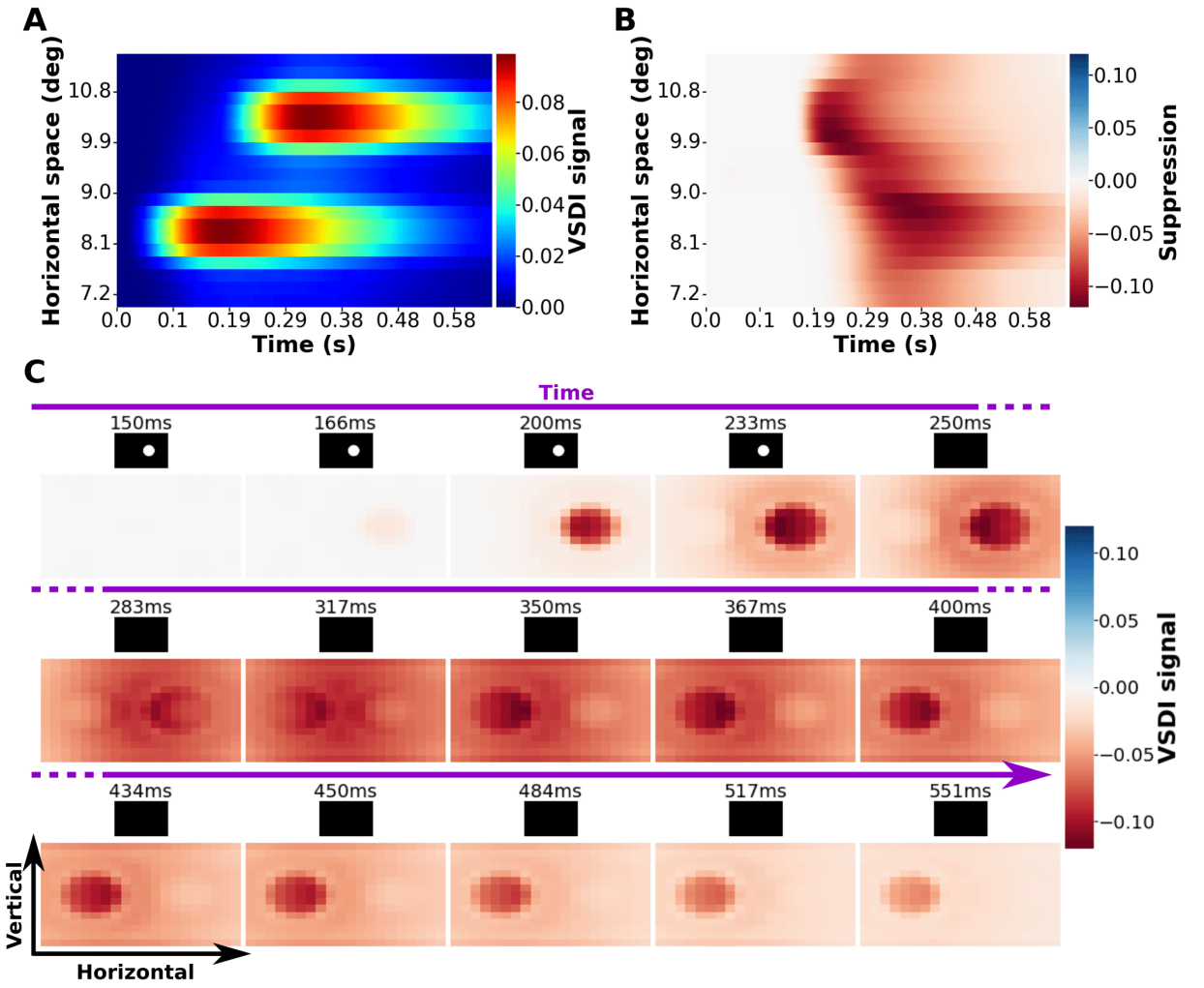

Figure 4.2: **The presence of the suppressive wave of apparent motion depends on the parameters.** Same presentation as Fig. 4.1. This simulation was carried out with the default parameter set (Appendix A.1). The size of the graph used is 15×83 cells. In contrast to Fig. 4.1 the horizontal axis of figures A, B and C has been cropped to keep only a square of 4.275 degree centered on the apparent motion and comparable to the graph of figure 4.1. Here, we don't see a clear wave propagation, in contrast to 4.1.

Figure 4.1 demonstrates the ability of our model to reproduce the suppressive wave observed by Chemla et al. We can actually go beyond as we also have the possibility of modifying the different model parameters, in particular those of the retina, to understand their respective roles. In this spirit, we studied the effects of some parameters variations on the suppressive wave. We run new simulations, this time using the default set that we have used throughout this thesis A.1, in particular in the chapter 3 on anticipation. We want to apply this default set because it is the closest to biology and the most stable. It is also the set that gave us the best results for anticipation. The question therefore arises as to whether it can also give good results in the context of apparent motion. In this default set we have modified : the amplitude of the OPL ($\mathcal{C}$), the retino-cortical weight (w_{RC}), the inhibitory quantal conductance (Q_I) of excitators, the probability of connection between neurons in the mean fields ($pconnec$), the connectivity distance of bipolar cells (σ_c), the characteristic time of bipolar cells (τ_B) and a non-zero external drive (ν_{ext}). This last choice was motivated by the

results obtained by the authors of the cortical model. Indeed, a non-zero external drive is normally essential for cortical mean fields models to function correctly [12, 13]. In [9] the authors actually conjectured that an external drive of zero would be detrimental to the suppressive wave. The comparative values of the default set and the set in figure 4.1 is illustrated by the table 4.1.

Figure 4.2 investigates this aspect, where we have dropped the stimulus representation as it is the same as in Fig. 4.1. In figure 4.2 A one observes as well a spot of activity at the bottom corresponding to the point on the left and then a second spot at the top corresponding to the point on the right. As in the previous case, the activity spot on the left-hand point is the first to arrive. Here, with a delay of 36 ms compared to 13 ms for the other set of parameters. The spots are spread over a radius of $1.8°$ and have a duration of about 500 ms instead of 400 ms. Figure 4.2 B also shows the presence of a suppressive wave propagating backwards for this parameter set. The maximum suppression only rises up to -11% of the sum of the responses from the right and left stimuli. This is 34% less than for the previous set. The peak of this maximum suppression moves from the position of the right stimulus to that of the left at a speed of 11.4 degrees/s, similarly to the previous example. In both sets, the region of the right stimulus is transformed into a suppression "shadow". This means that we do have a suppressive wave propagating. However, this suppressive wave remains almost impossible to see in the representation of Figure 4.2 C. We can actually see a suppression zone switching from right to left. But, the wave transiting between these two spots is too weak and noisy to be clearly visible. Overall, this new set of parameters seems to generate a suppressive wave but weaker, with less performance and longer compare to the Figure 4.1. Hence, the results in Figure 4.1 are the "better" ones we have obtained for reproducing the suppressive wave. As such, we decided to name this parameter set as the "better" set and distinguish it from the "default" set used in the rest of the thesis. Certain parameters must have affected the wave.

Parameter name	**Symbol**	**Default value**	**Better value**	**Expected effect**
Pixel per degree	ppd	300	30	More spatial precision
Width (X)	L_X	18.45	4.28	Less edge effects
Length (Y)	L_Y	3.15	0.9	Less edge effects
Frame rates	δ_t	60	188.68	No effect
OPL input amplitude	$\mathcal{C}$	0.025	0.5	Maintains the bipolar response amplitude equivalent
OPL center RF size	σ_c	0.2	0.3	Increases the extension of activity spots and suppression
OPL center characteristic time	τ_c	0.1	0.02	Increase activity spot and suppression duration
Bipolar characteristic time	τ_B	0.1	0.05	Increase activity spot and suppression duration
Ganglion characteristic time	τ_G	0.1	0.02	Increase activity spot and suppression duration
Retino-cortical amplitude	w_{RC}	2.5	4	Maintains the amplitude of the retinal output sent to the cortex.
Inhibitory quantal conductance of excitatory population	Q_{I_E}	3	4.5	Increases excitation to the detriment of inhibition.
Probability of connectivity	p_{connec}	0.0375	0.05	More stablity
External drive	ν_{ext}	2	0	Decrease the suppressive wave

Table 4.1: **Comparison between the default parameter set and the better one.** The "default" set corresponds to the parameters used in the rest of this thesis and in figure 4.2. The "better" set corresponds to the parameters used in figure 4.1, and is so named because it is the set that gave the best suppression results with apparent motion. For each parameter in our retino-cortical model, we give its name, symbol, its value in the best set, its value in the default set and the expected effect of this parameter on the retino-cortical model and suppression.

To go further, we are trying to understand which parameters may be responsible for these changes. The table 4.1 summarises all the different parameter values in the two sets and their assumed effects. First of all, we have the amplitude of the OPL and the weight of the retino-cortical connectivity. The aim is to see only a possible effect of the retina on the cortex through the spatio-temporal profile of its response and not through the intensity of its response. In theory, this parameter should smooth out some of the differences in response between the two sets rather than widening the difference. The decrease in the bipolar connectivity distance could theoretically lead to a shrinking of the activity spot or to suppression. In contrast, tests during the calibration of the model (Sec. 2.2.2) showed that the increase in the

probability of connection that we had carried out had very little effect on the response profile of the cortex. Its main effect was to stabilise the network.

The differences observed in the delay of the cortical response and in its duration could be explained by the characteristic times of OPL, bipolar and ganglion cells. All three have been considerably increased. The duration of the spots would be longer due to the slower decay phase of the Gaussian spot response. This effect on the Gaussian spots could be transferred to the suppression of which they are at the origin. Note that the change in characteristic time did not affect the speed of propagation of the suppressive wave. It is conceivable that the increase in the characteristic time could have contributed to the expansion in the size of the activity spot by slowing down the decay of the activity. Despite this, the most likely hypothesis for the reduction in the size of the activity spots is the involvement of the external drive (μ^{drive}) increased from 0 to 2 Hz.

In the presence of a non-zero external drive, the system is in an active state even at steady-state. The basic level of activity has risen compared with that of the better set. As it rose, this level of activity was able to completely drown out the low-intensity regions of the activity spot and its periphery. This would explain the shrinking of the activity spots observed with the non-zero external drive. In the case of the high-intensity regions of the activity spot, these were not drowned but their amplitude was drastically reduced. The amplitude of the VSDI depends both on the peak of activity and on the base level. This is why the maximum VSDI signal in the default set is divided by two compared with the better set. We assume that, in addition, the increase in the base level could also reinforce the network gain control carried by inhibitors and therefore also reduce the average discharge frequency of the cortical columns. This would contribute to reducing the VSDI response. Finally, a larger external drive screens the dynamics and diminishes the spread of the Gaussian spots, preventing them from interacting and generating the suppressive wave. In our case, the suppressive wave would be generated but with a very low intensity. The signal-to-noise ratio would be not enough to observe a salient wave. This observation is in line with that made by Chemla et al, where reducing the external drive increased the level of suppression. On the other hand, it is surprising because it contradicts their conjecture that a zero external drive should not generate a suppressive wave.

As a conclusion, we built a simulation set-up allowing us to reproduce the experiments of Chemla et al. in [9] for the apparent motion. We used an apparent movement stimulus with the same temporal and an adapted spatial dimensions as theirs. We fixed the connectivity extent and the conduction velocity of the cortical fibres at the value indicated by Frederic Chavane. All the cortical parameters are based on previous study on cortical mean field model [12, 13].

Our model is indeed capable of reproducing the suppressive wave of an apparent movement as studied by Chemla et al. This suppression wave is initiated by the appearance of the response to the most recent stimulus propagating back to the position of the oldest stimulus. This is the same observation made by Chemla et al. in the macaque. Despite differences in the temporal, spatial and speed properties of the wave and spots of activity, we think that our model have provided a better reproduction of the suppressive wave than that proposed by the cortical model used by Chemla et al. Indeed, the suppressive wave is much more visible in our time-horizontal representation than in theirs. In addition, our simulation setting (model + Macular plateform) allows us to go beyond the experimental setting by modifying both retinal and cortical physiological parameters in a way which is not accessible to experiments.

We used two sets of parameters to study the suppressive wave. The "better" set corresponds to the parameterisation that gave the best suppressive wave. The "default" set is the set of parameter values used in the rest of this thesis. The default set of parameters showed a weaker suppression wave. As we checked, some specific parameters could be good candidates for obtaining a highly visible suppressive wave. This is especially true for the background activity ν_{ext}. We confirm that a low external drive improves the level of the suppressive wave. We obtained the best result with a zero external drive. This is actually a surprising result given the importance of a non-zero external drive for the proper functioning of mean field cortical models[13]. For the moment we have no explanation for this contradiction.

Another interesting parameter that we didn't explore by lack of time could be the inhibitory quantal conductance Q_I of excitatory cells. The effect of this parameter on the suppression wave would confirm the importance of inhibition or the inhibition/excitation balance. Finally, the characteristic time of bipolar cells (τ_B) could play a role in extending the duration of the suppressive wave. A separate, more in-depth study of these different parameters could confirm these different hypotheses. It could enable the parameters to be optimised to obtain a suppressive wave that is as close as possible to biology. In this context, we would need an external drive low enough to enhance suppression but high enough to be compatible with the proper functioning of mean field models. According to Chemla et al, the suppressive wave is a dynamic normalisation of lateral connections caused by the excitatory/inhibitory balance. We could investigate the impact of this balance in our model. This could be done by varying the strength of the excitators or inhibitors by increasing parameters such as the synapse amplification factor, characteristic times or quantal conductances. This exploration would also be an opportunity to test our hypothesis that the extension of the cortical response also depends on this excitatory/inhibitory balance in addition to their connectivity distance. The suppressive wave is thought to be supported by lateral connectivity. This assertion could be verified by assessing the extent to which changing the

conduction velocity of this lateral connectivity can affect the speed at which the suppressive wave propagates. Finally, for the sake of simplicity, we have so far used a passive retina. This is not realistic because in the biological retina there are amacrine cells whose modulatory role by inhibition is essential. They create a dynamic gain control that is constantly present in the retina. If we want to get even closer to the Chemla et al. experiment, we need to add this amacrine connectivity or gain control directly. This change could make it possible to correct the difference observed between our quantification of the suppressive wave and that of Chemla et al. In addition, experiments have shown the importance of the retina in saccadic suppression [84].

4.2 Simulated saccades

4.2.1 Introduction to simulated saccade

Simulated saccades are a means of reproducing the saccade phenomenon [5] in a psycho-physics context where the gaze is fixed [8]. This is a way of isolating the visual component of the saccadic omission from the motor component. Recall that saccadic omission is the fact of not perceiving the movement of a saccade. Its visual component is carried by a peri-saccadic masking mechanism. In the case of a saccadic movement without peri-saccadic elements, a blurry smear is percepted during the saccade. In the presence of static phases before or after saccades, this smear is removed, leaving only a clear continous perception of a visual scene [7]. In particular Mark Wexler from the "Psychologie de la Perception" laboratory was able to reproduce this result with simulated saccades without eye movement (unpublished work). He has also shown with Duyck et al. that simulated saccades with masks were perceived with a shorter amplitude of motion [8]. In some other preliminary experiments, at the origin of the ANR shooting star, Mark Wexler and Patrick Cavanagh [96] have demonstrated the existence of an illusion induced by saccades, called "shape-dragging" (See Fig. 4.8 for an illustration). When the moving shape differs from the static shape, observers reported a clear moving shape corresponding to the static shape.
To construct simulated saccades, they used three essential elements. Firstly, a movement reproducing a standard saccade which he measured in subjects. The measured average amplitude of the saccade is 6 degrees, its average duration is 34 ms and its average speed is 176 degrees/s. Secondly, he used stimuli consisting of a movement phase preceded and followed by forward and backward static phases respectively: static-movement-static (SMS). They compared this with a stimulus with only movement, no static phases: -movement- (_M_). The duration of the static phases was set to 100 ms by default but could be varied. Finally, these stimuli had to be displayed using a video projector with a refresh rate of 1440 Hz. Using our model we would like here to investigate the impact that the different properties of a simulated saccade have on the retino-cortical response: high speed, presence of static phases, high versus low frame rate. In particular, we look more closely at effect of static phases on smear masking and shape-dragging.

We carry out our simulations with simulated saccade stimuli strongly inspired by the stimuli that Mark Wexler sent to us. However, he didn't communicate us the actual dimensions (in degrees) of these stimuli. For this reason, we decided to infer these dimensions on the basis that the distance between the two static phases should be of 6 degrees. From this we could determine a degree/pixel ratio of 0.078. From this ratio, we could calculate any dimension in degrees from the pixel sizes. Mark's stimuli have all the same width but can have two different heights when testing shape-dragging. There are high bars, called "wide" (W), and small ones called "narrow" (N). Calculating the height of the wide bar from the degree/pixel ratio of 0.078 gives 2.96 degrees. This dimension fits into our simulated area but we preferred to reduce it to 2.15 degrees to leave 0.5 degrees of margin with the edges. This choice was made to limit edge effects and also to see if the cortical activity extends beyond the stimulus size. We also changed the height value for the narrow bar. We indeed thought it was important to keep the same proportion as Mark's between the heights of the narrow and wide bars. We ended up with a wide bar dimension of 1.08×2.15 degrees and a narrow bar dimension of 1.08×0.45 degrees. We set the saccade speed at 200 degrees/s and the static phase duration at 100 ms on the advice of Mark. Finally, we chose to use a motion amplitude of 12 degrees. This is a correction that we decided to make in order to obtain high-speed, low-frame-rate simulations where the bar flashes several times along the trajectory instead of just once. We used all these measurements to create SMS, _M_ but also S_S stimuli at different speeds, frame rates and bar heights. The axis chosen for the movement of the bar is the horizontal axis, to be compatible with our horizontal graphs. In the remainder of this section, we use a three-letter nomenclature to describe these stimuli. The first letter refers to the first static phase, the second to movement and the last to the second static phase. Three possibilities are possible for each of these letters: N for a narrow bar, W for a wide bar and '_' for the absence of a bar. The difficulties encountered in using these high frame rate stimuli in Macular simulations are detailed in the section 2.1.4.

4.2.2 Role of the refresh rate in simulated saccade

We examine first the effect that a simulated saccade can have on the cortical activity using the setup presented in the section 4.2.1. A saccade is characterised by high speed, the presence of static phase and a high frame rate. Before going any further, we want to evaluate what the activity generated by a non-saccadic movement in the context of the SMS stimulus with high frame rate (1440 Hz). To set up a non-saccadic movement, we take care not to use the main property of a saccade: a high speed of movement. We have therefore chosen a bar moving at 6 degrees/s. The purpose of this

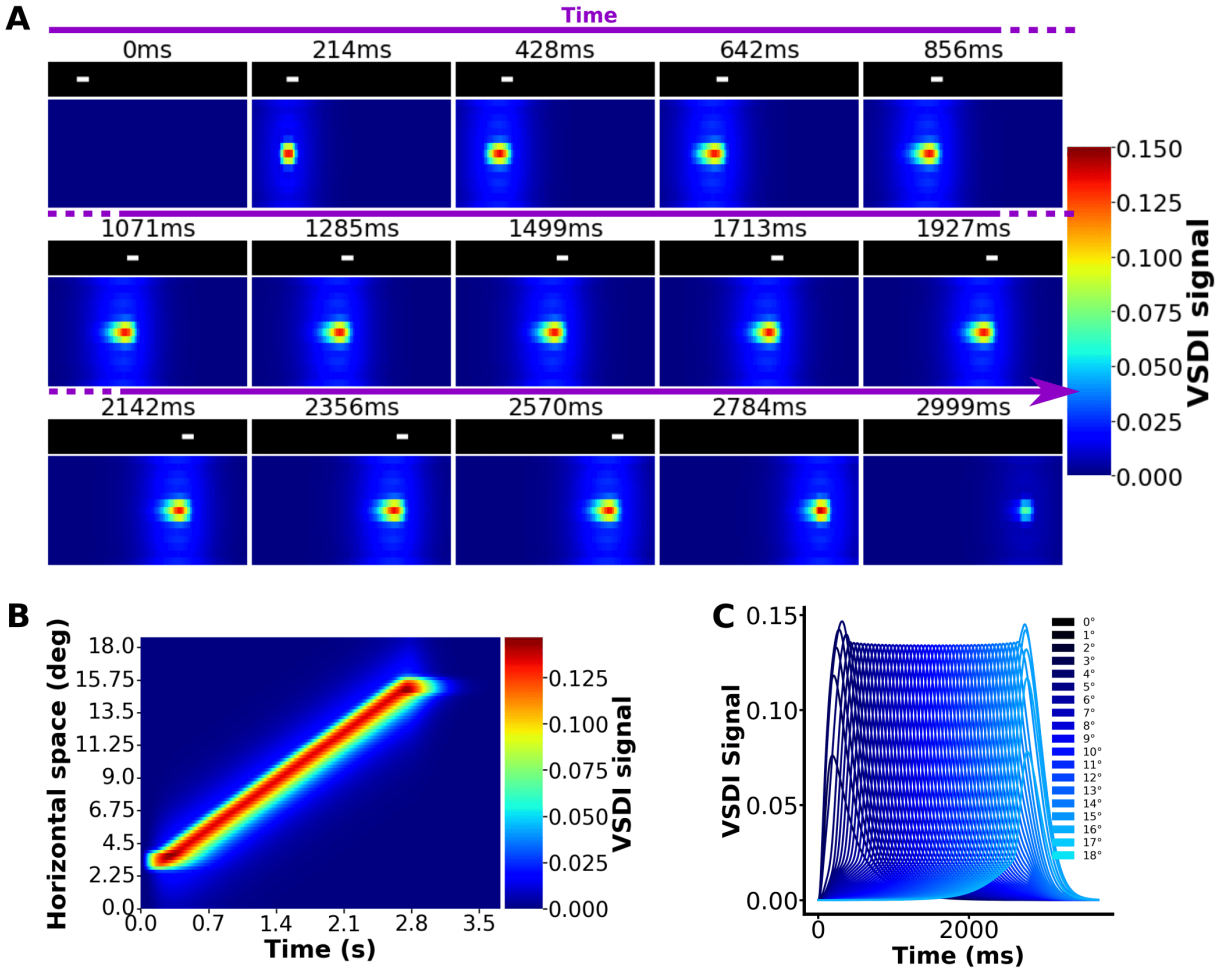

Figure 4.3: **The activity generated by slow movement is indistinguishable from that of successive static phases. A)** Time sequences of the VSDI signal (bottom) for a 6 degrees/s NNN stimulus (top) displayed at a frame rate of 1440 Hz. There is a static phase, with a narrow bar, from 0 to 100 ms, followed by the motion of the narrow bar, in the interval $[100, 2520]$ ms, finally ending by a static phase, still with a narrow bar. The time is indicated by the purple arrow above each time sequence. **B)** Time-horizontal heatmap representation of the VSDI signal in response to the stimulus displayed in A. **C)** Time-horizontal VSDI curves representation for the same conditions as A using the same color gradient as chapter 3

first simulation is to serve as a control condition that we will compare in the simulations that follow, which will have the properties of a saccade (fast movement and SMS). This control condition will give us a better idea of the specific characteristics of the response to a true saccadic movement.

In Fig. 4.3 A we show the evolution of the stimulus and the activity of the simulated cortical area over time. The static phase of the stimulus begins in the first frame (0 ms). In the next frames, from 214 to 2356 ms, we can see the slow progression of the movement of the bar with a speed of 6 degrees/s) between the positions of the two static phases. The movement lasted for 2520 ms, representing the majority of the stimulus duration. The first static phase produces a very large spot of activity. The movement phase that follows generates a strong activity looking like a continuous translation of the spot of activity initiated by the static phase. The amplitude and size of this spot is constant during movement. Moreover, no trace of residual activity remains behind this spot. Figure 4.3 B corresponds to the same condition using the representation already used in the previous section (Sec. 4.1, Fig. 4.1 B). The first static phase, on the left, is shown at the bottom of this representation, while the second static phase, on the right, is at the top. The translation of the activity generated by the initial static phase is clearly visible. Note the 37 ms delay before the response of the left static phase. This delay is identical to that observed in the apparent motion with the same default parameter set (Sec.

4.1). The duration of the activity generated by the static phases is about 570 ms, the same for that generated by the movement.

Figure 4.3 C is another representation of the VSDI activity as a function of time and horizontal position. It is similar to the one used in the chapter on anticipation (Sec. 3, Fig. 3.1 A). The VSDI signal is plotted as a function of time for each horizontal position. A blue gradient is associated with the horizontal coordinate of the cortical column. The closer a cortical column is to the left edge (0 degrees), the darker its colour; conversely, the closer it is to the right edge (18 degrees), the lighter its colour. On the far left and right of the graph one observes the VSDI peaks of the cortical columns close to the static phases. In between are the VSDI peaks of the cortical columns situated on the trajectory of the movement. The difference between the static phase peaks and the movement peaks is very small (-6%). We can also see that when the cortical columns of the second part of the movement is activated, the response of the first static phase is over. In addition, when the cortical columns of the second static phase are activated, the response of the first part of the movement is over.

The activity spots of the movement and static phases are almost identical. This means that *the cortex should not be able to distinguish the static phases from the movement*. This phenomenon happens because the movement is slow enough for the bar to remain in the receptive field for a long time and generate a response equivalent to a static bar flashed for 100 ms. We conjecture that no trace of residual activity remains behind the spot because of the slowness of the bar, 6 degrees/s, quite smaller here than saccadic speed. This is because the time required for the bar to cross the receptive field of the cortical column is quite a bit longer than the characteristic time of integration of this column. In this context, the cortical columns have time to inactivate completely when the bar has just left their receptive field. On this basis we raise the hypothesis that the interaction between static phases and movement depends largely on two temporal ratios.

The first is the ratio between the characteristic integration time of the cortical column and the time that the bar stays in its receptive field (shaping parameter rho in C). The higher this ratio, the earlier the static phase arrives. The static phase will be flashed even before the movement activity has a chance to develop. The two activities will thus increase almost simultaneously, facilitating their interaction.

The second ratio is between the duration of the static phase and the entire movement. The greater this ratio, the greater the difference in amplitude between the VSDI peaks in favour of the static phases. We can assume that the higher the amplitude of the VSDI peak of the static phase, the greater the suppression it causes. Moreover, this also generates a difference in VSDI signal slope between the peaks of the static phases and those of the movement. The slope of the VSDI signal in the second static phase is much steeper than the slopes caused by the movement. If the difference in slope is sufficient, then the response to the second static phase could catch up with or even exceed the response of the cortical columns at the start of the movement trajectory. All this means that the speed of the movement, its amplitude, the duration of the static phases, the size of the receptive field and the characteristic time of the cortical columns are crucial parameters. This could be a sign of the influence of shapings parameters (C).

With a bar moving at 6 degrees/s, the ratio between the characteristic time of the cortical column and the duration of the movement is extremely low (1.2). The cortical columns of the first part of the movement have time to inactivate before the end of the movement. It is therefore impossible for the second static phase to influence the cortical columns of the first part of the movement. The same assumption applies to the interaction between the columns in the first static phase and those in the second part of the movement. The ratio between the time of the static phase and that of the moving phase is low (0.04). The small difference between the amplitude of the static phase and the movement therefore suggests that here the static phase could not exert much influence on the activity generated by the movement. This is reinforced by the fact that the VSDI signal from the static phase will become lower than that caused by the movement even though we are still at the start of the movement. All this suggests that the static phases for such a low speed has a little impact on the movement.

In this section, we want to observe the impact that the frame rate can have on the response of the cortical columns in the case of a fast, saccadic, motion. We therefore first carried out simulations with a bar speed of 200 degrees/s, static phases and a frame rate of 60 Hz or 1440 Hz. We then produce the same 3 graphical representations as used for the 6 degrees/s stimulus.

The stimulus and response for a low frame rate (60 Hz) is shown in Figure 4.4 A. The first static phase appears at 0 ms and remains until the onset of movement. The start of the movement can be seen in frame 116 ms of the figure, while its end can be seen in frame 166 ms. Here, the movement lasts 60 ms, which is shorter than the static phases. We could only display two frames of movement because the speed is too high to have more in our representation. The second static phase can be seen in the 200 and 250 ms frames. The VSDI response barely begins to appear at the 33 ms frame. Note the progressive spreading over a long distance of a spot of Gaussian activity on the left of the spot, generated by the static phase.

The response caused by the moving phase of the bar is present in 166 ms frame. In contrast to the case when the speed is 6 degrees/s, it appears discontinuous. It is made up of 3 rectangular motion spots of low amplitude and very little spatial spread. There is no trace of these spots of motion activity in the 116 ms frame while the movement has already begun. Here we have a delay in the cortical response. This delay is also particularly noticeable for the second static phase, which is not yet visible in frame 200 ms, i.e. 34 ms after the start of the static phase. The second Gaussian spot of activity associated with the second static phase becomes clearly visible in frame 250 ms. Here too, its Gaussian spread is quite wide. Unlike the 6 degrees/s condition, when the spot of activity from the second stimulus appears, the motion spots are still clearly present.

With the representation in figure 4.4 B, the three motion activity spots are located in-between the spots corresponding to the first and second static phases (located at the bottom and top respectively). These three motion spots have very similar onset times. The static phases last longer (400 ms) than the motion phases (300 ms). Added to this is a delay of 37 ms before activation associated with the first static phase. This time is similar to that observed with the control condition at 6 degrees/s. The motion and static phase activity spots measure 0.48 degrees high, 1.06 degrees wide and are spaced 1.6 degrees apart.

The VSDI curves as a function of time and horizontal coordinate reveal maximum VSDI amplitudes for static phase that are 4.2 times greater than those for motion (Fig. 4.4 C). The response to the second static phase was slightly lower than to the first (1.09 times less). Their slope is also much steeper. So, when the VSDI signal peaks at the beginning of the trajectory reaches its maximum, the cortical columns excited by the second static phase are already at the same level of activity. We can also see that the activity associated with the first static phase is always much higher than the activity generated by the movement, including the columns located at the end of the trajectory. This is a notable difference from the 6 degrees/s condition, which showed little difference between the static and motion phases. Within the motion trajectory, we can see fluctuations in the maximum VSDI signal due to the response in the form of spots.

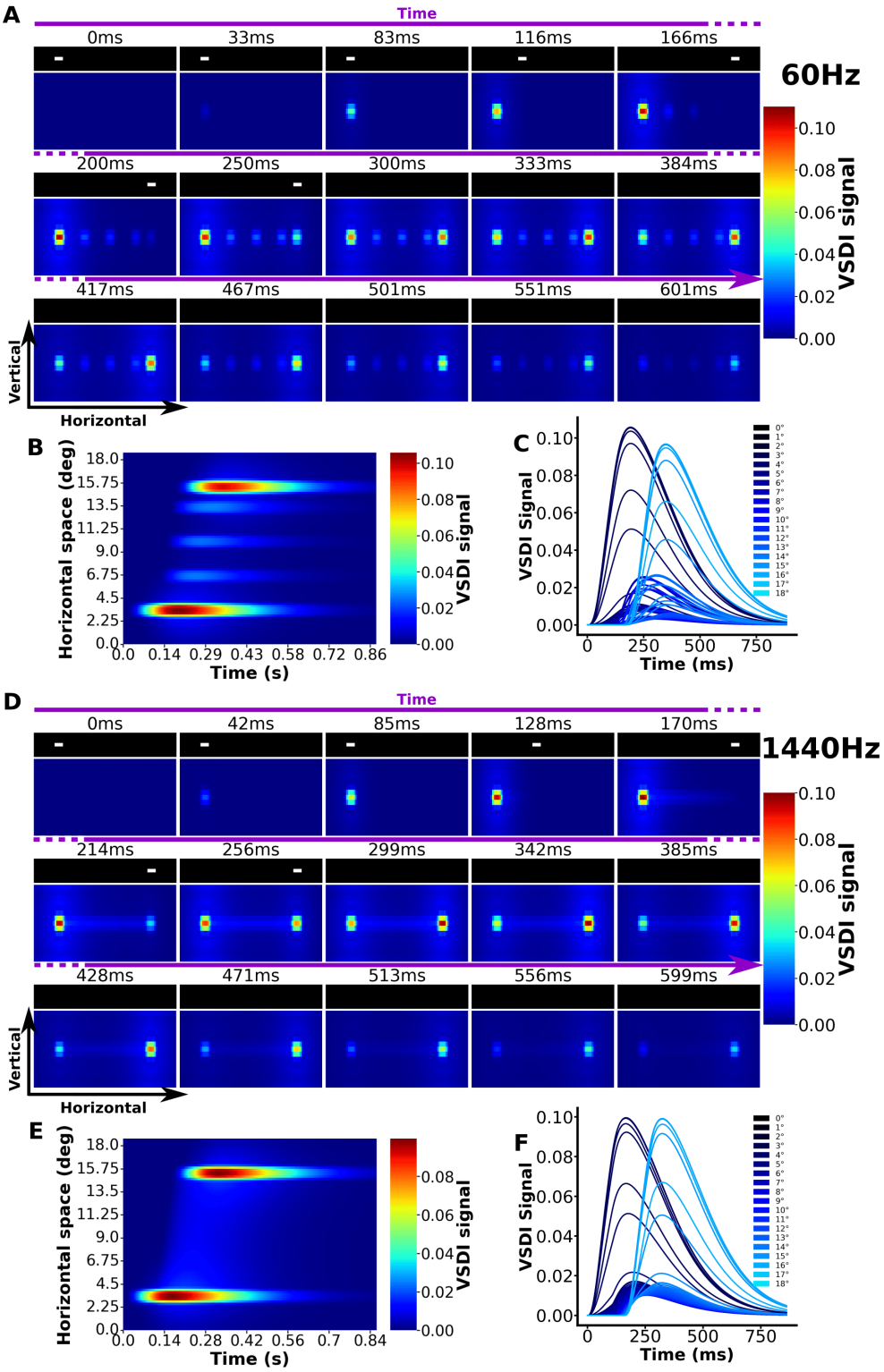

Figure 4.4: **The bar speed and the frame rate of the video projector modifies the response of the cortex. A, B)** Time sequences of the VSDI signal for a 200 degrees/s NNN stimulus displayed at a frame rate of 60 Hz **(A)**, or 1440 Hz **(D)**. The time is indicated by the purple arrow above each time sequence. **B, E)** Time-horizontal heatmap representation of the VSDI signal for the 1440 Hz **(B)** and 60 Hz **(E)** case. **C, F)** Time-horizontal curves representation of the VSDI signal for the 1440 Hz **(C)** and 60 Hz **(F)** case.

What becomes this experiment for a high frame rate of 1440 Hz ? Here, the evolution of the stimulus over time seems very similar to that at 60 Hz (Fig. 4.4 D). However, if we look at the response, a continuous band of residual activity gradually develops between the two static phases. There is a delay between the start of the bar movement and the appearance of the band. This band has a pitch of 0.44 degrees, equal to the pitch of the activity generated by the static phases. As for the response to the static phases, it doesn't seem any different from that with the slow frame rate (60 Hz). The band of activity remains long enough to be present at the same time as the response to the second static phase.

However, the result obtained differs both from the response at 60 Hz. It is smooth and does not show the discontinuous motion spots of Fig. 4.4 A. In addition it differs from the response to the 6 degrees/s movement for its residual activity and time scale. Figure 4.4 E confirms that the duration of the static phases and their size at 1440 Hz is the same as at 60 Hz. The delay also remains unchanged. The time elapsed between the start of the movement and the second static phase is extremely short (Fig. 4.4 F). This very short lapse of time explains why, as at 60 Hz, the first static phase generates activation that remains throughout the movement and the second static phase has time to respond sufficiently to equal or exceed the activity generated by the movement, including the start of its trajectory. The slope of activation of the static phases is much steeper than that of the movement phases. In contrast to 60 Hz, the maximum VSDI is the same for both static phases and is 10 times larger than that caused by movement. However, the maximum activity generated by the movement is lower.

In the two figures Fig. 4.4 A and D, the two stimuli look very similar despite the large difference in frame rate. The limited number of frames we were able to show did actually not allow us to have enough frames of movement to see a difference between those two stimuli. Despite this, the video of these two stimuli are very different. In the 1440 Hz stimulus, the movement of the bar appears fluid and continuous. All the fine details of the rapid movement of the bar are captured. Every cortical position is activated in the same way. In the 60 Hz stimulus, the bar remains static for a long time before jumping to a new position. However, this time is still much less than the duration of the static phase. The perceived movement is discontinuous and corresponds to an apparent motion. Only 3 shifts of the bar are observed within the trajectory of its movement.

At the cortical level, these two very different stimuli generate a spatio-temporal response whose structure is similar to theirs. Thus the discontinuous stimulus at 60 Hz provokes a discontinuous and heterogeneous response to a continuous movement. The bar activates a limited number of cortical columns in the trajectory of the bar. Conversely, at 1440 Hz, this leads in our model of V1 to a homogeneous and continuous band of activity. In comparison, at 1440 Hz, all the cortical columns in the trajectory of the bar are activated, but for less time than those in the activity spots at 60 Hz. With a high frame rate, the bar leaves the receptive field of the cortical columns too quickly to give them time to integrate. In contrast, with a low frame rate, the bar remains stationary for longer, leaving more time for the few cortical columns it activates to integrate. This is why the 60 Hz activity spots have a greater amplitude than the 1440 Hz band. The discontinuity in 60 stimulus is also responsible for the strongest response in the first static phase. When the movement starts, the first frame is in the same place as the static phase. The bar therefore remains at this position for one more frame before jumping to its next position. This means that the cortical columns at the position of the first static phase will be activated for one more frame.

In terms of spatial dimensions, the activity spots created at 60 Hz are identical to those in the static phase. A dimension not so far from their true spatial dimension. At 60 Hz, therefore, the spatial dimensions and the shape of the bar are preserved. This is very different from the case at 1440 Hz where only the vertical dimension is preserved. This observation was also made by Awen Louboutin, another doctoral student under the supervison of Olivier Marre in the ANR Shooting Star project (private communication). They are running simulations of a photoreceptor model from Rieke's laboratory to visualise the outputs sent by the photoreceptors to the rest of the retina. This photoreceptor model, which is more accurate than ours, takes into account the different processes that take place in a photoreceptor. All the simulation parameters were configured to create two different sets based on the monkey and macaque retina respectively. The stimulus used here belongs to the WNW category and is displayed at a frame rate of 60 or 1000 Hz. At 60 Hz, he observed spots of activity of the same shape as the bar, while at 1000 Hz there was only a blurred band of lower intensity (respectively 75% and 60% of the response of the static bar). Awen describes this effect as a loss of bar identity of the bar in the case of the high frame rate. He also speculates that this demonstrates the role of photoreceptors in this phenomenon.

For our part, we argue that these different effects are mainly caused by five parameters: the speed of the bar, the time it takes for the bar to cross the receptive field of the bipolar cells (or photoreceptors), the frame rate, the size of the receptive field and the characteristic time of the retinal cells. Their interaction can be summed up in two relationships. Firstly, there is a relationship between the frame rate and the speed of the bar. If the frame rate is much higher than the speed of the bar, then the corresponding stimulus will present a continuous movement that generates a real movement. Otherwise, the stimulus will be discontinuous and will only generate apparent movement. It is therefore the relationship between the frame rate and the speed of the bar that will be responsible for obtaining a discontinuous retinal or cortical

response. Then there is the relationship between the time taken for the bar to pass through the cells receptive field and the characteristic time of the cells, which we mentioned at the beginning of this section for its potential role in the interaction between the static phases and the movement phase. This is also the shaping parameter ρ presented in the appendix C. If the characteristic time is longer than the time of the bar in the receptive field, then residual activity will be observed to a greater or lesser extent. This explains the band at high frame rate and the presence of several visible spots at low frame rate. This phenomenon can be caused at the photoreceptor layer if the photoreceptors are slow enough to respond. It is important to stress that the natural visual environment is made up of continuous movements processed at high frame rates by our eyes. Low frame rates are only due to the limitations of human technology. Our results demonstrate the major impact that the frame rate can have on the stimulus of the moving object and also on the response of the visual system. This highlights the importance of not neglecting the frame rate in visual experiences, particularly in the context of fast movements such as saccades. It is very likely that the difference in spatio-temporal structure (continuous/discontinuous) at high and low frame rates can lead to radically different internal perceptions of bar movement. The succession of spots at 60 Hz could thus be perceived by the subject as a moving bar due to the apparent movement and clear shape that the spots take. The 1440 Hz band, on the other hand, could be perceived as a blurred bar with a smear.

These two frame rate conditions have one thing in common, that differs from the 6 degrees/s bar speed condition. Residual activity is left behind the bar. With a high speed of 200 degrees/s, the duration of the movement is extremely short. As a result, the cortical columns do not have time to inactivate before the movement ends. At 6 degrees/s, the opposite is true: the cortical columns have plenty of time to return to the state of equilibrium. This drag would increase with the ratio between the characteristic time and the duration of the movement phase. It would be a necessary point for good interaction with the activity generated by the static phases.

We believe that the results obtained here illustrate how the static phases, in particular the one after movement, can have a non-negligible influence on movement activity. With a bar speed of 200 degrees/s the ratio between the characteristic integration timescale of the cortical columns and the time necessary to cross the receptive field of the column is 40. In our opinion, this explains the capacity of the first static phase to generate an activity that lasts longer than the movement itself. This is how the activity created by the first static phase can influence the activity generated throughout the movement. This is also what allows the last static phase to become active before the cortical columns of the movement reach their maximum activity, including those at the start of the trajectory. This contrasts with the 6 degrees/s condition where this ratio is 33 times lower (1.2). Consequently, the activity of the static phase disappears well before the end of the movement and the activity of the second static phase appears well after the end of the movement.

The second ratio between the duration of the static phases and the entire movement phase is 1.7. This is a value 42 faith higher than that obtained with a bar speed of 6 degrees/s. We assume that this high value is responsible for the large difference in amplitude between the activity of the static phase and that of the movement. This difference in amplitude is accompanied by an equally large difference in VSDI slope. The activity of the static phases increases so quickly that the second static phase has time to catch up with, or even, exceeds the maximum activity generated by the movement, including that of the cortical columns at the start of the trajectory. This allows the second static phase to exceed the movement activity over a large part of the movement trajectory. This amplitude is also important to ensure that the activity of the first static phase always remains well above that of the movement. In contrast, when the bar speed is 6 degrees/s, there is virtually no difference in these amplitudes. As a result, the first static phase does not remain active throughout the movement and the second static phase does not activate with a sufficient slope to catch up with the activity of the movement.

We suggest that these effects result from a balance between 5 main parameters: the speed of movement, the amplitude of motion, the duration of the static phases, the size of the receptive field and the characteristic time of the cortical columns. These parameters greatly influence the opportunity for static phases to interact with movement. A balance that could be crucial for effective suppression between static phases and movement. All this would make it possible to justify that the effect of static phases comes into play in the context of saccade. This arises because the speed reaches a sufficiently high value. This would also provide a reason for the effect of the duration of static phases seen on saccade amplitude [8] and smear (unpublished work). Indeed, we believe that a reduction in the smear generated by the rapid movement of a saccade is associated with a strong suppression wave. A suppression wave which, according to Benvenuti et al. [3], should make it possible to erase the old representations of the movement and therefore the residual activity which generates the smear.

4.2.3 Effect of the static phases on smear

In this section, we study the implication of static phases on the absence of perception of a smear. This results from discussions with Mark Wexler (unpublished work). He has observed with psycho-physical tests on humans that the use of simulated saccades reduces the presence of a smear left behind the bar. The longer the static phase, the less visible this smear. As part of the ANR shooting star project, Mark Wexler is working with Frédéric Chavane to extend these

experiments to monkeys, where VSDI measurements are possible, and observe the cortical response. They are using only two stimuli, NNN and _N_. The aim of this section is to carry out the same experiment in our retino-cortical model. The characteristics of the stimuli we used are the same as those presented in section 4.2.1 and used in section 4.2.2.

In order to study smear, we first had to decide how to quantify it. We know that a smear is experienced, at the perceptual level, as a bar that is more or less elongated towards the back, and blurred. We think that this smear can be expressed by two components in the cortical response. A first horizontal component corresponding to residual activity upstream of the bar. A second vertical component corresponding to a greater spread of the cortical response. These two components were quantified using two methods developed by Mark Wexler and Frédéric Chavane (private communication).

The level of residual activity on the horizontal axis can be measured by constructing a horizontal section of activity along the stimulus trajectory (Fig. 4.5). This section is constructed by averaging over each vertical slice. This allows us to take into account the entire area behind the stimulus. As far as possible, we try to separate the two effects that make up the smear in order to understand how each behaves. This is why, in order to measure only the residual activity (horizontal smear), we have to take into account a restricted vertical zone in the wake of the moving bar. We only want to consider the cortical columns that were in direct contact with the passage of the bar. We can see in figure 4.4 D that the cortical columns directly in contact with the passage of the bar show an activity at least greater than 50% of the maximum activity of their vertical slice. With this in mind, we used a threshold to average out only those values in each vertical slice that exceed 50% of the vertical slice's maximum response. This creates a high-activity rectangle of interest centered on the same horizontal line as the spot of activity generated by the moving bar (Fig. 4.5 A). In this method, we keep the whole horizontal axis, including the static phases, because we also want to see how their activity evolves.

The spread along the vertical axis can be measured in a similar way by using a vertical section and averaging each horizontal slice (Fig. 4.5 A). This horizontal slice will nevertheless be defined to capture only the movement phase and not the static phases. It will also take into account the entire vertical axis, as no threshold will be applied. We abandoned this idea because of two issues. First, the presence of the static phases, even if truncated, risked to make the edges of the movement higher in intensity than the movement itself thereby attracting our measurement zone there. Second, the measurements would have been biased by the close proximity of the static phases.

The two smear quantification methods are illustrated in Figure 4.5 through a thought experiment. Figure 4.5 A represents a fictive spatial heatmap of the VSDI signal in response to a NNN stimulus accompanied by the frame of the labeled stimulus. We have pictured here 5 zones of increasing size represented by different colours. Each of these areas represents the movement response of different scenarios associated with an increasing smear. From the lowest to highest intensity of smear we have the red, orange, green, cyan and blue zones. Both (horizontal and vertical) smear components are increased.

First, the higher the smear, the more the active region lengthens horizontally. This corresponds to the increase in residual activity on the horizontal axis. This residual activity is reflected in the horizontal profile including all the vertical positions located in a zone of high activity ($> 50\%$ of the maximum of the integrated vertical line). This corresponds to a rectangle centered on the motion axis. The increase in the horizontal component of the smear causes the Gaussian-like activity to elongate backwards becoming gradually a plateau (Fig. 4.5 B). Second, the increase in the smear causes as well the activation zones to spread out vertically. This spread is reflected in the widening of the horizontal activity profile (Fig. 4.5 C) as the smear increases. If the smear increases sufficiently, the widening can lead to a plateau response.

The magenta zone in Fig. 4.5 B symbolises the core of high residual activity generated by the first static phase. For the sake of clarity, we have chosen to show it as invariant to smear levels. However, a smaller residual activity should also be accompanied by a stronger decrease in the residual activity of the static phase. In the vertical profile (Fig. 4.5 C), the activity cores of the static phases have been excluded from the calculation of the profile. We are only interested in the spread around the movement, not the static phases.

Figure 4.6 corresponds to the application of this method to quantify the smear to the NNN and _N_ conditions. The displayed profile shows the average response present on the horizontal axis, in the zone of high intensity located around the axis of movement. This profile was calculated for a series of frames ranging from 0 to 599 ms. This time interval was chosen in order to clearly see the decay of the cortical response over time. The speed of this decay is associated with the residual activity (horizontal component of the smear). For each frame, the scale of the y-axis was set to the same maximal value of 0.015. This value was chosen so that the motion response and part of the static phase response could be sufficiently visualised.

From frame 0 to 79 ms, only the horizontal NNN profile shows an activity, located to the left of the cortical area (blue). From frame 119 ms, a small amount of activity emerges to the left of the stimulus response profile (red). This activity continues to increase and to propagate from near to near in the next frame (159ms). At the same time, there is a slight increase in the VSDI signal to the right of the peak in the NNN profile, which is also propagating. In the second half

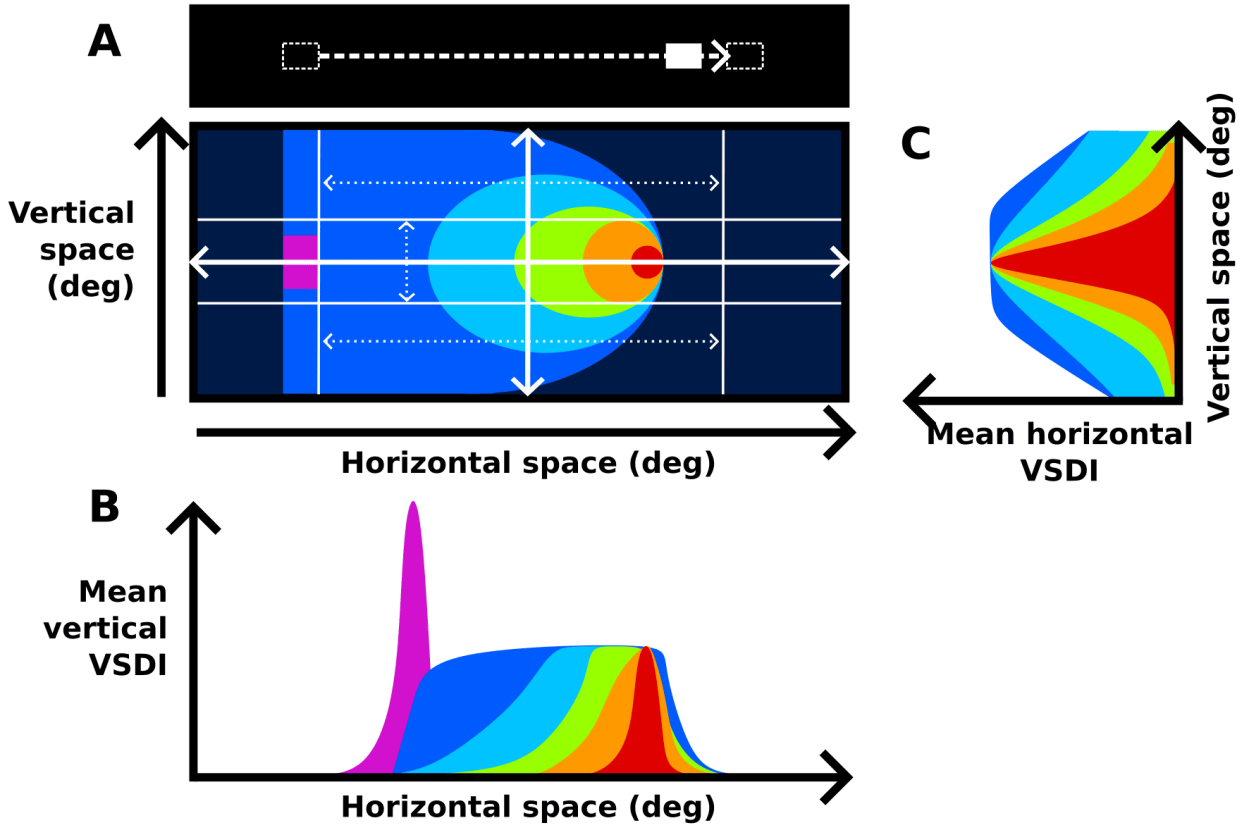

Figure 4.5: **The concept of mean sections. A), top.** A white square propagates from left to right, at a speed of 6 degree/s, on a black background, from a first position (dashed rectangle on the left), with a static phase lasting 100 ms, to a second position (dashed rectangle on the right) with a static phase of the same duration. This corresponds to a NNN stimulus. **A), bottom.** Sketch of the spatial VSDI response at the time corresponding to a specific stimulus position (a specific frame). The violet square represents the region directly activated by the first static phase. The colours red, orange, green, light blue and blue represent a discretisation of the activity generated by the movement of the bar. From red to blue, each colour corresponds to an increasing level of smear i.e., a spread of the response beyond the spatial region of the stimulus. This is associated to an increase in the horizontal residual activity and a vertical spread. The smear is first integrated vertically by averaging the contributions of the horizontal sections represented by the vertical dashed white arrow. The two horizontal white lines delimit the zone where the average is done. This is a dynamic zone obtained by applying a threshold of 50% to the maximum response of the vertical position. This vertical integration gives rise to **B),** horizontal profile of the VSDI signal at the corresponding frame. The more residual activity there is in the A spot, the more the horizontal profile shows a plateau. Similarly to B, an horizontal integration along vertical sections (horizontal dashed white lines) and only in the stimulus movement zone (vertical white lines) provides **C),** vertical profile of the VSDI signal for the same frame as A and B. The more the spot of activity in A spreads out, the wider the Gaussian-like profile.

of the horizontal profile, the responses of the two conditions are equal. In the 199 ms frame, a second response peak appears to the right of the horizontal axis. This peak continues to increase and at 239 ms creates an inequality in the responses between the two conditions for distant distances. At the same time, we observe a response from _N_ in the form of a straight plateau. From frame 439 ms, one can observe an asymmetric decrease in this plateau of activity. The anterior part of the response decreases before the posterior part. This reduction continues until the residual activity is almost non-existent. The residual activity of the NNN condition is also decreasing. At the center of the response profile, between the two peaks, the difference in response between NNN and _N_ appears to be gradually diminishing.

The same experiment carried out on monkeys by Frédéric Chavane and Mark Wexler revealed peaks of activity generated by static phases at the same height as the activity carried by the movement (private communication). Activity in static phases also lasts less time than in our simulation. They made a Gaussian fit of the horizontal profile for each frame. The aim was to determine the size of the residual activity spot and therefore the level of smear. The graph obtained showed

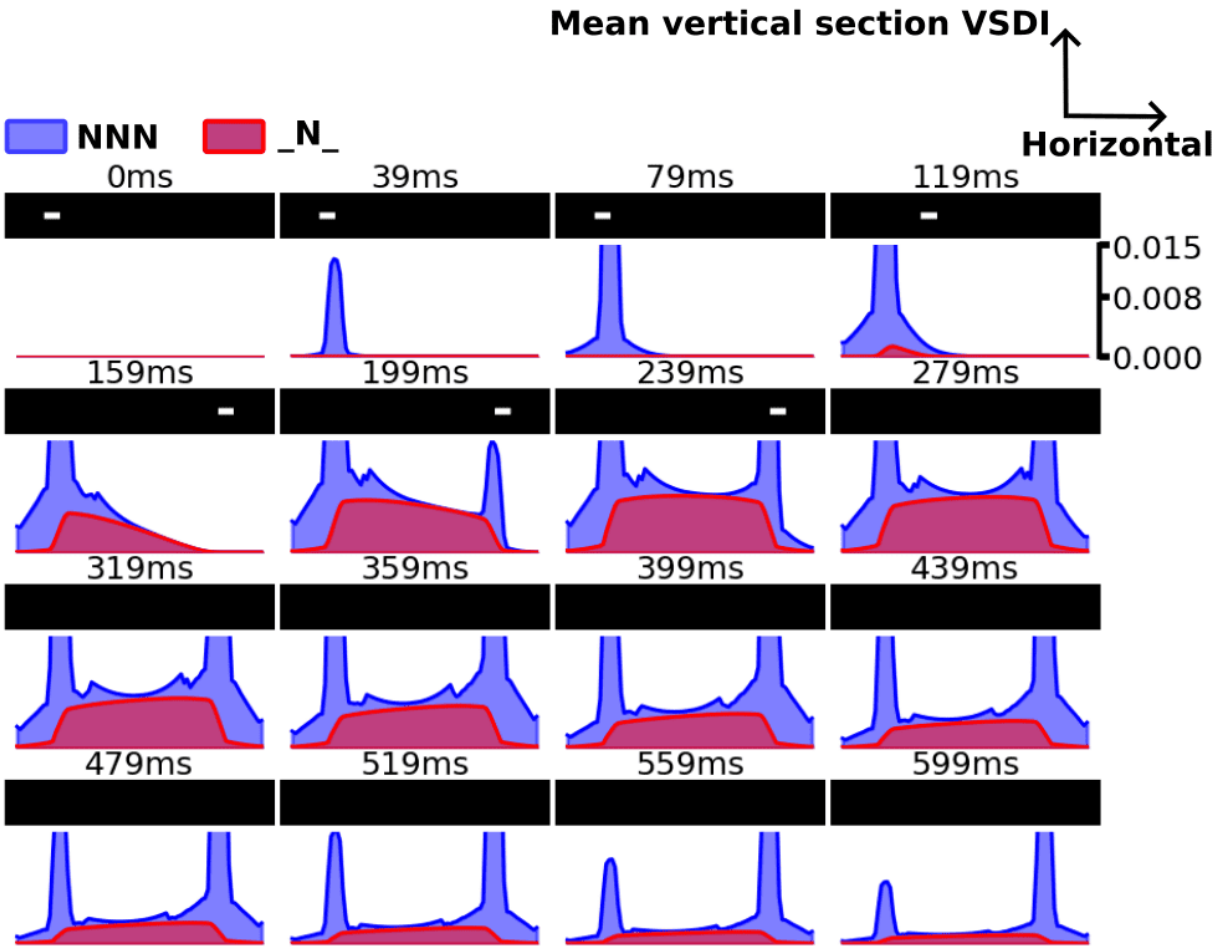

Figure 4.6: **Static phases increase the horizontal cortical smear.** Time sequences of the horizontal section averaged over the vertical axis defined in Figure 4.5 A. The blue curves correspond to the condition with static phase (NNN) and the red curves to those without (_N_). In both cases the moving phase has a velocity of 200 degree/s and the frame rate is 1440 Hz. The stimulus presented at the top of each frame is NNN.

that this spot was larger in the absence of a static phase than with one. In our case, the horizontal profile does not have a Gaussian shape to achieve the same kind of fit.

The activity associated with the static phases in our figure corresponds to the two large peaks on the left and right. The activity observed between the two is that generated by movement. This is visible in the _N_ condition, whereas it is drowned out by the activity of the static phases in the NNN condition. We can see that our static phases create a much higher level of activity than the movement and are less spread out. Their activity remains for almost the entire stimulus. Our static phases generate a response 10 times stronger than movement, whereas in the monkey experiments the static phases and the movement phase generate the same response amplitude. Our static phases are therefore too strong and less spread out compared with the movement phase. This can lead to an increased smear effect. We tried to set up Gaussian fits of the horizontal profile for each frame but without success. We were not surprised because we believe that the response obtained for the movement activity profile is a plateau, not a Gaussian. The use of a Gaussian fit does therefore not seem appropriate.

The way how this plateau decreases, with an asymmetry in favour of the anterior part, is linked to the fact that this is the oldest activated zone. The region near the second peak, on the other hand, decreases very little due to the very strong presence of the static phase peak, which comes last. We conjecture that the speed at which the different positions of the horizontal profile decrease depends strongly on the activity present there. With each new frame, the VSDI signal decreases by a fraction of the actual VSDI. Thus, the activity linked to the static phases in the last 3 frames (519, 559 and 599 ms) decreases by a much greater magnitude between frames than that of movement. We suggest that this

explains why the difference between NNN and _N_ decreases. In our opinion, this cannot be considered as a decrease in smear. Our results show that NNN activity is still greater than in _N_.

As a result, we could ask whether the increase in activity that we measure in NNN with our method should be considered as an increase in smear. Another solution would be to measure the smear as the amplitude of the movement response. This amplitude depends on the state of activation of the cortex before the start of the movement. With this second solution, we could explain why static phases would reduce the perceived smear. In fact, static phases lead to an increase in the level of global activity, particularly on the trajectory of the bar. Because of the non-linearity of the cortical response (dynamic gain), a high state of activation of the cortex causes a lower response from it. As a result, the amplitude of the movement response will be reduced, as will the smear. However, this is hardly visible in our case. The activity associated with our static phases seems too high and not spread out enough in relation to the length of the movement. This can be explained by our choice to use a movement amplitude twice as large as for a saccade. With well-spread static phases, part or all of the movement zone sees an increase in the activity of the cortical columns that make it up. The activity of the movement will then be reduced because it will be drowned in it.

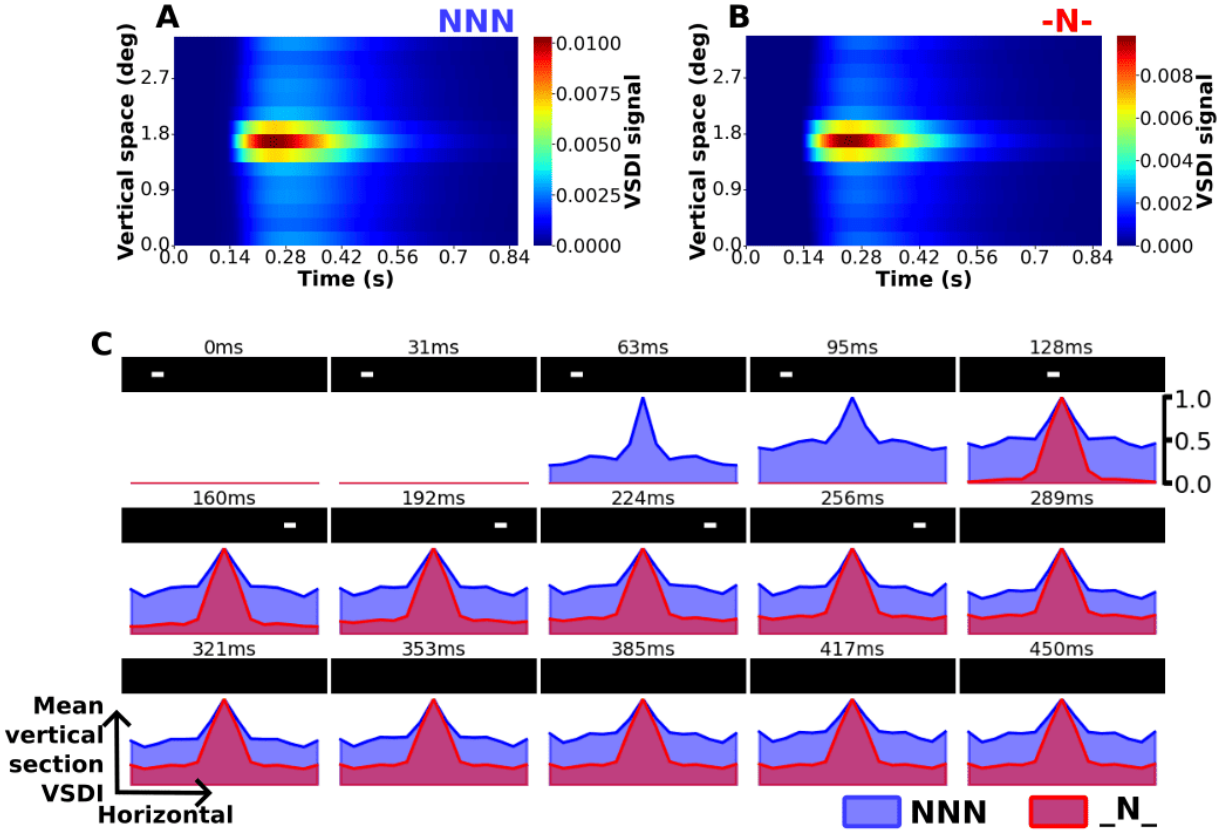

Figure 4.7: **Static phases increase the vertical cortical smear. A,B**)Time-vertical representation of the VSDI signal of the cortical columns located at the center of the horizontal axis with **(A)**, static phases (NNN), or **(B)** without (_N_). **C)** Time sequences of the normalized vertical section averaged over the horizontal axis and time for NNN (blue) and _N_ (red). For each frame of motion, a vertical section is calculated as shown in figure 4.5 B. The stimulus presented at the top of each frame is NNN.

We now study the vertical component of the smear, the spread (Fig. 4.7). We use a representation of the VSDI as a function of time and vertical position for the column at the center of the horizontal axis. We first apply it to the NNN condition (Fig. 4.7 A). On the left is the start of the stimulus. Here, we see an area devoid of VSDI signal up to about 0.14 s. Beyond this point, a central zone on the vertical axis becomes very active. This zone has a height of 0.44 degrees and a duration of around 400 ms. Around this zone of strong activity is a zone of activity half as strong and lasting half as long, which extends across the entire vertical slice. This organisation is symmetrical along the horizontal axis.

The result obtained with _N_ is very similar (Fig. 4.7 B). The only difference lies in the level of activity in the center of the spot but also in its vicinity. These are weaker and last a little less time. We change the representation in order to

use the vertical profile integrating the vertical sections as introduced in figure 4.5. We make a profile for several frames covering the duration between 0 and 450 ms (Fig. 4.7 C). We decided not to take more than this, because beyond this point the motion activity starts to become too small to be relevant. Each of the profiles has been normalised to make it easier to compare their shape. Shape is important for measuring spread. The vertical profile of NNN becomes non-zero from frame 63 ms, while that of $\_N\_$ becomes non-zero at frame 128 ms. For all the following frames, the profile created by NNN varies very little. The $\_N\_$ profile is invariant, but there is a gradual increase in activity around the central peak.

The spots of activity observed in 4.7 A and B have a height equal to that of the bar we used. This high-activity spot is formed by the positions that were in direct contact with the passage of the bar. We assume that the absence of VSDI before 140 ms can be explained by the use of the vertical profile of the cortical columns located at the center of the horizontal axis. These cortical columns receive very little excitation from static phases that are too far away from them. Taking into account that movement starts at 100 ms, this means that the delay before activation of these cortical columns is 40 ms. This delay is compatible with that observed so far in all the other figures in this section. In the NNN case, the increase in activity observed compared with $\_N\_$ reflects an overall increase in the level of activity generated by the static phases. There is also a change in shape, as shown by the normalised vertical profile. The NNN condition profile appears higher and wider. This change in shape seems to be consistent with a greater spread for the NNN condition and therefore a greater smear.

In conclusion, our work on smear showed very contradictory results to those of Mark Wexler and Frédéric Chavane. They found a significant difference between NNN and _N_ in the radius of the Gaussian fits performed on the horizontal profiles in their monkey experiments. In our case, we found no evidence of a decrease in smear in the NNN condition compared to the _N_ condition. This observation was made both for the horizontal smear, which we called residual activity, and the vertical smear, which we called spread. On the contrary, our measurements seem to reveal stronger residual activity and spread in the NNN condition. This would suggest an increase in smear in this condition. It should be noted that our horizontal profiles did not show any Gaussian profiles allowing a fit. We think that the most plausible explanation for all these changes lies in the very large difference in proportion between the response amplitude of the static phases and that of the movement phase compared with the experiments in monkeys. Our static phases are much too high, too sharp. The static phases of the monkey have a very spread out shape which could enable them to interact more strongly with all the cortical columns on the movement trajectory. In our case, we doubled the amplitude of the physiological saccade, which could also be partly responsible for the low overlap of the trajectory of the bar by the static phase. It would be interesting to modify the amplitude of our static phases, their spread and perhaps the amplitude of our movement in order to assess whether we obtain a reduction in the smear by correcting these deviations in our simulation compared with that of Chavane and Wexler. This would confirm the importance of the shape of the static phase and the equality of the amplitudes between the static and moving phases.

4.2.4 Shape-dragging effect in simulated saccades

When a simulated saccade is performed on humans an illusion called shape-dragging has been highlighted by Mark Wexler and Patrick Cavanagh [96]. To give an example, if the static phases correspond to a solid circle and the moving phase to a hollow circle, the subjects will see a solid circle in motion. This only happens in the context of a simulated saccade (high speed of movement, a high frame rate, and static phases) *where the shapes of the static phases differ from those of the moving phase (e.g. changing their size, shape or filling)*. Subjects perceive the slow movement of an object having all the properties of the one used for the static phases instead of the one of the moving phase. The moving object is masked by the static phase object. Mark Wexler and Frédéric Chavane have carried out another series of unpublished experiments in monkeys (private communication). In order to quantify, they used WNW and NWN stimuli in order to measure changes in the size of the cortical response. A region of the V1 cortex was recorded during the stimulus presentation. To check whether the size of the cortical has changed, they used the same method as we used and described in detail for the vertical smear (Sec. 4.2.3). They calculated vertical profiles by integrating each horizontal line in an area between the two static phases. This was averaged over 5 frames where motion occurs. A Gaussian fit was then used to calculate the thickness of the vertical profile. Their analyses revealed a non-significant difference between the width of the peak of the vertical profiles between NWN and WWW conditions and between WNW and NNN. In this section we simulate the same experiments and analysis with our retino-cortical model. To do this we will use the stimuli WNW, NWN, NNN and WWW, the creation and nomenclature of which is introduced in section 4.2.1. The extension of the bar (vertical) is therefore perpendicular to the direction of movement (horizontal). The speed of motion is 200 degrees/s and the frame rate is 1440 Hz.

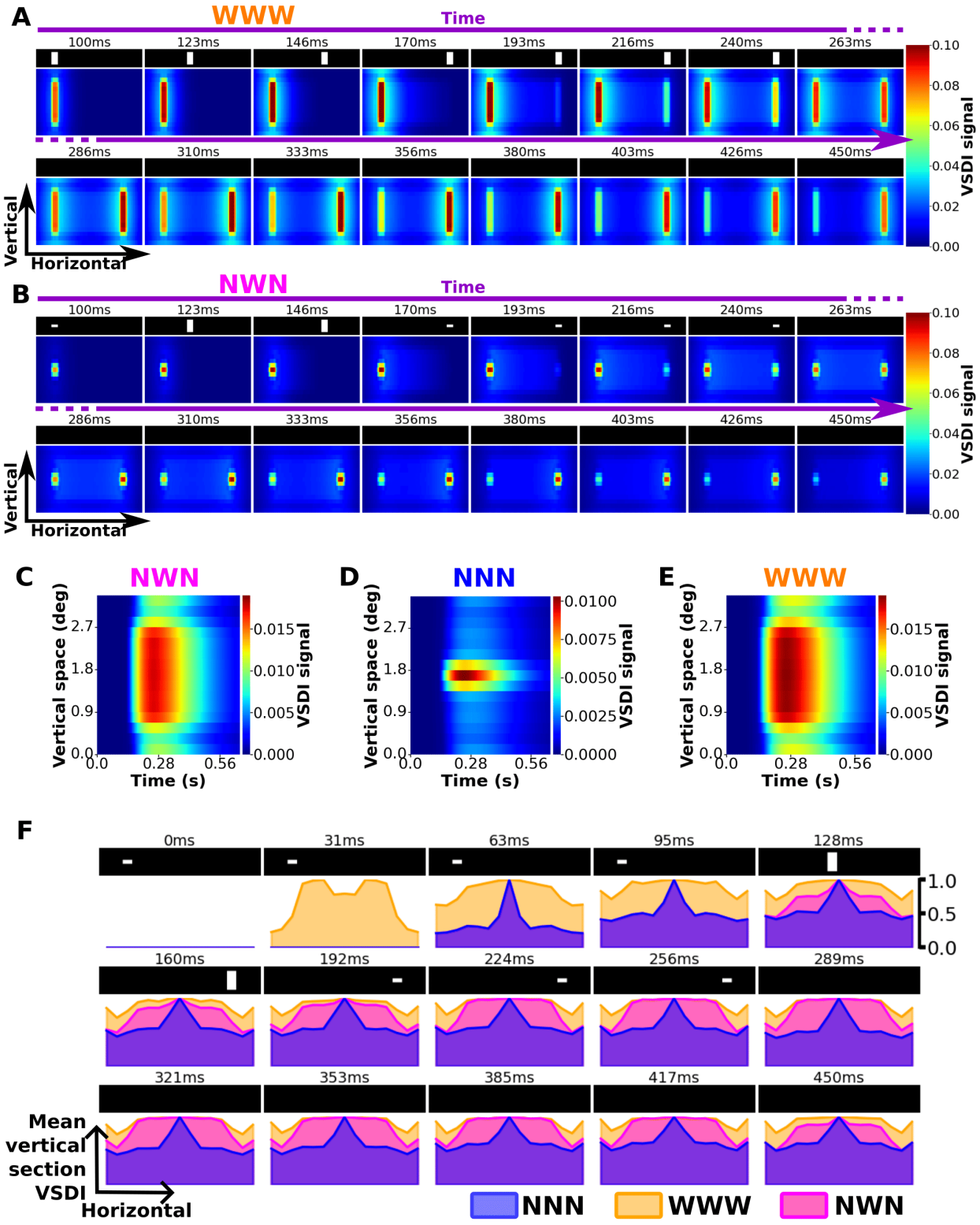

Figure 4.8: **Static phases with a bar height smaller than the height in the moving phase don't cause shape-dragging. A, B)** Time sequence of VSDI signal spatial heatmap and stimuli for WWW **(A)** and NWN **(B)**.**C, D, E)** Time-vertical representation of the VSDI signal of the cortical columns located at the center of the horizontal axis with NWN **(B)**, NNN **(C)** or WWW stimulus **(D)**. **F)** Time sequences of the normalized vertical section averaged over the horizontal axis and time for NNN (blue), WWW (orange) and NWN (pink). The stimulus presented at the top of each frame is NWN.

The results are shown in Fig. 4.8. The response of the cortex to the WWW stimulus generates the presence of a long rectangular spot of activity indicator in frame 100 ms and measuring 1.08×2.08 degrees (Fig. 4.8 A). The activity of this spot increases until the frame 193 ms. This spot radiates an activation halo of about half the size of the spot. In frame 146 ms, a band of activity extends from the spot to the right. This band stops at the position where a second spot of high activity appears, identical to the one on the left. Between 216 and 356 ms, the activity of this second spot continues to increase while that of the first spot decreases. After that, the activity of the second spot and the inter-spot region begin to decrease.

In the condition with the NWN stimulus, we can see the transition from the static phase to the movement phase between frames 100 and 123 ms (Fig. 4.8 B). The bar increases in height between these two frames before returning to its original shape in frame 170 ms, where the second static phase occurs. Here too, a spot of activity intensifies between 100 and 193 ms. However, the size of this spot is 4.3 times smaller (1.08×0.48 degrees) than that of the WWW stimulus. A band of activity extends from this spot between frames 146 and 193 ms. At the position where this band ends, a second spot of activity appears and develops between 216 and 356 ms. This is also the interval where the first spot of activity decreases. Beyond this, the second spot of activity and the motion activity decrease.

The evolution in time of the vertical profile at the center of the visual area shows a very intense response over the entire height of the cortical area (3.15 degrees) and for 330 ms for the NWN condition (Fig. 4.8 C). This response is preceded by a fairly long delay. In contrast, with the NNN stimulus, we see a much smaller spot of vertical profile activity (0.45 degrees) with a duration of 320 ms (Fig. 4.8 D). This spot also has much lower activity than the NWN condition. Surrounding this spot is a halo of VSDI activation twice as weak as the spot. The horizontal profile in response to a WWW stimulus is very similar to that of NWN (Fig. 4.8 E). The only difference is a stronger VSDI signal in the WWW case.

In order to take into account the whole length of the motion trajectory, we set up the same vertical profile integrating the horizontal positions as Mark Wexler did. However, we have decided not to average over time, as we believe it is important to see the evolution of size over time. A set of frames was chosen to display the profile. The time interval of these frames stops when the response to movement starts to reduce dans une simulation sans phase statique (_N_). We also decided to normalise the vertical profile in order to focus mainly on the shape of the response evoked by the movement. A change in the size of the cortical response will result in a change in the shape of the vertical profile of this response. If the size of the response increases, we will expect a flatter, more spread-out profile; conversely, if the size decreases, the profile will be narrower. Finally, we were unable to use a Gaussian fit to measure the width of the cortical response which was not Gaussian. The stimulus we chose to display in this figure 4.8 F is the NWN stimulus. It highlights the two frames of motion (128 and 160 ms) where the bar is higher than in the rest of the stimulus. Frames up to 95 ms show an identical NNN and NWN profile that is very different from the WWW profile. The WWW profile is flattened and wide, while the other two are pointed and narrow. The shape of the NNN and WWW profiles remained virtually unchanged for the duration of the stimulus. However, from frame 128 ms, the vertical profile of the response to the NWN stimulus gradually approaches the flat, wide shape of the WWW profile. The difference between the two shapes diminishes again after 450 ms.

We want to try and determine whether or not our result reveals shape-dragging. The two spots on the right and left of the spatial heatmaps (Fig. 4.8 A and B) correspond to responses to static phases. The one in between corresponds to movement. The static phases W of the stimulus are 4.7 times greater than those of N. This increase in the height of the stimulus generates an increase in the height of the activity spot of 4.3 between WWW and NWN. This means that there has been a slight change in the expected proportions of the height of the bar. The height of the WWW spot is smaller than that of NWN. We think that this is linked to the low spatial resolution that we have on the vertical axis. It is also possible that edge effects may play a role. The substitution of static N phases by higher static W phases generates an overall increase in activity. This is made possible by the very strong VSDI signal caused by the static phases. We do not believe that a simple increase in the overall level should be considered as an increase in the size of the perceived stimulus. It is the shape of the response profile that seems to be the best indicator. The main difference between our results and those of Mark is the shape of the vertical profiles obtained. In their case, the NNN and NWN vertical profiles resemble Gaussians. In our case, on the other hand, the profiles are very spread out and flat. It is possible that this difference in shape could be resolved by adding amacrines or gain controls. Despite this difference, we come to the same conclusion as Mark Wexler and Frédéric Chavane : there is no difference between the heights of movement with the NWN and WWW stimuli. Static phases do not affect the moving phase. We did not observe any effect in the V1 cortex that might be associated with shape-dragging in the case of the NWN and WWW stimuli.

In Fig. 4.9 we investigate the stimulation of the cortex by a WNW stimulus. The response begins with the development of an intense spot of size 1.08×2.08 degrees (Fig. 4.9 A). A thin band of activity appears in the central part of this spot, progressing until it stops where a second high spot of activity of the same size as the first appears. From 240 ms, the VSDI signal from the first spot is reduced while the second increases. This second spot and the response to the

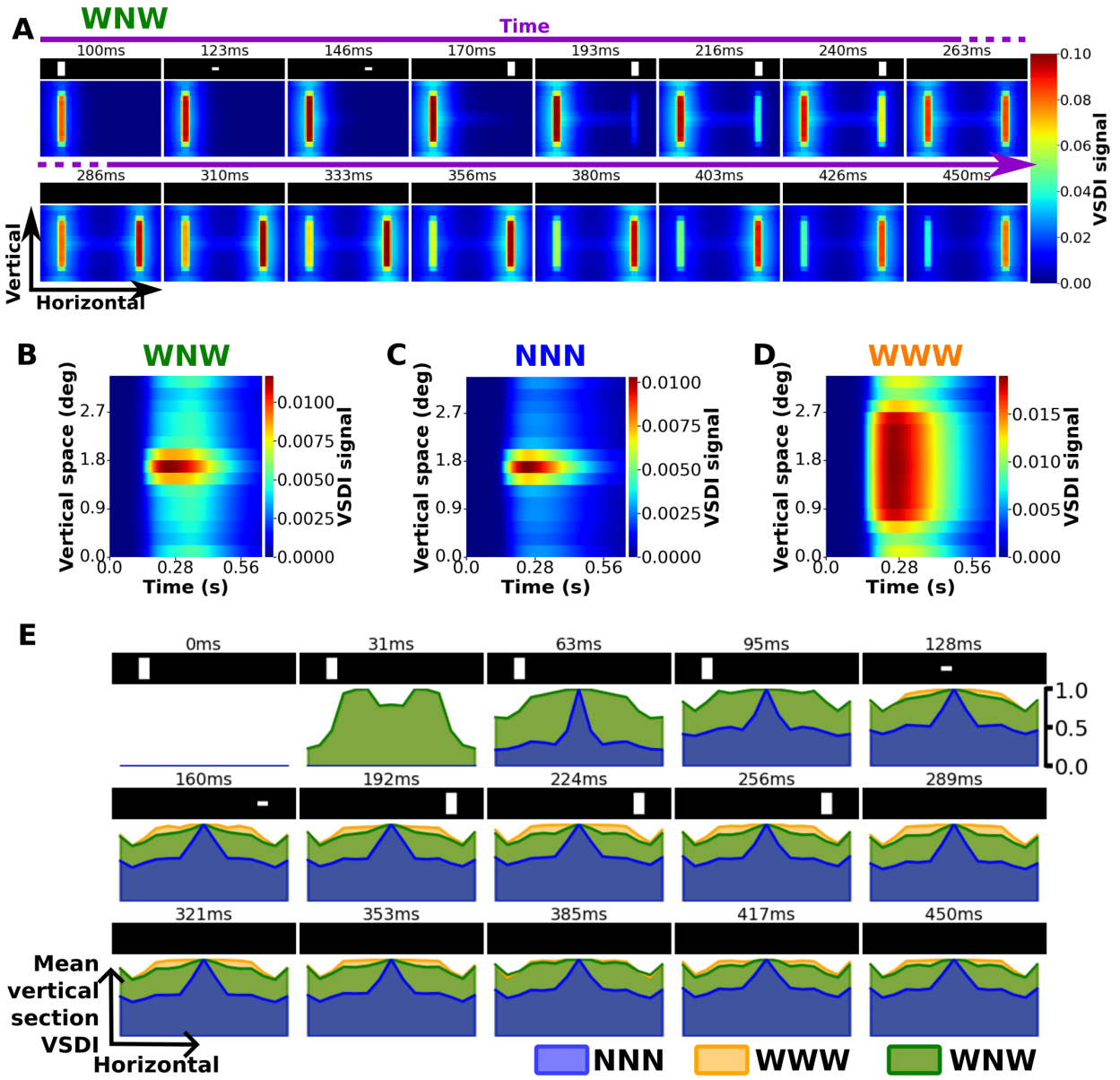

Figure 4.9: **Static phases with a bar height larger than the height in the moving phase cause shape-dragging.** **A)** Time sequence of VSDI response and stimulus for the WNW condition. **B, C, D)** Time-vertical representation of the VSDI signal of cortical columns located at the center of the horizontal axis with WNW **(B)**, NNN **(C)** or WWW stimulus **(D)**. **E)** Time sequences of the normalized vertical section averaged over the horizontal axis and time for NNN (blue), WWW (orange) and WNW (green). The stimulus presented at the top of each frame is WNW.

movement do not decrease until the 380 ms frame. A vertical section through the middle of the horizontal axis of each heatmaps in 4.9 A shows the vertical profile of the band of activity located between the two static phases (Fig. 4.9 B). This band measures 0.45 degrees and lasts 370 ms. Surrounding this band is an activation halo half as intense as its center. This vertical band appears to have a vertical profile at the center of the horizontal axis intermediate between that obtained with the NNN (Fig. 4.9 C) and WWW (Fig. 4.9 D) stimuli. For a more complete picture, we also use the vertical profile integrated on the horizontal axis (Fig. 4.9 E). In the early stages of the simulation, the profile of NWN merges with that of WWW. Both are spread out and flat, unlike that of NNN, which is sharp and narrow. The arrival of the movement causes a slight downward inflection in the WNW profile, which is slightly closer to the NNN profile. Despite this, the shape of the WNW condition remains much closer to that of WWW.

This experiment shows responses related to the static phases which are identical when we look at the temporal sequence of the spatial heatmaps. However, the height of the movement is much smaller, equal to that of the moving bar in the WNW stimulus. This band is the same size as that observed for NNN in the section 4.2.2. The vertical profile at the center of the cortical area of WNW is closer to that of the NNN condition than WWW. On the other hand, the normalised vertical profile incorporating horizontal positions tends to point in the direction of greater shape similarity between WNW and WWW. This difference is due to the fact that the vertical profile of figures B, C and D is only calculated for the central vertical line. This position is equidistant from the two static phases. It receives the least excitation from the static phases. This can be seen in the 356 ms frame in figure 4.9 A. The halo of the two static phases does not reach the center of the horizontal axis. In the vertical profile used in figure 4.9 E, the entire motion trajectory is integrated. This makes it possible to take into account all the variations on this trajectory, including those close to the static phases. It is in this context that we observe a proximity between the NWN and WWW vertical profiles. This suggests that the static phases do have an impact on the shape that could be perceived in the case of a WNW stimulus.

Overall, our simulations carried out to explore the effect of shape-dragging seem to have revealed effects that contradict those of Frédéric Chavane and Mark Wexler, as well as my own results. In their preliminary experiments with monkeys, Chavane and Wexler found no significant difference in the size of vertical profiles between NNN and WNW or WWW and NWN. To do this, they used Gaussian fits, which we were unable to do due to the lack of vertical profiles resembling a Gaussian. We decided to concentrate instead on the shape of the vertical profile by adding a normalisation not present in the monkey experiments. This process enabled us to identify a WNW vertical profile whose shape is closer to WWW than to NNN. This could indicate a shape-dragging effect. On the other hand, we were unable to observe the same change in the shape of the vertical profile of NWN and therefore no shape-dragging. We do not yet know why we obtained two contradictory results with respect to shape dragging in the cortex. We wonder whether it is conceivable that the effect of shape-dragging in humans is also stronger and more visible in the WNW case than in the NWN case. However, these results need to be put into perspective as it is possible that the change in shape is not sufficient to consider that the size of the response has changed and that the same level of activity is also potentially required. We think that our differences with the biological results may still be due to our static phases being too strong. Even though we don't integrate static phases directly into the calculation of the vertical profile, they still have an influence on the lateral connectivity. Another probable explanation is our use of normalisation. If Mark Wexler and Frédéric Chavane applied normalisation to their analyses of the temporal profile, perhaps they too could observe the same results as us. Finally, shape-dragging could be used in areas with a higher hierarchical level. This could require interaction between the 'what' and 'how' pathways.

4.3 Suppressive effect in simulated saccades

In section 4.1, we introduced Chemla et al.'s [9] demonstration of the presence of suppressive waves within apparent movement in macaques. They gave evidence of a suppressive wave which goes in the opposite direction of motion in order, according to Chemla et al, to suppress the earlier representation of the stimulus in the cortex. The section 4.2 investigated the impact that static phases can have on the smear of movement as well as the size or shape of the object perceived as moving (shape-dragging) during a saccade. The central question that we address in this final section establishes the bridge between these two phenomena. We believe that the effects of smear reduction and shape-dragging could be explained by a suppressive interaction between the static phases and the motion phase. This exploration has not yet been the subject of any previous experiments, nor simulations, to our best knowledge. The experimental set-up we are using was defined during discussions with members of the ANR ShootingStar. We ran simulations with the default set as in 4.1 for the three types of stimuli : SMS, S_S and _M_. SMS stimuli are extremely different from apparent movement. It's real continuous movement made up of a large number of frames. This movement is much faster and is bordered by long static phases. From advice of our partners, we calculate the difference between the SMS activity and the sum of the S_S and _M_ activities. This procedure allows us to highlight the non-linearities present in SMS and which originate in the interaction between the static phases and the movement phase. We will do this for three of the stimulus sets used: NNN, WNW and NWN.

Figure 4.10 A shows the response to the NNN stimulus. The bottom and top of the representation correspond respectively to the left and right of the cortical area. The first static phase generates a long, intense activation at the bottom, while the second creates an identical activation at the top. In between is a mixture of the response evoked by the movement of the bar and that of the two static phases. In figure 4.10 B we subtracted the responses generated by a stimulus with no movement phase (N_N) and another with no static phase (_N_). A first suppressive spot appears at 0.11 s, at the same time as the moving phase response develops. The position of this suppressive spot is identical to that of the first static phase. Its duration is 350 ms, slightly less than the static phase responses. We can also observe a spread of the suppression with time in the direction of movement. This spread reaches a maximum of 2.8 degrees, 110 ms after the start of suppression, and then starts to decrease. A second suppression spot occurs at 0.19 s when the response to the second static phase appears. From this spot, suppression spreads in the opposite direction to the

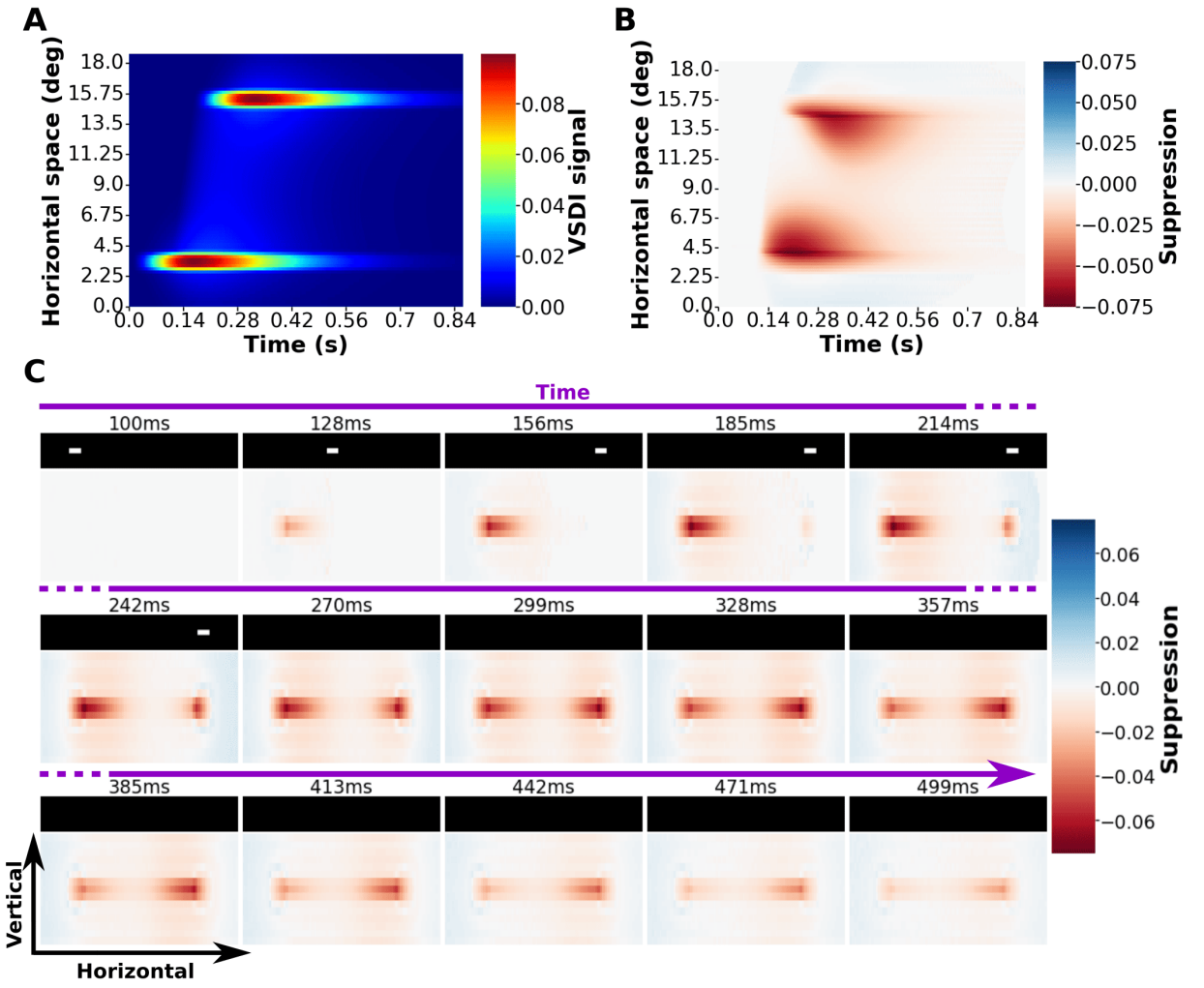

Figure 4.10: **The NNN stimulus creates suppressive spots spreading from static phases to motion phase. A)** Time-horizontal heatmap of the VSDI signal for the NNN stimulus. **B),** Time-horizontal heatmap, and **(C)**, time sequence of the suppressive non-linear effect generated by the saccade. This non-linearity is the difference in activity between the NNN condition and the sum of those generated by motion phase (_N_) or static phases alone.

movement. The suppression extends to 2.4 degrees after 140 ms before diminishing. The temporal sequence of this same suppression starts with a spot in frame 128 ms (Fig. 4.10 C). A suppression band extends from this spot in the direction of motion and gradually intensifies. A second spot then appears at 214 ms and extends in the opposite direction to the movement. Note the presence of a virtually suppression-free zone of 0.5 degrees at the center of the motion trajectory. The maximum value reached by suppression is only -7.5%.

The start of suppression here occurs at the moment when the movement starts, which is the earliest we can have. In fact, we couldn't have seen any suppression before because we're looking specifically at suppression between motion and the static phase. Actually, we don't really see a suppressive wave propagating in these results. The maximum of the two suppression spots always remains at the same position, that of the static phase, compare to Fig. 4.1 A where a propagation is clearly visible. Here we only have a suppression spot that spreads with time. The suppression generated by these spots doesn't cover the entire trajectory of the movement and their value is slightly less than that observed in the apparent motion for the same set of parameters (11%). In the case of the suppressive spot in the first static phase, the suppression is maximal in the static phase and then decreases in the same direction as the motion. This is the expected behaviour, if we omit the absence of a wave, that observed for the suppression of apparent motion (Sec. 4.1). However, this is not true for the second static phase. Its suppressive spot is maximal on the static phase and intensifies in the direction and in the opposite direction of the motion. This is the opposite of what we expected. This means that recent representations of the bar are more suppressed than earlier ones.

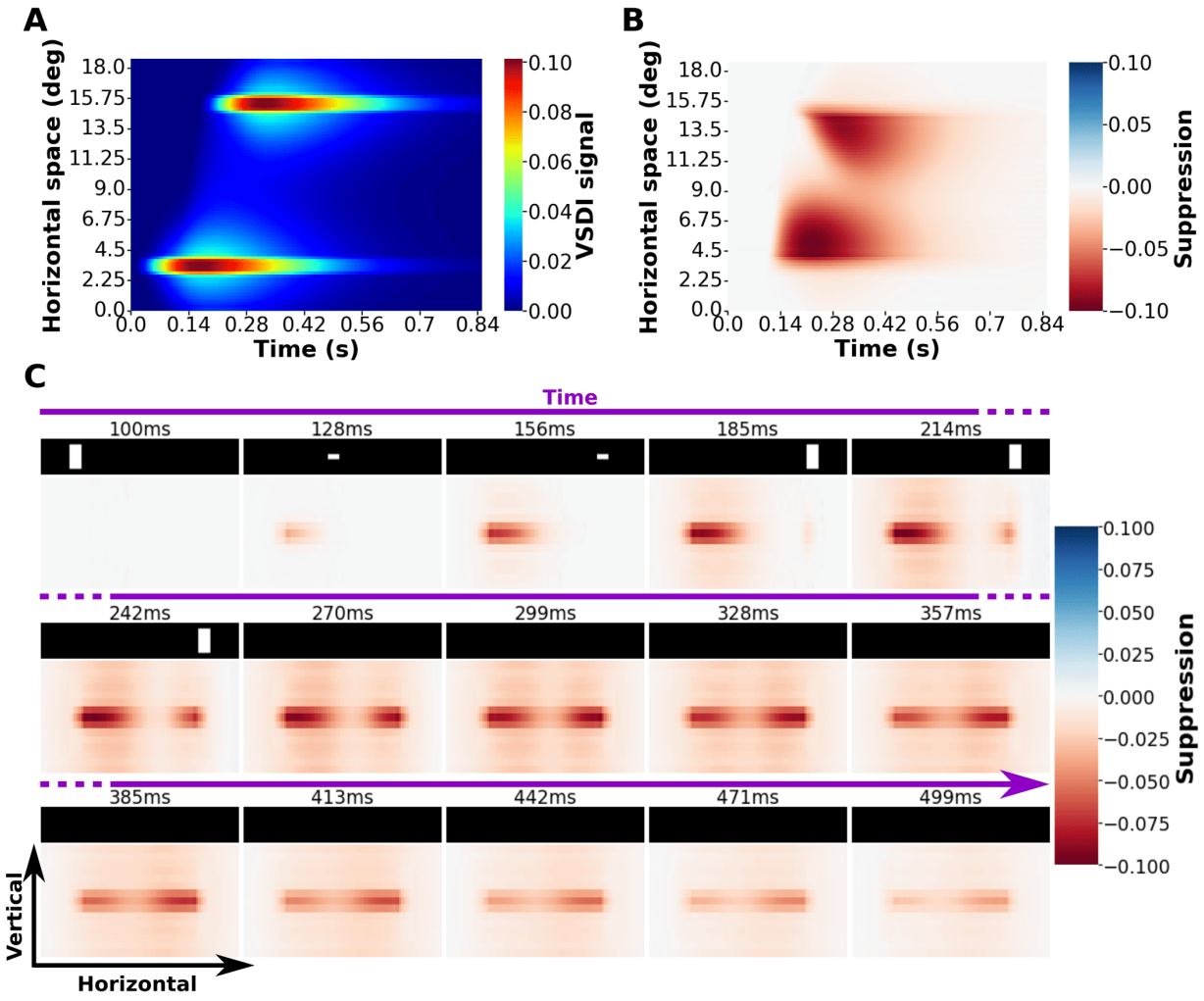

Figure 4.11: **The WNW stimulus creates suppressive spots spreading from static phases to motion phase**. Same description as figure 4.10 for WNW, _N_ and W_W stimuli.

Figure 4.11 A is the equivalent of figure 4.10 A in the case of a WNW stimulus. The horizontal size of the two activity spots is 0.48 degrees and lasts 400 ms as for NNN (Figure. 4.10 A). However, the activation halo is relatively strong and extended by 2 degrees. This figure shows the structure of the response to the WNW stimulus (Fig. 4.11 B). A first suppression spot arrives at the position of the first static phase and at the start of the movement. The spot lasts for 360 ms. From this spot, strong suppression spreads out in the direction of movement. After 110 ms the suppression extends to 4.8 degrees and then shortens. It is in this spot that the maximum suppression is observed (-10%). At the moment of response to the second static phase and its position, a second suppression spot appears, lasting 360 ms. This spot extends asymmetrically in the direction but in the opposite direction to the movement. It extends to 3.7 degrees after 150 ms. The temporal sequence of response to the WNW stimulus allows us to see the left suppression spot starting at 128 ms and then extending in the direction of movement (Fig. 4.11 C). It is accompanied by weaker suppression on either side of the motion trajectory. The appearance of the second spot on the right produces the same thing, but in the opposite direction to the movement. Note that only a very small part (1 degree) of the motion trajectory is not affected by the suppression of one of the two static phases.

This result and the conclusions to be drawn are almost identical to those in figure 4.10. No suppressive wave can be observed and the position of the suppression maximum does not vary. All that we have is a spot which spreads asymmetrically in the direction of motion. This results in a suppression whose gradient intensifies in the opposite direction to the movement for the first static phase and in the same direction for the second. The only two differences with the figure are the intensity and the spreading distance of the suppression. These two characteristics are higher here due to the presence of larger static phases. A larger static phase increases the VSDI signal sufficiently to generate an

activation halo, including on the horizontal axis. The maximum suppression value observed here is very close to that of the apparent motion (10% compared with 11%. This larger size and greater intensity could lead to better suppression of static phases in the movement.

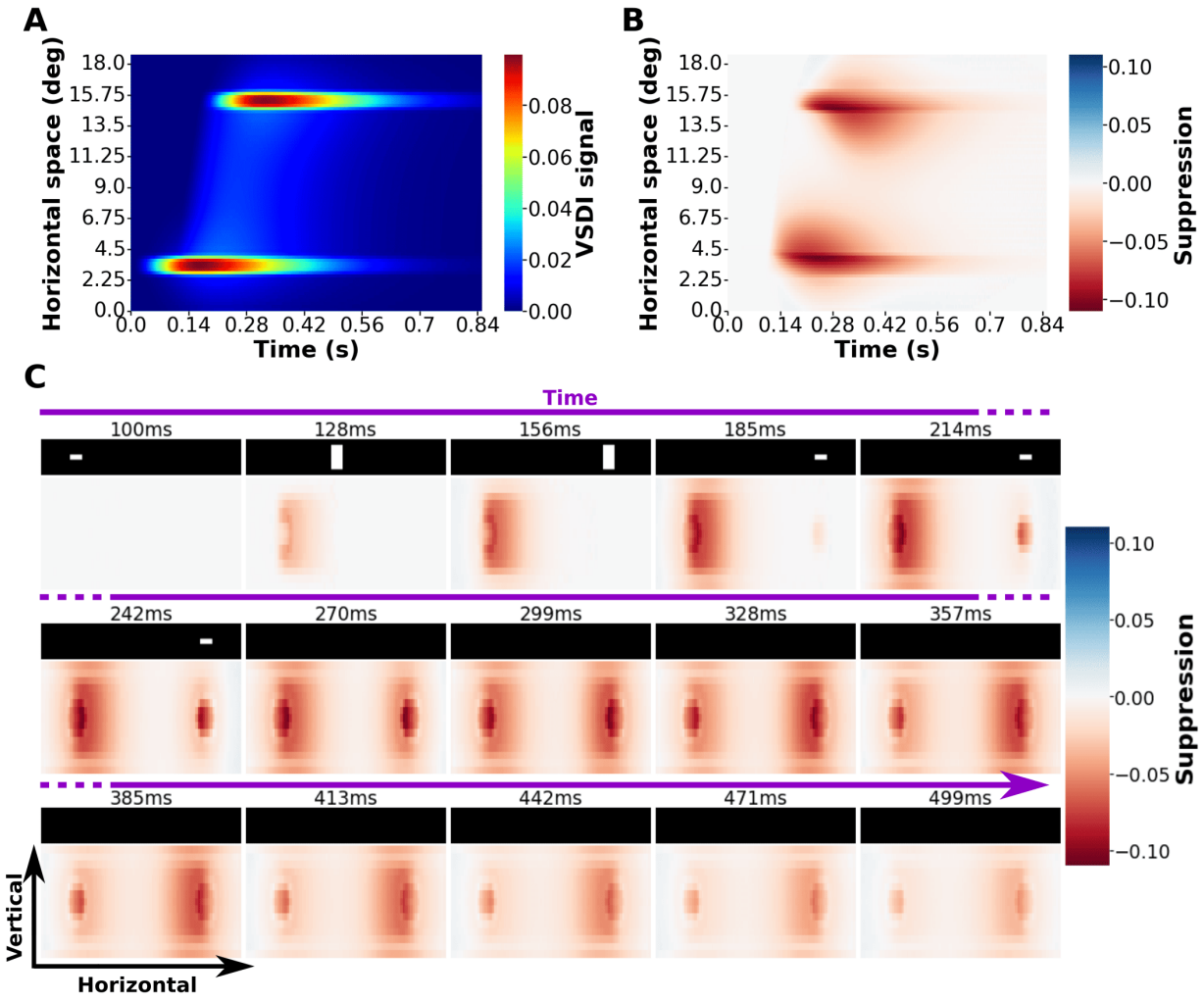

Figure 4.12: **The NWN stimulus creates suppressive spots spreading from static phases to motion phase.** Same description as figure 4.10 for NWN, _W_ and N_N stimuli.

We conclude our with the NWN stimulus. The spots of activity generated by the static phases for the response to the NWN stimulus (Fig. 4.12 A) are the same as those for NNN (Fig. 4.10 A). The activities generated by the two static phases last 400 ms and measure 0.48 degrees along the horizontal axis. The only difference lies in the activity generated between the two static phases, on the movement trajectory. This is stronger and lasts longer (230 ms). Suppression with the same representation reveals a spot of activity at the positions of the two static phases (Fig. 4.12 B). The first arrives at the start of the movement and lasts 490 ms. The second arrives at the start of the response to the second static phase and lasts 450 ms. Over time, these two spots both spread asymmetrically in the two directions of the horizontal axis. Both spread with greater intensity in the direction of movement than the other way round. In the case of the first spot, suppression spreads out to 2.7 degrees after 110 ms from the start of the suppression spot. In the opposite direction of movement, the suppression is barely visible. For the second spot, the suppression spreads out by a maximum of 2.2 degrees after 180 ms of spot. In the opposite direction, suppression also increases very slightly. The maximum suppression observed in this condition is 11%. The suppression time sequence also shows the arrival of two spots at 128 and 185 ms respectively (Fig. 4.12 C). From these two spots extends a suppressive band with a height of x degrees which covers part of the motion trajectory. The positions of the static phases are the areas where maximum suppression remains. An area 4.4 degrees long and free of suppression separates the two suppressive bands.

The difference in the VSDI signal of the motion phase observed with the NWN stimulus is justified by the presence of a larger moving phase, which therefore generates *stronger activity* during its passage. This greater activity also explains the greater height of the suppression band compared with that obtained with NNN or WNW. This height is very close to the true height of the bar. This means that the larger the moving bar, the larger the suppression generated. Once again, we conjecture that what we are observing is not a wave because the maximum suppression remains fixed. What we see is a spot of activity that spreads progressively from the static phases in the direction of motion. This explains why, in the case of the first static phase, the activity spreads out in the oldest positions but suppresses the most recent positions to a greater extent.

In conclusion, these incomplete results seem to show a kind of halo of suppression of the static phases towards the trajectory of movement. But no waves were observed in any of the three experiments. The simulation generating the strongest suppression was that of the NWN stimulus, followed by WNW and finally NNN. On the other hand, the WNW stimulus produced the greatest suppression, followed by NWN and NNN. The size of the bars is an important parameter in the level of suppression obtained.

We speculate that the difference between the suppression phenomena observed in the apparent motion and SMS stimuli with simulated saccade may be due to the nature of the stimuli being compared. In the case of apparent motion, we compare two identical stimuli. They are simple short flashes creating two Gaussian shapes of static and identical activity. On the contrary, SMS stimuli are made up of two radically different phases. In on one hand we have the static phase, which is a long flash creating intense static activity. On the other hand, we have the moving phase, which creates dynamic activity over time, homogeneous and of low intensity. Apparent motion and SMS are far too different to be comparable. The presence of a suppressive wave in apparent motion does not imply that one should be observed between static phases and motion. We further suggest that a suppressive wave may only appear in motion. This is the case in apparent motion as well as in the moving phase of the SMS stimulus. On the other hand, there is no movement, even apparent movement, between the static phases and the moving phase. The interval of time and space between the static phases and the moving phase is not regular. The duration of the static phases is too long compared with the moving phase, and they are at the same position as the first and last flashes of the moving phase.

This preliminary work actually suggests that there are no suppressive waves between the static phases and the motion. Instead, we would have a simple asymmetric suppression spot that grows in the direction of the motion trajectory. Despite the absence of a wave, this suppression spot can nevertheless have a significant impact on motion. If the suppression halo is sufficiently intense and extensive, the entire motion trajectory could be intensely suppressed. We believe that this could be enough for the static phases to exert their two potential roles: suppressing the smear by drowning it out and modifying the shape of the moving stimulus. The static phases could not therefore have the role of suppressing the early representations of movement. This role could be carried by the movement itself. In this way, each representation of the moving object would be responsible for suppressing previous representations. To explore this hypothesis, we would have to calculate the non-linearity from the difference between the _M_ stimulus and the sum of all the frames that make up the movement of this stimulus. It would be interesting to compare these two non-linearities within the movement itself and between the SMS phases with a global non-linearity. This global linearity would correspond to the difference between the SMS stimulus and the sum of all the frames that make up the movement of this stimulus as well as the two static phases. This global non-linearity would allow us to see how the other two non-linearities interact together. In particular, whether the suppression spot on the static phase modulates the suppression wave carried by the moving phase. We had initially thought of implementing such a procedure. Unfortunately, we had to give up because it requires an absolutely enormous number of simulations to be carried out. The most feasible thing would be to find an approximation with a reduced number of simulations.

The greater suppression intensity and distance of the WNW could partly explain why we obtain a difference in the shape of the moving phase in the case of the WNW. To confirm this, it would be interesting to run simulations with the "better" set of parameters used in the apparent motion (Sec. 4.1). This set gave results closer to those of Chemla et al. and could perhaps reveal a suppression wave. We should also try to reduce the motion distance to 6 degrees, as we think the results might be better with a shorter distance. The distance of a saccade is on average 6 degrees, so it is possible that the connectivity distances at the cortical level are carefully optimised to work at this motion size and not much more.

Discussion

4.4 Conclusion

We have completed the implementation of the chimera model within Macular. This task was an opportunity to participate in the final development of Macular by adding a number of important functionalities and improving existing ones. The Chimera model was then calibrated to reproduce in a qualitative way the results of Benvenuti's experiments on cortical anticipation [3].

This first step led us to explore all the parameters, physiological or otherwise, that can influence cortical anticipation. We were able to note the absolute importance of the amplitude of retinal output on the level of cortical anticipation. This was a parameter that we had to separate from the other effects that we subsequently observed. We also demonstrated that anticipation in our model is supported by lateral connectivity and depends on the excitation/inhibition balance as in biology. We also demonstrated an effect that is not observed in biology: anticipation by latency in the cortex is associated with a slight earlier shift in the cortical response peak.

The Chimera model enabled us to go further by studying the interaction between retinal anticipation and cortical anticipation. We started with adaptive anticipation, which we applied with gain control or amacrine connections on bipolars or ganglion cells. Overall, cortical anticipation was reduced by retinal anticipation despite the presence of compensatory effects and to different degrees depending on the condition. Anticipation was less affected in the case of gain control or when one of these two features was applied to bipolars. As a counterpart to the reduction in cortical anticipation, the shift in the cortical response peak was strongly shifted in each of these conditions. This indicates a transfer of retinal anticipation to the cortex. On the other hand, the peak shift that is specific to cortical anticipation was reduced. We can easily understand how the peak shift can contribute to the system's anticipation, but we wonder about the role of accentuated latency slopes. Do they generate the shift or do they play a more specific role in anticipation? It is possible that anticipation by peak shift informs 'something has happened' while anticipation by latency could inform certain cells that 'something is happening' to trigger different processes.

A second retinal anticipation by 'predicting' has recently been discovered [2]. No retinal model has yet reproduced this new mode of anticipation. We have succeeded in reproducing it by adapting our model to incorporate an amacrine with a biphasic profile. We have shown that this profile is essential for creating predicting anticipation as conjectured by Menz. We propose that this biphasic profile depends both on connectivity between two different types of amacrine, including one with a large receptive field, and one with a very high characteristic time of the biphasic amacrine cell. This predicting anticipation greatly improves anticipation by latency and peak shift, although here again the proportion of peak shift attributable to the cortex is reduced. However, we observed a somewhat strange behaviour in the cortical response with a rounded peak following the first. This could be a biological effect or an artefact of our model.

The addition of bipolar or ganglion gain control makes it possible to study how predicting anticipation behaves in the presence of adapting anticipation. On one hand, predicting anticipation increases the range of anticipation and its maximum latency, but reduces the peak shift generated by the cortex. On the other hand, anticipation has the opposite effect on these three anticipation indicators. The two together therefore make it possible to improve all the anticipation indicators while slightly increasing the shift in the cortical response peak. We think it is possible that these two anticipations could be complementary by compensating for each other's defect. This would make it possible to obtain strong retinal anticipation with less impact on cortical anticipation. It is possible that a balance needs to be found between the two that allows the indicators of anticipation to be improved as much as possible. This is particularly the case for the speed of anticipation, which is the only one deleteriously impacted by the addition of predicting with adaptation. We think this would explain why we have two anticipations in the retina: a synergy of anticipation.

The Chimera model also enabled us to investigate the impact of a simulated saccade on the cortical response and to compare it with a non-saccadic movement. The non-saccadic movement at 1440Hz is a translation of the response to the static phase without any residual activity. Increasing the speed to 200°/s makes the motion response much

weaker and with residual activity (smear). The main difference in reducing the frame rate to 60 Hz is that the activity is discontinuous compared with 1440 Hz. This discontinuity is due to the stimulus being displayed at 60Hz, which results in a loss of information. The strength of the smear depends on the ratio between the time for the bar to cross the receptive field and the characteristic time of the cell. These results led us to reflect on the ability of static phases to act on the motion phase. We believe that two ratios make this possible. A first ratio between the characteristic time of the cortical columns and the duration of the movement in the receptive field. The static phase will have more time to grow and suppress the movement. A second ratio between the duration of the static phase and the moving phase. This would make it possible to increase the intensity of the response to the static phase compared with that to movement, as well as its slope so that it grows faster than the response of the cortical columns to movement.

Despite good timing in the interaction between the response to static phases and to movement, the smear (horizontal and vertical) did not disappear in the presence of static phases. On the contrary, it seems to have increased. This result nevertheless reveals that the response to our static phases is far too high compared to the motion phase. In unpublished preliminary results by Wexler and Chavane, their static phases have the same amplitude as the motion. This goes in the opposite direction to the second ratio mentioned above. Nevertheless, it might be thought that a lower but more spread-out static phase would allow the entire movement to be impacted equally. It's also possible that to observe a difference in smear, you don't need static phases that are too strong. The shape-dragging results were contradictory. Using a larger static phase than the WNW movement alters the shape of the movement response, which becomes closer to the shape of the static phase (WWW) than the movement. In contrast, there is no difference in shape in the case of smaller static phase (NWN). It is possible that the shape-dragging effect is more easily observed, including in psychophysical experiments, with the WNW condition than NWN.

Finally, we studied the suppressive wave in the context of simulated saccades. To this end, we first succeeded in reproducing the anticipation wave described by Chemla et al. [9] with apparent motion. This wave propagates from the most recent representation of the apparent motion to the oldest, as detailed in their paper. This suppressive wave seems to be particularly influenced and reduced by certain parameters such as the increase in constant background noise received by the cortical columns from the rest of the cortex (external drive). The characteristic time of the retinal cells also causes a significant change in the duration of suppression. The three simulated saccade conditions showed asymmetric suppression in the direction of motion. However, this is only a spreading spot of suppression rather than a suppressive wave. We suggest that the difference in nature between the static and motion phases may play a role in this observation. We also hypothesise that static phases may be involved in the suppression of smear or the creation of shape-dragging solely via this Gaussian spot. At the same time, the role of suppressing each previous representation in the movement would be assumed by the cortical columns activated later.

The work carried out throughout this thesis has made it possible to present a model of the retino-cortical pathway that is highly parameterisable and adaptable by adding new cells or functions. This model makes it possible to study the parallels between the retina and the cortex, while offering the ability to act on both in order to better understand their interaction. This model has been able to reproduce numerous mechanisms associated with movement processing: the two retinal anticipations (adaptation, predicting), cortical anticipation and the suppressive wave. It was in this context that we were able to note the crucial importance of the different mechanisms of anticipation, gain control or adaptation on movement processes such as saccades. We believe that it is essential to take all these mechanisms into account if we want to study motion processing. In the end, we have provided a suitable environment for modelling motion processing and this environment could be extended to other visual processes.

4.5 Future work

Chimera model

Our Chimera model demonstrated a good ability to qualitatively reproduce the results of latency anticipation [3] but also of suppressive wave in apparent motion [9]. Despite this, it has presented some limitations in terms of reproducing these experiments in a more qualitative way. There are still many directions in which this model can be improved. Some of the parameters used are still not sufficiently inspired by biology. For example, the distance between bipolar cells could be too large [117]. The δ_x value for ganglion cells has yet to be found in the literature. The problem is that to vary δ_x we must not touch the size of the simulated area because it doesn't change between bipolars and ganglion cells. What varies in the retina is the cell density. Bipolars are much more numerous than ganglion cells. For this reason, we suggest using a bipolar area that is larger than the ganglion area. Another parameter that needs to be improved is the characteristic times of amacrines and bipolars. To do this, we need to be able to determine these values from biological experiments in the literature. Finally, we could modify the amplification of inputs from the retina so that inhibitors receive 2/3 of retinal inputs and excitators only 1/3 [109]. To go further, we could try to insert bipolar and ganglion cells from the magnocellular or parvocellular pathways and then compare the impact this may have on the perception of movements, anticipation and also saccades. It would be interesting to confirm the greater ability of magnocellular cells to detect movement [38].

We could also undertake more extensive modifications such as adding new cell types, a variety of synapses and more realistic types of connectivity than the nearest neighbours. This would make it possible to implement more realistic retinal circuits and access their role in motion analysis or anticipation. In particular, it would be interesting to study the effect of gap junction and amacrine connectivity, and whether their collaboration can improve cortical anticipation as suggested by [115]. The current cortex model is very unstable, and we could study the ability of amacrines to reduce these oscillations in the model. We would also like to add dynamic adaptation [115] to the current model, as well as second-order dynamics [105, 118] involving the co-variances of all the sub-threshold variation statistics. In particular the second order model introduces corrections in the Jacobian of the cortical model at the steady state. These corrections increase the value at which the retinal output amplitude triggers a Hopf bifurcation generating pathological oscillations. This would make our model more stable and allow us to test wider ranges of the different parameters whose effect on cortical anticipation has been tested. Another major change is the addition of a thalamus mean field model obtained by Overwiening etal. [11] and based on the same principle as the current cortical model. This model takes into account the particularities of thalamo-cortical neurons, such as their burst/tonic regime change. Rather than adding the thalamus model to Macular, it is planned to put the thalamus in TVB and then set up the interface between Macular and TVB with the aim of simulating a whole brain with realistic retinal inputs. This final step would enable us to study the impact of the retina, thalamus and V1 on other cortical regions.

Anticipation corticale

We reproduced anticipation faithfully and were able to explore how it was affected by adapting anticipation and by predicting. However, we noted discrepancies between the values measured by Benvenuti and those of our model, which were much lower. The implementation of a gain or amacrine connectivity control reduced this discrepancy. For this reason, we would like to carry out all the experiments that we anticipated in chapter 3 but in the presence of gain control or amacrine connectivity. It would be interesting to note whether or not there were any new effects or changes to those already known. To go even further, we could tune our parameters with gain control or amacrine connectivity until we get as close as possible to Benvenuti's results. In doing so, we could note whether the parameters we obtain are consistent with biology, but we could also start from a perfectly calibrated model in order to study the impact of the chimera model's parameters on anticipation. Among the possible new effects, we expect to observe potentially a preferential speed of bars in the retina as observed by Selma, but also in the latency of the cortex.

During this thesis, we also did not have the time to test the effect of a certain number of parameters on anticipation. If we had more time, we would have liked to test the impact of the width and height of the bar or simulated area, the number of cells and their separation distance, the characteristic times of the retinal cells and their connection length. This would allow us to see in a little more detail the impact of the retina on the cortex. We would also have liked to see the consequences on the anticipation of other types of connectivity, such as a Gaussian in the case of amacrines towards bipolars or ganglion cells. We were interested in comparing the effect of gain control with one-to-one amacrine connectivity to determine the extent to which gain control can be reduced to a particular type of amacrine connectivity. It would have been relevant to perform simulations in the presence of surround/center receptive fields. Finally, as Macular easily allows us to do, we could change stimulus to evaluate anticipation in more complex cases than a simple bar: curved trajectory, back-and-forth trajectory, two moving objects (See [108]).

Anticicipation par prédiction

Our retinal model is the first to demonstrate predicting anticipation. These results need to be put into perspective, however, as we are still at the beginning of this new model, which still needs a lot of fine-tuning. To begin with, we need to reproduce the predicting anticipation result in a larger graph in order to avoid observing saturated anticipation ranges in our simulations. We also need to increase the frame rate to compensate for the frame rate artefact observed in amacrines, which have a very low characteristic time. The use of Gaussian connectivity would seem much more relevant at the biological level. We also need to understand whether the strange activity with a second peak in the cortex and very strong edge activity in the retina is an artefact that we can remove or a authentic behaviour that can be observed in biology.

It would be interesting to modify the different parameters that we think are the most important for predicting anticipation: the characteristic time of the biphasic amacrine, the size of the bipolar-amacrine connection and the amplitude and symmetry of the biphasic profile. On the contrary, we could vary the characteristic time of the amacrines to confirm that it doesn't have that much impact. Successfully varying these different elements would make it possible to confirm their importance and to obtain an optimised set of parameters in which predicting anticipation is optimal. To influence the balance of the profile, the characteristic time at 1 s could be necessary unless we find an alternative.

With this new optimised set, we will study the combined effect of predicting and adaptive anticipation. We want to confirm our hypothesis of complementarity between these two anticipations. Experiments should be carried out with varying levels of gain control and predicting in order to obtain the combination that maximises the beneficial effects on cortical anticipation. We believe that the key lies in the balance between these two modes of anticipation. All this could

also be extended with amacrine connectivity instead of gain control. Once we have found the balance between the two anticipations, we suggest using this set to carry out the experiments we did in our chapter on anticipation 3. This dual-anticipation model could be more relevant than the single-anticipation model mentioned above for reproducing a cortical anticipation that is as close as possible to Benvenuti.

Simulated saccades

The simulated saccade experiments showed a large difference in the smear and shape dragging results compared to the unpublished results of Wexler and Chavane. We would like to try to improve them by first using a saccade size corrected to 6 degrees like in biology. We want to increase the height of the simulated area to better see the vertical section of the 'W' (wide) bars and limit the edge effects on them. However, the most important thing will be to reduce the height of the responses to static phases so that it is as high as the response to movement. This can be done by adjusting the amplitude of the static phases and their spread. With all these corrections, we would be able to determine whether these changes were sufficient to explain the differences in shape dragging and smear. If this were the case, it would indicate the importance of these parameters on these two effects. We would also like to test the veracity of our hypothesis that the ratio of bar time in the receptive field to characteristic time has a strong impact on smear.

Suppressive wave

The SMS suppressive waves reproduced by our model seem to testify to an effect of the static phases on the motion that is only due to a suppression Gaussian. However, we would need to test other parameter sets to ensure that we continue to observe this. An interesting first set would be the 'better' set described in section 4.1.This set showed a much stronger suppression wave in the case of apparent motion and this could also be for SMS. A second set that would be interesting is the optimised set mentioned earlier in the presence of gain control or amacrine. Gain control has been shown to participate in the saccadic suppression mechanism, so it could play a role here too. We believe that in the presence of gain control, the strength of our static phases would be considerably reduced while that of movement would be less impacted. We can also prefer this set to one that includes predicting anticipation to determine to what extent it can participate in motion processing in the case of a movement as fast as a saccade.

To extend our knowledge of suppression in simulated saccades, we need to experiment with certain parameters. Firstly, we want to separate the calculation of the non-linearity between SMS and _M_ + S_S by deciding to separate the two static phases: _M_ + __S + S__. We want to evaluate the possibility that the two static phases can suppress each other, in particular by working at 6 degrees of amplitude of movement. It is possible to go even further by summing the system response to a single frame of motion. This would allow us to see the effect of the suppression wave that we think is propagating from a recent representation to an older one. We want to finish confirming our initial impressions of the negative impact of the external drive. But we also want to explore new ones with the balance between inhibition and excitation, which seems to determine the strength of a suppression wave. We could do this by changing the strength of the exc/inh synapses, their characteristic time, their quantal conductances and the size of their connections. Another parameter that could have an impact on suppression is the conduction velocity of the fibres, we should have a suppression Gaussian propagating more slowly. Finally, we need to see if the two ratio hypothesis we have developed is correct. That is, the ratio between the travel time of the bar in the receptive field and the characteristic time, and the ratio between the duration of the static phase and the moving phase. The first must allow the second static phase to arrive at the same time as the responses to the movement trajectory. The second must increase the amplitude of the response to the static phase and the slope to catch up with the activity evoked by the movement. Simulations varying the parameters of these two ratios will be used to determine whether this has an impact on suppression in the simulated saccades.

Shaping parameters

Finally, during this thesis we began to characterise the response of the retina to a stimulus as a function of three dimensionless parameters. We began to confirm the impact of these parameters by means of simulation in Macular. However, we are not finished yet. We still have to test varying κ by changing the value of the bar thickness to change only κ and not ρ. But also, to get better results for r.

Appendix A

Parameters sets

A.1 Model parameters (default values)

Parameter category	Parameter Name	Symbol	Value	Unit
Simulated area	Number of cells (X)	n_{cells_X}	83	Dimensionless
	Number of cells (Y)	n_{cells_Y}	15	Dimensionless
	Width (X)	L_X	18.45	degrees
	Height (Y)	L_Y	3.15	degrees
	Cell distance	δ	0.225	degrees
	mm retina per degree	rpd	0.3	mm/degrees
	mm cortex per degree	cpd	3	mm/degrees
Stimulus video (moving bar)	Speed	v_B	6	degrees/s
	Width (X)	l_X	0.67	degrees
	Height (Y)	l_Y	0.9	degrees
	Frame rates	δ_t	60	Hz
	Pixel per degree	ppd	300	pixel/degrees
OPL	OPL input amplitude	$\mathcal{C}$	0.025	Dimensionless
	Integration time step (ODE solver)	dt	0.0004	s
	RF size	σ_c	0.2	degrees
	Characteristic time	τ_c	0.1	s
Bipolar cells	Characteristic time	τ_B	0.1	s
	Activity characteristic time	τ_{a_B}	0.1	s
	Threshold	θ_B	0	mV
	Activity rate	h_B	[0,9.2]	mV^{-1}Hz
Amacrine cells	Characteristic time	τ_A	0.05	s
	Weight bipolar to amacrine	$\lvert w_A^B \rvert$	[0,12]	Hz
	Weight amacrine to bipolar	w_B^A	[0,12]	Hz
	Weight amacrine to ganglion	w_G^A	[0,1]	Hz
Ganglion cells	Radius bipolar to ganglion	σ_G	0.3	degrees
	Characteristic time	τ_G	0.1	s
	Activity characteristic time	τ_{a_G}	0.189	s
	Threshold	θ_G	0	mV
	Activity rate	h_G	[0,0.54]	mV^{-1}Hz
	Weight bipolar to ganglion	w_G^B	0.15	Dimensionless
	Pooling extent	σ	0.09	mm
	Non linear rectification	α_G	1110	Hz/mV
	Non linear rectification limit	$N_{G_{max}}$	212	Hz

Cortical shared parameters values	Membrane capacitance for cortical columns	C_m	0.2	nF
	Excitatory reversal potential	V_E	0	mV
	Inhibitory reversal potential	V_I	-80	mV
	Leak reversal potential	V_L	-65	mV
	Cell number in network	N_{tot}	10 000	Dimensionless
	Excitatory quantal conductance	Q_E	1.5	nS
	Leak conductance	g_L	10	nS
	Excitatory characteristic time	τ_E	0.005	s
	Inhibitory characteristic time	τ_I	0.005	s
	External drive	ν_{ext}	2	Hz
	Mean field characteristic time	T	0.005	s
	Fraction of inhibitory cells	g_{ei}	0.2	Dimensionless
	Probability of connectivity	p_{connec}	0.0375	Dimensionless
	Mean voltage initial fit value	μ_V^0	-60	mV
	Mean voltage initial fit variation	$\delta\mu_V^0$	10	mV
	Sigma initial fit value	σ_V^0	4	mV
	Sigma initial fit variation	$\delta\sigma_V^0$	6	mV
	Normalized tau initial fit value	$(\tau_V^N)^0$	0.5	Dimensionless
	Normalized tau initial fit variation	$(\delta\tau_V^N)^0$	1	Dimensionless
Cortical excitators (RS)	Sigma extent	σ_E	1.67	degrees
	Initial activity	ν_{E_0}	1.86	Hz
	Inhibitory quantal conductance	Q_I	3	nS
	P parameters	P_E	[-49.8, 5.06, -25, 1.4, -0.41, 10.5, -36, 7.4, 1.2, -40.7]	mV
Cortical inhibitors (FS)	Sigma extent	σ_I	0.3	degrees
	Initial activity	ν_{I_0}	12.66	Hz
	Inhibitory quantal conductance	Q_I	5	nS
	P parameters	P_I	[-51.4, 4, -8.3, 0.2, -0.5, 1.4, -14.6, 4.5, 2.8, -15.3]	mV
Cortical column connectivity	Retino-cortical amplitude	w_{RC}	2.5	Dimensionless
	Cortical density	ρ_{cort}	4000	mm^{-2}
	Retinal density	ρ_{ret}	400	mm^{-2}
	Fiber conduction velocity	v_C	300	mm/s
	Weight excitatory to excitatory	A_E^E	1	Dimensionless
	Weight inhibitory to inhibitory	A_I^I	1	Dimensionless
	Weight excitatory to inhibitory	A_I^E	1.5	Dimensionless
	Weight inhibitory to excitatory	A_E^I	1	Dimensionless

Table A.1: **Model parameters.** For each parameter in our retino-cortical model, we give its name, symbol, unit and the default value used in control condition.

A.2 Initial Chimera parameters

The use of these parameters is described in the section 1.4.1 and 1.4.2.

Parameter category	Parameter Name	Symbol	Value	Unit
Simulated area	Number of cells (X)	n_{cells_X}	20	Dimensionless
	Number of cells (Y)	n_{cells_Y}	20	Dimensionless
	Width (X)	L_X	12	degrees
	Length (Y)	L_Y	12	degrees
	Cell distance	δ	0.633	degrees
	mm retina per degree	rpd	0.3	mm/degrees
	mm cortex per degree	cpd	3	mm/degrees
Stimulus video	Speed	v_{stim}	20	degrees/s
	Width (X)	l_X	1	degrees
	Length (Y)	l_Y	3	degrees
	Frame rates	δ_t	200	Hz
	Pixel per degree	ppd	5	pixel/degrees
OPL	OPL input amplitude	amp_{OPL}	1	Dimensionless
	Integration time step	dt	0.002	s
	Center RF size	σ_c	0.3	degrees
	Center characteristic time	τ_c	0.02	s
	Weight surround	w_{surr}	0	Dimensionless
	Surround RF size	σ_{surr}	0.967	degrees
	Surround characteristic time	τ_{surr}	0.005	s
Bipolar cells	Characteristic time	τ_B	0.1	s
	Activity characteristic time	τ_{a_B}	0.1	s
	Amacrine input characteristic time	τ_{ext_A}	0.1	s
	Threshold	θ_B	5.32	mV
	Activity rate	h_B	0	$mV^{-1}Hz$
Amacrine cells	Characteristic time	τ_A	0.05	s
	Weight bipolar to amacrine	w_A^B	0	Hz
	Weight amacrine to bipolar	w_B^A	0	Hz
	Weight amacrine to ganglion	w_G^A	0	Hz
Ganglion cells	Radius bipolar to ganglion	σ_G	1.8	degrees
	Characteristic time	τ_G	0.02	s
	Activity characteristic time	τ_{a_G}	0.189	s
	Threshold	θ_G	0	mV
	Activity rate	h_G	0	$mV^{-1}Hz$
	Weight bipolar to ganglion	w_G^B	0.15	Dimensionless
	Non linear rectification	α_G	1110	Hz/mV
	Non linear rectification limit	$N_{G_{max}}$	212	Hz
Cortical shared parameters values	Membrane capacitance	C_m	0.2	nF
	Excitatory reversal potential	V_E	0	mV
	Inhibitory reversal potential	V_I	-80	mV
	Leak reversal potential	E_L	-65	mV
	Cell number in network	N_{tot}	10 000	Dimensionless
	Excitatory quantal conductance	Q_E	1	nS
	Inhibitory quantal conductance	Q_I	5	nS
	Leak conductance	g_L	10	nS

	Excitatory characteristic time	τ_E	0.005	s
	Inhibitory characteristic time	τ_I	0.005	s
	External drive	ν_{ext}	2	Hz
	Mean field characteristic time	T	0.005	s
	Fraction of inhibitory cells	g_{ei}	0.2	Dimensionless
	Probability of connectivity	p_{connec}	0.05	Dimensionless
	Mean voltage initial fit value	μ_V^0	-0.06	mV
	Mean voltage initial fit variation	$\delta\mu_V^0$	0.01	mV
	Sigma initial fit value	σ_V^0	0.004	mV
	Sigma initial fit variation	$\delta\sigma_V^0$	0.006	mV
	Normalized tau initial fit value	$(\tau_V^N)^0$	0.5	Dimensionless
	Normalized tau initial fit variation	$(\delta\tau_V^N)^0$	1	Dimensionless
Cortical excitators (RS)	Sigma extent to excitators	σ_{E_E}	1.2	degrees
	Sigma extent to inhibitors	σ_{E_I}	0.9	degrees
	Initial activity	ν_{E_0}	0	Hz
	P parameters	P_E	[-5.66e-02, 7.29e-03, -2.85e-02, -5.79e-03, -4.22e-03, 0, 0, 0, 0, 0]	mV
Cortical inhibitors (FS)	Sigma extent to excitators	σ_{I_E}	0 (one-to-one)	degrees
	Sigma extent to inhibitors	σ_{I_I}	0.6	degrees
	Initial activity	ν_{I_0}	0	Hz
	P parameters	P_I	[-5.41e-02, 5.45e-03, 1.97e-03, 1.04e-03, 3.18e-05, 0, 0, 0, 0, 0]	mV
Cortical column connectivity	Retino-cortical amplitude	w_{RC}	20	Dimensionless
	Cortical density	ρ_{cort}	4000	mm^{-2}
	Retinal density	ρ_{ret}	400	mm^{-2}
	Fiber conduction velocity	v_C	1	mm/s
	Weight excitatory to excitatory	A_E^E	1	Dimensionless
	Weight inhibitory to inhibitory	A_I^I	1	Dimensionless
	Weight excitatory to inhibitory	A_I^E	1	Dimensionless
	Weight inhibitory to excitatory	A_E^I	1	Dimensionless

Table A.2: **Model parameters.** For each parameter in our retino-cortical model, we give its name, symbol, unit and the default value used in the initial set.

A.3 Calibration parameter sets

A.3.1 Connectivity and parameter consistency set change

- $dt = 0.0004$ s

- $ppd = 10$ pixel/degrees
- $L_X = L_Y = 6$ degrees
- $dx = dy = 0.31$ degrees
- $\delta_t = 43.47$ Hz
- $v_{stim} = 3$ degrees/s
- $\mathcal{C} = 0.2$ Hz
- $C_m = 150$ pF
- $\nu_{Aff} = 0$ Hz
- $\nu_{ext} = 4$ Hz
- $A_I^E = 1.5$
- $v_C = 300$ mm/s
- $(\tau_V^N)^0) = 0.67$
- $(\delta\tau_V^N)^0 = 1.33$
- $\mu_V^0 = -60$ mV
- $\delta\mu_V^0 = 10$ mV
- $\sigma_V^0 = 4$ mV
- $\delta\sigma_V^0 = 6$ mV
- Excitatory TF parameters (mV) : $-51.4, 6.1e^{-3}, 7.4e^{-3}, 5.8e^{-5}, -1.5e^{-4}, 5.6e^{-4}, 2.7e^{-4}, 5.3e^{-4}, -6.8e^{-4}, 4.9e^{-4}, 1.2e^{-3}$
- Inhibitory TF parameters (mV) : $-54.6, 4.6e^{-3}, -1.8e^{-3}, 6.6e^{-4}, -3e^{-4}, 3.9e^{-4}, -5.1e^{-4}, -6.4e^{-6}, -1.4e^{-3}, -4.9e^{-4}, -3.6e^{-4}$

A.3.2 Optimized distance set change

- $ppd = 7.41$ pixel/degrees
- $L_X = L_Y = 8.1$ degrees
- $dx = dy = 0.225$ degrees
- $l_X = 0.67$ degrees
- $l_Y = 2$ degrees
- $\delta_t = 32.26$ Hz
- $v_{stim} = 6$ degrees/s
- $\mathcal{C} = 0.65$
- $\tau_B = \tau_{ext} = 200$ ms
- $\sigma_G = 90$ µm
- $\nu_{ext} = 0.004$ Hz

A.3.3 Cortical model stabilisation set change

- $ppd = 30$ pixel/degrees
- $L_X = 4.28$ degrees
- $L_Y = 0.9$ degrees
- $l_y = 0.9$ degrees
- $\delta_t = 188.68$ Hz
- $C_m = 0.2$ nF

- $Q_E = 1.5$ nS
- $(\tau_V^N)^0 = 0.5$
- $(\delta\tau_V^N)^0 = 1$
- Excitatory P params (mV) : $-49.8, 5.06, -25, 1.4, -0.41, 10.5, -36, 7.4, 1.2, -40.7$
- Inhibitory P params (mV) : $-51.4, 4, -8.3, 0.2, -0.5, 1.4, -14.6, 4.5, 2.8, -15.3$

A.3.4 Excitatory inhibitory balance set change

- $\mathcal{C} = 0.5$
- $\tau_B = 50$ ms
- $\Theta_B = 0$ mV
- $w_{RC} = 4$
- $Q_i = 4.5$ nS

A.3.5 Steady-state cortical activity

- $ppd = 300$ pixel/degrees
- $L_X = 9$ degrees
- $\delta_t = 60$ Hz
- $\mathcal{C} = 0.025$
- $\sigma_C = 60$ µm
- $\tau_c = \tau_B = \tau_G = 100$ ms
- $w_{RC} = 2.5$
- $\nu_{ext} = 2$ Hz
- $Q_{I_{exc}} = 3$ nS

Appendix B

Retino-cortical model

B.1 Mean-field cortical equations

We summarize here the mean-field equations derived in a series of paper [105, 12, 9, 13, 119]. The goal is to propose dynamical equations characterising the average dynamics of the two populations of neurons, excitators and inhibitors, at the level of a cortical column. In the core paper, we have given the main equations ruling the dynamics. Here, we give more detail of their constitutive elements. For clarity we rewrite the dynamical equations (1.9), giving the evolution of the excitatory population rate, $\nu_E(\vec{x},t)$, for the cortical column located at $\vec{x}$ at time t, (resp. $\nu_I(\vec{x},t)$ for the inhibitory population rate), in the form:

$$\begin{cases} T\,\frac{\partial \nu_E(\vec{x},t)}{dt} \;=\; -\nu_E(\vec{x},t) \;+\; F_E\left[\,\mathcal{I}_E^E(\vec{x},t),\,\mathcal{I}_E^I(\vec{x},t)\,\right] \\ \\ T\,\frac{\partial \nu_I(\vec{x},t)}{dt} \;=\; -\nu_I(\vec{x},t) \;+\; F_I\left[\,\mathcal{I}_I^E(\vec{x},t)\;,\,\mathcal{I}_I^I(\vec{x},t)\,\right]. \end{cases} \tag{B.1}$$

where:

$$\begin{cases} \mathcal{I}_E^E(\vec{x},t) \;=\; \nu^{aff}(\vec{x},t) \;+\; \nu^{drive} \;+\; A_E^E\,\nu_E^{input}(\vec{x},t), \\ \mathcal{I}_E^I(\vec{x},t) \;=\; A_E^I\,\nu_I^{input}(\vec{x},t), \\ \mathcal{I}_I^E(\vec{x},t) \;=\; \nu^{aff}(\vec{x},t) \;+\; \nu^{drive} \;+\; A_I^E\,\nu_E^{input}(\vec{x},t), \\ \mathcal{I}_I^I(\vec{x},t) \;=\; A_I^I\,\nu_I^{input}(\vec{x},t). \end{cases} \tag{B.2}$$

Here, $\mathcal{I}_X^Y(\vec{x},t)$, $X,Y = \{\,E,I\,\}^2$, is the total contribution (firing rates) of population Y controlling the time evolution of population X.

Note a few important differences with the aforementioned papers. First, the retino-thalamic input ν^{aff} is, in our case, acting on the two populations, excitatory and inhibitory. Also, we have introduced the coefficients A_X^Y weighting the relative contributions of excitatory and inhibitory populations, $\nu_E^{input}, \nu_I^{input}$, from the other columns. These coefficients were implicitly set to 1 in these papers and, in this case, $\mathcal{I}_E^E = \mathcal{I}_I^E$, $\mathcal{I}_E^I = \mathcal{I}_I^I$ so that the superscript Y becomes useless.

We then define, dropping the $(\vec{x},t)$ dependence for legibility:

$$\mu_{G_X^Y} = \mathcal{I}_X^Y K_X \tau_X Q_X \tag{B.3}$$

$$\sigma_{G_X^Y} = Q_X\sqrt{\tfrac{\mathcal{I}_X^Y K_E \tau_X}{2}};\; X,Y = \{\,E,I\,\}^2. \tag{B.4}$$

where, $\mu_{G_X^Y}$ is contribution of population Y to the mean conductance of population X and σ_{G_X} the corresponding standard deviation, computed from shot-noise theory [120]. K_E (resp. K_I) is the number of excitatory synapses (resp. inhibitory), Q_E (resp. Q_I) the unitary excitatory conductance (resp. inhibitory), and τ_E (resp. τ_I) the excitatory decay (resp. inhibitory). See table in appendix A.1 for the value of these parameters.

The total input conductance of the neuron μ_G and its effective membrane time constant τ_m^{eff} are controlled by the mean conductances as follows:

$$\begin{aligned}\mu_G &= \sum_{X,Y\in\{E,I\}^2} \mu_{G_X^Y} + g_L, \\ \tau_m^{\text{eff}} &= \frac{c_m}{\mu_G},\end{aligned} \tag{B.5}$$

where C_m is the membrance capacitance, assumed to be the same for all neurons and g_L is the leak conductance.

The transfer functions of excitatory (resp. inhibitory) neurons appearing in eq. (B.1) take the form:

$$F_X(\mathcal{I}_E^X, \mathcal{I}_X^I) = \frac{1}{2\tau_{V,X}}\, erfc(\frac{\nu_{thr,X}^{eff} - \mu_{V,X}}{\sqrt{2}\sigma_{V,X}}), \quad X = E, I. \tag{B.6}$$

The quantity:

$$\mu_{V,X} = \frac{\sum_{Y=E,I} \mu_{G_X^Y} V_Y + g_L V_L}{\mu_G}, \quad X = E, I, \tag{B.7}$$

is the mean-voltage of the population X in the cortical column, where V_E, V_I, V_L are respectively the reversal potentials for excitatory (E), inhibitory (I) neurons and for the leak. Likewise:

$$\sigma_{V,X} = \sqrt{\sum_{Y=E,I} K_Y\, \mathcal{I}_X^Y\, \frac{(U_Y\,\tau_Y)^2}{2\,(\tau_{\text{m}}^{\text{eff}} + \tau_Y)}}, \tag{B.8}$$

$$\tau_{V,X} = \frac{\sum_{Y=E,I} \left(K_Y\, \mathcal{I}_X^Y\, (U_Y\,\tau_Y)^2\right)}{\sum_{Y=E,I} \left(K_Y\, \mathcal{I}_X^Y\, (U_Y\,\tau_Y)^2/(\tau_{\text{m}}^{\text{eff}} + \tau_Y)\right)}, \tag{B.9}$$

where we defined $U_Y = \frac{Q_Y}{\mu_G}(V_Y - \mu_{V,Y})$ and where $X = (E, I)$.

Finally, in eq. (B.1), $\nu_{thr,X}^{eff}$ is a phenomenological threshold expressed as a first order expansion (eq. (B.10)) of the three sub-threshold statistical quantities : $\mu_{V,X}$, $\sigma_{V,X}$, $\tau_{V,X}$. As it does not exist an analytic formulation of the transfer function for complex models such as the Adaptive Exponential IF or Hodgkin Huxley, Zerlaut et al. [12] have developed a semi-analytic method based on a phenomenological threshold which carries the single neuron non-linearities mechanisms (spike/reset and adaptation). This leads to the following expression for the phenomenological threshold:

$$\nu_{thr,X}^{eff} = P_{X,0} + \sum_{u\in\{\mu_{V,X},\sigma_{V,X},\tau_{V,X}^N\}} P_{X,u}\cdot\Big(\frac{u-u^0}{\delta u^0}\Big) + \sum_{u,v\in\{\mu_{V,X},\sigma_{V,X},\tau_{V,X}^N\}^2} P_{X,uv}\cdot\Big(\frac{u-u^0}{\delta u^0}\Big)\Big(\frac{v-v^0}{\delta v^0}\Big), \tag{B.10}$$

where $\tau_{V,X}^N = \tau_{V,X} G_l/c_m$ is an unitless parameter. Coefficients $P_{X,u}$ have been fitted on numerical simulations of a given single AdEx neuron model with conductance-based exponential synapses [121]. Note that they are different for excitators and inhibitors. The value of these coefficients in our model are given in the table of appendix A.1, as well as the coefficients μ_V^0, $\delta\mu_V^0$, σ_V^0,$\delta\sigma_V^0$, $(\tau_V^N)^0$, $(\delta\tau_V^N)^0$ which are actually assumed to be constant over the populations E, I.

Finally, the VSDI signal is given by:

$$VSDI(\vec{x},t) = 0.8\,\times\, VSDI_E(\vec{x},t) + 0.2\,\times\, VSDI_I(\vec{x},t), \tag{B.11}$$

where the coefficient 0.8 and 0.2 corresponds to the fraction of excitators and inhibitors in the colum population and:

$$VSDI_X(\vec{x},t) = \frac{\mu_{V,X}(\vec{x},t) - \mu_{V,X_0(\vec{x})}}{\mu_{V,X_0(\vec{x})}}, \quad X = E, I,$$

where $\mu_{V,X_0}(\vec{x})$ is the average membrane potential at rest (i.e. when $\nu^{aff} = 0$, for the population X). Note that it depends on $\vec{x}$, due to boundary conditions.

B.2 Connectivity type

Our retino-cortical model contains three different connectivity types :

- **One to one** connectivity link cells or cortical column populations with the same spatial position. This is the case for the connectivity from bipolar to amacrine or from ganglion cell to excitatory/inhibitory cortical column population.
- **Nearest neighbor + 1** connects a cells or cortical column with its 4 nearest adjacent cells or cortical columns. This is used to connect BCs to ACs and reciprocally.
- **Gaussian** connectivity connects the pre- and post-synaptic cell (column) with a weight proportional to a Gaussian function of the distance $d_{[pre,post]}$ between the pre- and post-synaptic cell (eq. (1.11) in the text).

Appendix C

Shaping retino-cortical response

C.1 Introduction to dimensionless shaping parameters

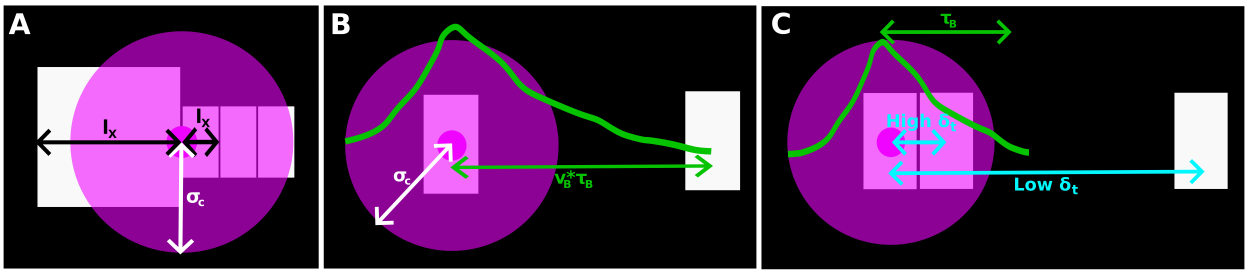

Figure C.1: **Description of shaping parameters** for a white bar of width on a black background. The purple disc corresponds to the bipolar cell's receptive field and the green curves its temporal response. **A)** ρ shaping parameter based on the ratio between the thickness of the bar l_X and that of the receptive field σ_c. On the left is the case where the thickness of the bar is greater than the radius of connectivity and on the right when it is much less. **B)** κ shaping parameter based on the distance travelled by the bar during the bipolar response time $v_B \times \tau_B$, all expressed as a number of σ_c. **C)** r shaping parameter based on the ratio between the time between two frames δ_t, here illustrated by the displacement of the bar, and the bipolar response τ_B. Se represent here the high frame rate case where the successive bars are closer together and the low frame rate case where the bars are further apart. This corresponds to the continuous and static regimes respectively.

During our work on refresh rate, Bruno undertook an analysis of the impact of different parameters on a simplified model containing only bipolar cells and no Macular. Their default parameters were : $l_X = 1.33$ degrees, $v_B = 33.3$ degrees/s, $\delta_t = 0.01s$, $\sigma_c = 0.33$ degrees and $\tau_B = 0.01$ s. The aim of this analysis was to identify how each parameter and their combination could explain the shape of the temporal response. The result was 3 dimensionless parameters derived from the combination of other spatial or temporal parameters. All these parameters are illustrated in Figure C.1.

These three parameters and their equations are :

- $\kappa = \frac{2}{5}\frac{l_X}{\sigma_c}$. The term l_X corresponds to the thickness of the bar while σ_c is the radius of the connectivity Gaussian between the OPL and the bipolars. κ measures the size of the bar compared to the radius of bipolar connectivity. It controls the shape of the response to the moving bar. This shape can be a Gaussian when κ is small and sees its peak flatten as κ increases too much (Fig. C.2A). This is because when the bar exceeds $\frac{2}{5}$ of the receptive field, the bar is too large and the bipolar cell saturates. The $\frac{2}{5}$ ratio is used to normalise and ensure that the transition between the Gaussian and saturated regimes occurs for $\kappa \sim 1$.
- $\rho = \frac{v_B \times \tau_B}{\sigma_c}$. The term v_B is the speed of the bar and τ_B the characteristic time of the bipolar cell. ρ measures the distance travelled by the bar in σ_c during the characteristic time of the bipolar cell. It is responsible for the amplitude and time at which the peak of the response occurs (Fig. C.2B and C). When ρ is high, the peak is earlier and lower. The bar leaves the bipolar cell's receptive field very quickly and integration is stopped early.

- $r = \frac{\delta_t}{\tau_B}$. The term δ_t is the time between each frame of the video (inverse of the frame rate). r evaluates the reaction time of the cell to the frames it sees. This determines how it will perceive the movement in the video. If the frame rate is much faster than the bipolar characteristic time ($r \ll 1$) then the cell doesn't have time to react and integrate each frame. The movement is perceived as continuous (Fig. C.2D). When the frame rate is slower ($r \gg 1$), the cell will have time to react fully and even more before the next frame arrives. The movement is perceived as a static image. The cell therefore integrates for longer and saturates (Fig. C.2F). In this case, the bipolar cell acts as a low-pass integrator over the duration δ_t. Finally, in the case of equality ($r \sim 1$), we obtain an intermediate regime of a series of low pass filters. The cell has just enough time to react fully before the frame changes. The movement will therefore be perceived, but as a more or less apparent movement. The response remains similar to the continuous response, with a more or less delayed and reduced response (Fig. C.2E). In both continuous and intermediate domain everything depends on κ and ρ, not in static one.

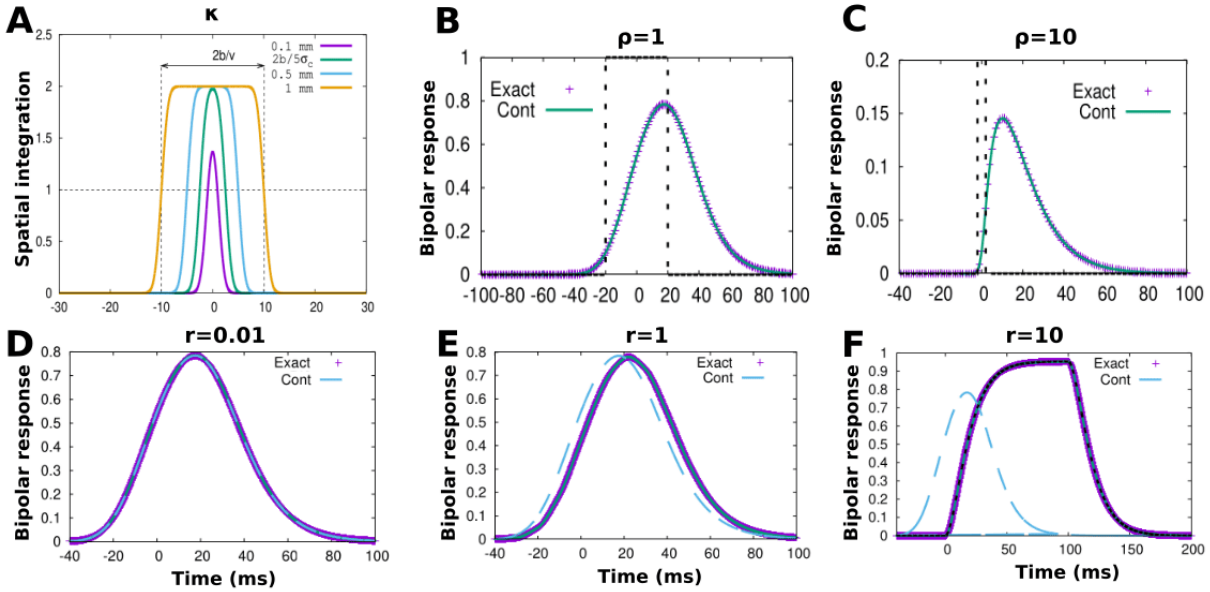

Figure C.2: **Results of experiments on shaping parameters. A)** Spatial integration of bipolars as a function of time for a kappa varying at 0.4 (violet), 1 (green), 2 (blue) and 4 (yellow). **B - F)** Bipolar response as a function of time. The "Exact" curve (pink crosses) corresponds to the model response whereas "Cont" (blue or green) represents the equivalent response with a continuous regime. **B, C)** Response of the bipolar cells to the parameter ρ by varying the speed of the bar. The dotted lines represent the passage of the bar through the receptive field. **B)** Result with $\rho = 1$ ($v = 10$ mm/s). **C)** Result with $\rho = 10$ ($v = 100$ mm/s). **D, E, F)** Response of the bipolar cells to the three regimes of r by modifying δ_t. **D)** Continuous regime with $r = 0.01$ ($\delta_t = 0.1$), the exact curve is the same as the continuous response. **E)** Intermediate regime with $r = 1$ ($\delta_t = 10$), the exact curve is slightly behind the continuous response. **F)** Static regime with $r = 10$ ($\delta_t = 100$), the exact curve is very late as well as saturated compared to that of the continuous regime.

C.2 Shaping effect in Macular simulation

We decided to continue these initial experiments by transposing them to Macular. In the case of our retino-cortical model we have a $\tau_B = 0.1$. For simulations running at 60 Hz frame rate, $r = 0.17$. We are typically in the intermediate regime. On the other hand, when the frame rate is increased to 14440 Hz, $r = 0.007$. This is a continuous regime for the bar. The size of the bar is 0.67 degrees and $\sigma_c = 0.2$ degrees. This gives us a $\kappa = 1.34$ which is larger than 1 but despite this we are not yet in the flat regime. As for ρ, it is equal to 3 with a default speed of 6deg/s. I then carried out simulations by varying the three formatting parameters.
We start with κ which flattens the response when it is large. We vary κ from 0.0133 to 100 by changing the value of σ_c from 20.15 degrees to 0.00357 degrees (Fig. C.3A, B). The more blue the gradient of the curves, the more kappa increases. Our bipolar responses behave very differently from those expected in Bruno's code (Fig. C.3A). The amplitudes of the responses increase and their shape remains Gaussian despite the κ being much greater than 1. The

same thing is observed in the cortex, although the differences in amplitude are tempered there (Fig. C.3B). We think this is because the variable σ_c also plays a role in the variable ρ which impacts the amplitude of the response. Varying the two shaping parameters therefore does not allow us to clearly see the individual effect of each. A new simulation would have to be run with a different bar thickness.
We then move on to the ρ shaping variable, which should decrease the amplitude of the peak and shift it to later times as it increases. We produce a graph with ρ ranging from 2.25 to 15 by accelerating the bar speed from 4.5 degrees/s to 30 degrees/s (Fig. C.3C, D). In this graph, the redder the curve, the higher the ρ. The behaviour of the bipolars is identical to that identified in Bruno's code (Fig. C.3C). The more ρ is increased, the more the amplitude and shift are reduced. Note also that these two effects decrease exponentially as ρ increases. The behaviour observed in the cortex is identical except that the characteristic times of the curves are slower (Fig. C.3D).
The last shaping parameter to be studied here is r. Increasing this shaping parameter should lead to saturation of the activity in addition to its later offset. We increase the r from 0.01 to 100, i.e. a change in frame rate from 1000 Hz to 0.1 Hz (Fig. C.3E, F). Here, the bluer the curves, the greater the increase in r. The observed behaviour is only partly consistent with Bruno's code. While bipolar activity saturates and reaches a plateau when a very large r is used, the peak here is earlier (Fig. C.3E). In addition, if we compare the peak times of the frame rates at 10, 100 and 1000Hz, we see no clear relationship between the decrease in frame rate and the amplitude of the peak. At the cortical level, there is no great difference in these dynamics apart from their greater spread over time (Fig. C.3F).

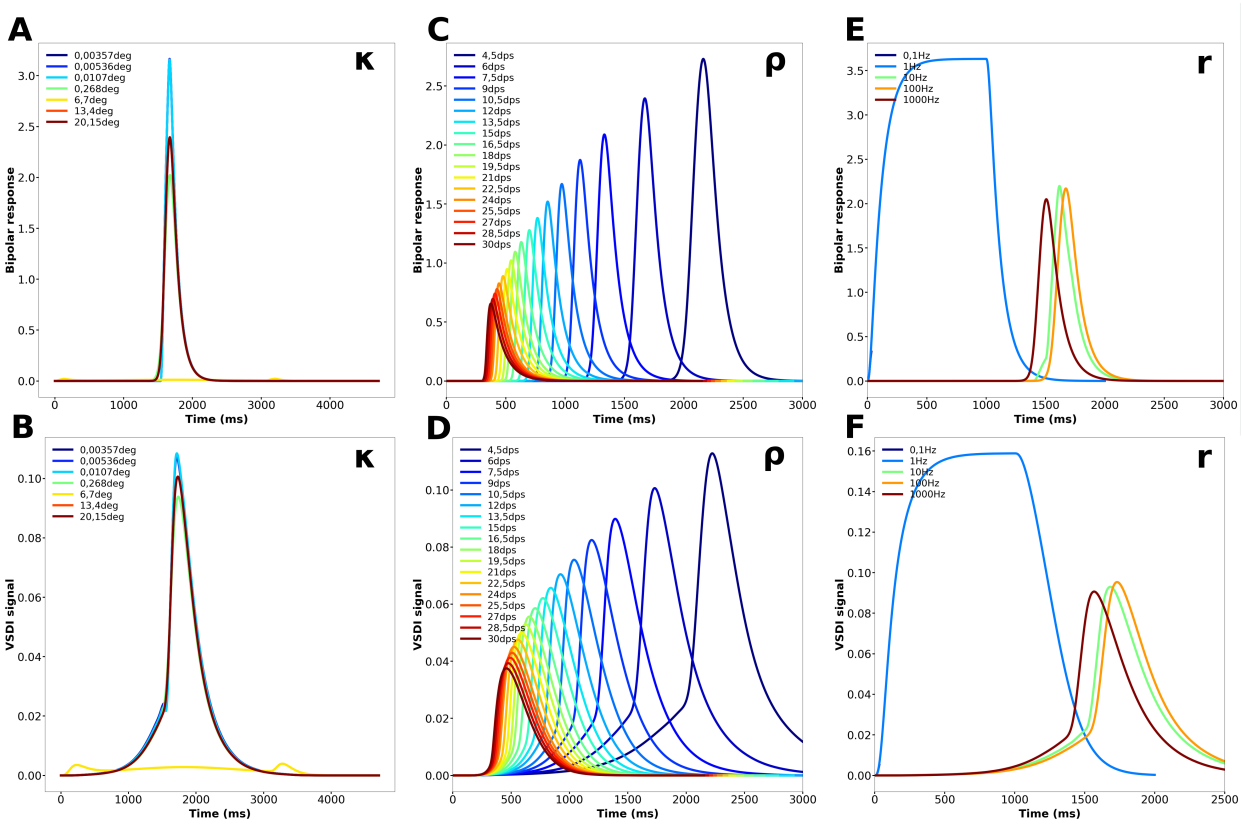

Figure C.3: **Effect of shaping parameters on bipolar and cortical response in Macular A,B)** Variation of the value of the connectivity distance σ_C to change the value of κ in bipolar **(A)** and cortical layers **(B)**. **C,D)** Variation of the bar speed value to change that of ρ in bipolar **(C)** and cortical layers **(D)**. **E,F)** Variation of the frame rate value to change the value of r in bipolar **(E)** and cortical layers **(F)**.

Bibliography

[1] M. Berry, I. Brivanlou, T. Jordan, and M. Meister, "Anticipation of moving stimuli by the retina," Nature, vol. 398, no. 6725, pp. 334—338, 1999.

[2] M. D. Menz, D. Lee, and S. A. Baccus, "Representations of the amacrine cell population underlying retinal motion anticipation," bioRxiv, 2020.

[3] G. Benvenuti, S. Chemla, A. Boonman, L. Perrinet, G. S. Masson, and F. Chavane, "Anticipatory responses along motion trajectories in awake monkey area v1," bioRxiv, 2020.

[4] G. Westheimer, "Mechanism of saccadic eye movements," A.M.A. Archives of Ophthalmology, vol. 52, pp. 710–723, 1954. Place: US Publisher: American Medical Association.

[5] M. F. Land, "Motion and vision: why animals move their eyes," Journal of Comparative Physiology A, vol. 185, pp. 341–352, Oct. 1999.

[6] R. H. Wurtz, "Corollary Discharge Contributions to Perceptual Continuity Across Saccades," Annual Review of Vision Science, vol. 4, pp. 215–237, Sept. 2018.

[7] F. W. Campbell and R. H. Wurtz, "Saccadic omission: Why we do not see a grey-out during a saccadic eye movement," Vision Research, vol. 18, pp. 1297–1303, Jan. 1978.

[8] M. Duyck, M. Wexler, E. Castet, and T. Collins, "Motion Masking by Stationary Objects: A Study of Simulated Saccades," i-Perception, vol. 9, p. 2041669518773111, Apr. 2018. Publisher: SAGE Publications.

[9] S. Chemla, A. Reynaud, M. di Volo, Y. Zerlaut, L. Perrinet, A. Destexhe, and F. Chavane, "Suppressive traveling waves shape representations of illusory motion in primary visual cortex of awake primate," Journal of Neuroscience, vol. 39, no. 22, pp. 4282–4298, 2019.

[10] A. Destexhe, "Self-sustained asynchronous irregular states and up-down states in thalamic, cortical and thalamocortical networks of nonlinear integrate-and-fire neurons," J Comput Neurosci., vol. 27, no. 3, pp. 493–506, 2009.

[11] J. Overwiening, F. Tesler, D. Guarino, and A. Destexhe, "A multi-scale study of thalamic state-dependent responsiveness," bioRxiv, 2024.

[12] Y. Zerlaut, S. Chemla, F. Chavane, and A. Destexhe, "Modeling mesoscopic cortical dynamics using a mean-field model of conductance-based networks of adaptive exponential integrate-and-fire neurons.," Journal of Computational Neuroscience, 2018.

[13] M. Di Volo, A. Romagnoni, C. Capone, and A. Destexhe, "Biologically realistic mean-field models of conductance-based networks of spiking neurons with adaptation," Neural Computation, vol. 31, pp. 653–680, Apr. 2019.

[14] S. Souihel and B. Cessac, "On the potential role of lateral connectivity in retinal anticipation," J. Math. Neurosc., vol. 11, no. 3, 2021.

[15] B. Cessac, "Retinal processing: Insights from mathematical modelling," Journal of Imaging, vol. 8, no. 1, 2022.

[16] E. Kartsaki, G. Hilgen, E. Sernagor, and B. Cessac, "How does the inner retinal network shape the ganglion cells receptive field : a computational study," Neural Computation, vol. 36, pp. 1041–1083, June 2024.

[17] C.-H. Sung and J.-Z. Chuang, "The cell biology of vision," The Journal of Cell Biology, vol. 190, pp. 953–963, Sept. 2010.

[18] C. Salesse, "Physiologie du signal visuel rétinien : de la phototransduction jusqu'au cycle visuel," Journal Français d'Ophtalmologie, vol. 40, pp. 239–250, Mar. 2017.

[19] T. D. Lamb, "Why rods and cones?," Eye, vol. 30, pp. 179–185, Feb. 2016. Publisher: Nature Publishing Group.

[20] M. Helmstaedter, K. L. Briggman, S. C. Turaga, V. Jain, H. S. Seung, and W. Denk, "Connectomic reconstruction of the inner plexiform layer in the mouse retina," Nature, vol. 500, pp. 168–174, Aug. 2013.

[21] J. S. Diamond, "Inhibitory Interneurons in the Retina: Types, Circuitry, and Function," Annual Review of Vision Science, vol. 3, pp. 1–24, Sept. 2017.

[22] W. Thoreson and S. Mangel, "Lateral interactions in the outer retina," Prog Retin Eye Res., vol. 31, no. 5, pp. 407–441, 2012.

[23] R. Rodieck, "Quantitative analysis of cat retinal ganglion cell response to visual stimuli," Vision Research, vol. 5, pp. 583–601, Dec. 1965.

[24] H. Kolb, E. Fernandez, and R. Nelson, eds., Webvision: The Organization of the Retina and Visual System. Salt Lake City (UT): University of Utah Health Sciences Center, 1995.

[25] S. R. y. Cajal, La rétine des vertébrés. Typ. de Joseph van In & Cie., 1892. Google-Books-ID: kmBHnQEACAAJ.

[26] S. Baccus, "Timing and Computation in Inner Retinal Circuitry," Annual review of physiology, vol. 69, pp. 271–90, Feb. 2007.

[27] S. Lee, K. Kim, and Z. J. Zhou, "Role of ACh-GABA cotransmission in detecting image motion and motion direction," Neuron, vol. 68, pp. 1159–1172, Dec. 2010.

[28] S. W. Kuffler, "Discharge patterns and functional organization of mammalian retina," Journal of Neurophysiology, vol. 16, pp. 37–68, 1953.

[29] S. Weng, W. Sun, and S. He, "Identification of ON–OFF direction-selective ganglion cells in the mouse retina," The Journal of Physiology, vol. 562, pp. 915–923, Feb. 2005.

[30] D. Kerschensteiner, "Feature Detection by Retinal Ganglion Cells," Annual Review of Vision Science, vol. 8, pp. 135–169, Sept. 2022.

[31] J. Sanes and R. Masland, "The types of retinal ganglion cells: current status and implications for neuronal classification," Annu Rev Neurosci, vol. 38, pp. 221–246, 2015.

[32] T. Baden, P. Berens, K. Franke, M. R. Rosón, M. Bethge, and T. Euler, "The functional diversity of retinal ganglion cells in the mouse," Nature, 2016.

[33] R. H. Masland, "The Neuronal Organization of the Retina," Neuron, vol. 76, pp. 266–280, Oct. 2012.

[34] E. E. M. Stewart, M. Valsecchi, and A. C. Schütz, "A review of interactions between peripheral and foveal vision," Journal of Vision, vol. 20, no. 12, 2020. Place: US Publisher: Assn for Research in Vision & Ophthalmology (ARVO).

[35] C. A. Curcio, K. R. Sloan, R. E. Kalina, and A. E. Hendrickson, "Human photoreceptor topography," The Journal of Comparative Neurology, vol. 292, pp. 497–523, Feb. 1990.

[36] E. Kaplan, "The M, P and K pathways in the Primate Visual System," in Invest. Ophthalmol. Vis. Sci. (L. Chalupa and J. Werner, eds.), vol. 46, pp. 481–494, CogNet, Nov. 2003. Journal Abbreviation: Invest. Ophthalmol. Vis. Sci.

[37] B. B. Lee, P. R. Martin, and U. Grünert, "Retinal connectivity and primate vision," Progress in Retinal and Eye Research, vol. 29, pp. 622–639, Nov. 2010.

[38] M. B. Manookin, S. S. Patterson, and C. M. Linehan, "Neural Mechanisms Mediating Motion Sensitivity in Parasol Ganglion Cells of the Primate Retina," Neuron, vol. 97, pp. 1327–1340.e4, Mar. 2018.

[39] M.-T. Herrero, C. Barcia, and J. M. Navarro, "Functional anatomy of thalamus and basal ganglia," Child's Nervous System: ChNS: Official Journal of the International Society for Pediatric Neurosurgery, vol. 18, pp. 386–404, Aug. 2002.

[40] C. G. De Moraes, "Anatomy of the visual pathways," Journal of Glaucoma, vol. 22 Suppl 5, pp. S2–7, 2013.

[41] S. M. Sherman, "Functioning of Circuits Connecting Thalamus and Cortex," Comprehensive Physiology, vol. 7, pp. 713–739, Mar. 2017.

[42] J. A. Hirsch, X. Wang, F. T. Sommer, and L. M. Martinez, "How inhibitory circuits in the thalamus serve vision," Annual Review of Neuroscience, vol. 38, pp. 309–329, July 2015.

[43] D. H. Hubel and T. N. Wiesel, "Integrative action in the cat's lateral geniculate body," The Journal of Physiology, vol. 155, pp. 385–398.1, Feb. 1961.

[44] X. Wang, V. Vaingankar, C. Soto Sanchez, F. T. Sommer, and J. A. Hirsch, "Thalamic interneurons and relay cells use complementary synaptic mechanisms for visual processing," Nature Neuroscience, vol. 14, pp. 224–231, Feb. 2011.

[45] W. Chen, X. Zhu, et al., "Retinotopic mapping of lateral geniculate nucleus in humans using functional magnetic resonance imaging," Proc. Natl. Acad. Sci. USA, vol. 96, pp. 2430–2434, Mar. 1999.

[46] E. J. Ramcharan, J. W. Gnadt, and S. M. Sherman, "Burst and tonic firing in thalamic cells of unanesthetized, behaving monkeys," Visual Neuroscience, vol. 17, no. 1, pp. 55–62, 2000.

[47] M. A. Goodale and A. D. Milner, "Separate visual pathways for perception and action," Trends in neurosciences, vol. 15, pp. 20–25, Jan. 1992.

[48] J. Norman, "Two visual systems and two theories of perception: An attempt to reconcile the constructivist and ecological approaches," The Behavioral and Brain Sciences, vol. 25, pp. 73–96; discussion 96–144, Feb. 2002.

[49] L. M. DiNicola and R. L. Buckner, "Precision estimates of parallel distributed association networks: evidence for domain specialization and implications for evolution and development," Current Opinion in Behavioral Sciences, vol. 40, pp. 120–129, Aug. 2021.

[50] D. C. Van Essen, C. H. Anderson, and D. J. Felleman, "Information processing in the primate visual system: an integrated systems perspective," Science (New York, N.Y.), vol. 255, pp. 419–423, Jan. 1992.

[51] D. Hubel and T. Wiesel, "Receptive fields and functional architecture in two nonstriate visual areas (18 and 19) of the cat," Journal of Neurophysiology, vol. 28, pp. 229–289, 1965.

[52] K. Tanaka, "Inferotemporal cortex and object vision," Annual Review of Neuroscience, vol. 19, pp. 109–139, 1996.

[53] L. L. Glickfeld and S. R. Olsen, "Higher-Order Areas of the Mouse Visual Cortex," Annual Review of Vision Science, vol. 3, pp. 251–273, Sept. 2017.

[54] E. H. Adelson and J. R. Bergen, "The plenoptic function and the elements of early vision," in Computational Models of Visual Processing, pp. 3–20, MIT Press, 1991.

[55] P. Haueis, "The death of the cortical column? Patchwork structure and conceptual retirement in neuroscientific practice," Studies in History and Philosophy of Science Part A, vol. 85, pp. 101–113, Feb. 2021.

[56] D. Hubel and T. Wiesel, "Functional architecture of macaque monkey," Proceedings of the Royal Society, London [B], pp. 1–59, 1977.

[57] V. Mountcastle, An organizing principle for cerebral function. The unit module and the distributed system. The mindful brain, Cambridge, MIT Press, 1978.

[58] J. Szentágothai, "The Ferrier Lecture, 1977 The neuron network of the cerebral cortex: a functional interpretation," Proceedings of the Royal Society of London. Series B. Biological Sciences, vol. 201, pp. 219–248, Jan. 1997. Publisher: Royal Society.

[59] J. C. Horton and D. L. Adams, "The cortical column: a structure without a function." Published online, Jan. 2005.

[60] J. A. Bednar and S. P. Wilson, "Cortical Maps," The Neuroscientist: A Review Journal Bringing Neurobiology, Neurology and Psychiatry, vol. 22, pp. 604–617, Dec. 2016.

[61] M. Connolly and D. Van Essen, "The representation of the visual field in parvicellular and magnocellular layers of the lateral geniculate nucleus in the macaque monkey," The Journal of Comparative Neurology, vol. 226, pp. 544–564, July 1984.

[62] M. G. P. Rosa, "Visual maps in the adult primate cerebral cortex: some implications for brain development and evolution," Brazilian Journal of Medical and Biological Research = Revista Brasileira De Pesquisas Medicas E Biologicas, vol. 35, pp. 1485–1498, Dec. 2002.

[63] W. Bosking, Y. Zhang, B. Schofield, and D. Fitzpatrick, "Orientation selectivity and the arrangement of horizontal connections in tree shrew striate cortex," The Journal of Neuroscience, vol. 17, no. 6, pp. 2112–2127, 1997.

[64] B. A. Wandell, S. O. Dumoulin, and A. A. Brewer, "Visual field maps in human cortex," Neuron, vol. 56, pp. 366–383, Oct. 2007.

[65] M. Lavidor and V. Walsh, "The nature of foveal representation," Nature Reviews. Neuroscience, vol. 5, pp. 729–735, Sept. 2004.

[66] P. Azzopardi and A. Cowey, "Preferential representation of the fovea in the primary visual cortex," Nature, vol. 361, pp. 719–721, Feb. 1993.

[67] L. Nurminen, S. Merlin, M. Bijanzadeh, F. Federer, and A. Angelucci, "Top-down feedback controls spatial summation and response amplitude in primate visual cortex," Nature Communications, vol. 9, p. 2281, June 2018.

[68] N. Kruger, P. Janssen, S. Kalkan, M. Lappe, A. Leonardis, J. Piater, A. J. Rodriguez-Sanchez, and L. Wiskott, "Deep hierarchies in the primate visual cortex: What can we learn for computer vision?," IEEE Trans. Pattern Anal. Mach. Intell., vol. 35, pp. 1847–1871, Aug. 2013.

[69] D. Hubel and T. Wiesel, "Receptive fields, binocular interaction and functional architecture in the cat visual cortex.," J Physiol, vol. 160, pp. 106–154, 1962.

[70] L. M. Martinez and J.-M. Alonso, "COMPLEX RECEPTIVE FIELDS IN PRIMARY VISUAL CORTEX," The Neuroscientist : a review journal bringing neurobiology, neurology and psychiatry, vol. 9, pp. 317–331, Oct. 2003.

[71] G. A. Orban, H. Kato, and P. O. Bishop, "End-zone region in receptive fields of hypercomplex and other striate neurons in the cat," Journal of Neurophysiology, vol. 42, pp. 818–832, May 1979.

[72] M. Kaestner, M. L. Evans, Y. D. Chen, and A. M. Norcia, "Dynamics of absolute and relative disparity processing in human visual cortex," NeuroImage, vol. 255, p. 119186, July 2022.

[73] G. A. Orban, "Higher order visual processing in macaque extrastriate cortex," Physiological Reviews, vol. 88, no. 1, pp. 59–89, 2008.

[74] R. Shapley and M. Hawken, "Color in the Cortex—single- and double-opponent cells," Vision research, vol. 51, pp. 701–717, Apr. 2011.

[75] E. M. Callaway, "Feedforward, feedback and inhibitory connections in primate visual cortex," Neural Networks: The Official Journal of the International Neural Network Society, vol. 17, no. 5-6, pp. 625–632, 2004.

[76] K. Martin, "Microcircuits in visual cortex," Current opinion in neurobiology, vol. 12, no. 4, pp. 418–425, 2002.

[77] K. Kim, J.-H. Kim, Y.-H. Song, and S.-H. Lee, "Functional dissection of inhibitory microcircuits in the visual cortex," Neuroscience Research, vol. 116, pp. 70–76, Mar. 2017.

[78] H. Zhou, H. S. Friedman, and R. von der Heydt, "Coding of border ownership in monkey visual cortex," The Journal of Neuroscience, vol. 20, no. 17, pp. 6594–6611, 2000.

[79] L. Liu, L. She, M. Chen, T. Liu, H. D. Lu, Y. Dan, and M.-m. Poo, "Spatial structure of neuronal receptive field in awake monkey secondary visual cortex (V2)," Proceedings of the National Academy of Sciences, vol. 113, pp. 1913–1918, Feb. 2016. Publisher: Proceedings of the National Academy of Sciences.

[80] D. C. Burr, J. Holt, J. R. Johnstone, and J. Ross, "Selective depression of motion sensitivity during saccades," The Journal of Physiology, vol. 333, pp. 1–15, Dec. 1982.

[81] D. C. Burr, M. C. Morrone, and J. Ross, "Selective suppression of the magnocellular visual pathway during saccadic eye movements," Nature, vol. 371, pp. 511–513, Oct. 1994. Publisher: Nature Publishing Group.

[82] R. Sylvester, J.-D. Haynes, and G. Rees, "Saccades differentially modulate human LGN and V1 responses in the presence and absence of visual stimulation," Current biology: CB, vol. 15, pp. 37–41, Jan. 2005.

[83] J. B. Reppas, W. M. Usrey, and R. C. Reid, "Saccadic eye movements modulate visual responses in the lateral geniculate nucleus," Neuron, vol. 35, pp. 961–974, Aug. 2002.

[84] B. Roska and F. Werblin, "Rapid global shifts in natural scenes block spiking in specific ganglion cell types," Nature Neuroscience, vol. 6, pp. 600–608, June 2003. Publisher: Nature Publishing Group.

[85] L. A. Riggs, P. A. Merton, and H. B. Morton, "Suppression of visual phosphenes during saccadic eye movements," Vision Research, vol. 14, pp. 997–1011, Oct. 1974.

[86] M. A. Sommer and R. H. Wurtz, "What the brain stem tells the frontal cortex. I. Oculomotor signals sent from superior colliculus to frontal eye field via mediodorsal thalamus," Journal of Neurophysiology, vol. 91, pp. 1381–1402, Mar. 2004.

[87] H. Deubel, B. Bridgeman, and W. X. Schneider, "Immediate post-saccadic information mediates space constancy," Vision Research, vol. 38, pp. 3147–3159, Oct. 1998.

[88] J. Cavanaugh, R. A. Berman, W. M. Joiner, and R. H. Wurtz, "Saccadic Corollary Discharge Underlies Stable Visual Perception," The Journal of Neuroscience: The Official Journal of the Society for Neuroscience, vol. 36, pp. 31–42, Jan. 2016.

[89] J. R. Duhamel, C. L. Colby, and M. E. Goldberg, "The updating of the representation of visual space in parietal cortex by intended eye movements," Science (New York, N.Y.), vol. 255, pp. 90–92, Jan. 1992.

[90] M. Kusunoki and M. E. Goldberg, "The time course of perisaccadic receptive field shifts in the lateral intraparietal area of the monkey," Journal of Neurophysiology, vol. 89, pp. 1519–1527, Mar. 2003.

[91] R. A. Berman, J. Cavanaugh, K. McAlonan, and R. H. Wurtz, "A circuit for saccadic suppression in the primate brain," Journal of Neurophysiology, vol. 117, pp. 1720–1735, Apr. 2017.

[92] S. L. Macknik and M. S. Livingstone, "Neuronal correlates of visibility and invisibility in the primate visual system," Nature Neuroscience, vol. 1, pp. 144–149, June 1998.

[93] E. Castet and G. Masson, "Motion perception during saccadic eye movements," nature neuroscience, vol. 3, pp. 177–183, Feb. 2000.

[94] E. Castet, S. Jeanjean, and G. Masson, "Motion perception of saccade-induced retinal translation," Proceedings of the National Academy of Sciences USA, vol. 99, no. 23, pp. 15159–15163, 2002.

[95] Y. Kuroki, T. Nishi, S. Kobayashi, H. Oyaizu, and S. Yoshimura, "3.4: Improvement of Motion Image Quality by High Frame Rate," SID Symposium Digest of Technical Papers, vol. 37, no. 1, pp. 14–17, 2006. _eprint: https://onlinelibrary.wiley.com/doi/pdf/10.1889/1.2433276.

[96] M. Wexler and P. Cavanagh, "Fast motion drags shape," Journal of Vision, vol. 19, p. 288c, Sept. 2019.

[97] M. R. Ibbotson and S. L. Cloherty, "Visual Perception: Saccadic Omission — Suppression or Temporal Masking?," Current Biology, vol. 19, pp. R493–R496, June 2009.

[98] J. Johnston and L. Lagnado, "General features of the retinal connectome determine the computation of motion anticipation," Elife, 2015.

[99] D. Jancke, W. Erlaghen, G. Schöner, and H. Dinse, "Shorter latencies for motion trajectories than for flashes in population responses of primary visual cortex," Journal of Physiology, vol. 556, pp. 971–982, 2004.

[100] G. Benvenuti, S. Chemla, A. Boonman, G. Masson, and F. Chavane, "Anticipation of an approaching bar by neuronal populations in awake monkey v1," Journal of Vision, 2015.

[101] M. Subramaniyan, A. S. Ecker, S. S. Patel, R. J. Cotton, M. Bethge, X. Pitkow, P. Berens, and A. S. Tolias, "Faster processing of moving compared with flashed bars in awake macaque v1 provides a neural correlate of the flash lag illusion," Journal of Neurophysiology, 2018.

[102] E. Y. Chen, O. Marre, C. Fisher, G. Schwartz, J. Levy, R. A. da Silviera, and M. Berry, "Alert response to motion onset in the retina," Journal of Neuroscience, vol. 33, no. 1, pp. 120–132, 2013.

[103] S. Chemla, A biophysical cortical column model for optical signal analysis. PhD thesis, School of Information and Communication Sciences, 2010.

[104] L. G. Nowak, R. Azouz, M. V. Sanchez-Vives, C. M. Gray, and D. A. McCormick, "Electrophysiological classes of cat primary visual cortical neurons in vivo as revealed by quantitative analyses," J Neurophysiol, vol. 89, pp. 1541–1566, Mar. 2003.

[105] S. ElBoustani and A. Destexhe, "A master equation formalism for macroscopic modeling of asynchronous irregular activity states," Neural computation, vol. 21, no. 1, pp. 46–100, 2009.

[106] J. S. Goldman, L. Kusch, B. H. Yalcinkaya, D. Depannemaecker, T.-A. E. Nghiem, V. Jirsa, and A. Destexhe, "Brain-scale emergence of slow-wave synchrony and highly responsive asynchronous states based on biologically realistic population models simulated in The Virtual Brain," Dec. 2020. Pages: 2020.12.28.424574 Section: New Results.

[107] R. Veltz, "An analytical method for computing Hopf bifurcation curves in neural field networks with space-dependent delays," Comptes Rendus Mathematique, vol. 349, pp. 749–752, July 2011.

[108] S. Souihel, Generic and specific computational principles for visual anticipation of motion trajectories. Phd thesis, Université Nice Côte d'Azur ; EDSTIC, Dec. 2019.

[109] Y. Bereshpolova, X. Hei, J.-M. Alonso, and H. A. Swadlow, "Three rules govern thalamocortical connectivity of fast-spike inhibitory interneurons in the visual cortex," eLife, vol. 9, p. e60102, Dec. 2020.

[110] N. Drasdo and C. W. Fowler, "Non-linear projection of the retinal image in a wide-angle schematic eye," The British Journal of Ophthalmology, vol. 58, pp. 709–714, Aug. 1974.

[111] G. Montesano, G. Ometto, R. E. Hogg, L. M. Rossetti, D. F. Garway-Heath, and D. P. Crabb, "Revisiting the Drasdo Model: Implications for Structure-Function Analysis of the Macular Region," Translational Vision Science & Technology, vol. 9, p. 15, Sept. 2020.

[112] S. Strauss, M. M. Korympidou, Y. Ran, K. Franke, T. Schubert, T. Baden, P. Berens, T. Euler, and A. L. Vlasits, "Center-surround interactions underlie bipolar cell motion sensitivity in the mouse retina," Nature Communications, vol. 13, p. 5574, Sept. 2022. Publisher: Nature Publishing Group.

[113] U. S. Kim, O. A. Mahroo, J. D. Mollon, and P. Yu-Wai-Man, "Retinal Ganglion Cells-Diversity of Cell Types and Clinical Relevance," Frontiers in Neurology, vol. 12, p. 661938, 2021.

[114] S. Souihel, B. Cessac, M. D. Volo, A. Destexhe, F. Chavane, S. Chemla, and O. Marre, "Anticipation in the retina and the primary visual cortex : towards an integrated retino-cortical model for motion processing," in NeuroMod 2019 - First meeting of the NeuroMod Institute, (Fréjus, France), July 2019.

[115] S. Souihel and B. Cessac, "Anticipation in the retina and the primary visual cortex : towards an integrated retino-cortical model for motion processing," in ICMNS 2019 - The 5th International Conference on Mathematical NeuroScience, (Copenhague, Denmark), June 2019.

[116] S. Ebert, Dynamical synapses in the retinal network. Phd thesis, Université Côte d'Azur, Dec. 2023.

[117] G. W. Schwartz, H. Okawa, F. A. Dunn, J. L. Morgan, D. Kerschensteiner, R. O. Wong, and F. Rieke, "The spatial structure of a nonlinear receptive field," Nature Neuroscience, vol. 15, pp. 1572–1580, Nov. 2012. Publisher: Nature Publishing Group.

[118] D. Aquilué-Llorens, J. S. Goldman, and A. Destexhe, "High-Density Exploration of Activity States in a Multi-Area Brain Model," Neuroinformatics, vol. 22, pp. 75–87, Jan. 2024.

[119] M. DiVolo and I. M. Férézou, "Nonlinear collision between propagating waves in mouse somatosensory cortex," Scientific Reports, vol. 11, p. 19630, 2021.

[120] A. Papoulis, Probability, Random Variables and Stochastic Processes. McGraw-Hill, New York, 1965.

[121] M. Carlu, O. Chehab, L. Dalla Porta, D. Depannemaecker, C. Héricé, M. Jedynak, E. Köksal Ersöz, P. Muratore, S. Souihel, C. Capone, Y. Zerlaut, A. Destexhe, and M. Di Volo, "A mean-field approach to the dynamics of networks of complex neurons, from nonlinear Integrate-and-Fire to Hodgkin-Huxley models," Journal of Neurophysiology, vol. 123, pp. 1042–1051, Mar. 2020.